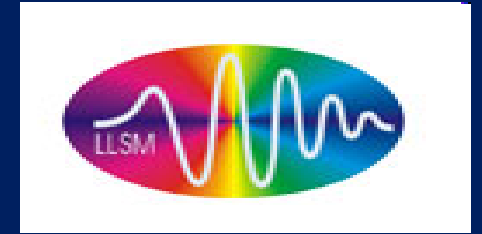




MIĘDZYRESORTOWY INSTYTUT TECHNIKI RADIACYJNEJ
WYDZIAŁ CHEMICZNY POLITECHNIKI ŁÓDZKIEJ

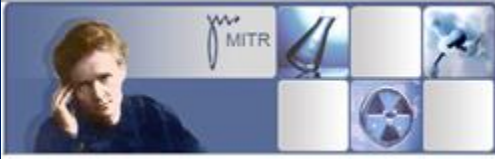


Biospektroskopia

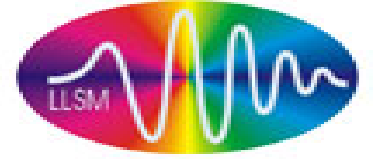
Prof. dr hab. Halina Abramczyk

<http://www.mitr.p.lodz.pl/raman/>

**Politechnika Łódzka, Międzyresortowy Instytut Techniki Radiacyjnej, Laboratorium Laserowej
Spektroskopii Molekularnej, Łódź**



MIĘDZYRESORTOWY INSTYTUT TECHNIKI RADIACYJNEJ
WYDZIAŁ CHEMICZNY POLITECHNIKI ŁÓDZKIEJ



- **Biospektroskopia, st. 1., sem. 6, specjalność
CHEMIA BIOMEDYCZNA**

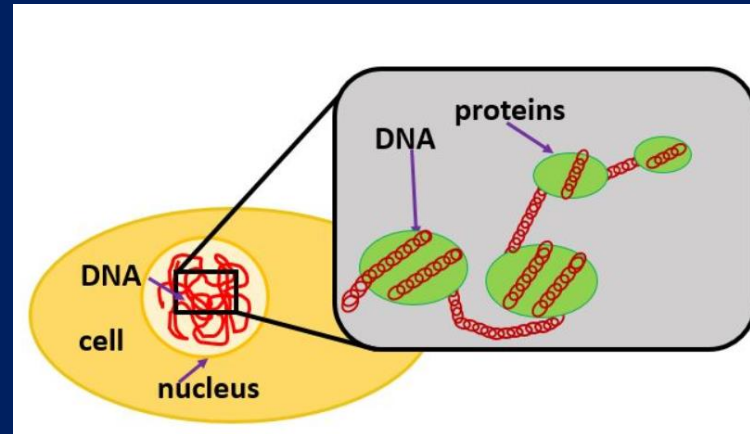
High throughput biology

- **High throughput cell biology** is the use of automation equipment with classical cell biology techniques to address biological questions that are otherwise unattainable using conventional methods. It may incorporate techniques from optics, chemistry, biology or image analysis to permit rapid, highly parallel research into how cells function, interact with each other and how pathogens exploit them in disease.
- High-throughput biology serves as one facet of what has also been called "omics research" - the interface between large scale biology (genome, proteome, transcriptome), technology and researchers. High throughput cell biology has a definite focus on the cell, and methods accessing the cell such as imaging, gene expression microarrays, or genome wide screening. The basic idea is to take methods normally performed on their own and do a very large number of them without impacting their quality. High throughput research can be defined as the automation of experiments such that large scale repetition becomes feasible. This is important because many of the questions faced by life science researchers now involve large numbers. For example, the Human Genome contains at least 21,000 genes, all of which can potentially contribute to cell function, or disease. To be able to capture an idea of how these genes interact with one another, which genes are involved in and where they are, methods that encompass from the cell to the genome are of interest.

Separately, cancer biology with genomics and proteomics protocols provides only a partial picture of cancer

- Separately, cancer biology with genomics and proteomics protocols provides only a partial picture of cancer

Conventional molecular biology

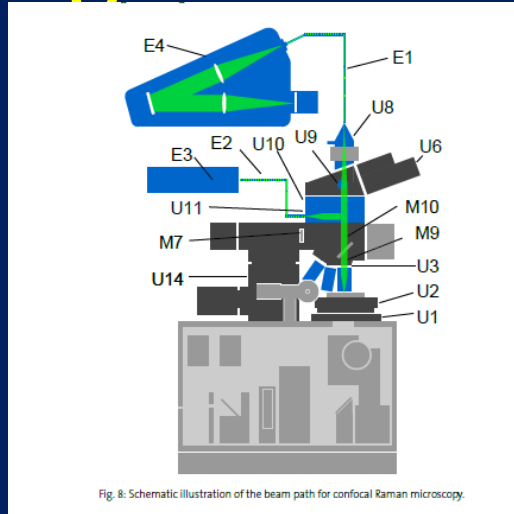


- **Isolation of DNA from Cells and Tissues**
- DNA can be extracted from many types of cells. The first step is to lyse or break open the cell. This can be done by grinding a piece of tissue in a blender. After the cells have broken open, a salt solution such as NaCl and a detergent solution containing the compound SDS (sodiumdodecyl sulfate) is added.
- **Isolation of Mitochondria from Cells and Tissues**
- Mitochondrial isolation protocols involve two processes – cell disruption to break open the cells and release the cellular structures, and differential centrifugation to recover fractions that are enriched for mitochondria.

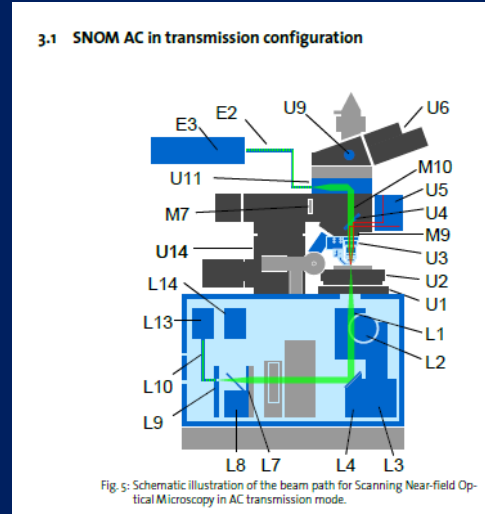
Biomedical applications

- **High spacial resolution (far below the diffraction limit, TERS) RAMAN IMAGING**
- **High temporal resolution (FEMTOSECOND PUMP-PROBE SPECTROSCOPY)**
- **Strong signal enhancement enabling monitoring the genetic and immunological responses in biological systems (SERS COMBINED WITH NANOPARTICLES)**
- **Specificity of interactions (BIOCONJUGATES)**

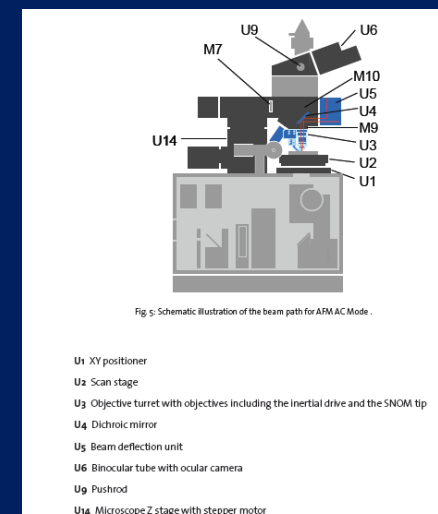
Methods of molecular and laser microspectroscopy imaging



Raman imaging



SNOM imaging



AFM imaging

We do not need to disrupt cells to break open the cells and release the cellular structures

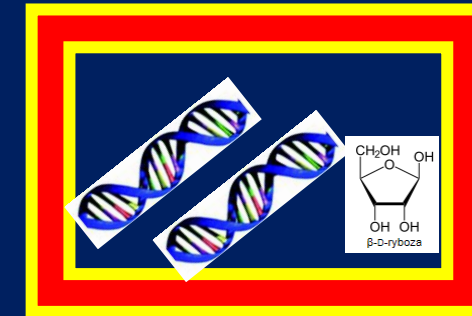
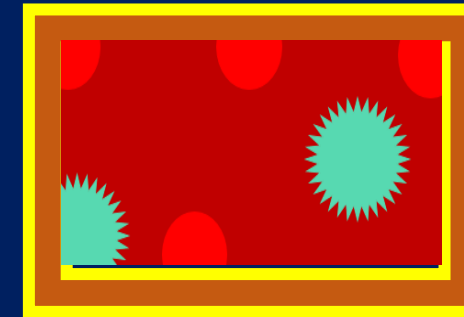
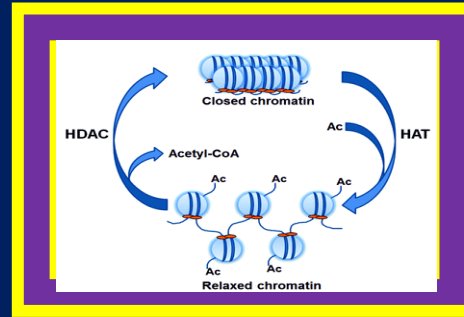
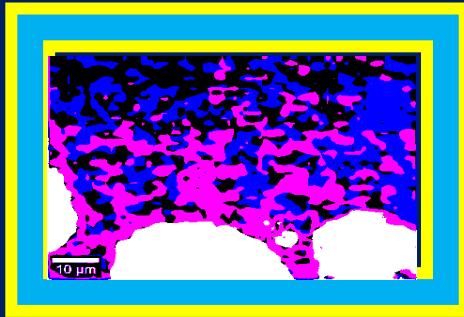
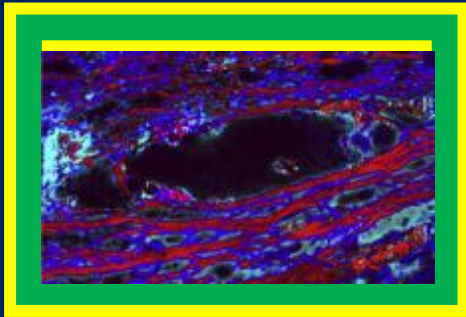
Concentration (molar)

mM

μ M

nM

pM



STRUCTURAL

METABOLIC

EPIGENETIC

IMMUNOLOGIC

GENETIC

- epithelium
- connective
- nerves
- muscle

- lipids
- proteins
- carbohydrates
- minerals
- enzymes

- DNA methylation
- histone methylation
- histone acetylation

- receptors
- growth factors
- cytokines
- hormones

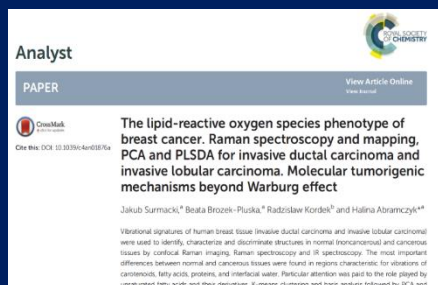
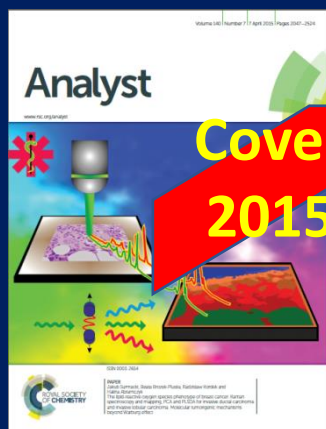
- DNA
- mRNA

EASE OF DETECTABILITY

POTENTIAL SPECIFICITY INCREASE

Detectable molecular features in tissue can be divided into six physiological categories: structural, metabolic, epigenetic, immunologic and genetic. The key factor limiting most imaging methods is signal-to-noise related to the concentration of the feature to be imaged. Fig.1 shows detectable molecular features in tissue (specificity) vs. concentration (sensitivity). Metabolic markers and immunologic markers (growth factors, cytokines or hormones) can be secreted at concentrations several times higher than surface receptors, which make them easier to detect.

HOW DOES RAMAN SPECTROSCOPY AND IMAGING BENEFIT BIOLOGICAL RESEARCH?



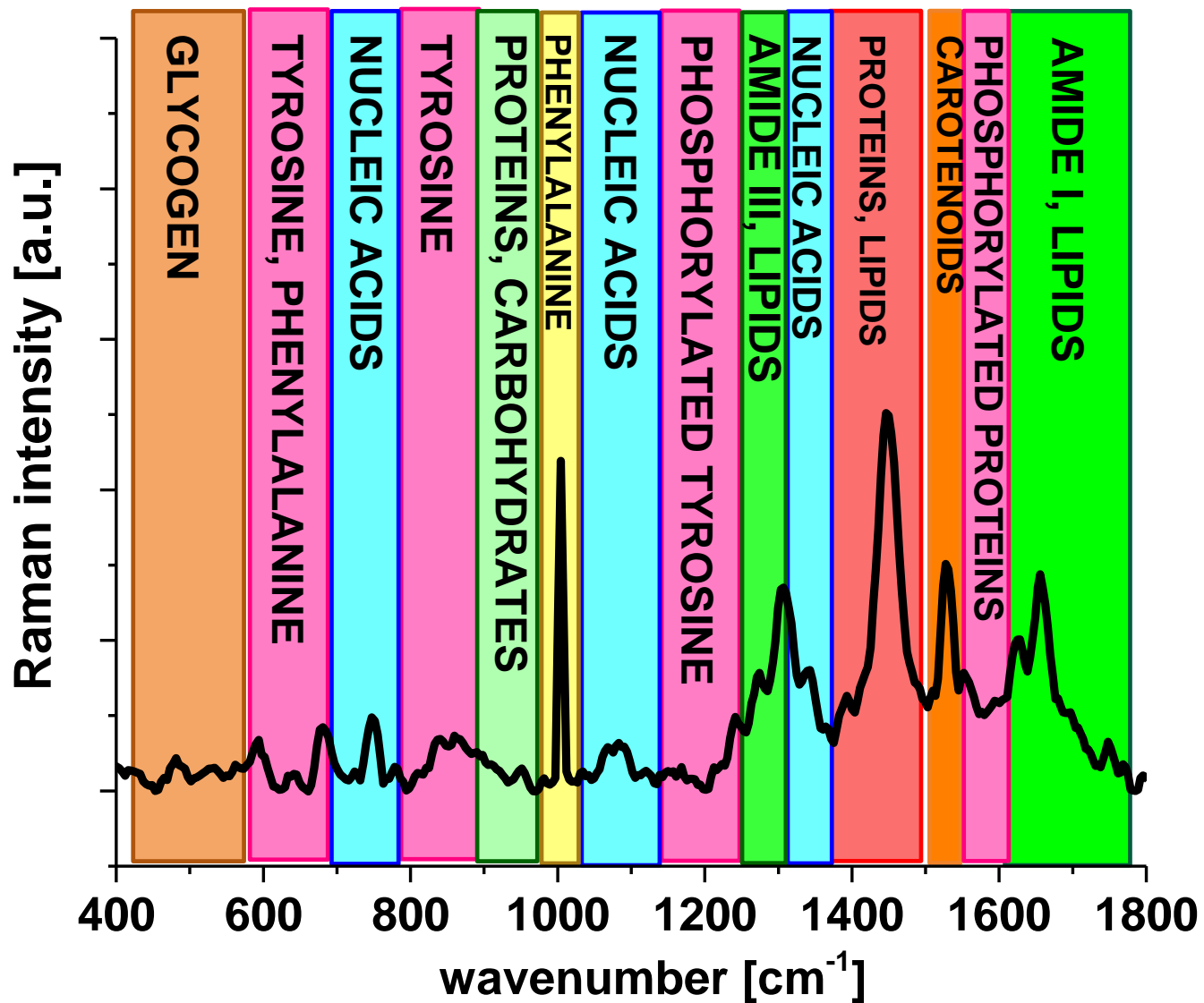
Surmacki J, Brozek-Pluska B, Kordek R, Abramczyk H, The lipid-reactive oxygen species phenotype of breast cancer. Raman spectroscopy and mapping, PCA and PLSDA for invasive ductal carcinoma and invasive lobular carcinoma. Molecular tumorigenic mechanisms beyond Warburg effect, Analyst, 2015, 140, 2121 – 2133, (IF=4.2)

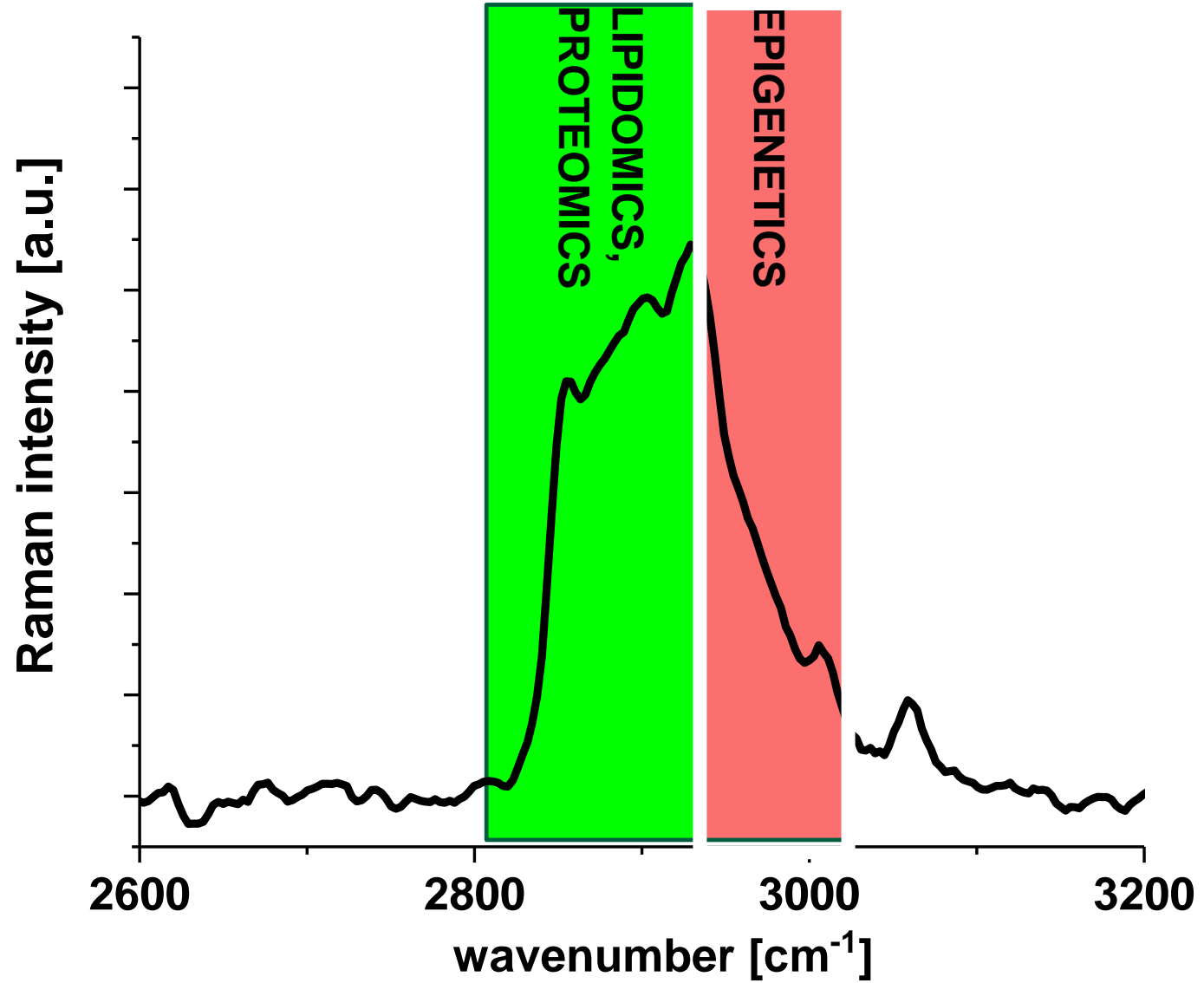
METABOLOMICS

GENOMICS/TRANSCR
IPTOMICS

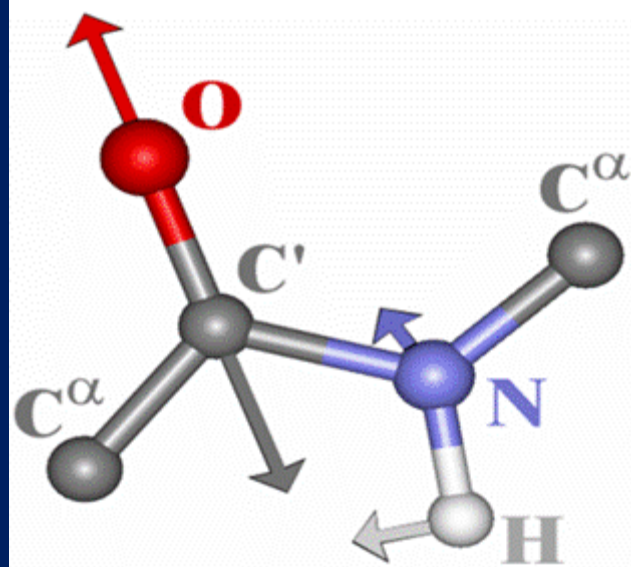
LIPIDOMICS

PROTEOMICS



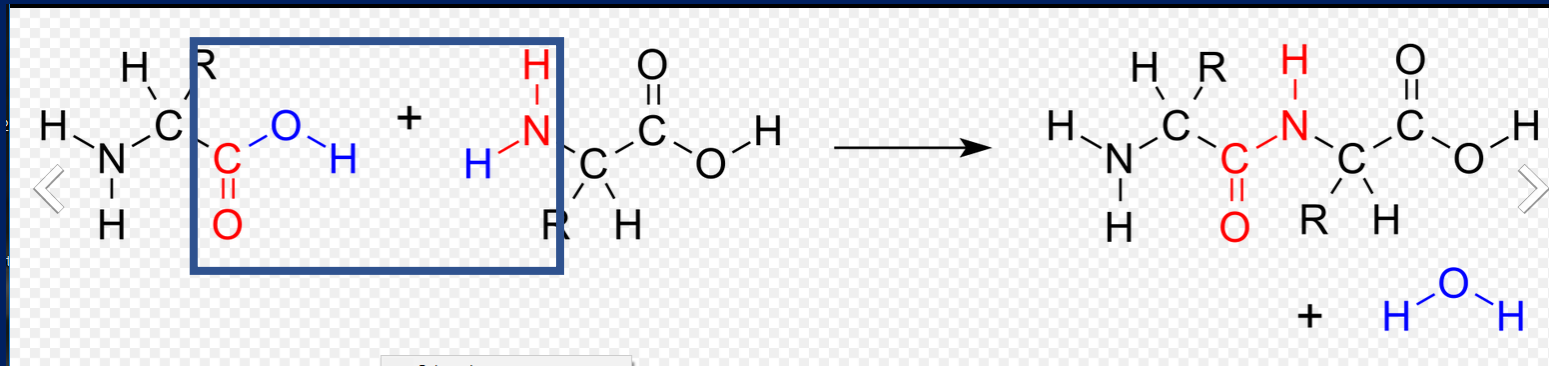


Amide I Vibrational Mode



PROTEINS

- Proteins are linear polymers consisting of 20 different amino acids. All amino acids have the same backbone, consisting of one nitrogen and two carbon atoms. The chemical and physical properties of each amino acid are determined by its side chain, which is connected to the C α atom. Two amino acids can be connected by a chemical bond, the so called peptide bond. Short amino acid oligomers are also called peptides



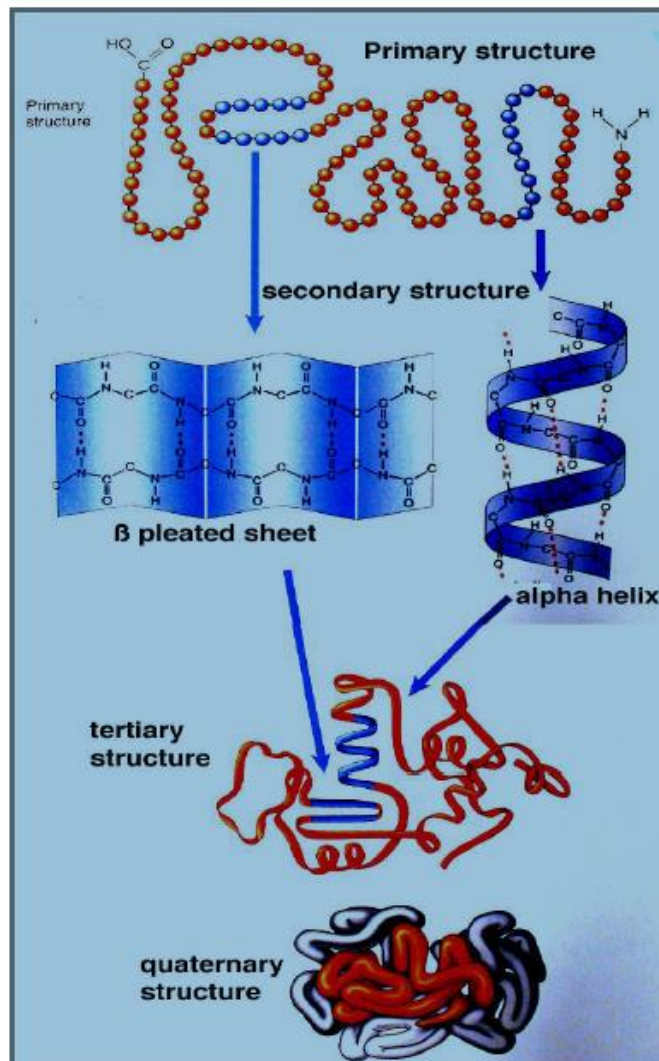
The dehydration condensation of two amino acids to form a peptide bond (red) with expulsion of water (blue).

- Grupę 20 uniwersalnych α -aminokwasów, budujących białka, możemy u człowieka podzielić na dwie równoliczne podgrupy: **AMINOKWASY EGZOGENNE** - te, które muszą być dostarczone w pożywieniu:

fenyloalanina (Phe)
izoleucyna (Ile)
leucyna (Leu)
lizyna (Lys)
metionina (Met)
treonina (Thr)
tryptofan (Trp)
walina (Val)
arginina (Arg)
histydyna (His)

- **AMINOKWASY ENDOGENNE** - te, które organizm jest w stanie sobie w wystarczającej ilości wyprodukować: alanina (Ala), asparagina (Asn), kwas asparaginowy (Asp), cysteina (Cys), kwas glutaminowy (Glu), glutamina (Gln), glicyna (Gly), prolina (Pro), seryna (Ser) i tyrozyna (Tyr).

Raman spectrum of proteins

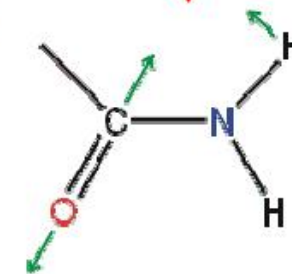


Secondary structure of the protein

Spatial arrangement of bonds (C=O)

Coupling between individual vibrations (C=O)

Amide I Raman band



The precise positions of bands depend on inter and intra molecular effects, including peptide-bond angles and hydrogen-bonding patterns

- The structure of proteins is described by four different levels.
- The primary structure of a protein is its amino acid sequence, which is coded in DNA or RNA. Each protein is identified by its primary structure.

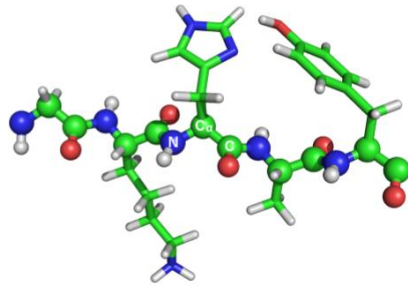


Figure 2.1: A sample peptide consisting of five different amino acids. Backbone atoms are drawn as spheres. The order of the residues from left to right is Glycine-Lysine-Histidine-Alanine-Tyrosine.

SECONDARY STRUCTURE

- Short amino acid segments can arrange into recurring local structure elements, referred to as secondary structure. Secondary structure elements include for example α -helices, β -sheets, and random coils. Both α -helices and β -sheets are defined by stabilizing hydrogen bonds involving the protein backbone. Amino acid side chains do not contribute to secondary structure elements. α -helices (Figure 2.2 A) are regular spiral staircase like structures. A hydrogen bond is formed between the $C\beta=O$ group from residue n and the N-H group from residue $n + 4$. Each helix turn consists of 3.6 residues, leading to an average angle of 100° per residue. The side chain atoms are oriented towards the helix outside. β -sheets (Figure 2.2 B) are similarly stabilized by hydrogen bonds between the $C\beta=O$ and the N-H group. But unlike α -helices, β -sheets are formed by two adjacent peptide chains rather than one single chain. According to the orientation of the two strands relative to each other, parallel and anti-parallel β -sheets are distinguished.

SECONDARY STRUCTURE

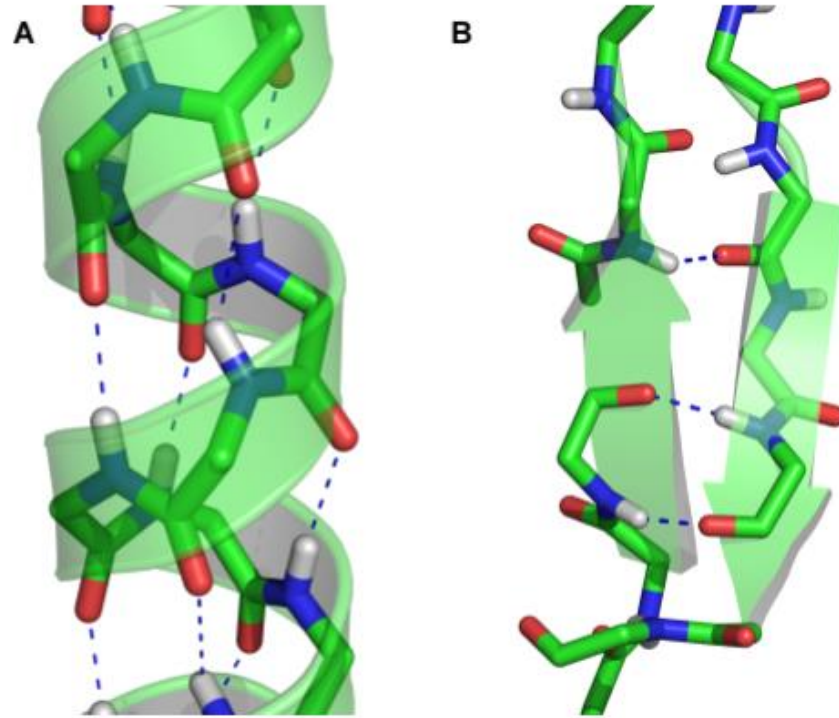


Figure 2.2: Secondary structure elements. Backbone atoms are shown in a stick representation. Hydrogen bonds appear as dotted blue lines. A: α -helix B: β -sheet

tertiary structure

- Proteins arrange into a well-defined spatial shape termed tertiary structure, defined by their primary structure, in a process called protein folding. With only few exceptions, the folded protein has a minimal free energy G . Unlike the secondary structure, the tertiary structure is not mainly stabilized by hydrogen bonds inside the protein backbone, but also by van-der-Waals forces, by electrostatic forces, and by the hydrophobic effect. Additionally, side chain atoms are involved in the folding process. Even other molecules than amino acids or ions can contribute to the tertiary structure of a protein

quarternary structure

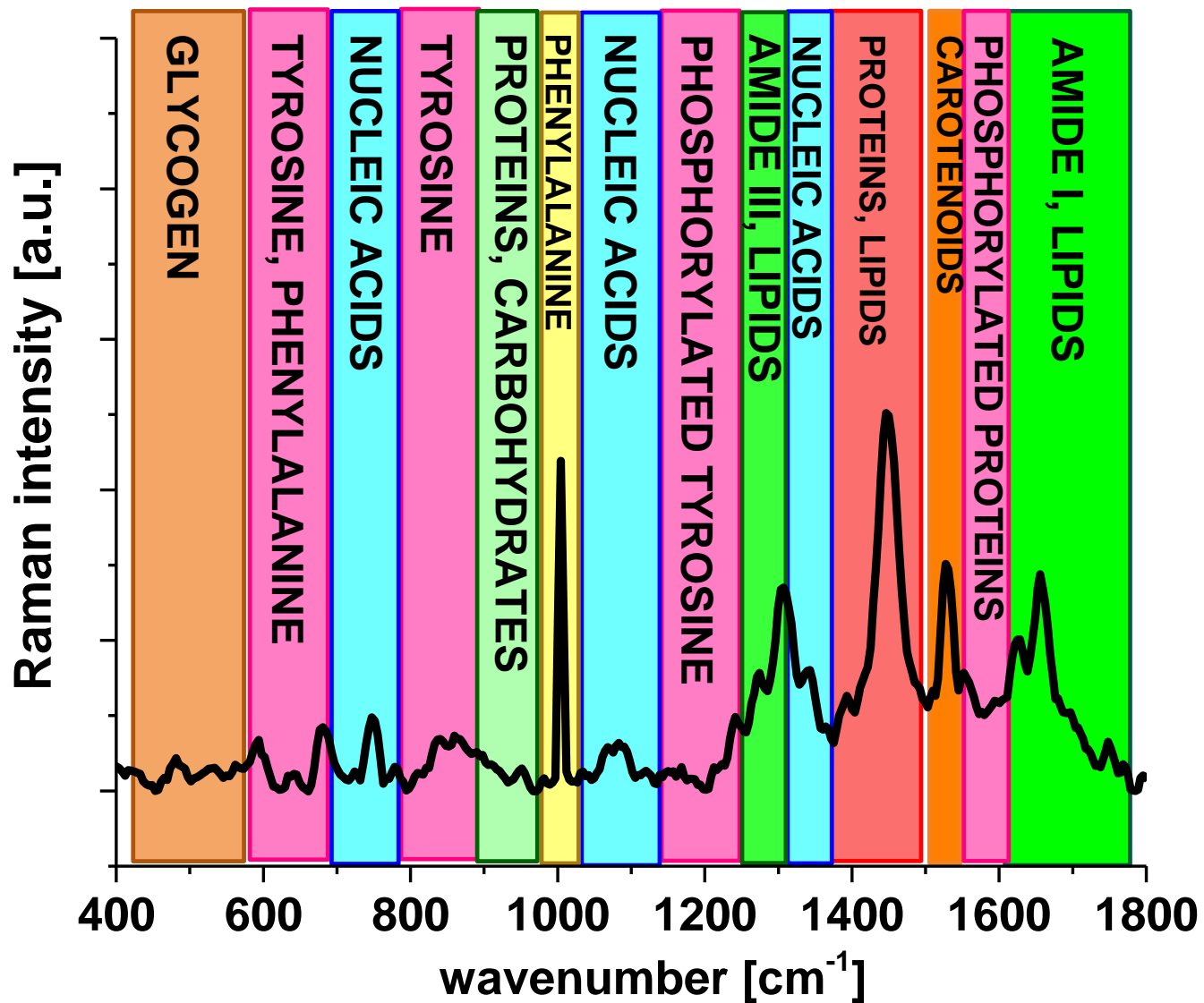
- For functional purposes, folded proteins sometimes form larger assemblies. These structures of several folded proteins are called quarternary structure. The association forces are, as for the tertiary structure, van-der-Waals forces, electrostatic forces, and the hydrophobic effect.

METABOLOMICS

GENOMICS/TRANSCR
IPTOMICS

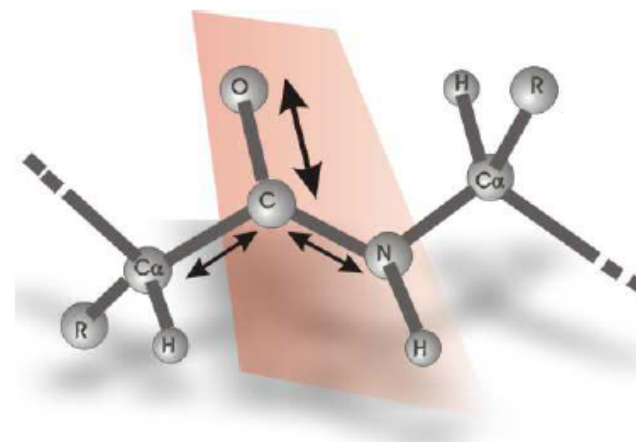
LIPIDOMICS

PROTEOMICS



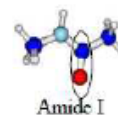
Secondary structure analysis

- Nine normal modes are allowed for the amide band of proteins.
- These are called A, B, and I-VII in order of decreasing frequency

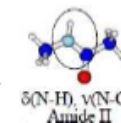


Amide Raman bands

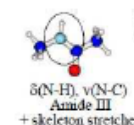
Amide I band 80% C=O stretch, near 1650cm⁻¹



Amide II band 60% N-H bend and 40% C-N stretch, near 1550 cm⁻¹

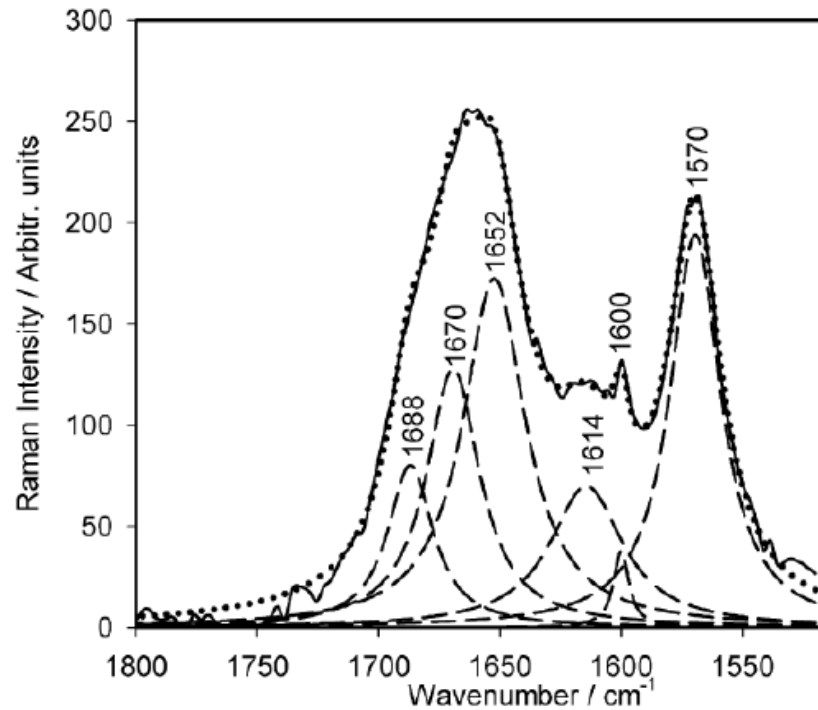


Amide III band 40% C-N stretch, 30% N-H bend, near 1300 cm⁻¹

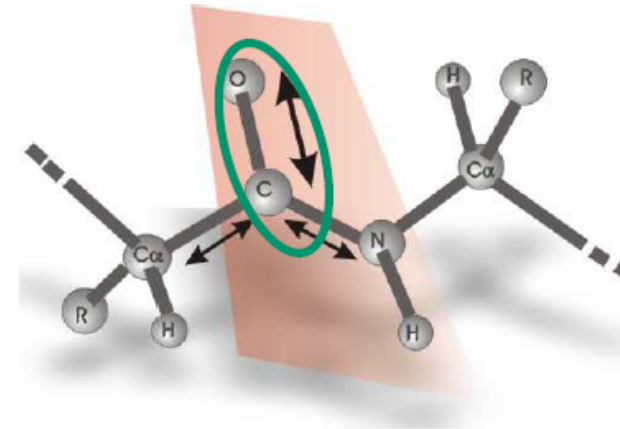


Raman spectrum of proteins

Amide I bands



The different types of secondary structures are characterized by amide I bands slightly different in position and shape

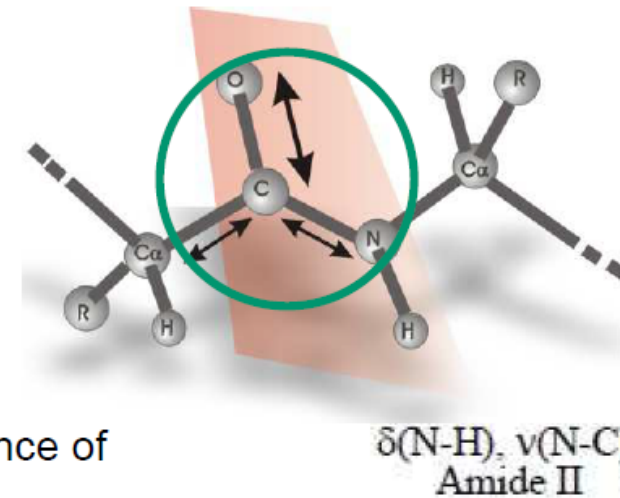


Principal Amide I Frequencies Characteristic of Protein Secondary Structures

Conformation	H ₂ O	D ₂ O
α -helix	1650–1657	1647–1654
Antiparallel β -sheet	1612–1640; 1670–1690 (weak)	1628–1635
Parallel β -sheet	1626–1640	
Turn	1655–1675	
Unordered	1680–1696	1643

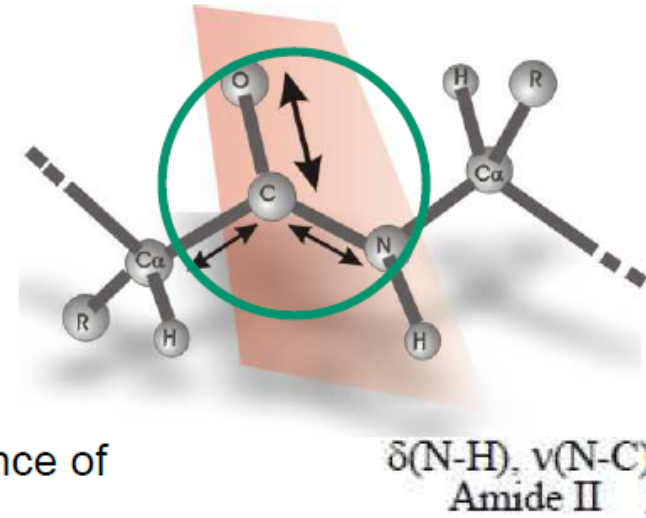
Amide II band

- Parallel / antiparallel β - sheet structure $\sim 1550 \text{ cm}^{-1}$
- It is a weak band It can not be observed in the absence of resonance excitation
- It is hardly affected by the side-chain vibrations but the correlation between secondary structure and frequency is less straightforward than for the amide I vibration.
- It can be sensitive to H/D exchange



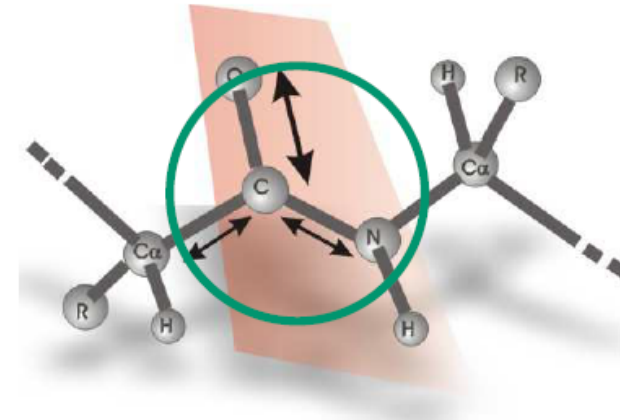
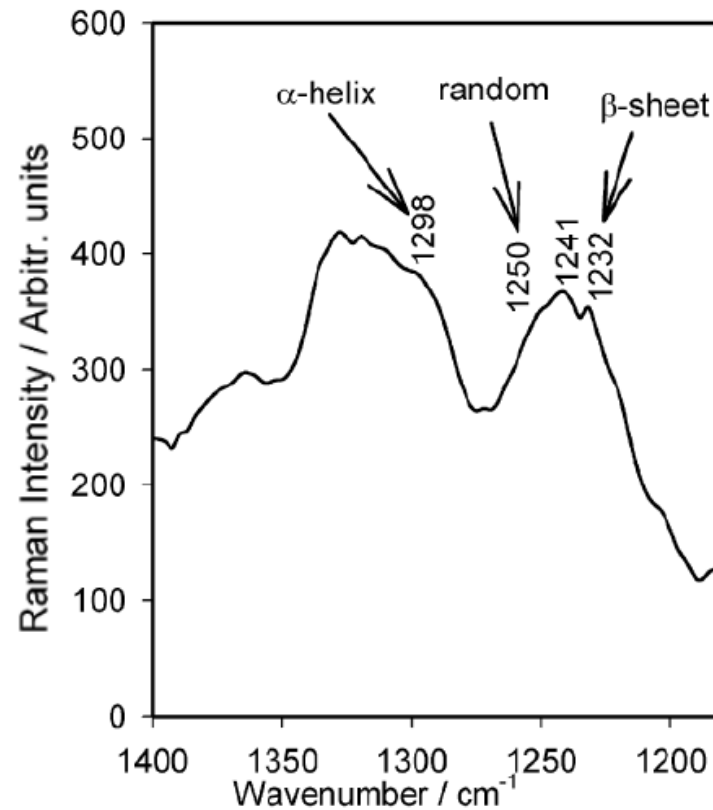
Amide II band

- Parallel / antiparallel β - sheet structure $\sim 1550 \text{ cm}^{-1}$
- It is a weak band It can not be observed in the absence of resonance excitation
- It is hardly affected by the side-chain vibrations but the correlation between secondary structure and frequency is less straightforward than for the amide I vibration.
- It can be sensitive to H/D exchange



Raman spectrum of proteins

Amide III bands



$\delta(\text{N-H}), \nu(\text{N-C})$
Amide III
+ skeleton stretches

- Assignment

α -helix : 1270-1300 cm^{-1}

Random coil : 1243-1253 cm^{-1}

β -sheet : 1229-1235 cm^{-1}

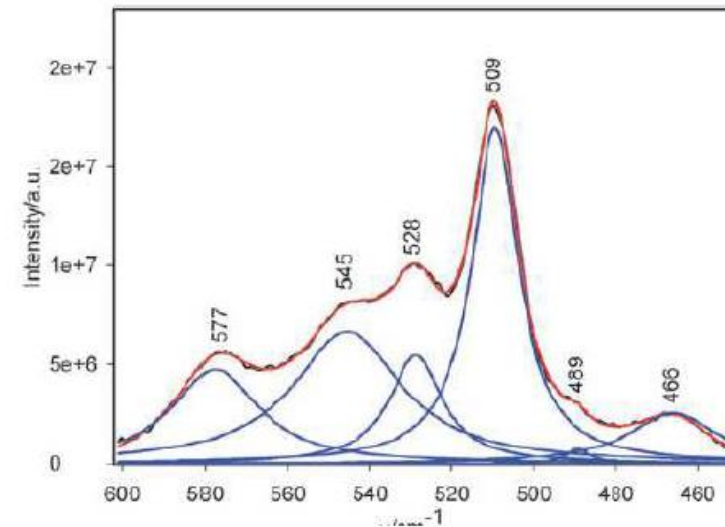
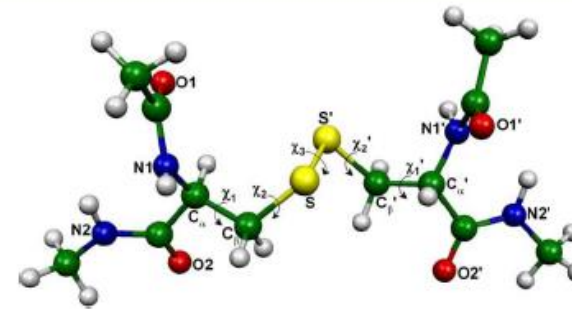
- The structure of amide III band can be correlated to the amide I band = complementary structural information on the protein structure and in this way it is possible to get some additional details to the amide I

Other important spectral features in proteins spectra

- Disulphide Bridges (S-S bonds)
- Aromatic aminoacids (Phenylalanine - Phe, tryptophan - Trp, tyrosine - Tyr, hystidin - His)

S-S bond stretching

- Experimental studies, shows that for the proteins whose structure contains S-S bridges, the S-S Raman bands are located in the spectral range 500-550 cm^{-1} .
- The factors affecting the frequency of vibration are: the relative conformation of atoms C_{α} - C_{β} -S-S'- C'_{β} - C'_{α} around C_{β} -S and C_{β} -S' bonds, the mode coupling and the hydrogen bonds



The analysis of the lysozyme Raman spectrum in the 450–600 cm^{-1} spectral range using Lorentzian functions. Experimental spectrum in black and simulated spectrum in red (band decomposition in blue)

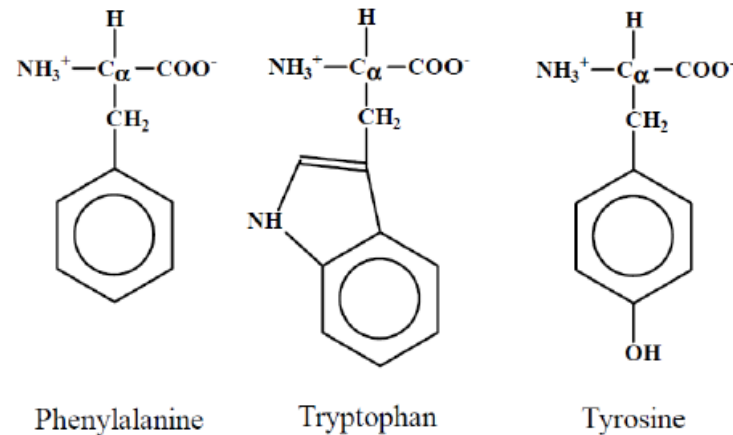
David et al, PCCP, 2009



Raman spectrum of proteins

Aromatic aminoacids

- Some of the vibrational bands of tyrosine (Tyr), tryptophan (Trp) or phenylalanine (Phe) are sensitive to the microenvironment
- Theirs band positions may vary up to 5 cm^{-1} in the Raman spectra of proteins.

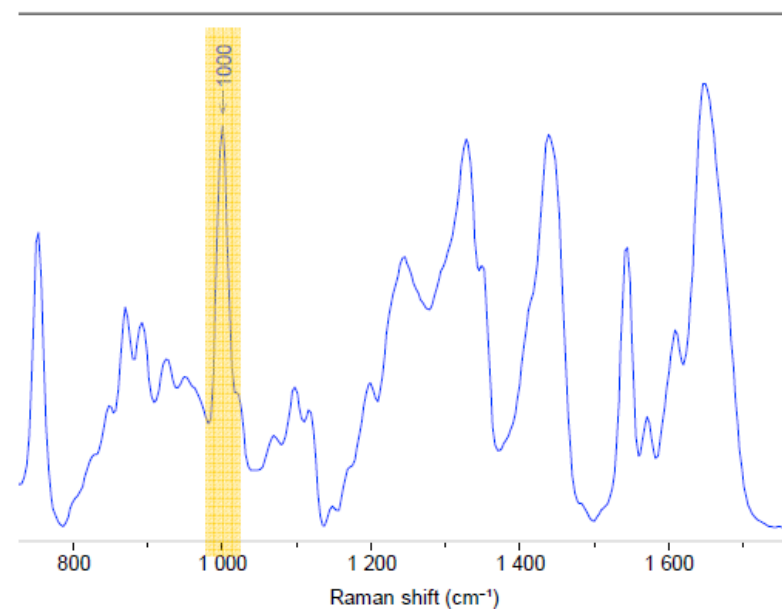
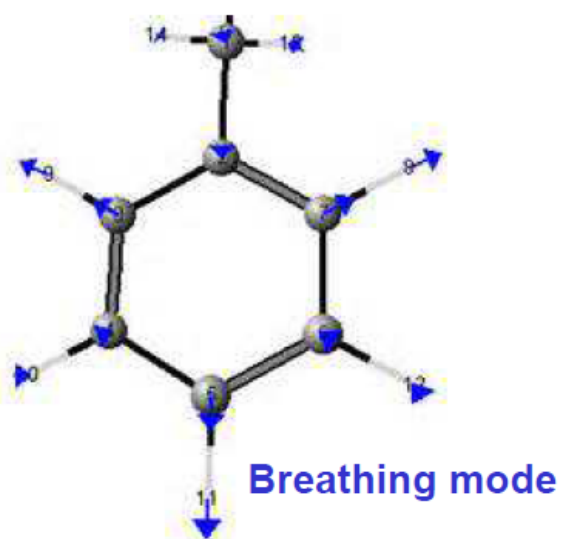


Aromatic residues	Mean frequency (cm^{-1})
Phe	620
Tyr	640
Trp	750
Tyr	830, 850
Phe	1000, 1030
Trp	1011
Tyr, Phe	1170-1200
Trp	1340-1360
Trp	1582
Phe, Trp	1584
Tyr	1590
Phe	1605
Trp, Phe, Tyr	1610-1616
Trp	1618-1621
His	3110-3160

Important Raman modes of aromatic aminoacids within the protein structure

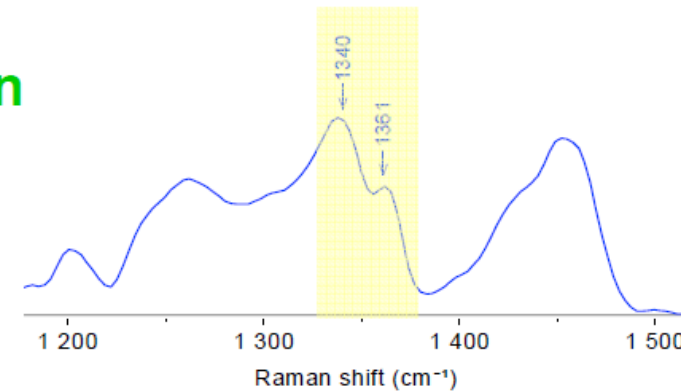
Aromatic aminoacids - Phenylalanine

- Phe shows very intense band around 1000 cm^{-1}
- This band is not sensitive to conformational changes of protein and therefore can be used for normalization of the Raman spectra of protein



Aromatic aminoacids - **Tryptophan**

■ The components of the Fermi doublet of Trp : 1340 and 1360 cm^{-1} .



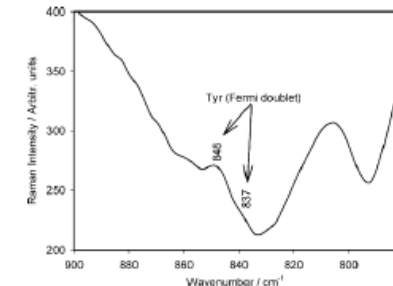
- I_{1360}/I_{1340} serves as a hydrophobicity marker.
- The 1360 cm^{-1} band is strong in hydrophobic solvents ($I_{1360}/I_{1340} > 1.1$)
- The 1340 cm^{-1} band is stronger in hydrophilic environment ($I_{1360}/I_{1340} < 0.9$)

■ The 1010 cm^{-1} band is sensitive to the strength of van der Waals interactions of the Trp ring with surrounding residues

- ν near or below 1010 cm^{-1} indicates weak or no van der Waals interactions
- ν near 1012 cm^{-1} or higher reflect stronger van der Waals interactions

Aromatic aminoacids - Tyrosine

- Tyrosine doublet Raman bands near 830 and 850 cm⁻¹.
- They are caused by Fermi resonance between the in-plane breathing mode of the phenol ring and an overtone of out-of-plane deformation mode
- The intensities of these two bands depend on the hydrogen bonding condition of the phenol side chain.



Relative intensity of sensitive Raman bands in rabbit lenses with induced cataract

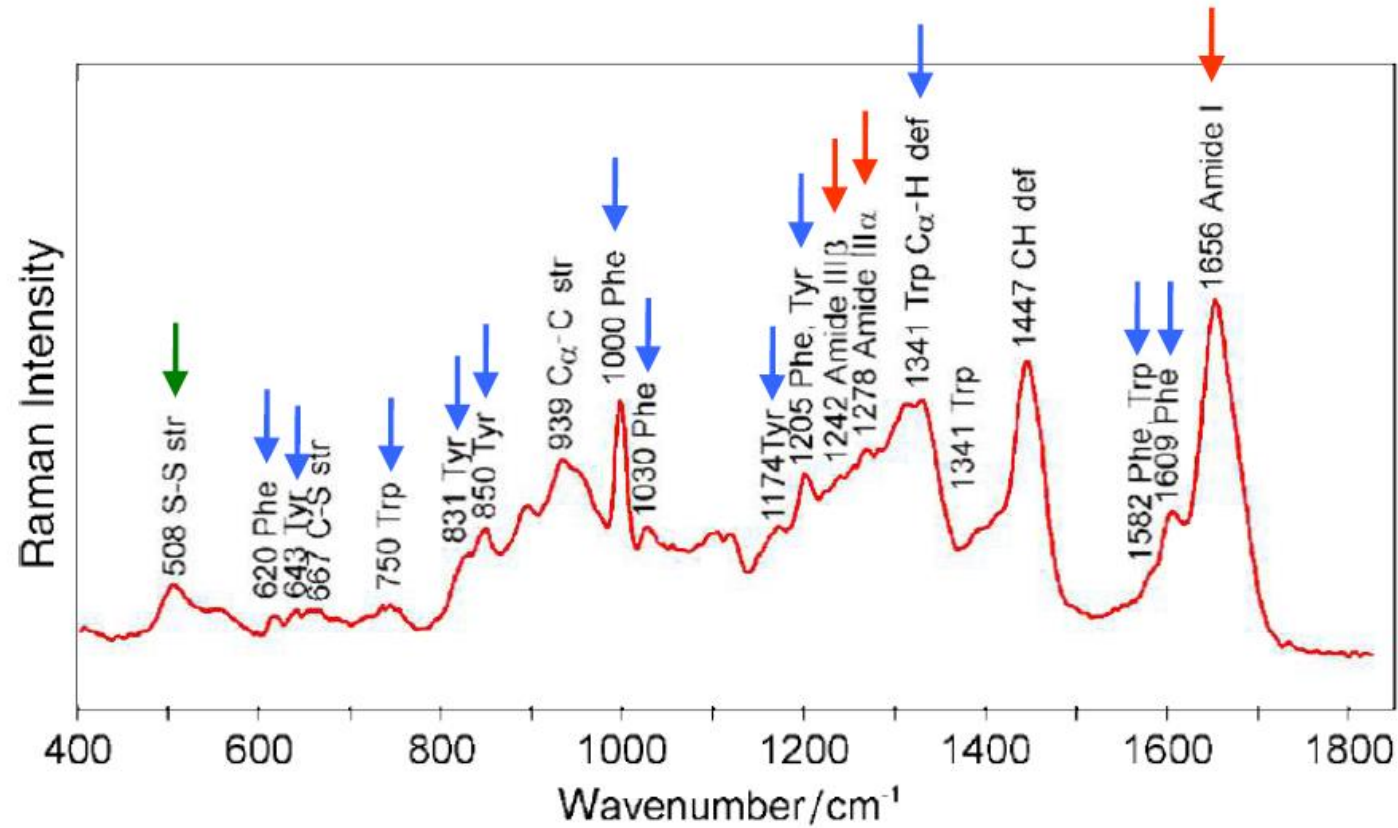
		Rabbit lenses	
		Normal	Cataractous
H ₂ O	I_{3390}/I_{2935}	0.40	0.50
S-H	I_{2580}/I_{2730}	1.53	1.38
TYR	I_{830}/I_{855}	0.92	0.96
TRP	I_{890}/I_{700}	0.78	0.66
Amide	I and III		No change
TYR/PHE	I_{644}/I_{624}	1.77	1.44

- The ratio I₈₅₀/I₈₃₀ is often analyzed
 - 6.7 corresponds to non-hydrogen bonded
 - 2.5 the OH group of tyrosine is a strong
 - 0.3 corresponds to tyrosine as a donor
 - 1.25 shows that the OH group serves both as an acceptor and a donor of a hydrogen bond.

Journal of Molecular Structure, 214 (1989) 111-117



Raman analysis of proteins



backbone amino acids S-S

Conclusions

- Raman spectroscopy can be successfully used as a method for probing the structure and conformation of native proteins
- Important structural information can be deduced from specific Raman vibrational bands as: amide I, amide II and amide III bands.
- The influence of chemical reactions mechanism involving proteins (folding/unfolding, oxidation, reduction, phosphorylation, and polymerization) can be monitored by following the evolution over the time of Raman bands: the disulphide bridges stretching, aromatics ring vibrations, protein side chain deformation etc

CHARACTERISTIC BANDS OF PROTEINS

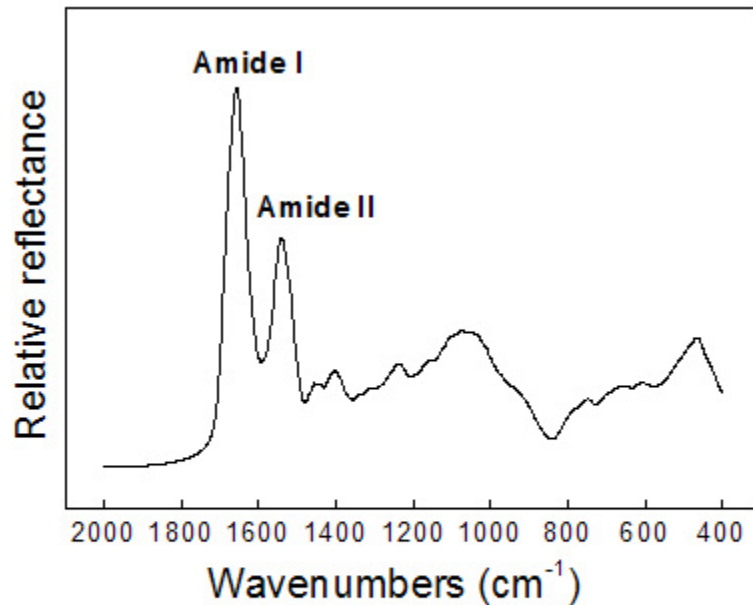


Figure 1. Infrared spectrum for the lysozyme film deposited on vitreous fragments with diameters of 0.3 mm. The tops amide I and amide II correspond to 1542 and 1659 cm^{-1} , respectively.

the peptide group, the structural repeat unit of proteins, has 9 characteristic bands named amide (A, B, I, II ... VII). Amide I and amide II bands are two major bands of the protein infrared spectrum. The amide I band (ranging from 1600 to 1700 cm^{-1}) is mainly associated with the C–O stretching vibration (70-85%) and is directly related to the backbone conformation. Amide II results from the N–H bending vibration (40-60%) and from the C–N stretching vibration (18-40%)²⁰. The amide III band is usually weak in the FTIR spectroscopy but can be found in the region from 1250 to 1350 cm^{-1} .

CHARACTERISTIC BANDS OF PROTEINS

- ν_{NH} stretch is a localized mode. Usually it
- appears as a doublet called as Amide A and Amide
- A' (or sometimes Amide B), respectively. The
- other interacting components are either the overtone
- of the Amide II mode or a combination band.
- In hydrated state and/or in water solution the NH
- stretching is partially screened with OH stretching
- of H₂O molecules.

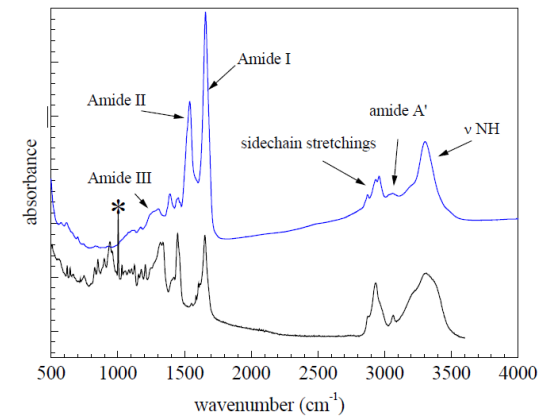


Fig. 1. IR spectrum of dried BSA cast film (upper spectrum) and Raman spectrum of BSA solution in phosphate buffer (lower spectrum)

CHARACTERISTIC BANDS OF PROTEINS

- The Amide I
 - mode is primary a C=O stretching
 - band. It may have some contributions from CN stretching and CCN deformation.
- The Amide II
 - mode is an out-of-phase combination of largely NH in plane bending and CN stretching and smaller contributions from C=O in-plane bending and NC stretching.
- The Amide III
 - mode is the inphase combination of NH in-plane bending and CN stretching.

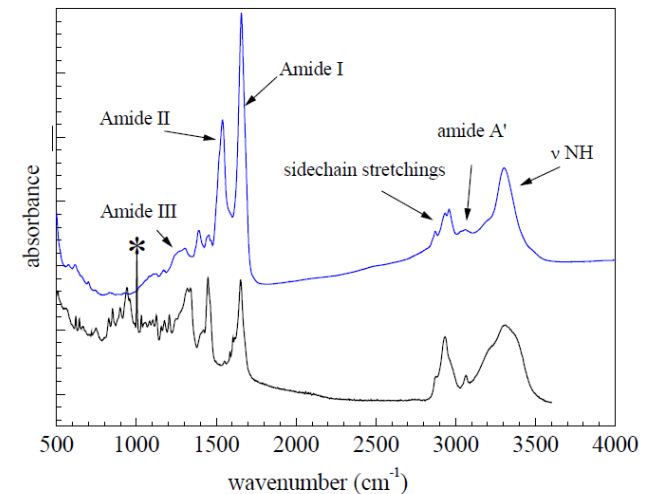


Fig. 1. IR spectrum of dried BSA cast film (upper spectrum) and Raman spectrum of BSA solution in phosphate buffer (lower spectrum)

CHARACTERISTIC BANDS OF PROTEINS

- Less intensive is contribution from
- CC stretching and CO bending.
- Other Amide modes (from IV to VII) are less
- intensive in both infrared and Raman spectra and
- therefore not practical for a conformation study.
- These modes are mainly due to in and out-of plane
- deformation vibrations of amino groups, strongly
- coupled, and less sensitive to conformational
- changes. 0.6

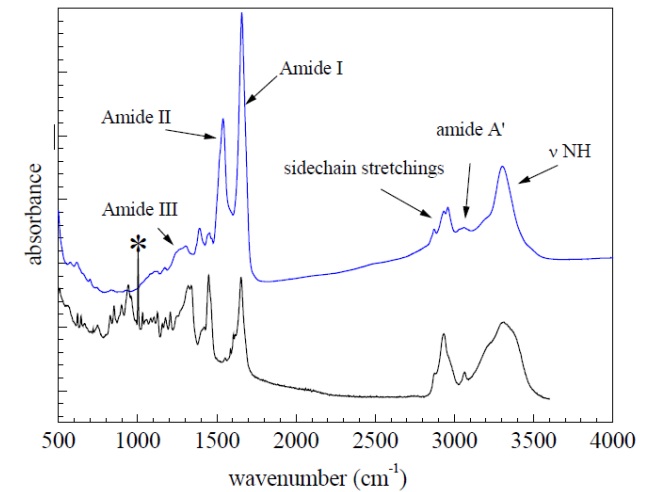


Fig. 1. IR spectrum of dried BSA cast film (upper spectrum) and Raman spectrum of BSA solution in phosphate buffer (lower spectrum)

A short history of rise and fall of hydrophobia and hydrophilia

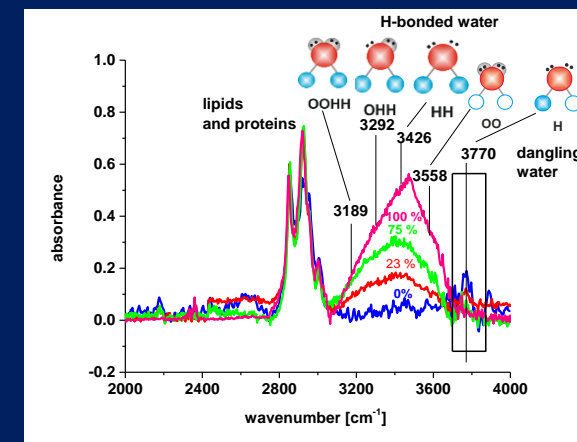
- To understand the Raman and IR spectral differences in hydrations of the normal and cancerous breast tissue, at least three fundamental questions must be addressed.
- **How do proteins interact with water in the cellular environment?**
- **How do biological membranes interact with the interfacial water?**
- **How do fatty acids interact with water under realistically crowded conditions?**

Although interactions at cellular surfaces involve large numbers of forces and molecular interactions, at first glance, the interactions between water and cell surfaces seem to embody the similar principles as those between molecules in hydrophobic, and hydrophilic environments.

interfacial water at the biological surface of human breast cancer tissue

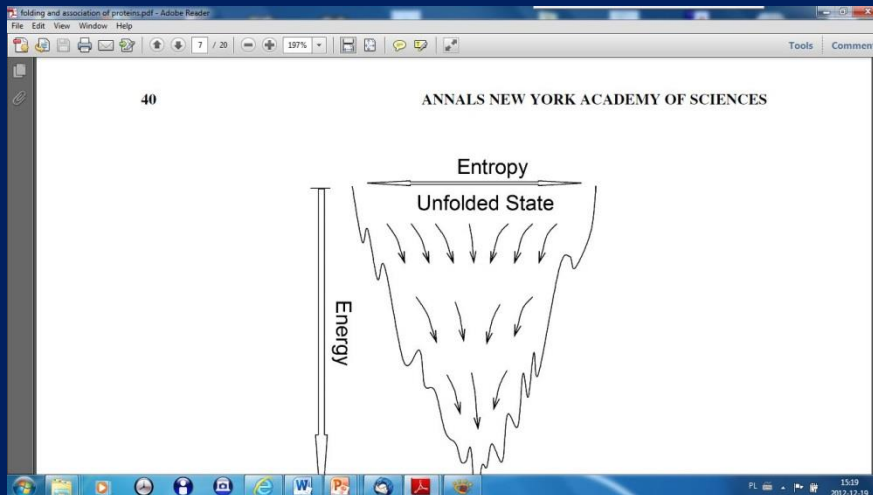
The next step is to study spectral properties of water under realistically crowded conditions, since these conditions are typical property of all cells and crowding may be essential for the efficient operation of most biological processes. While there are many papers reporting on water static and dynamic properties at model interfaces there is limited number of papers on properties of water at the interfacial regions under realistically crowded conditions of biological tissue .

Ultrafast Dynamics of Metal Complexes of Tetrasulfonated Phthalocyanines at Biological Interfaces: Comparison between Photochemistry in Solutions, Films, and Noncancerous and Cancerous Human Breast Tissues
Halina Abramczyk, Beata Brozek-Pluska, Marc Tondusson, and Eric Freysz J Phys Chem C, 2013



Water in the cellular environment of the cancerous human tissue

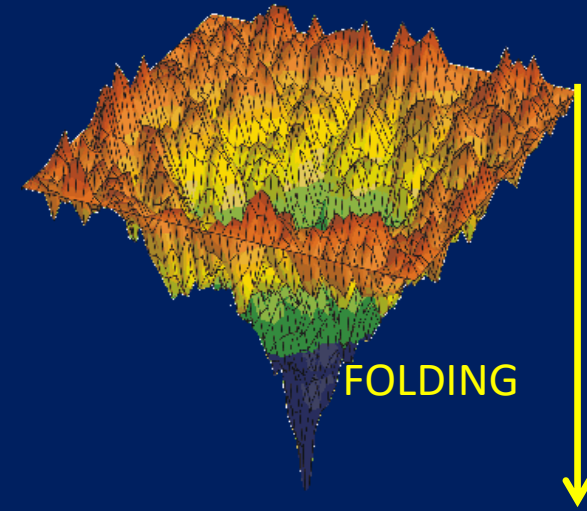
Most proteins are functional only in an aqueous environment. The internal molecular motions in proteins, necessary for biological activity, are very dependent on the degree of plasticizing, which is determined by the level of hydration



The idealized funnel-shaped free energy landscape of proteins. The unfolded state has the highest energy and entropy, while the folded state has the lowest energy and entropy. Folding progresses through multiple pathways; in the extreme, any path that crosses over the rim of the funnel will lead to the minimum

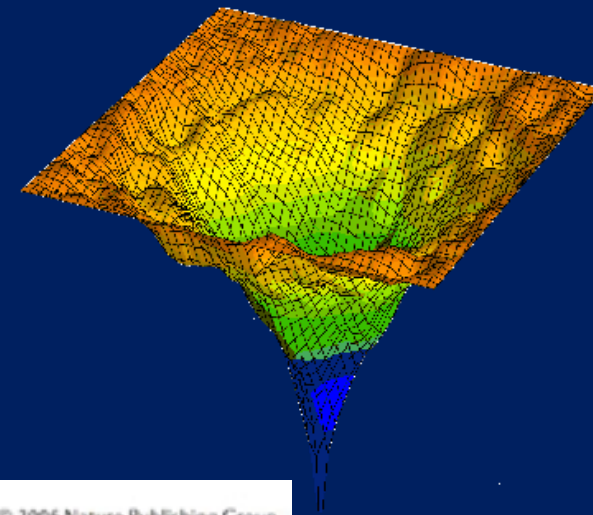
Schematic potential energy funnel for the folding of proteins

Potential energy funnel for the folding of proteins without sufficient water presence.



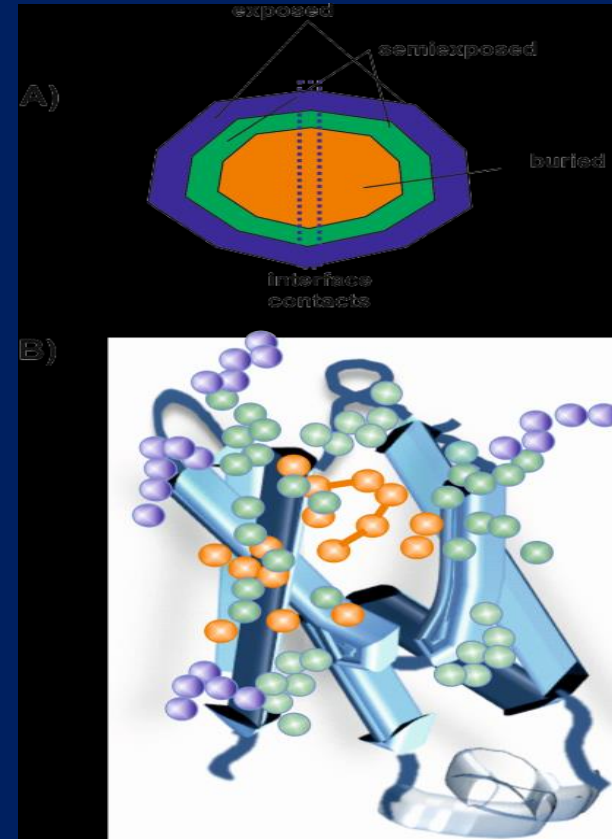
the structural changes due to hydration of the protein

When a protein is fully hydrated, the potential energy landscape is seen to be considerably smoothed. Under conditions of sufficient hydration, this allows proteins to attain their active minimum-energy conformation in a straightforward and rapid manner.



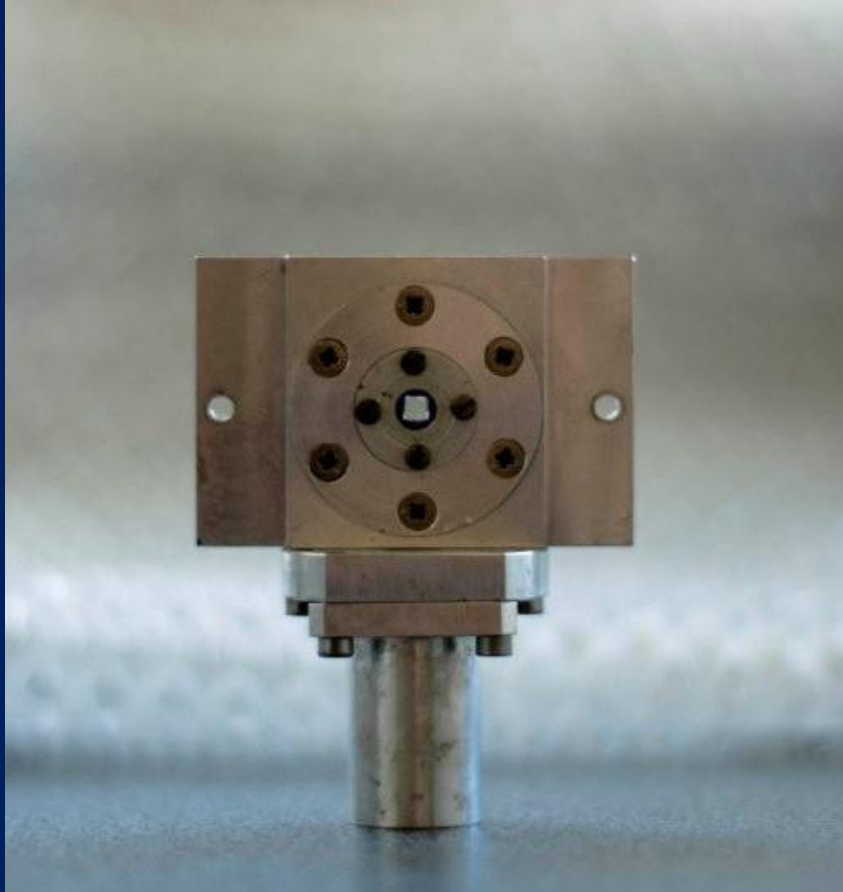
HOW DO PROTEINS FOLD IN THE CELLULAR ENVIRONMENT?

Interactions with the solvent (water) contribute to many aspects of stabilization effects. First of all, as a polar molecule, water interacts with charges on the surfaces of proteins and disfavors exposure of hydrophobic side chains. It is entropically costly to have residues with hydrophobic (nonpolar) side chains on the surface of the protein, which leads to ordering of polar water molecules on the nonpolar surface. Therefore, hydrophobic residues tend to point toward the interior of proteins, stick together and form a “hydrophobic core” while exposing polar or charged residues to the solvent. Hydrophobic interactions are the major driving force for protein folding, and major contributors for protein thermal stability.



The selected conformations at the top illustrate the water expulsion as the folding progresses along the reaction coordinate Q .

HYDRATION OF THE BREAST TISSUE



- **humidity:**
- **0%, 23%, 75%, 100% (H₂O, D₂O)**
- **windows**
- **Si₃N₄ substrate 0.5 μm**
- **BaF₂ substrate 1 mm**
- **Tissue section 6 μm**

0% in P₂O₅

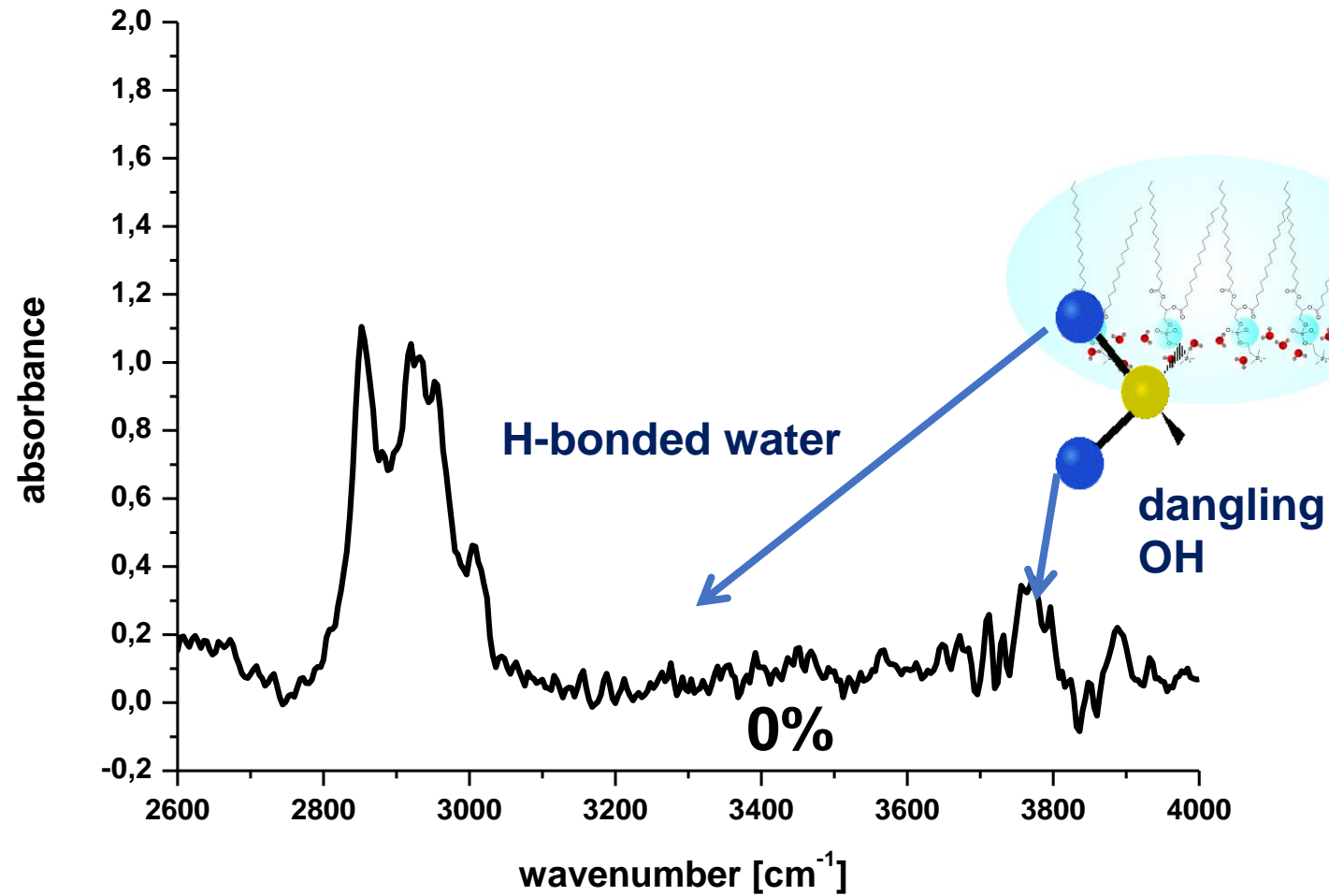
23%

75 % NaCl

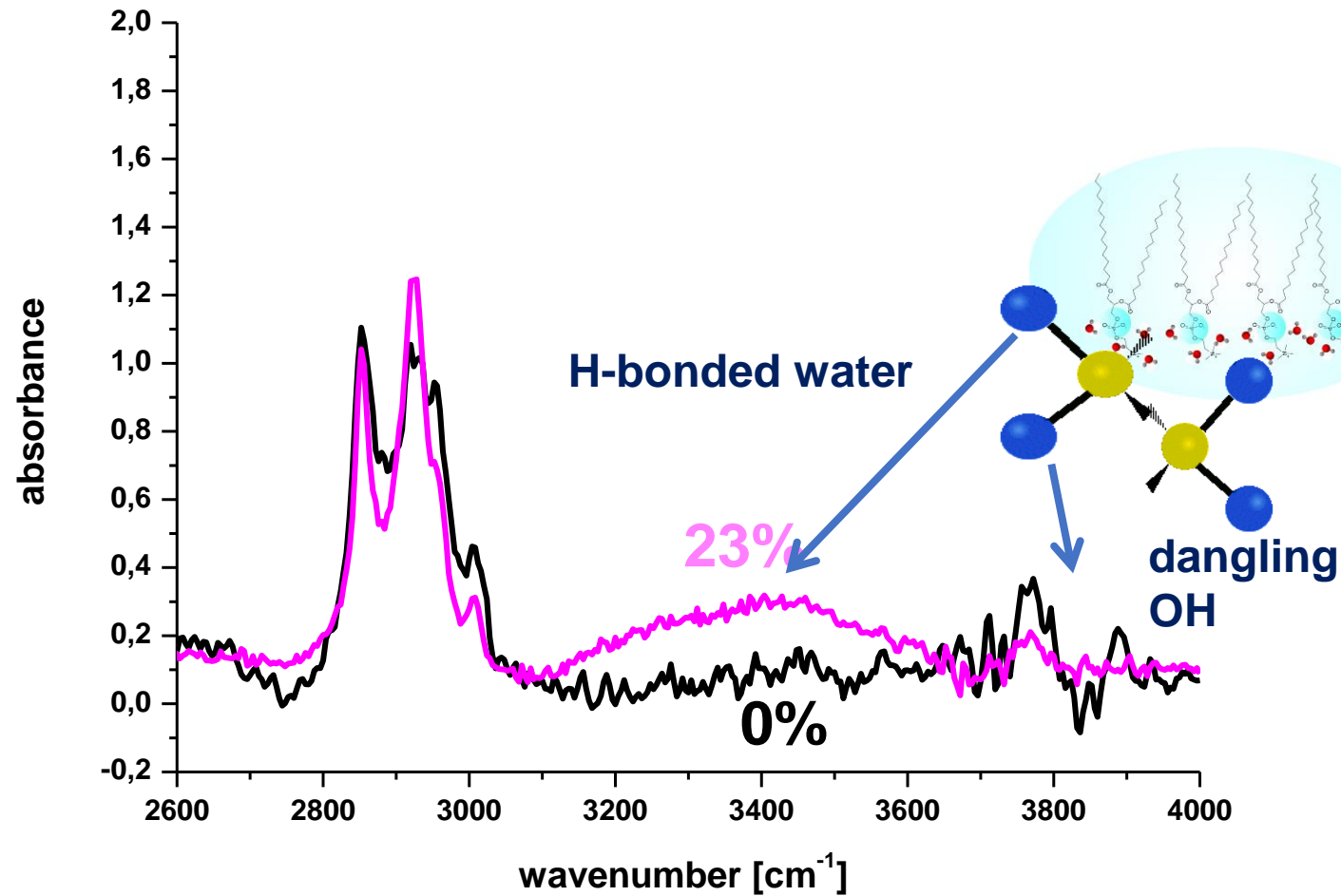
100% H₂O

Jarota, A; Brozek-Pluska, B; Czajkowski, W;
Abramczyk H. J. Phys. Chem. C 2011, 115,
24920–24930

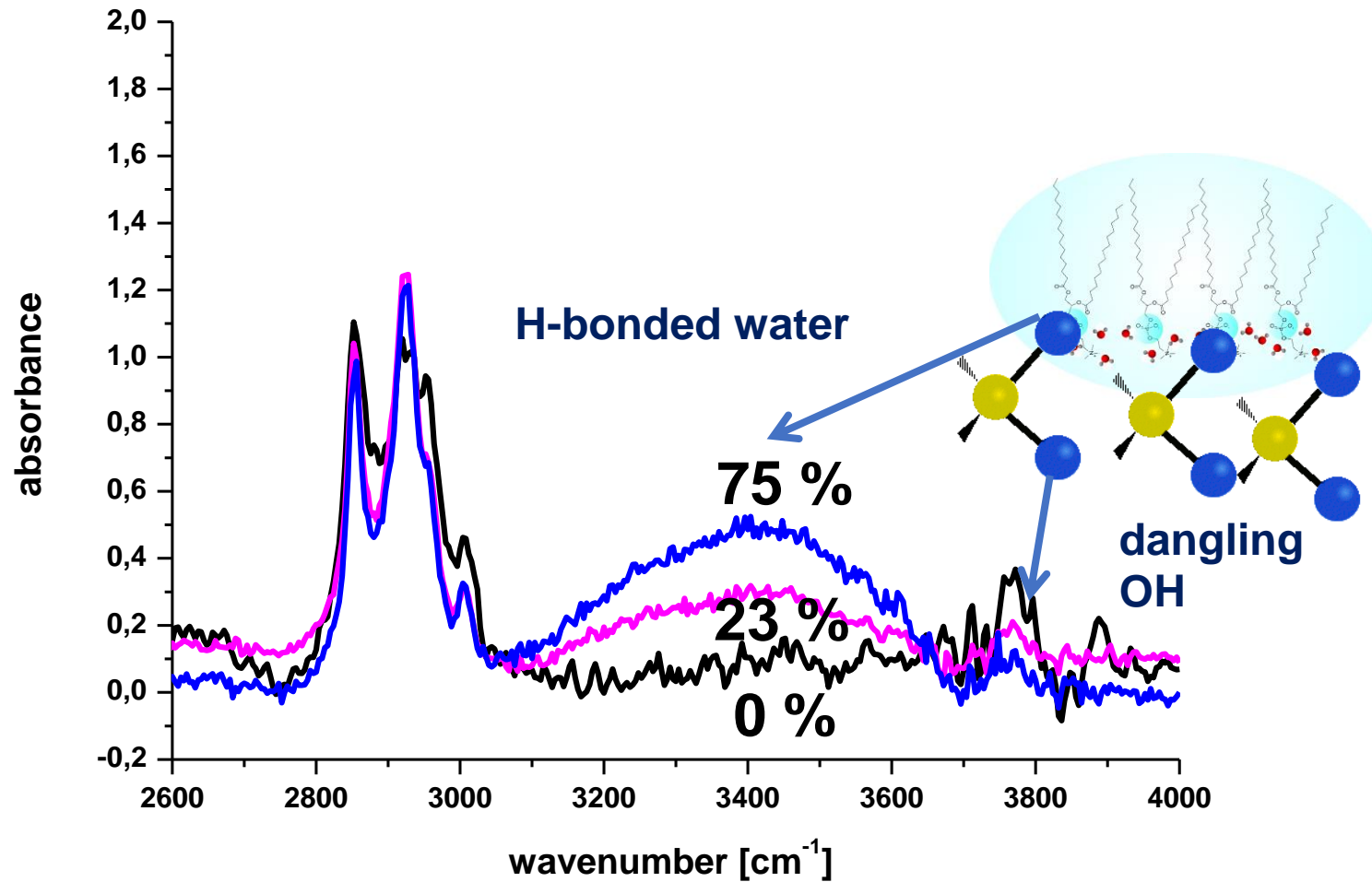
Interfacial water in human breast tissue (normal) (16 μm)



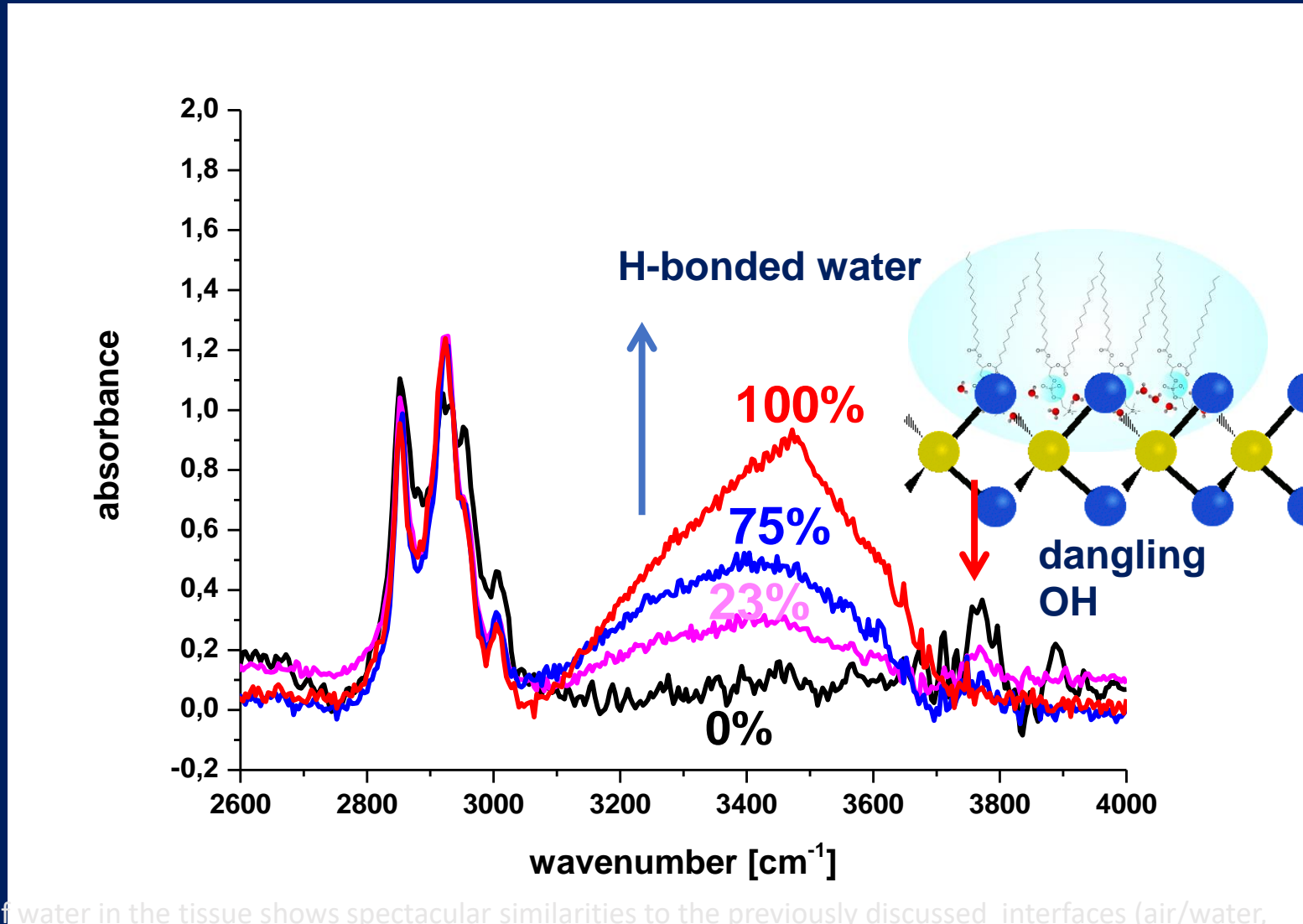
Interfacial water in human breast tissue (normal) (16 μm) (P94)



Interfacial water in human breast tissue (normal) (16 μm) (P94)

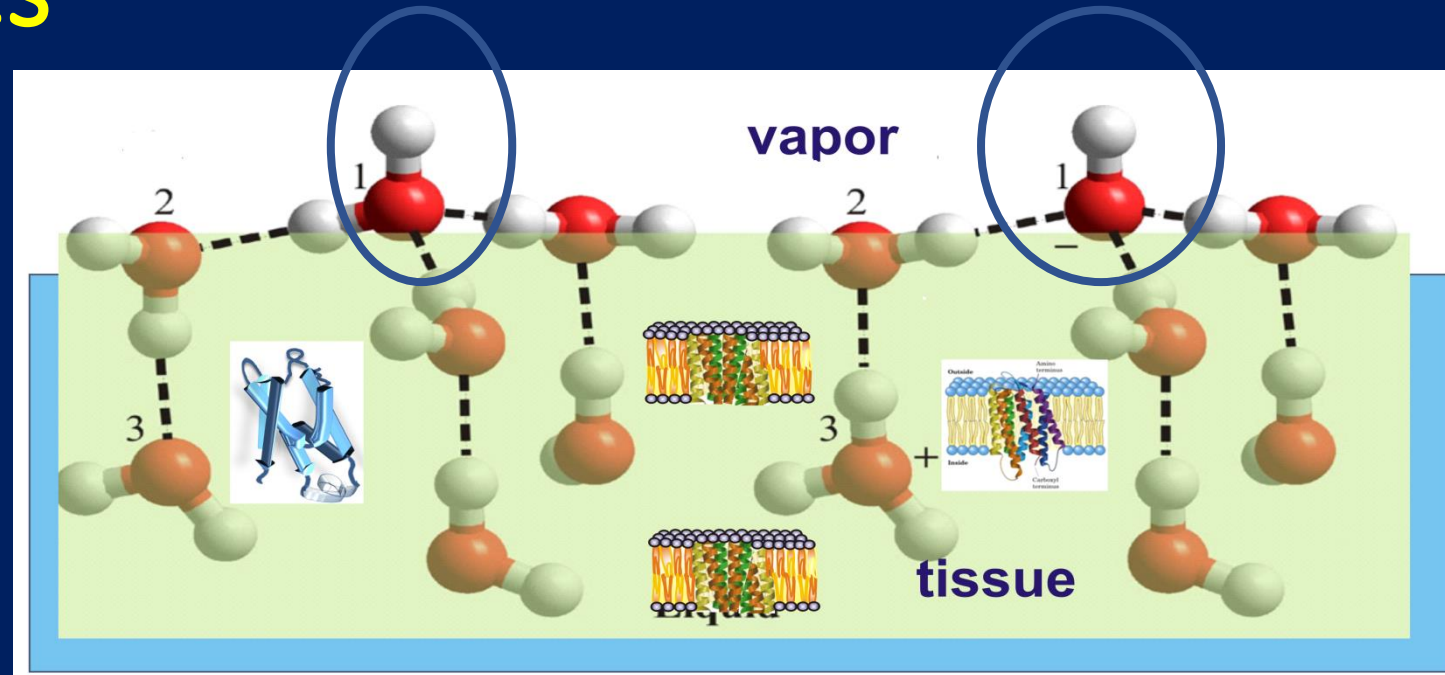


Interfacial water in human breast tissue (normal) (16 μm) (P94)



The spectrum of water in the tissue shows spectacular similarities to the previously discussed interfaces (air/water, hydrophobic liquids/water, water /Langmuir layer)

Conclusion -1- Interactions at biological tissue surfaces



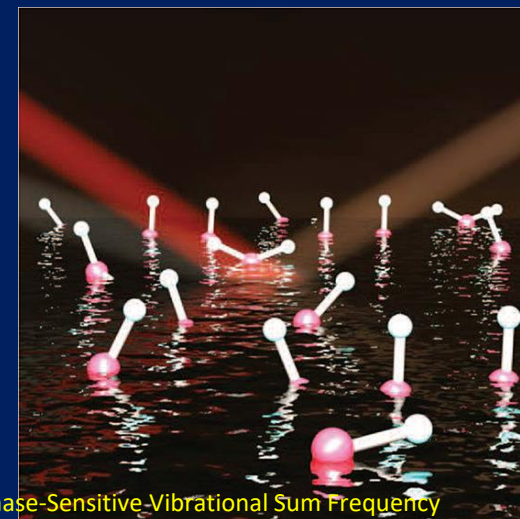
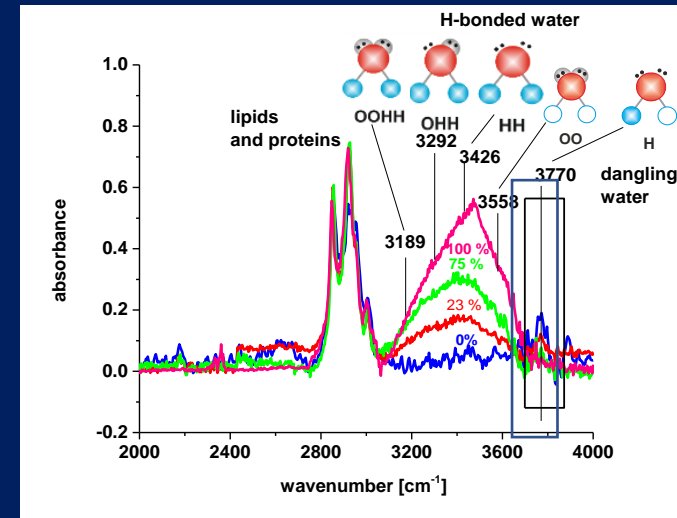
In liquid water and ice , all molecules are part of H-bond 3D networks and nearly all of them are tetra-coordinated. This is not so at surfaces of the biological tissue. In the vicinity of the biological surface, water is not able to maintain its four coordination hydrogen-bonding configuration, but it must sacrifice one of its hydrogen bonds by forming a dangling OH .

The vibrational spectrum of the vapor/ water in cancerous tissue

The vibrational spectrum of the vapor/ water at cancerous tissue interface consists of a very broad band ranging from 3000 to $\sim 3600\text{ cm}^{-1}$ and a narrow band centered at around 3700 cm^{-1} . The broad structure in the region $3000\text{-}3600\text{ cm}^{-1}$ has been attributed to distinct substructures of interfacial O-H groups with weak and strong hydrogen bonds, and have been referred to as “icelike” and “waterlike,” respectively .

The most fascinating feature of the interfacial water has been observed at around 3700 cm^{-1} . This narrow band is typically assigned to the dangling OH stretching of topmost surface water molecules with the OH bond directed towards the hydrophobic phase (vapor and air).

Scatena et al. Science 2009



From Conventional to Phase-Sensitive Vibrational Sum Frequency Generation Spectroscopy: Probing Water Organization at Aqueous Interfaces Dominique Verreault, Wei Hua, and Heather C. Allen

Conventional molecular biology imaging vs Raman imaging

Conventional techniques (e.g. SEM, IHC, H&E, and fluorescence imaging)	Raman spectroscopy-based diagnostics
Destructive	Non-invasive and non-destructive
Requires prior knowledge in order to target molecules	Provides the full range of chemical information in the spectrum
Laborious preparation procedures	Minimal preparation required can be directly applied to living cells and animals
Protocol optimization –often time consuming	Measurement condition is easy and quick to optimize
Fixation often required, not suitable for live cells	Living cells –can be analyzed without causing damage to the cells
Labelling required possibility of creating artefacts	Label free
Not suitable for heterogeneous samples conventional methods often required a large number of pure samples for characterization	Can be performed on individual samples or get information <i>in situ</i> (without moving it to some special medium)
High sensitivity(concentration) but lower specificity (molecular features)	Lower sensitivity but higher specificity

Conventional diagnostics methods vs Raman spectroscopy-based diagnostics

Conventional techniques in histology, cytology and molecular biology (H&E, IHC, qPCR, mass spectroscopy)	Raman spectroscopy-based diagnostics
Destructive	Non-invasive and non-destructive
Requires prior knowledge in order to target molecules	Provides the full range of chemical information in the spectrum
Sample processing can take hours to days (e.g. DNA preparation, PCR and western blots runs)	Minimal to no sample processing is required
Protocol optimisation – often time consuming (e.g. western blots and PCR)	Measurement condition is easy to optimise. Rapid measurement can be enabled
Loss of spatial information (e.g. PCR and mass spectroscopy)	Retains spatial information High spatial resolution (sub-micrometre)
Labelling required (e.g. PCR and western blots) possibility of creating artefacts and costly (time, reagents and labour)	Label free

qPCR
Quantitative
reverse
transcription

Conventional-omics molecular techniques vs Raman spectroscopy-based-omics

Conventional techniques (DNA microarray, sequencing, mass-spectroscopy, PCR, immunoprecipitation, western blotting)	Raman spectroscopy and imaging
Destructive (e.g. qPCR and mass spectroscopy)	Non-invasive and non-destructive
Requires prior knowledge in order to target molecules (e.g. IHC and qPCR)	Provides the full range of chemical information in the spectrum
Sample processing can take days to weeks (e.g. tissue sectioning and staining, microbiology cultures)	Minimal to no sample processing is required and therefore is faster and cheaper to perform -> quicker patient diagnosis and less cost to hospital
Protocol optimisation –often time consuming(e.g. IHC and qPCR)	Measurement condition is easy and quick to optimise
Loss of spatial information (e.g. qPCR and mass spectroscopy)	Retains spatial information High spatial resolution (sub-micrometre)
Fixation often required not suitable for live cells	Living cells –can be analysed without causing damage to the cells
Labelling required (e.g. IHC and qPCR) possibility of creating artefacts and costly (time, reagents and labour)	Label free

HOW DOES RAMAN SPECTROSCOPY AND IMAGING BENEFIT CANCER RESEARCH?

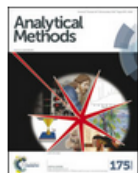
- **EPIGENETIC MODIFICATIONS**

Reprogrammed metabolic pathways that are essential for cancer cell survival and growth affect epigenetics.

EPIGENETICS BY RAMAN IMAGING

- We developed a novel Raman based alternative for currently existing epigenetics research approaches. The proposed Raman approach can 'upgrade' cancer epigenetic tests and answer many of the biochemical questions of cancer

Issue 48, 2016



From the journal:
[Analytical Methods](#)

2016

Development of a new diagnostic Raman method for monitoring epigenetic modifications in the cancer cells of human breast tissue

[Beata Brozek-Pluska](#)^a [Monika Kopeć](#)^a and [Halina Abramczyk](#)^{*a}

Previous Article

Issue 19, 2016



From the journal:
[Analyst](#)

2016

Epigenetic changes in cancer by Raman imaging, fluorescence imaging, AFM and scanning near-field optical microscopy (SNOM). Acetylation in normal and human cancer breast cells MCF10A, MCF7 and MDA-MB-231

[Halina Abramczyk](#)^{*a} [Jakub Surmacki](#)^a [Monika Kopeć](#)^a [Alicja Klaudia Olejnik](#)^b [Agnieszka Kaufman-Szymczyk](#)^c and [Krystyna Fabianowska-Majewska](#)^c

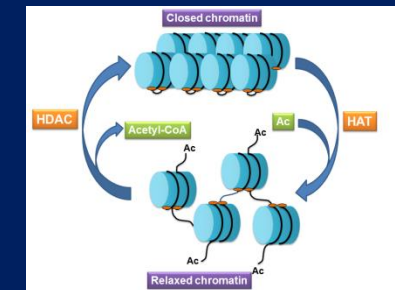
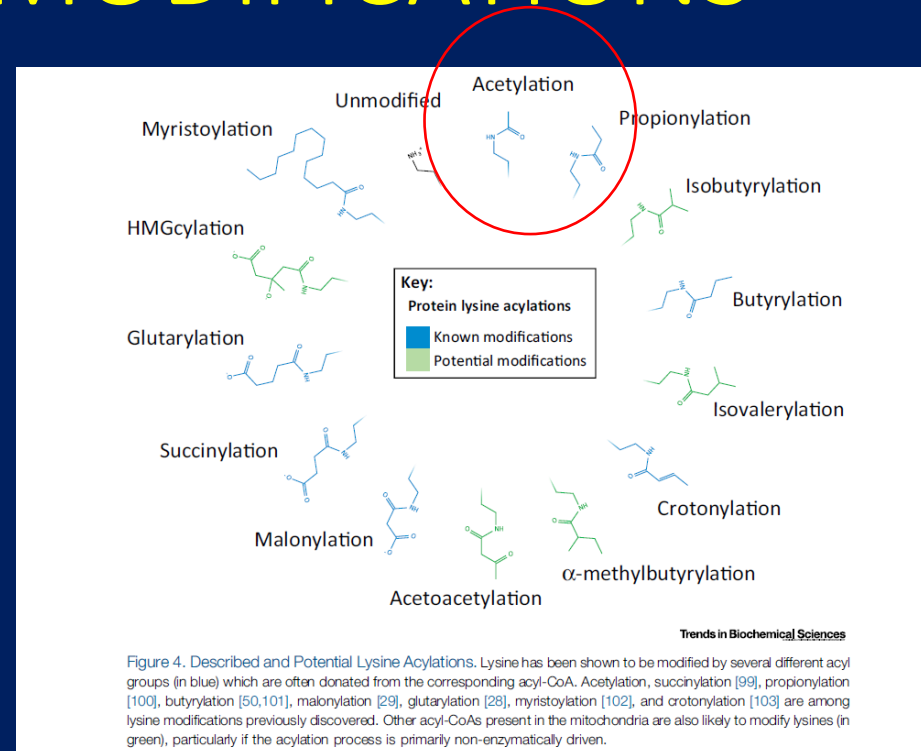
Previous Article

Next Article

Raman Single cell analysis: The new frontier in 'omics

- A combination of immunohistopathology and gene profile approaches are considered as gold standards to identify many cancer subtypes. Diagnostic approaches have limitations, such as, false positives, time delays, pain and trauma of patients, encouraging researchers to explore new non-invasive, reagent-free and less painful methodologies. Raman spectroscopy (RS), a vibrational spectroscopic technique, not only provides real time biochemical profile of tissues but also understanding of the disease as it progresses.

EPIGENETIC MODIFICATIONS



Now is just the beginning of our understanding of epigenetic factors involved in development of cancer diseases, but it has become evident that cancer cells have many epigenetic differences compared to normal cells in the same patient. The list of all possible epigenetic modifications is not yet complete, but it is obvious that in the future the manipulation of the epigenetic landscape will become a key element of cancer therapy. We have concentrated on Lysine acetylation and methylation because they are involved in diverse cellular processes, such as chromatin remodeling.

EPIGENETICS BY RAMAN IMAGING

2017

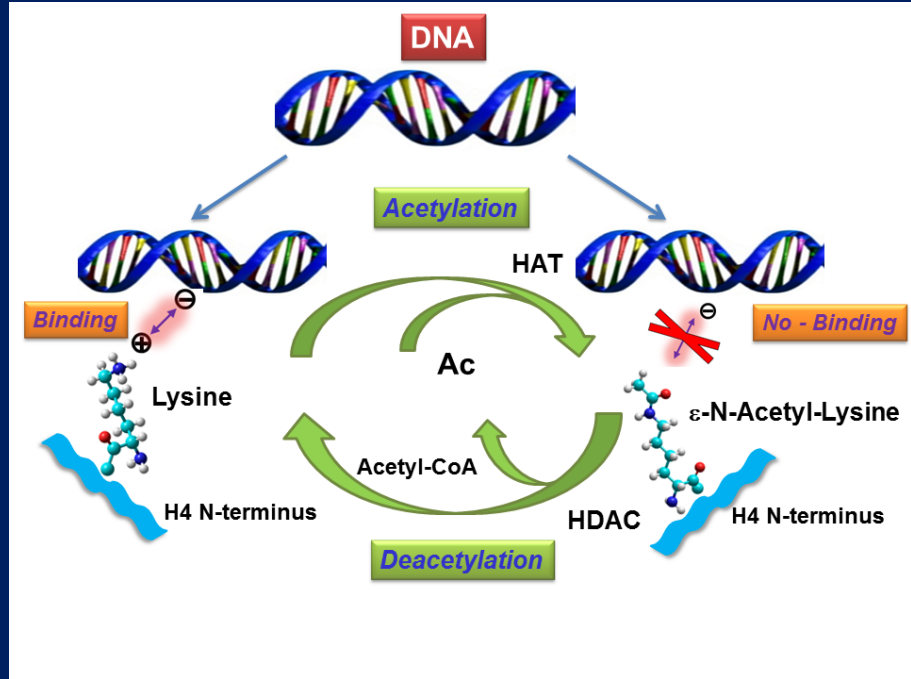
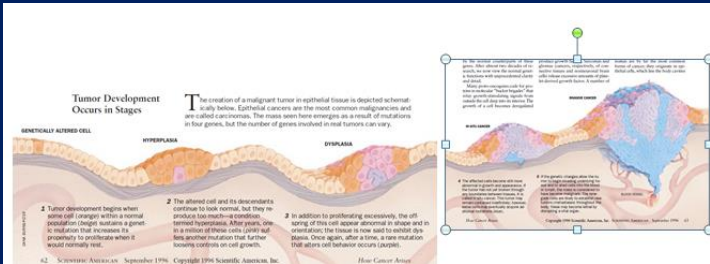
Issue 48, 2016

Analytical Methods

From the journal:
Analytical Methods

Development of a new diagnostic Raman method for monitoring epigenetic modifications in the cancer cells of human breast tissue

Beata Brozek-Pluska,^a Monika Kopeć^a and Halina Abramczyk^{*a}

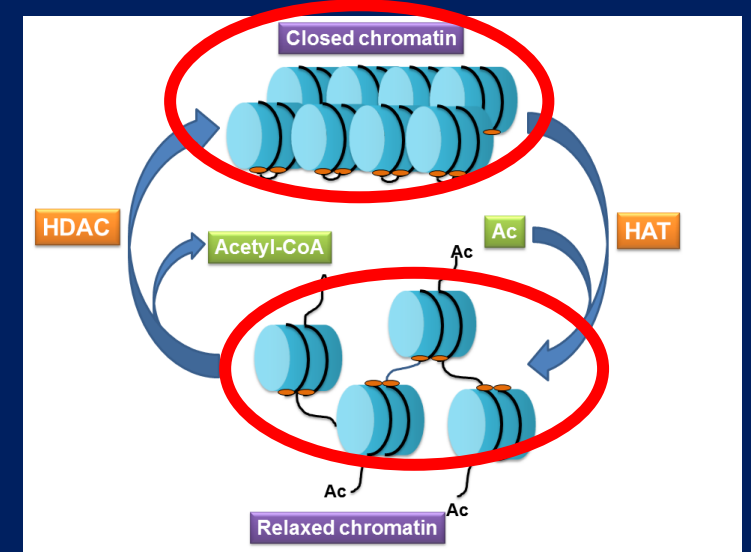
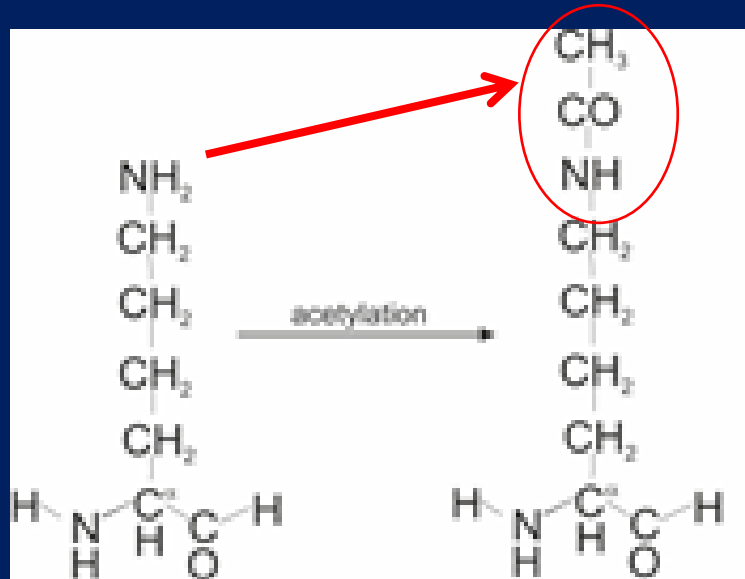
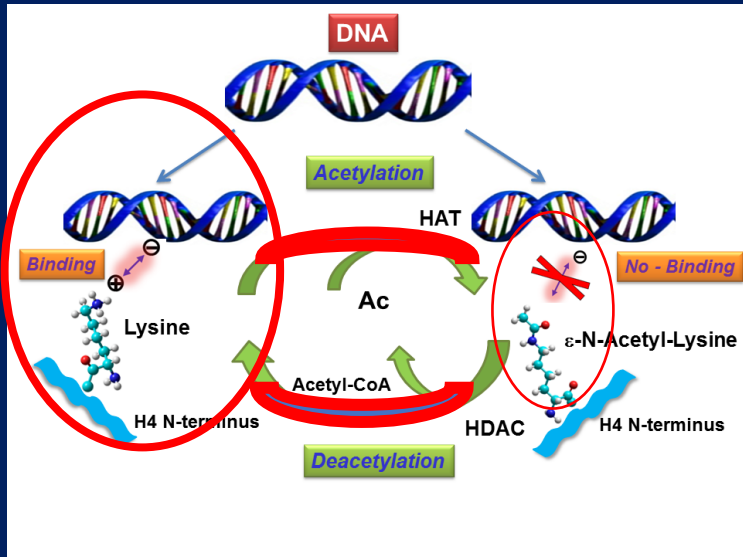


For many years it was thought that cancer is a genetic disease in which changes in the sequence of certain genes, oncogenes and tumor suppressors cause the disease. In recent years it has become evident, however that changes in cancer are also based on the epigenetic factors such as DNA methylation and histone acetylation, phosphorylation that modify transcriptional and posttranslational potential of the cell.

Acetylation

- Acetylation has the effect of changing the overall charge of the histone tail from positive to neutral. Nucleosome formation is dependent on the positive charges of the H4 histones and the negative charge on the surface of H2A histone fold domains. Acetylation of the histone tails disrupts this association, leading to weaker binding of the nucleosomal components.^[4] By doing this, the DNA is more accessible and leads to more transcription factors being able to reach the DNA. Thus, acetylation of histones is known to increase the expression of genes through transcription activation. Deacetylation performed by HDAC molecules has the opposite effect. By deacetylating the histone tails, the DNA becomes more tightly wrapped around the histone cores, making it harder for transcription factors to bind to the DNA. This leads to decreased levels of gene expression and is known as gene silencing.^{[5][6][7]}
- · · de Ruijter, AJ; van Gennip, AH; Caron, HN; Kemp, S; van Kuilenburg, AB (Mar 15, 2003). "Histone deacetylases (HDACs): characterization of the classical HDAC family.". *The Biochemical journal* **370** (Pt 3): 737–49. doi:[10.1042/BJ20021321](https://doi.org/10.1042/BJ20021321). PMC [1223209](https://pubmed.ncbi.nlm.nih.gov/1223209/). PMID [12429021](https://pubmed.ncbi.nlm.nih.gov/12429021/). Retrieved 8 April 2014.
- · · Gallinari, P; Di Marco, S; Jones, P; Pallaoro, M; Steinkühler, C (Mar 2007). "HDACs, histone deacetylation and gene transcription: from molecular biology to cancer therapeutics.". *Cell research* **17** (3): 195–211. doi:[10.1038/sj.cr.7310149](https://doi.org/10.1038/sj.cr.7310149). PMID [17325692](https://pubmed.ncbi.nlm.nih.gov/17325692/).
- · Struhl, Kevin (1998). "Histone acetylation and transcriptional regulatory mechanisms" (PDF). *Genes & Dev.* **12** (5): 599–606. doi:[10.1101/gad.12.5.599](https://doi.org/10.1101/gad.12.5.599). Retrieved 7 August 2012.

EPIGENETICS BY RAMAN IMAGING



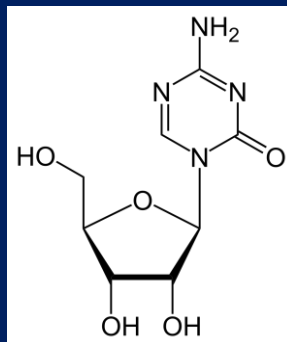
Here we can see interaction between DNA and histone protein via lysine residue. Briefly, mechanism of acetylation and deacetylation presented in Fig. 1 is maintained by opposing activities of histone acetyltransferases (HAT) and deacetylases (HDAC). The acetylation transfers an acetyl group from acetyl CoA to form ε-N-acetyl lysine. The acetylation mechanism induced by HAT is particularly important in post translational alterations of histone proteins, because the positive charge of the histone tail can be changed to neutral by acetylation. Ultimately, such a modification leads to weaker binding via electrostatic forces between the histone proteins and DNA of the nucleosome components that results in structure alteration of chromatin (less compact euchromatin) and affects the expression of genes making them more active. The opposite effect is due to the HDAC, which removes the acetyl groups from the lysine residues, making the DNA more tightly wrapped around the histone cores (and resulting in a repression of gene activity known as a gene silencing). These opposite effects of HAT/HDAC on chromatin structure are presented in Fig. 2.

Chromatin remodeling plays an important role in the regulation of expression of certain genes

- Chromatin remodeling also plays an important role in the regulation of expression of certain genes. The basic unit of chromatin is the nucleosome, which consists of 146 bp of DNA wrapped around a histone octamer. Modification of the N-terminal group of lysine in histones by acetylation or deacetylation changes the configuration of nucleosomes. The positive charge on unacetylated lysines in the histones is attracted to the negatively charged DNA producing a compact chromatin state that is repressive for transcription. On the other hand, acetylation of the lysines by histone acetylase removes their positive charge and results in an open chromatin structure, which facilitates gene transcription. HDAC removes the acetyl groups from lysine, which reverses this process and silences gene expression (**Fig. 2**). Aberrant deacetylation of histones in nucleosomes is probably a result of a dysregulation of the specificity of HDAC and may be associated with neoplastic transformation. For example, gene translocations in some types of leukemia can generate fusion proteins that recruit HDAC and bind to promoters to silence genes involved in differentiation (**46**).

Histone Methylation

- In addition to acetylation of H3 and H4 tails, methylation in lysine residues (Lys4 and Lys9) of histone 3 occur. The methylation of lysine in histones by specific histone methylases is also implicated in changes in chromatin structure and gene regulation. The methylation of lysine-4 in histone-3 is associated with an open chromatin configuration and gene expression. On the other hand, the methylation of lysine-9 in histone-3 is associated with condensed and repressive chromatin. This histone modification and the acetylation/deacetylation of histones to influence gene expression are called the histone code. A hypermethylated promoter is surrounded by methylated lysine-9 in histone-3, whereas an unmethylated promoter is surrounded by methylated lysine-4 in histone-3. Treatment of tumor cells with 5-AZA reduces the level of methylated lysine-9 in histone-3 and increases the level of methylated lysine-4 in histone-3 in the promoter region of genes silenced by aberrant DNA methylation.



Azacitidine

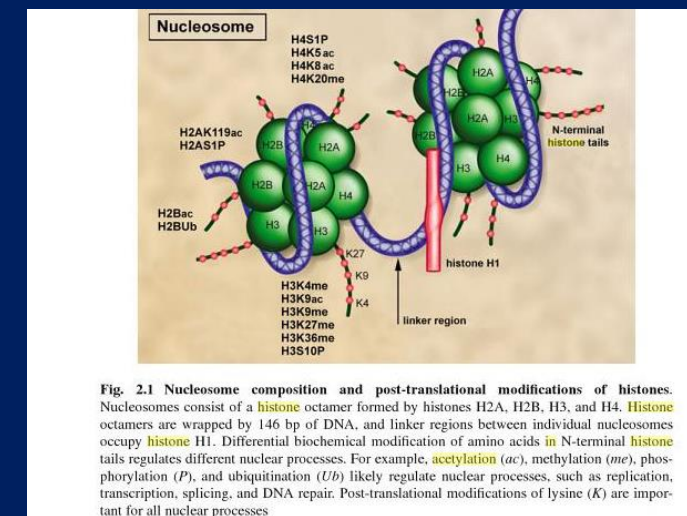
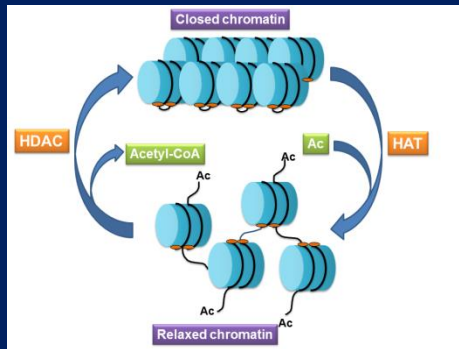
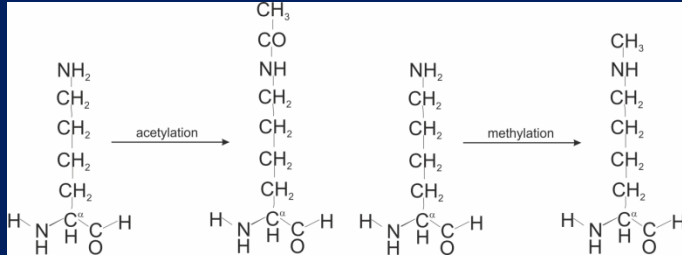
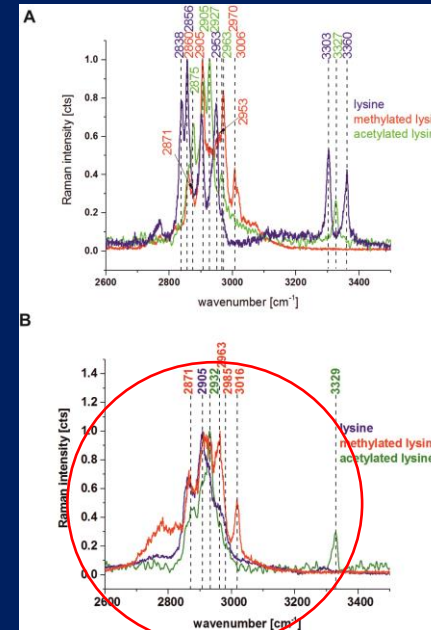


Fig. 2.1 Nucleosome composition and post-translational modifications of histones. Nucleosomes consist of a **histone** octamer formed by histones H2A, H2B, H3, and H4. **Histone** octamers are wrapped by 146 bp of DNA, and linker regions between individual nucleosomes occupy **histone** H1. Differential biochemical modification of amino acids in N-terminal **histone** tails regulates different nuclear processes. For example, **acetylation** (*ac*), **methylation** (*me*), **phosphorylation** (*P*), and **ubiquitination** (*Ub*) likely regulate nuclear processes, such as replication, transcription, splicing, and DNA repair. Post-translational modifications of lysine (*K*) are important for all nuclear processes

EPIGENETICS BY RAMAN IMAGING



Histone acetylation/deacetylation by HAT and HDAC enzymes alters chromatin structure by decreasing/increasing accessibility of exposed sites on DNA to silencing/activating gene transcription.



Raman spectrum of lysine, acetylated lysine and methylated lysine, solid crystalline powder (A), Raman spectrum of lysine, acetylated lysine and methylated lysine amorphous phase evaporated from aqueous solution $c=10^{-2}$ M (B).

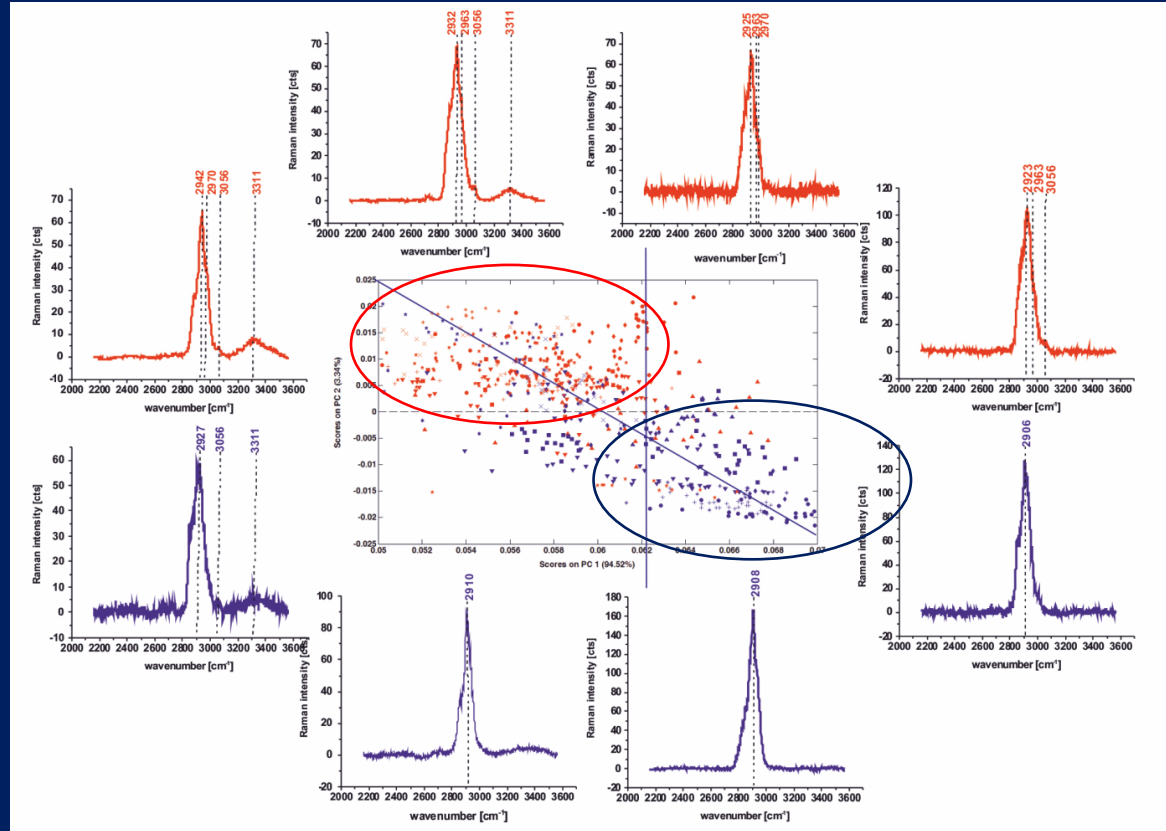
Raman spectroscopy and Raman imaging have strong diagnostic potential for monitoring acetylation and methylation processes in cancer cells of human breast tissues. We will show that Raman spectroscopy and Raman imaging can detect the relative amounts of acetylated and methylated lysine by monitoring the vibrations of the acetyl and methyl chemical functional groups. In comparison to existing tests and assays, Raman-based methods represent a powerful alternative that allows non-invasively detect cellular acetylation and methylation processes that are not limited to only those events that are sensitive to a specific antibody.

epigenetics in breast cancer

- Over the past few years there has been an explosion in studies of epigenetics in breast cancer, reflected by the exponential increase of published manuscripts . A PubMed search for the keywords 'epigenetic' and 'breast cancer' reveals that the first publication was in 1983. Progress was slow until approximately 10 years ago when the number of studies started to steadily increase, at least in part fueled by improved technologies. In the present review, we focus on recent advances in the understanding of histone methylation and demethylation, a relatively new area with promise for clinical translation. We also review recent studies that have utilized genomewide technologies for the study of DNA methylation. Much progress has been made in the characterization of noncoding RNAs, and the effect of higher order chromatin structure on gene expression in
- breast cancer.

EPIGENETICS BY RAMAN IMAGING

In order to visualize chemical similarities and differences in level of acetylation and methylation in cancerous and normal tissues we have evaluated the predictive validity and potential of Raman spectroscopy by using multivariate statistical methods for data interpretation.

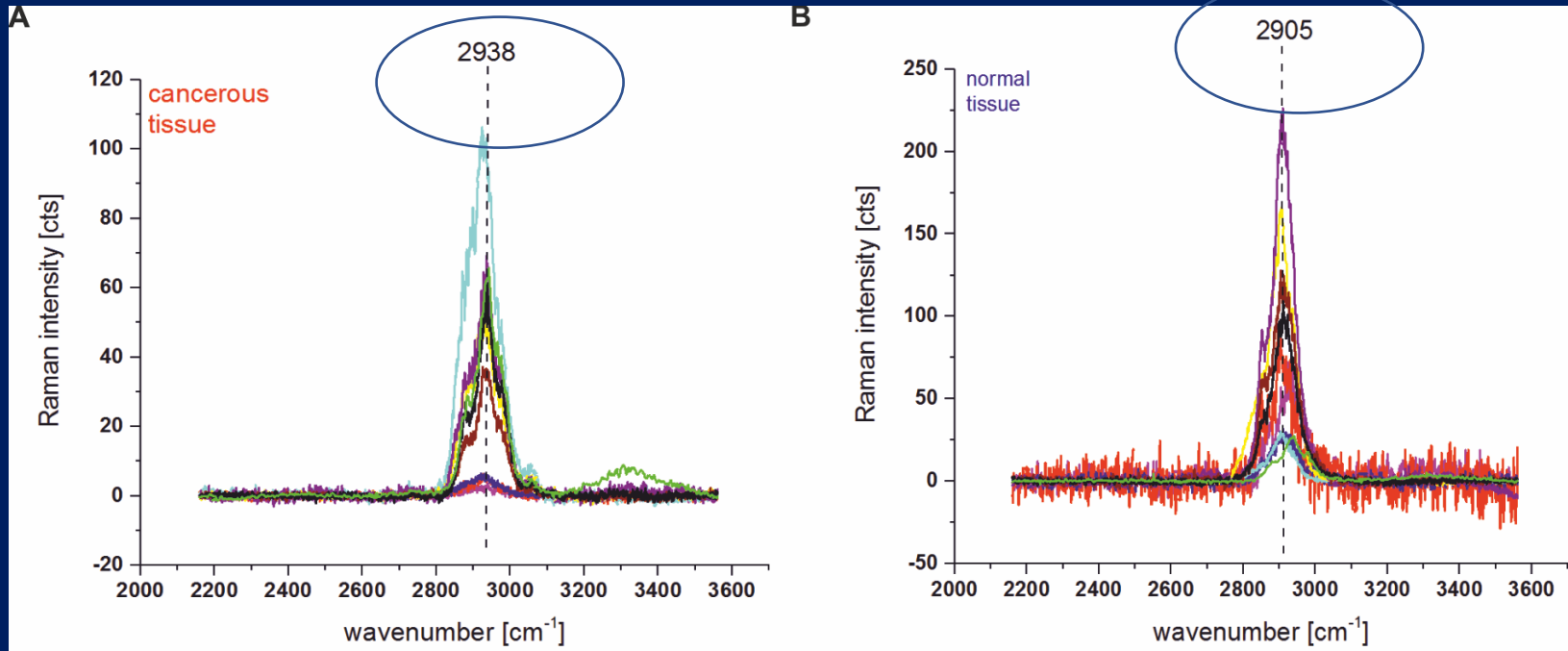


The results of the PCA reveal separation of the cancer and normal tissues. The similarities and differences are clearly visible by grouping the Raman spectra in two separate clusters, where the spectra with similar or identical vibrational properties for the samples from the tumor mass (red points) are grouped in the upper area while the samples from the safety margin (blue points) are grouped in the lower area of the plot.

PCA score plot (model: area normalized to 1) for the Raman spectra from the region (2000 cm⁻¹ -3700 cm⁻¹) of the human breast tissue samples from the tumor mass (red points) and the safety margin (blue points), integration time 0.5 s, laser power 10 mW;

The characteristic spectra corresponding to the various coordinates of the PC1-PC2 score plot.

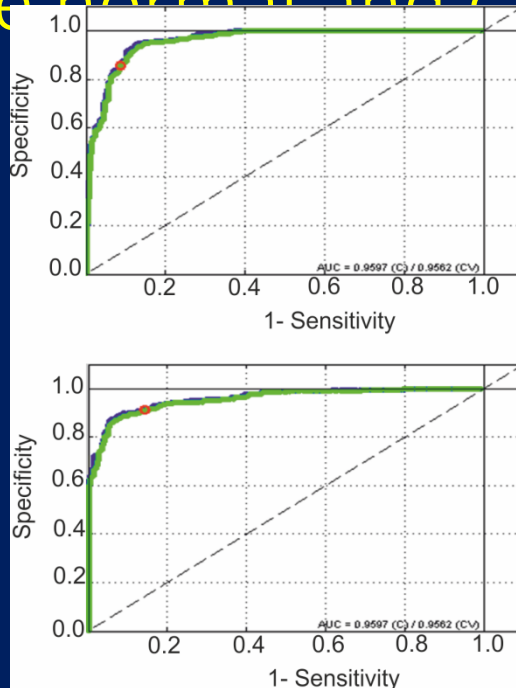
EPIGENETICS BY RAMAN IMAGING



In the view of the results presented so far one can provide strong evidence that the global acetylation level of histone and non-histone proteins increases in human breast cancer cells.

One can see that the samples of the cancerous tissue from the tumor mass have the Raman peak frequency at 2938 cm⁻¹ correlating quite well with the Raman peak position of acetylated lysine. The samples of normal tissue from the safety margin have the Raman peak frequency at 2905 cm⁻¹ corresponding to the vibrations of non-methylated/non-acetylated proteins (CH₂ symmetric stretching vibration).

Bimodal ROC (Receiver operating characteristic) curves graph for the normal and cancerous human samples



To further evaluate and compare the performance of the PCA and PLSDA based diagnostic algorithm for breast cancer diagnosis, the receiver operating characteristic (ROC) analysis was performed.

Fig. 10 shows a bimodal ROC (Receiver operating characteristic) curves graph for the normal and cancerous human samples. The sensitivity and specificity obtained directly from the ROC curve are 0.861 and 0.913, respectively. The ROC curve in Fig. 10 illustrates the ability of Raman spectroscopy to separate enhanced methylation/acetylation of proteins occurring in cancerous breast tissue. A simulated ROC curve of two indistinguishable populations is included for comparison.

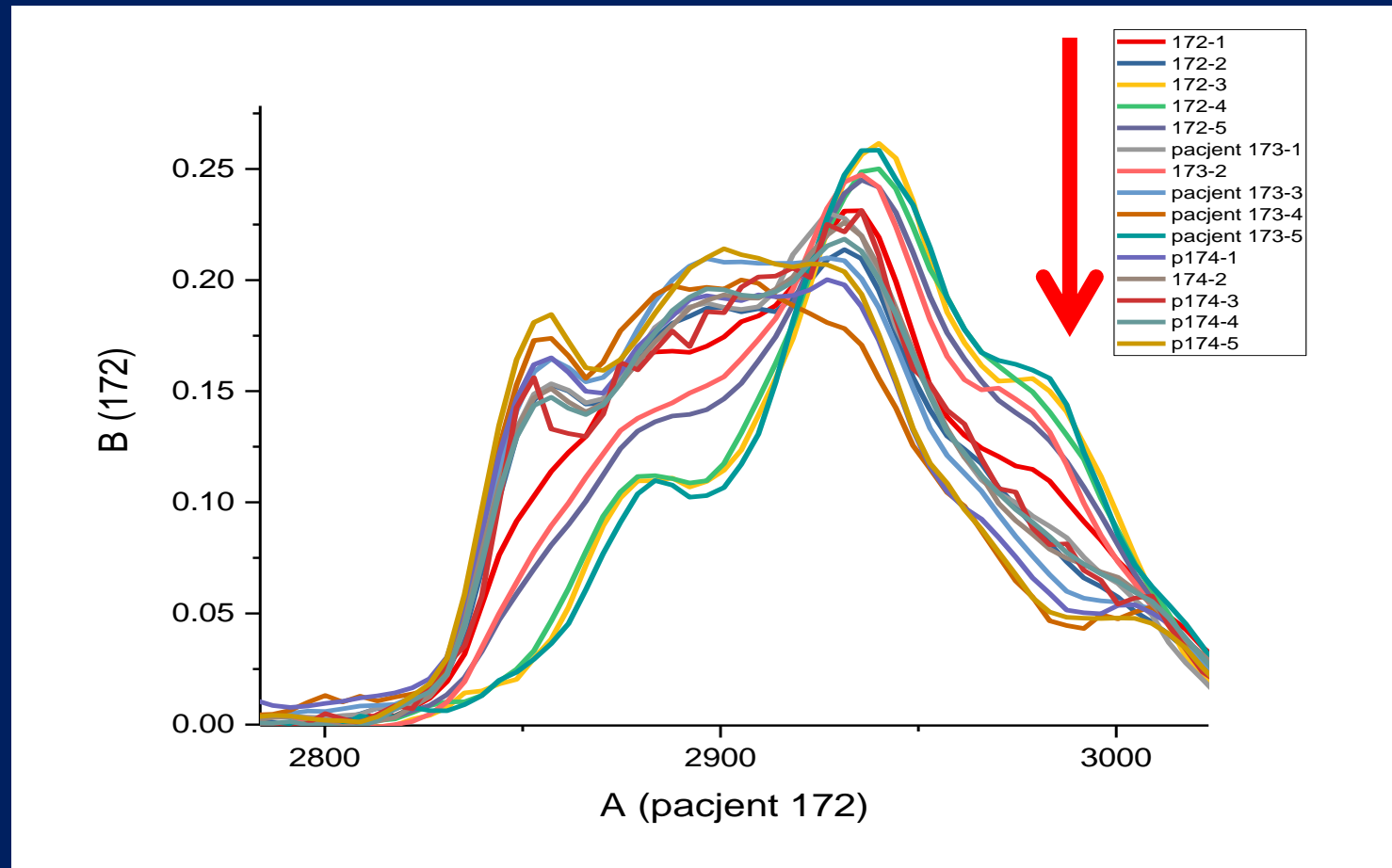
Although PCA method is useful for visualization of data trends, it cannot be used as Supervised Learning classification method, where the previous knowledge of the samples under study must be known. In our case the class membership of every sample is a priori known from a 'gold standard' method of histopathology performed by the certified doctors.

We used supervised learning algorithm PLSDA to calculate the sensitivity .

The sensitivity and specificity obtained directly from PLSDA and cross validation for a chosen model gives a sensitivity and specificity of 86.1% and 91.3% for calibration and 85.3% and 91.3% for cross-validation, respectively.

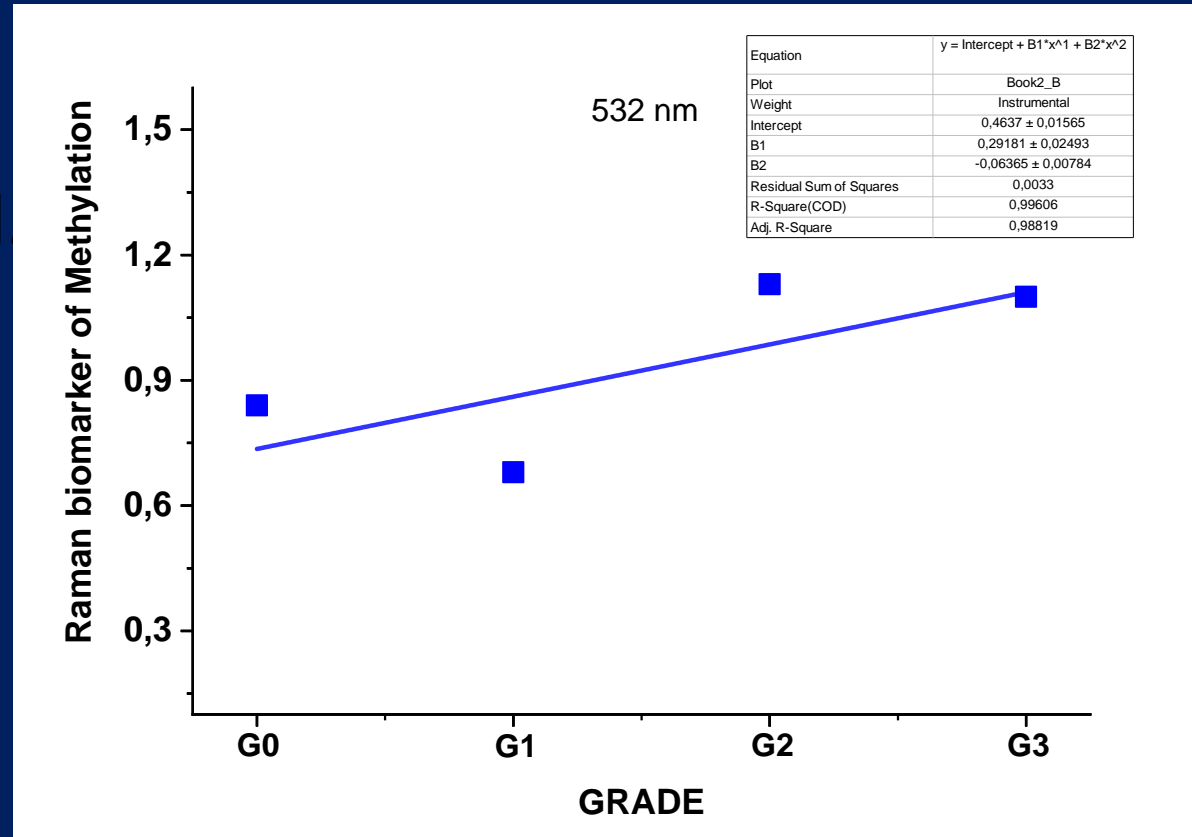
BREAST Ductal cancer , grade 2

METHYLATION



LEVEL OF METHYLATION VS BREAST CANCER GRADE

- Abramczyk et al
- 2019



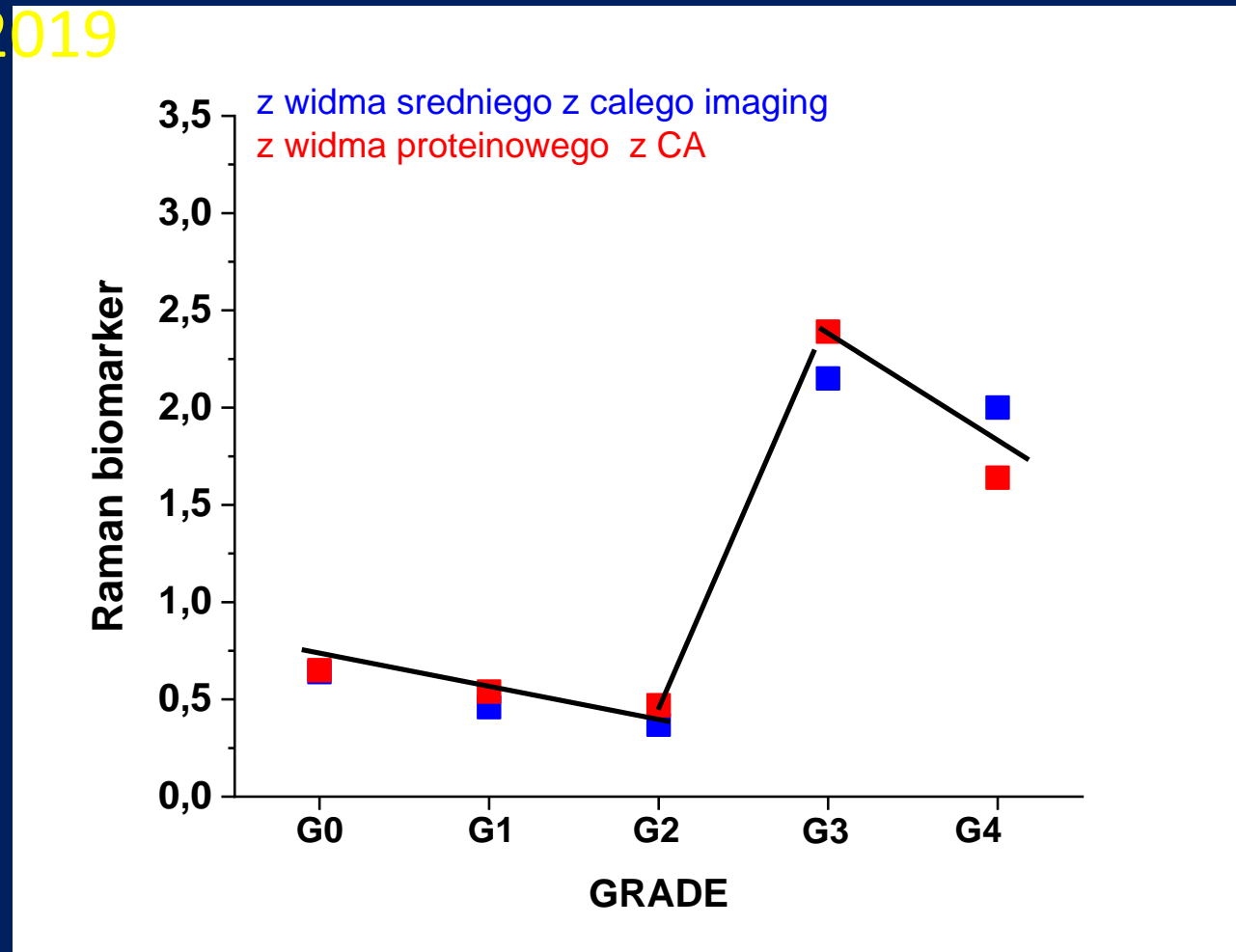
The global methylation level of DNA and histone and non-histone proteins increases in human breast cancer cells.

LEVEL OF PHOSPHORYLATION VS BRAIN TUMOR GRADE

- Abramczyk et. al. 2019

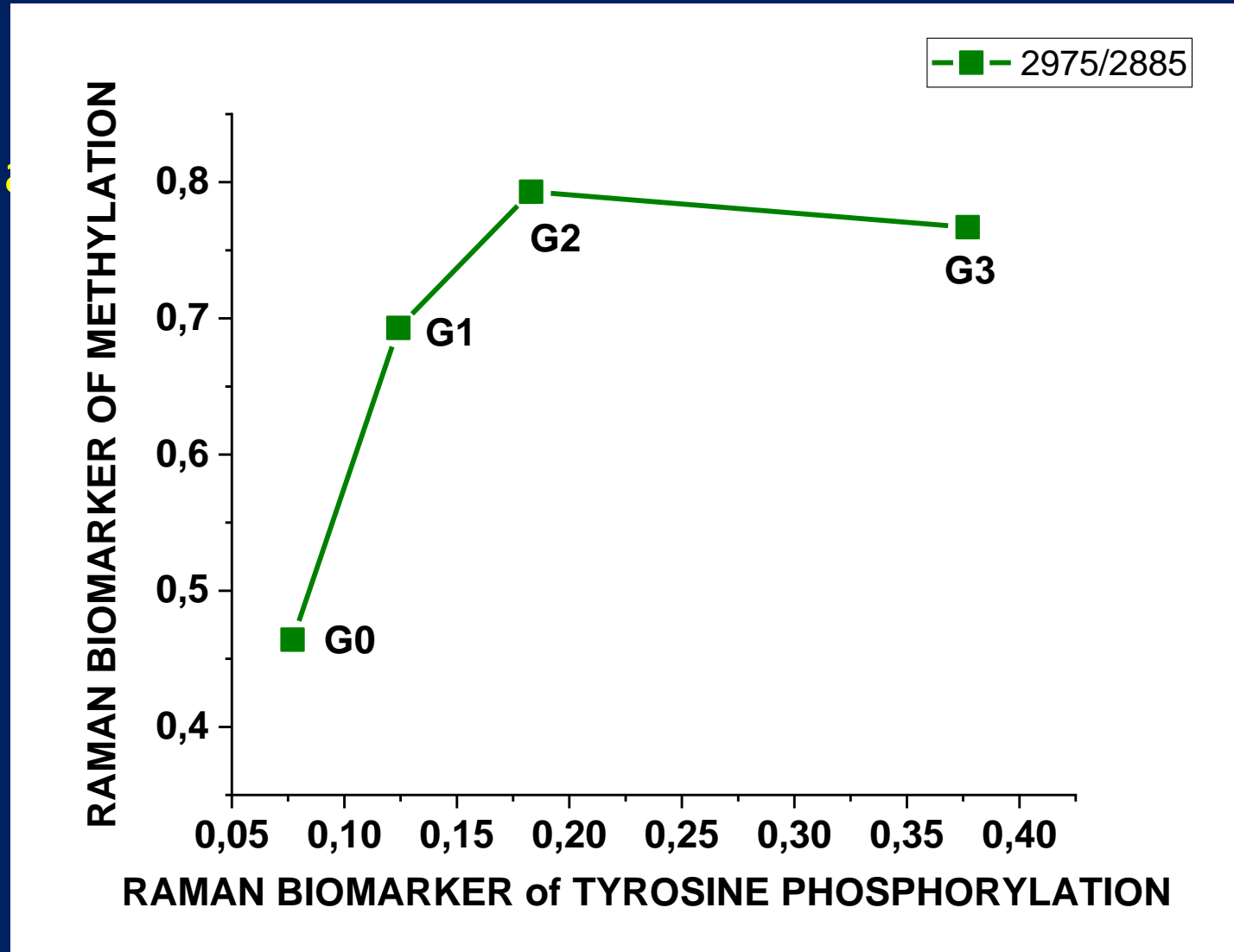
2018

The global protein phosphorylation level increases in human brain cancer cells.

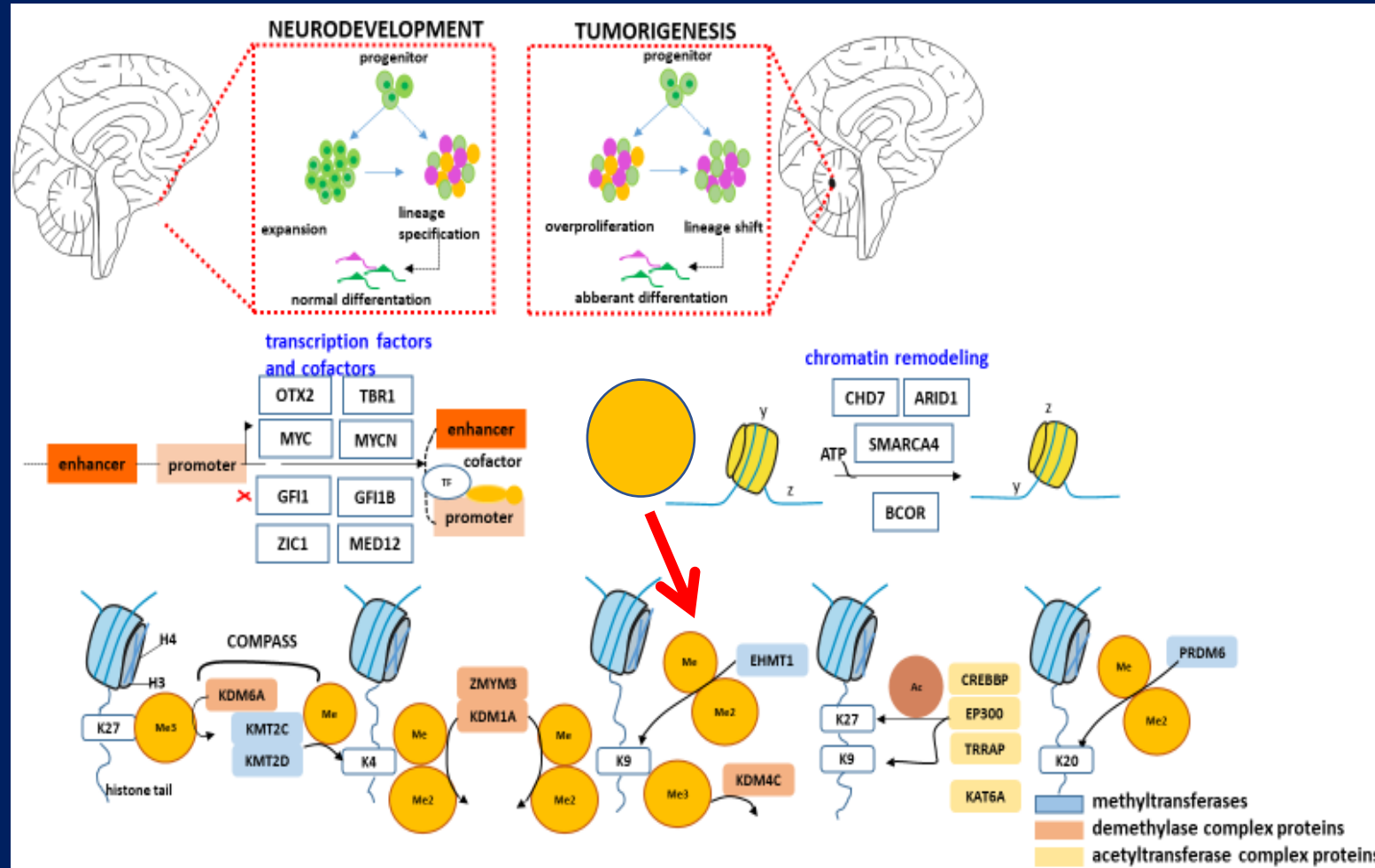


2D PLOT RAMAN BIOMARKER OF METHYLATION –RAMAN BIOMARKER OF TYROSINE PHOSPHORYLATION VS BREAST GRADE

- Abramczyk et al
- 2019



histone -modifying genes and epigenetic alterations in medulloblastoma



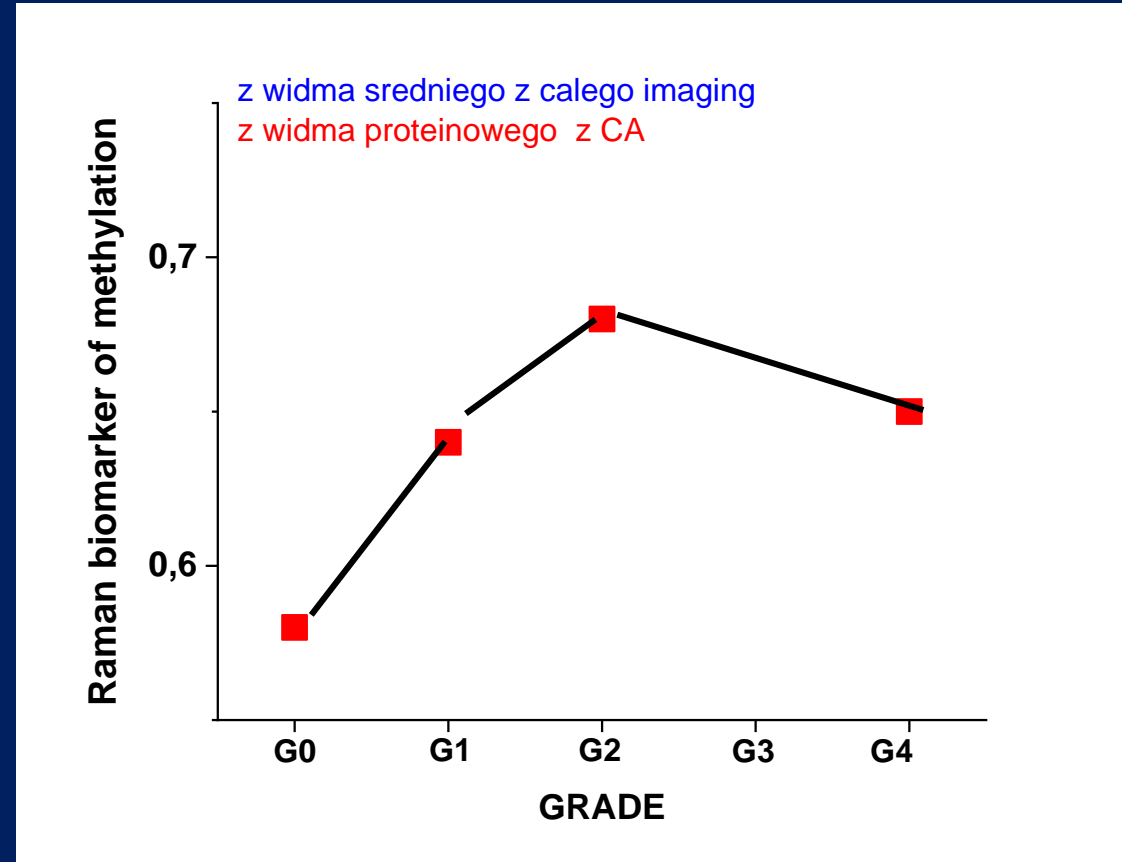
NATURE REVIEWS, 2019

Epigenetic modifications in brain tumor pathogenesis

- There is an increasing evidence that retinoic acid and retinoic acid receptors (RAR) play important role in inducing epigenetic changes, and regulate epigenetic changes in carcinogenesis. [Subcell. Biochem. 2014, 70, 129-149]

Is Glioblastoma an Epigenetic Malignancy?

LEVEL OF METHYLATION VS BRAIN TUMOR GRADE



The global methylation level increases in human brain tumor cells.

DNA methylation

- DNA methylation remains the best-studied epigenetic mechanism. Methylation is needed for the normal development of cells because it facilitates static long-term gene silencing and confers genomic stability. Abnormal methylation, which confers growth advantages, is tightly connected to cancer development. Methylation of cytosines within the CpG dinucleotide (60% of human genes contain a CpG island) by transfer of a methyl group from the methyl donor S-adenosylmethionine to the carbon 5 position of cytosines is catalyzed by DNA methyltransferases: DNA methyltransferases 1 (DNMT1; responsible for DNA methylation maintenance during cell division, development, and cancer), DNMT3a, and DNMT3b (responsible for *de novo* methylation during early development).

Cancer epigenomics: DNA methylomes and histone-modification maps

Manel Esteller

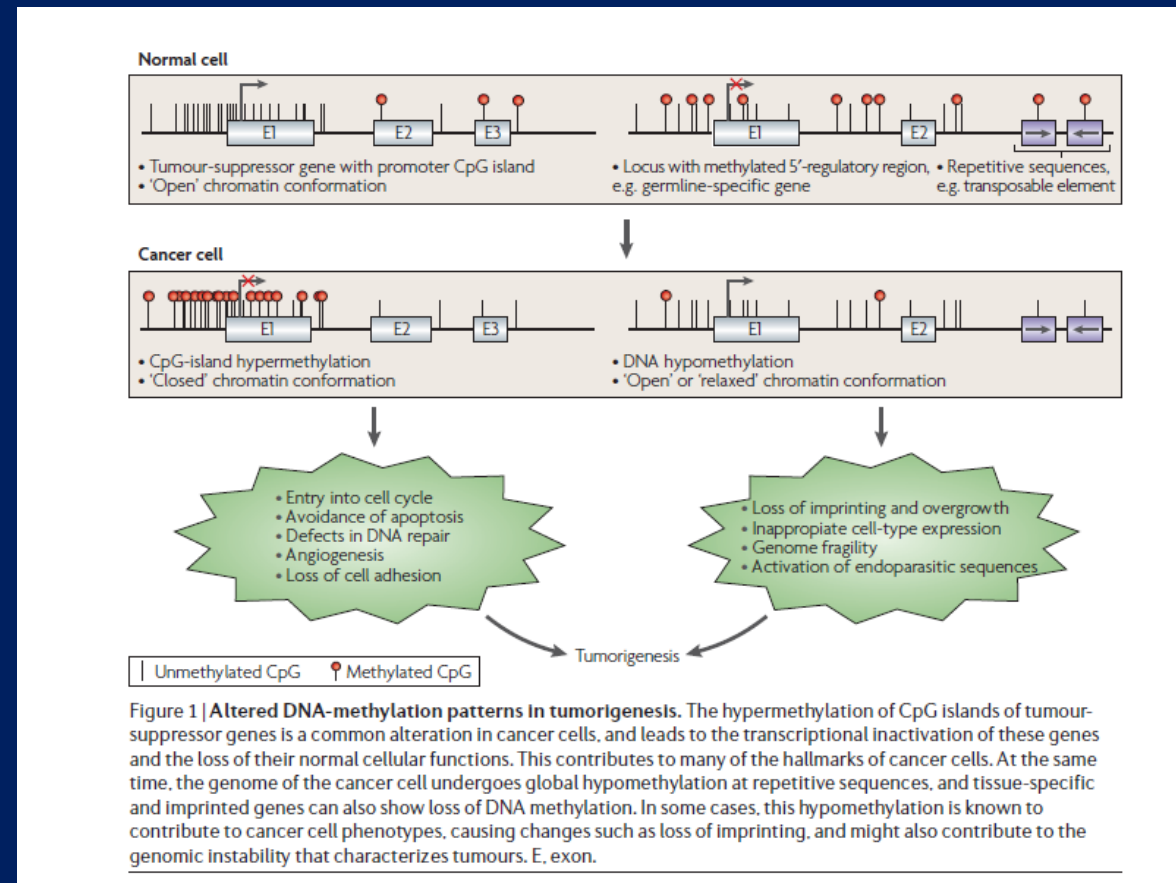
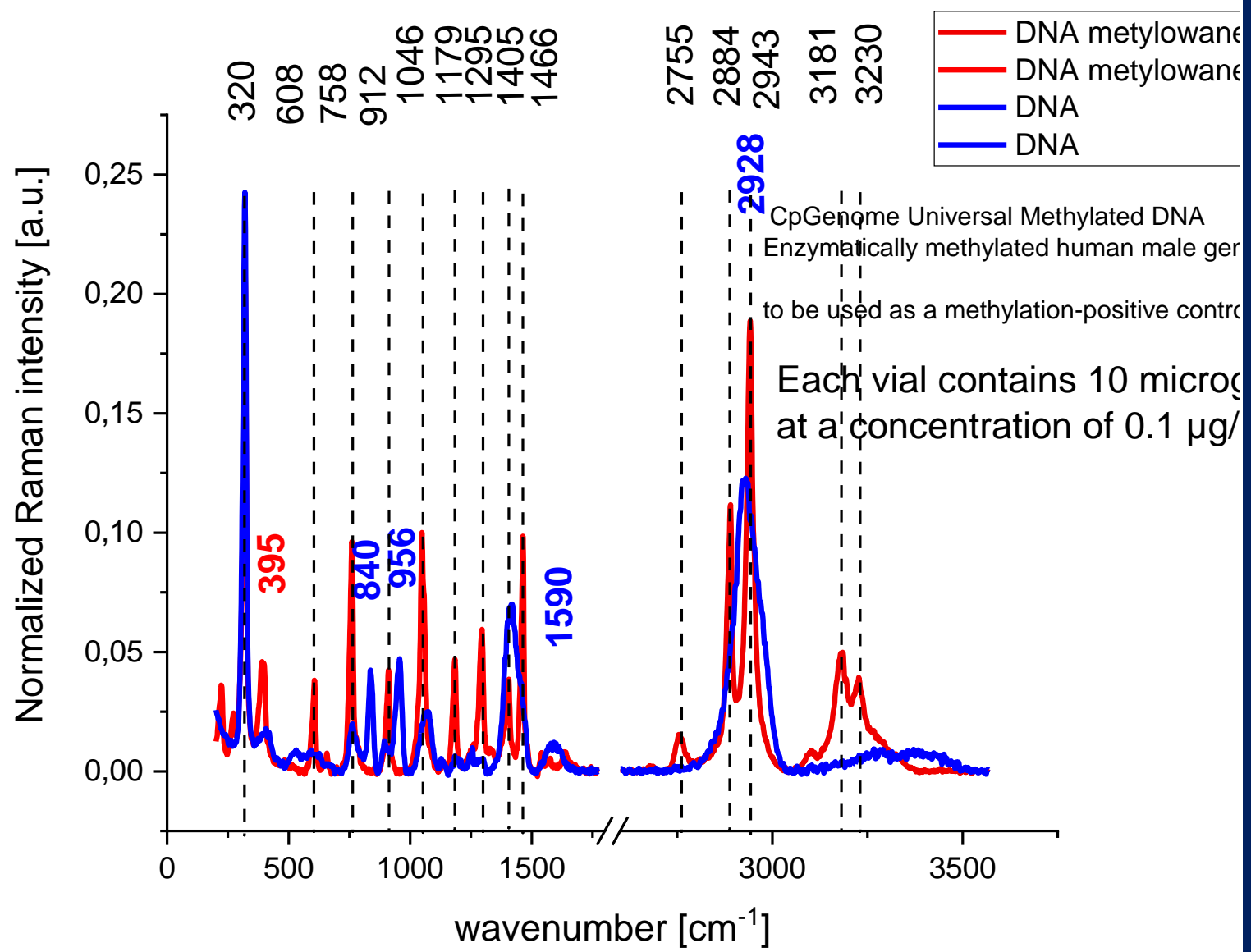


Figure 1 | **Altered DNA-methylation patterns in tumorigenesis.** The hypermethylation of CpG Islands of tumour-suppressor genes is a common alteration in cancer cells, and leads to the transcriptional inactivation of these genes and the loss of their normal cellular functions. This contributes to many of the hallmarks of cancer cells. At the same time, the genome of the cancer cell undergoes global hypomethylation at repetitive sequences, and tissue-specific and imprinted genes can also show loss of DNA methylation. In some cases, this hypomethylation is known to contribute to cancer cell phenotypes, causing changes such as loss of imprinting, and might also contribute to the genomic instability that characterizes tumours. E, exon.

The hypermethylation of CpG Islands of tumour-suppressor genes is a common alteration in cancer cells



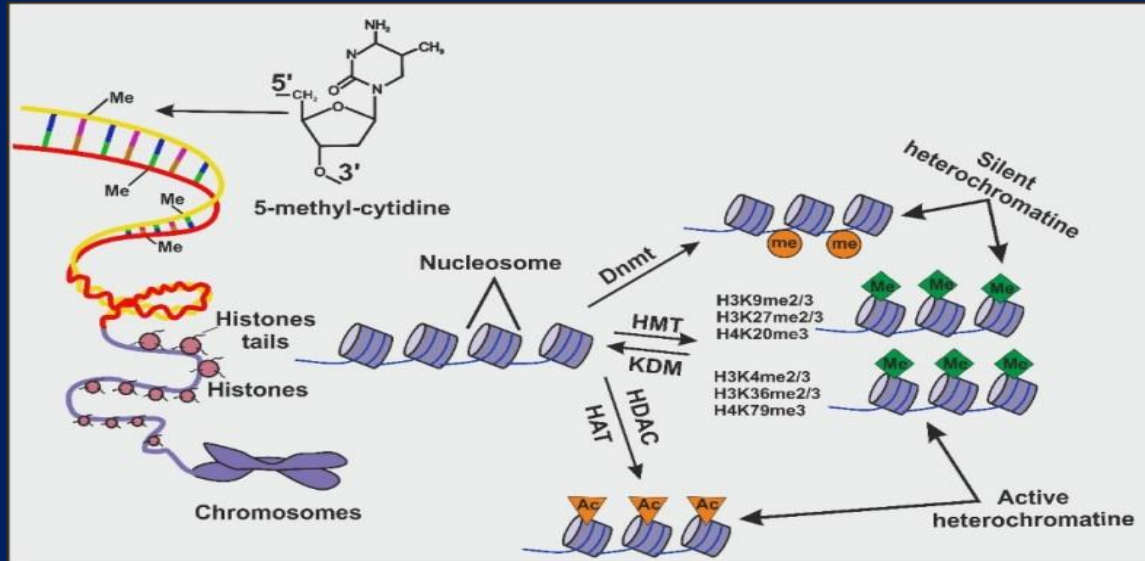
Double-Stranded DNA Damage Assessed with Raman Spectroscopy

- Auner AW^{1,2} and Thomas JC^{1*} ¹ Department of Natural Sciences, University of Michigan-Dearborn, Dearborn, MI 48128, USA ² Children's Hospital of Michigan, Detroit Medical Center, Detroit, MI 48201, USA
- Double stranded DNA breaks [DSBs] and subsequent repair can correct DNA damage or may mistakenly cause mutations leading to cell damage and disease. DSBs can be by measured with Raman spectroscopy, using inelastic scattered light resulting from distinct molecular vibrations from purified DNA samples
- Raman spectroscopy is a rapid and simple method to comparatively estimate the extent of relative DSBs. Unlike comet assays, which require analysis of living and dying cells, isolated DNA can be easily recovered from virtually any cell, stored, and DSB analysis done later.

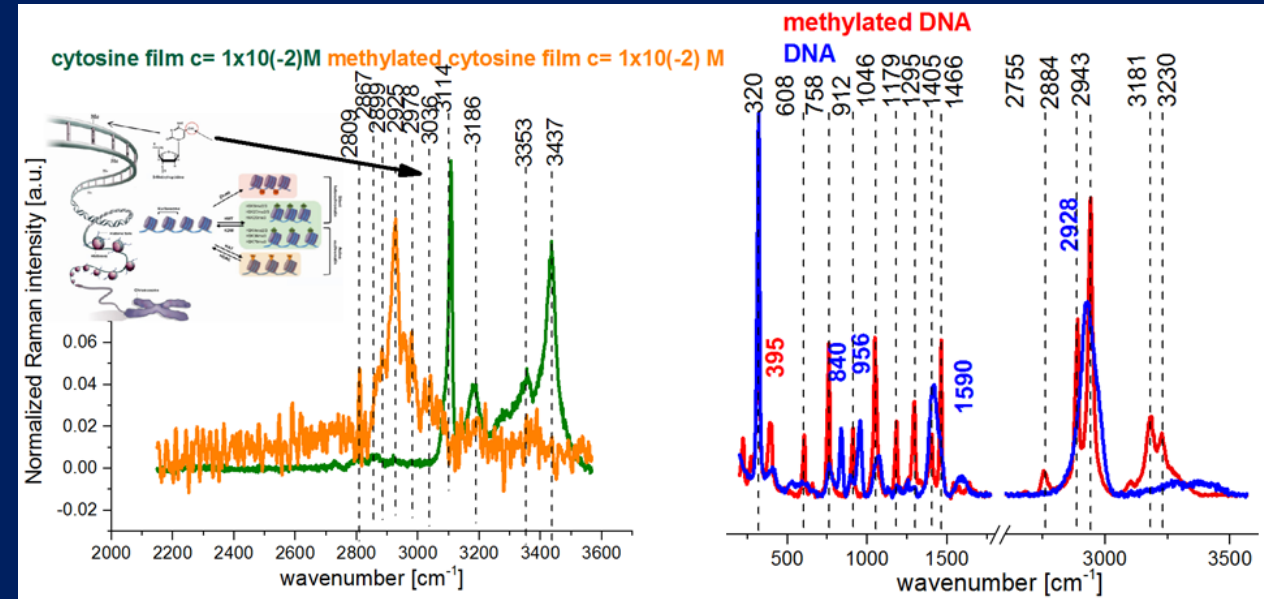
CpG ISLAND methylation in DNA



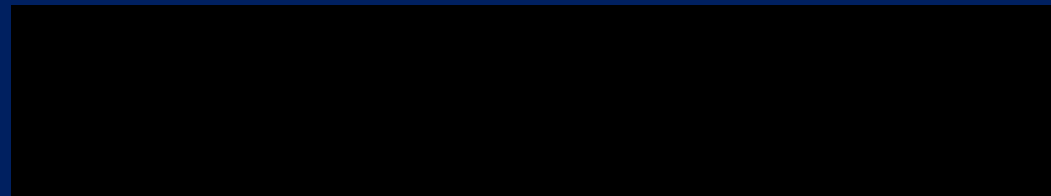
Cytosines in CpG dinucleotides can be methylated to form 5-methylcytosines.



CpG is shorthand for 5'—C—phosphate—G—3', that is, cytosine and guanine separated by only one phosphate group; phosphate links any two nucleosides together in DNA



Raman spectra of DNA and methylated DNA and cytosine /methylated cytosine, which will be useful in monitoring total CpG methylation DNA status.



Double-Stranded DNA Damage Assessed with Raman Spectroscopy

Auner AW1,2 and Thomas JC1* 1 Department of Natural Sciences, University of Michigan-Dearborn, Dearborn, MI 48128, USA 2 Children's Hospital of Michigan, Detroit Medical Center, Detroit, MI 48201, USA

Wave number (cm ⁻¹)	Macromolecule	Vibration Source
764-772	Cytosine, Thymine	Pyrimidine ring breathing
880	DNA	Possible C-C backbone vibration
926	DNA	Possible C-C backbone vibration
1044	DNA	PO ₄ ⁻³ stretch backbone
1084	DNA	PO ₂ stretch backbone
1280	DNA	Nucleic Acid Vibration
1456	DNA	Deoxyribose or Guanine vibrations
1485	Adenine, Guanine	Purine ring breathing
1645	DNA or substrate	DNA ring breathing or strong substrate artifact

Table 1: Peaks assignments for Raman spectra of DNA. (For references see [29,30]).

Recently Raman tip scattering combined with Atomic Force microscopy detected DSBs from UVC radiation cleavage at the 3'- and 5'-bonds of deoxyribose [19].

Western blot analysis indicated the 2 and 4 day incubations with Bleocin™ promoted the accumulation of 53BP1 compared to control cells (Figure 5A). 53BP1 is a critical repair protein that binds chromatin near double strand breaks and promotes nonhomologous end-joining to repair double strand breaks [37]. An isoform of p53, TAp73 protein is known to facilitate apoptosis in Jurkat cells and hepatocytes following DNA damage [35,38,39]. Here, p73 and p63 kD proteins were accumulated above controls at 2d and 4d of Bleocin™ treatment (Figure 5B) [25,40]. For a loading control, blots were also reacted with an anti-α tubulin antibody, subsequently revealed with a secondary antibody linked to alkaline phosphatase (Figure 5C).

To confirm enhanced DNA breakage in Bleocin™ treated cells compared to controls, a 3' end labeling biotin - dUTP procedure was used [34-36]. Two day Bleocin™ treated cells contained DNA with 1.12 (0.05 SD) (or 12% free ends) in excess of controls. When treatment was extended to 4d Bleocin™, 1.20 (0.05 SD) (or 20% free ends above controls) were estimated. This data represents 4 separate DNA treatments and isolations.

Western blot analysis indicated the 2 and 4 day incubations with

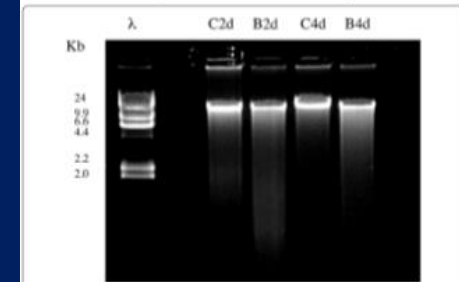


Figure 4: Approximately 1 µg/lane of genomic DNA isolated from Jurkat cells after 2 and 4 days of Bleocin™ treatment. Kilobase markers are indicated with the Hind III ladder. Genomic DNA is largely intact and greater than 24 Kb. Lambda Hind III marker was used as a size reference. Slightly more smearing in DNA from cells in the Bleocin™ treatments was observed.

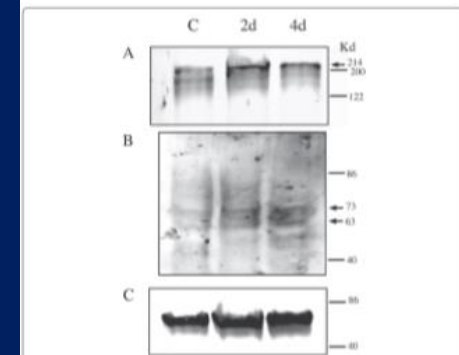
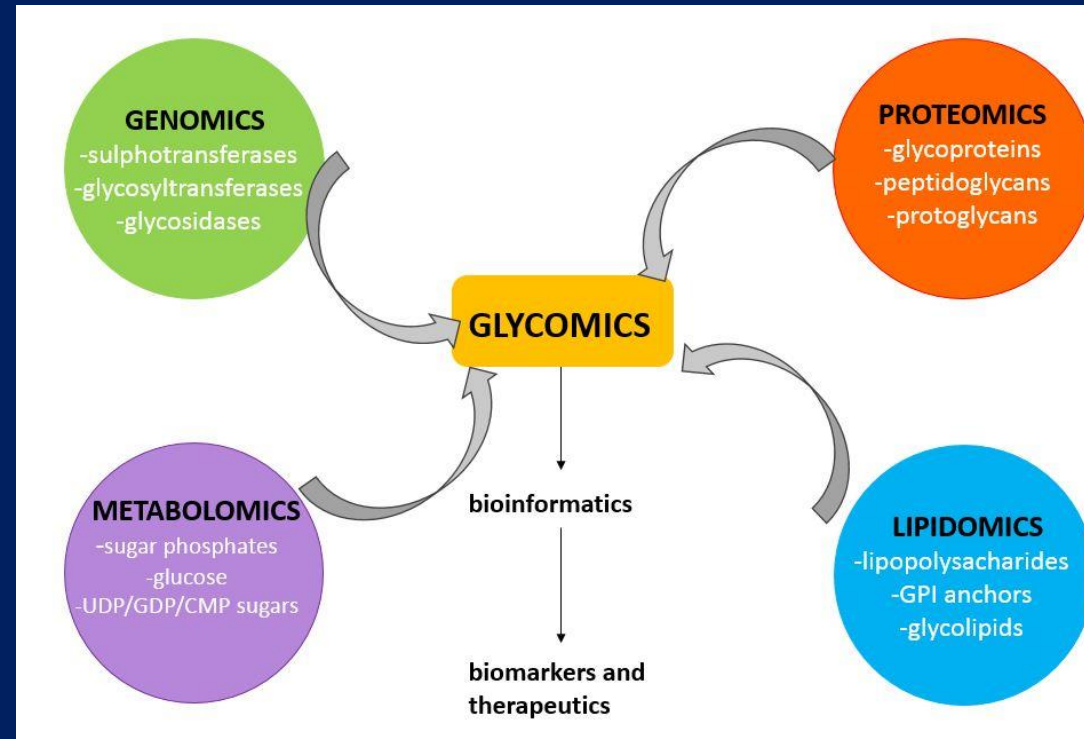


Figure 5: 50µg of total protein extract/lane from C(control) or cells treated with 10 µg/ml Bleocin™ for 2 days or 4 days. Samples were separated on a 10% (A, C) or 12% (B) (w/v) SDS-Laemmli gel, blotted to nitrocellulose. Blots were reacted with (A) anti - 53BP1 (214 Kd), (B) anti - TAp73 (73Kd), or (C) anti - alpha tubulin (50 Kd) antibodies. Data shown is a representative blot from three experiments.

FUTURE DIRECTIONS OF CANCER RESEARCH



Monitoring glycosylation metabolism in brain and breast cancer by Raman and AFM imaging

- Our recent results opened a new window for exploration of processes occurring in non-cellular space - glycocalyx –a coat on the external surface of their plasma membranes of epithelial cells consisting of several carbohydrates, several carbohydrate moieties of membrane glycolipids and glycoproteins, which serve as backbone molecules for support.

a non-invasive monitoring of cellular epigenetic processes BY RAMAN

- Compared to the currently existing methods of molecular biology IR and Raman- based methods (spectroscopy, imaging) show an interesting alternative, which allows for a non-invasive monitoring of cellular epigenetic processes.
- In the presentation we will assess the diagnostic potential of acetylation and methylation processes in normal and brain cancer cells and tissues by IR/Raman-based methods. Since IR and Raman methods are label free, and do not involve any staining or antibody attachment for detecting methylated and acetylated proteins, they offer straightforward sample handling over complex assays that must take into account sensitivity and specificity to antibody. Our algorithm based on epigenetic modifications in the cancerous cells that cover the entire IR/Raman spectra regions associated with lipids, DNA, and proteins and using a machine-learning algorithm will be capable to classify different tissue types. The IR and Raman-driven methods will be verified and compared with the methods of molecular staining, histopathology imaging, fluorescence imaging and methods of conventional biology, such as expression protein profiles, methylated DNA Quantification Kits, western blotting with specific selected primary antibodies such as H3K4me3, H3K9me3 and H3 (used as a loading control).

-

CONCLUSION

- Raman spectroscopy and Raman imaging have strong diagnostic potential for monitoring acetylation and methylation processes in cancer cells of human breast and brain tissues.

Warburg effect

The best characterized metabolic phenotype observed in tumour cells is the Warburg effect, which is a shift from ATP generation through oxidative phosphorylation to ATP generation through glycolysis, even under normal oxygen concentrations. This effect is regulated by the PI3K, hypoxia-inducible factor (HIF), p53, MYC and AMP-activated protein kinase (AMPK)–liver kinase B1 (LKB1) pathways.

However, metabolic adaptation in tumours extends beyond the Warburg effect. It is becoming clear that alterations to metabolism balance the need of the cell for energy with its equally important need for macromolecular building blocks and maintenance of redox balance.

TRENDS IN CANCER RESEARCH

- Presently, a growing number of reports have initiated a discussion about the benefits of metabolic regulation in cancers. The Warburg effect, a great discovery approximately 90 years ago, addresses the “universality” of cancer characteristics. For instance, most cancer cells prefer anerobic glycolysis instead of mitochondrial respiration.

Biomol Ther (Seoul) 2015; 23(2): 99-109 <https://doi.org/10.4062/biomolther.2015.013>

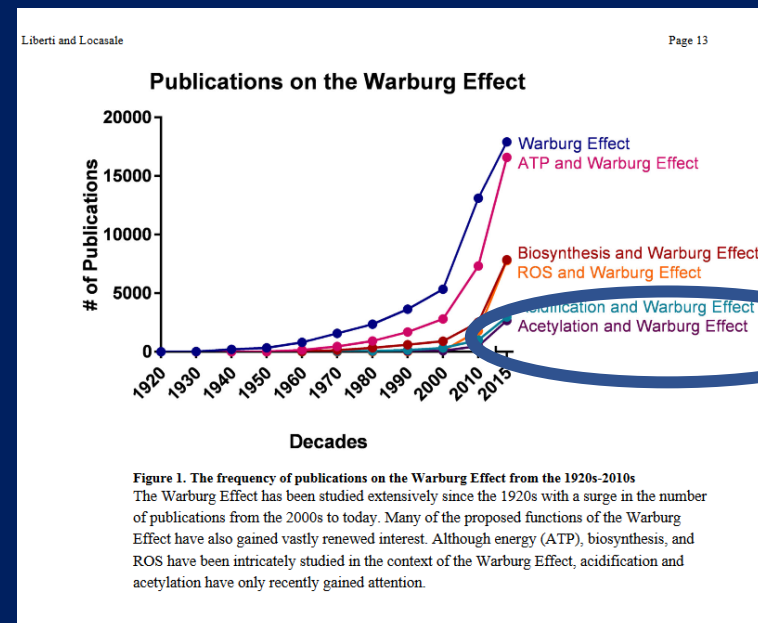
Cancer Metabolism: Strategic Diversion from Targeting Cancer Drivers to Targeting Cancer Suppliers

Current ideas in cancer metabolism

- The Raman –driven oncological platform will help to analyze proposed biological explanations for the Warburg effect and enhanced fatty acid synthesis de novo, emphasize their rationale, and discuss their controversies.

Although energy (ATP), biosynthesis, and ROS have been studied in the context of the Warburg Effect, epigenetic modifications (acetylation) have only recently gained attention.

Trends Biochem Sci. 2016 March ; 41(3): 211–218



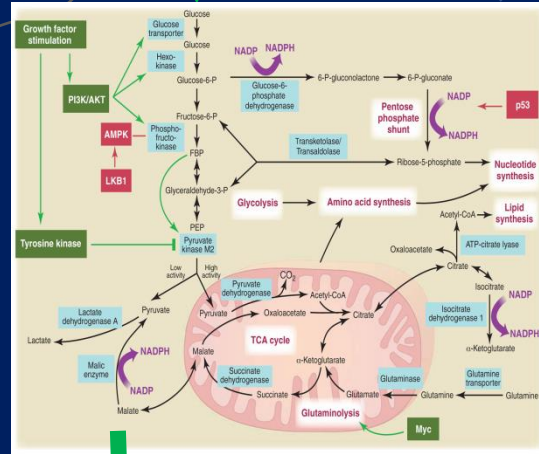
Rapid ATP synthesis

Proposal: Increases access to a limited energy source

Questions:

- Why are ATP demands not limiting for proliferation?
- Why are there other mechanisms for rapid ATP synthesis?

Glucose



Tumor microenvironment

Proposal: Enhances disruption of tissue architecture

Questions:

- Why do unicellular organisms and cultured cells use aerobic glycolysis?
- Why do oncogenes induce the Warburg Effect cell-intrinsically?

LIPIDS Fatty acids de novo

Cell

Signaling

Proposal: Allows for signal transduction through ROS and/or chromatin modulation

Questions:

- Why is specificity unclear?
- Why would metabolite levels be influenced by flux?

Biosynthesis

Proposal: Promotes flux into biosynthetic pathways

Questions:

- Why is most glucose not retained?
- Why does optimal biosynthesis not require aerobic glycolysis?

Lactate

Function of the Warburg Effect and Fatty Acids de novo synthesis?

METABOLISM

THE FUTURE OF GLIOMA CELL

- METABOLISM
- Recent years have yielded exciting findings in the field of cancer cell metabolism, suggesting that Warburg is only a small part of the larger story. While glioma cells do partially metabolize glucose, releasing lactate into the extracellular space, other substrates are being oxidized. Yet the questions remain:
- What fraction of ATP is produced from glycolysis, and what fraction from oxidation? What substrates are preferentially oxidized? How easily can a glioma cell change its metabolic strategy upon exposure to hypoxia, nutrient deprivation, or acidic environment? Do different cells within the tumor have different metabolic strategies or preferred metabolic substrates? Do gliomas with different oncogenic driver mutations (e.g., in p53, NF1, or IDH) have different metabolic strategies or preferred

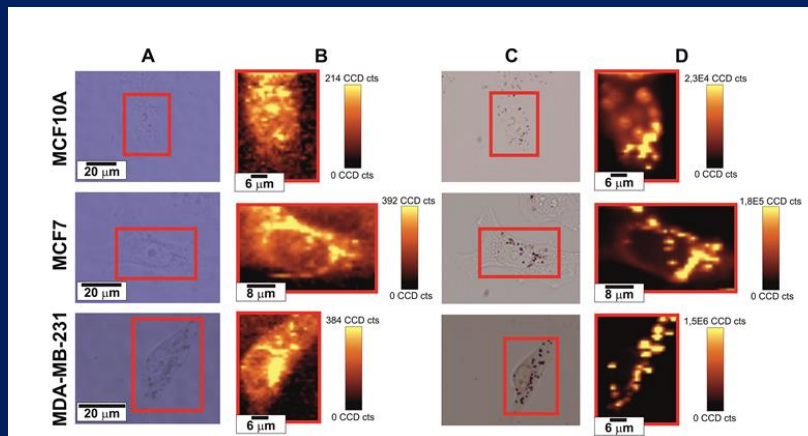
CANCER PHENOTYPE

Lipid metabolic reprogramming in cancer cells

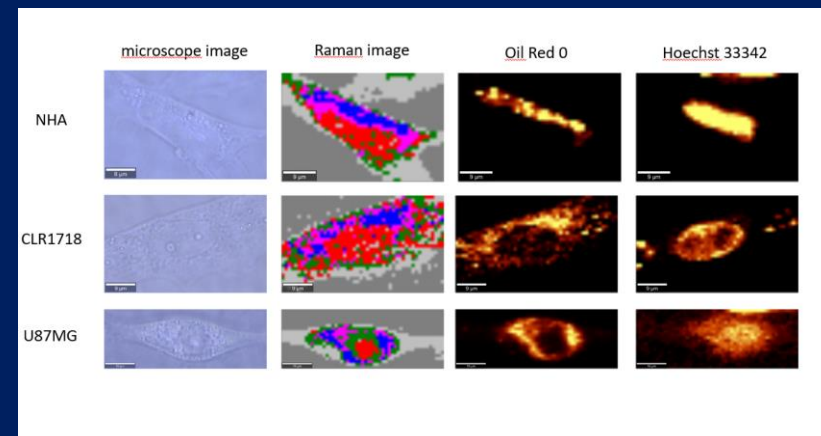
Warburg proposed that dysfunctional mitochondria is the root of aerobic glycolysis. Warburg further hypothesized that this event is the primary cause of cancer. A higher rate, but lower yield, of ATP production may gain a selective advantage when competing for shared and limited energy resources

We want to verify the hypothesis that metabolic adaptation in tumours extends beyond the Warburg effect and that commonly disregarded in the past alterations in lipid metabolic reprogramming encountered in tumors are very important in cancer development.

To address these important questions on lipid phenotypic alterations we will study compositional mapping of cellular compartments, such as lipid droplets (LDs), mitochondria, nucleus in cell cultures



Abramczyk et al. Analyst , 2015

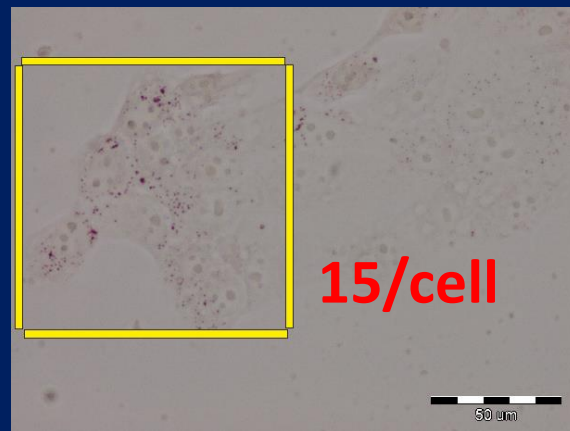


Abramczyk et al. LLSM, 2018

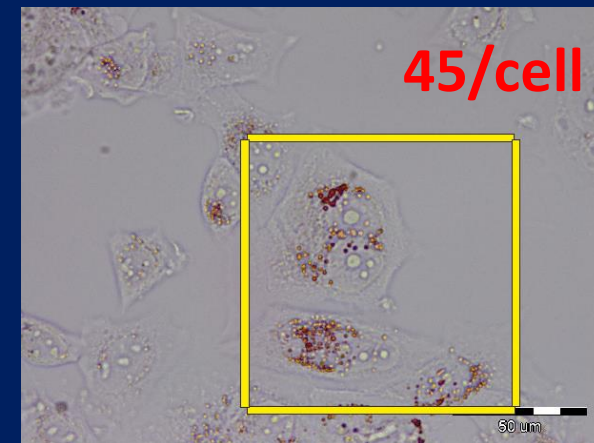
- Recent advances in lipid analytical and imaging technologies, including Raman scattering microscopy, have greatly progressed such lipidomic analysis. Raman-based imaging offers lipid compositional mapping of cellular compartments, such as LDs. These complementary approaches provide crucial information on tumor lipid phenotype, in particular abundance, FA composition and spatial distribution of lipid classes within tumors

LIPID DROPLETS IN NORMAL MCF10A EPITHELIAL CELLS OF BREAST vs MILDLY MALIGNANT MCF7 AND AGGRESSIVELY MALIGNANT MDA-MB-231

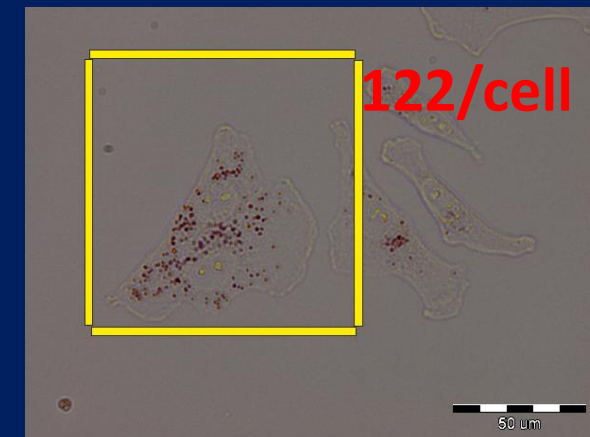
MCF10A - normal cells



MCF7 - mildly malignant

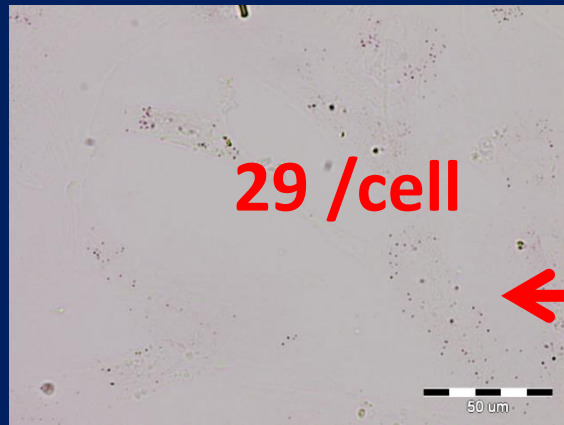


MDA-MB-231 - Aggressively malignant

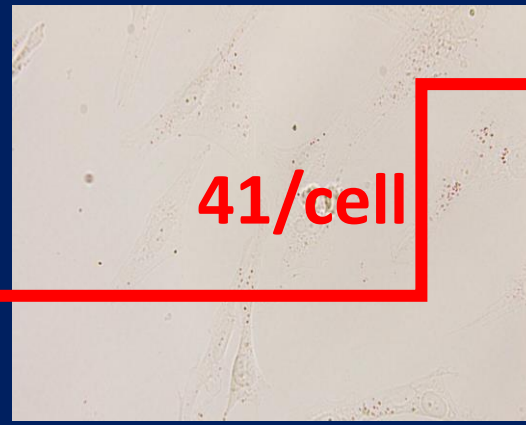


The goal of our study will be to assess the impact of cancer aggressiveness on the amount of cytosolic lipid droplets and their chemical composition in non-malignant and malignant human epithelial cell lines.

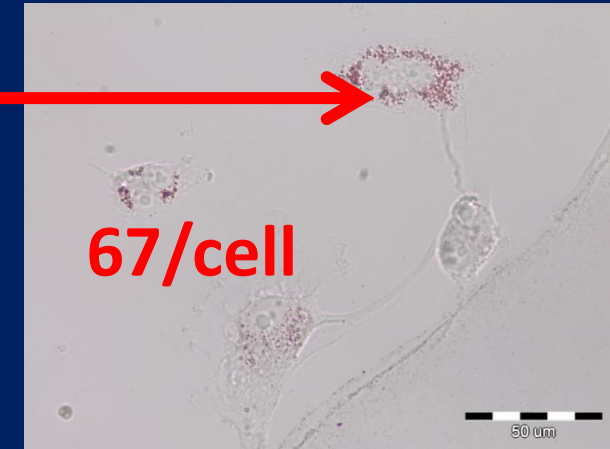
LIPID DROPLETS in Astrocytes vs Glioblastoma U89



Astrocytes –normal cells



Astrocytoma –malignant cells



Glioblastoma U89- highly malignant cells

- Cancer cells contain increased numbers of lipid droplets compared with normal cells.
- Increased amount of lipid droplets correlates with increased aggressiveness of cancer.
- The increased amount of cytoplasmic lipid droplets in the human cancer cells may be closely related to increased rate of lipid synthesis in cancerous tissues.

Tissue preparation

Frozen Tissue Blocks

Frozen Tissue Arrays

Frozen Tissue Sections

Frozen Tissue Section Panels

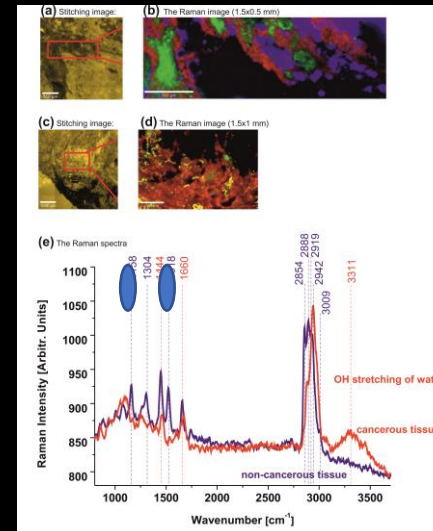
Matched Pair Tissue Frozen Sections

Paraffin Tissue Blocks

Paraffin Tissue Arrays

Paraffin Tissue Sections

Paraffin Tissue Section Panels **deparafinization**



Do not waste valuable information!!!!

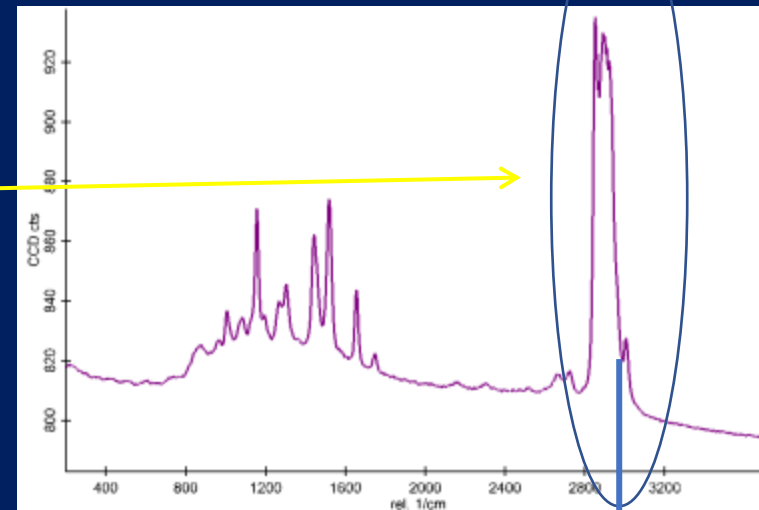
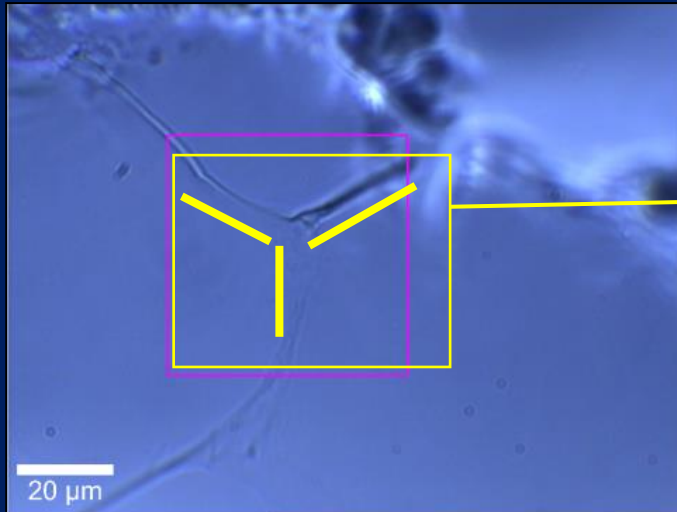
An essential role in spectroscopic methods is played by the preprocessing of tissues, as they naturally occur at the expense of introducing some fixatives, matrices, adhesives, which may generate their own vibrational spectra overlapping the signals from the native tissue. To obtain reliable results one must be sure that the method of tissue processing does not distort the vibrational spectra of the studied tissue.

FRESH TISSUE – the best solution

B. Brozek-Pluska, J. Musial, R. Kordek, E. Bailo, T. Dieing, H. Abramczyk, *Raman spectroscopy and imaging: Applications in human breast cancer diagnosis*. Analyst, 137, 2012, 3773. (IF=4.2)

P80 crio sample

Figure 4 shows the Raman image (a) (150 μm x 100 μm) and the averaged spectra (b). The average spectrum was achieved from the region marked in (a).



P80 Sample after deparafinization

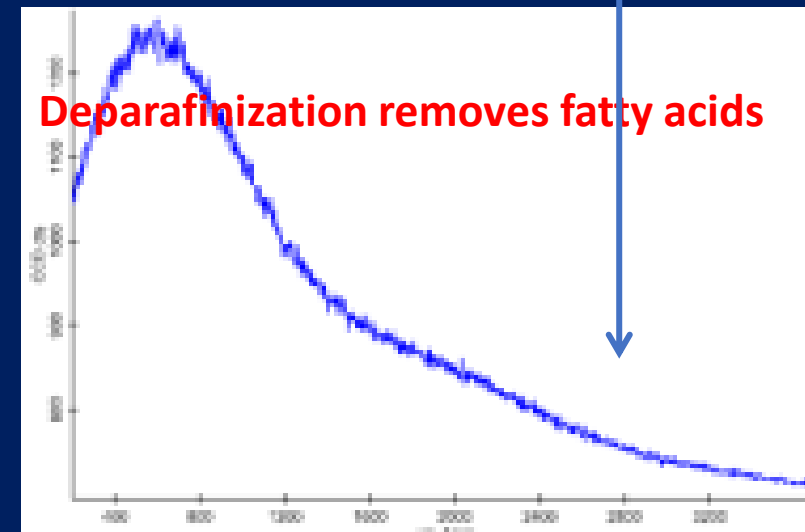
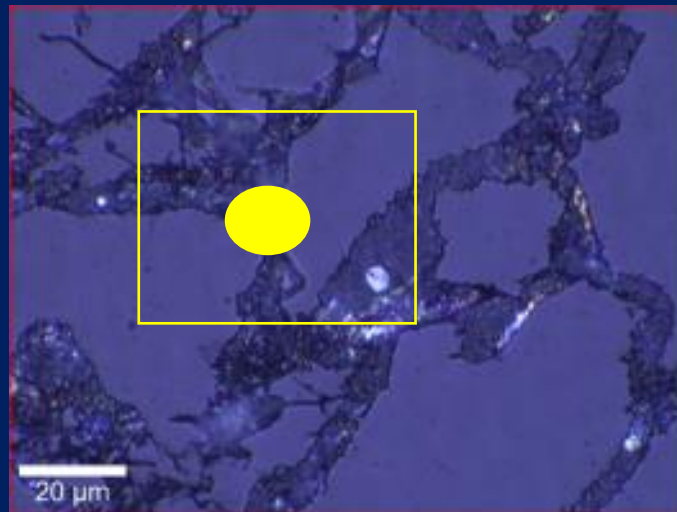
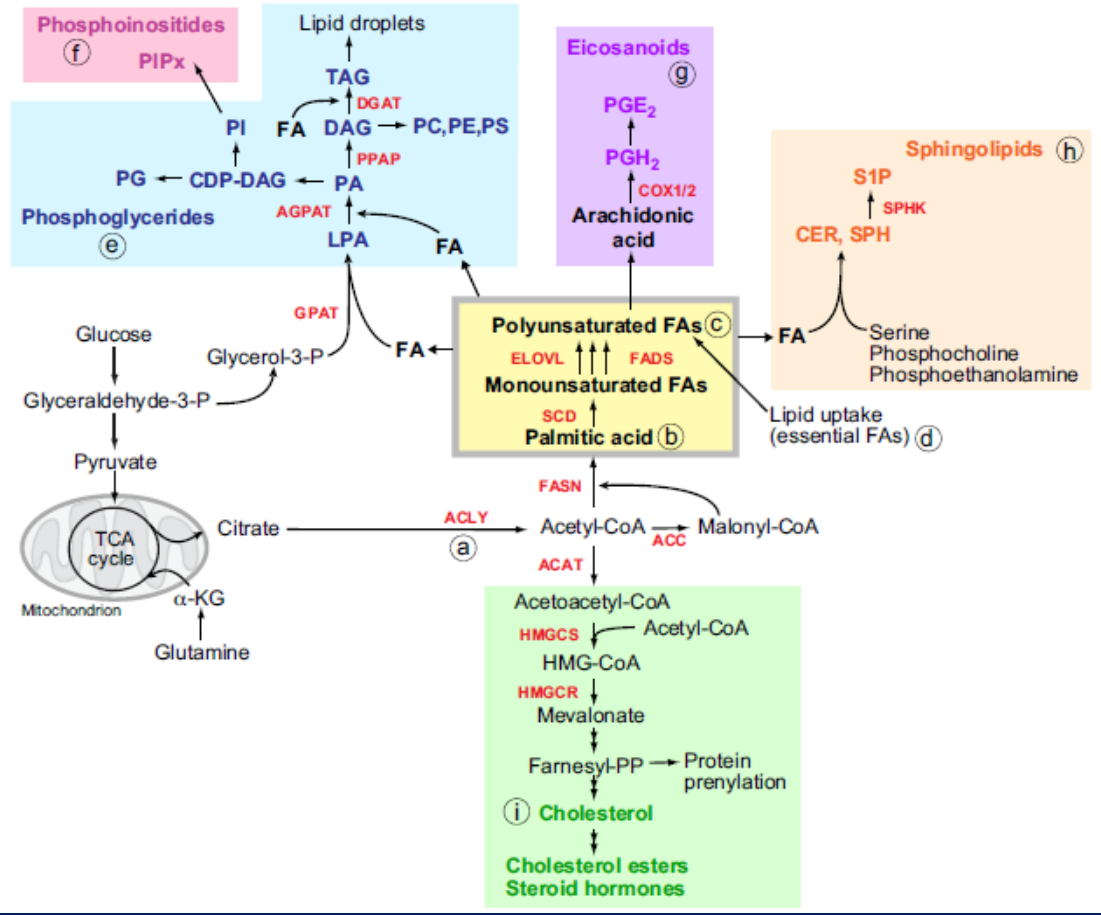


Figure 7 shows the stitching image recorded for a overview of the sample; width [μm]: 150.00 height [μm]: 100.00; objective 5x 0.10NA , the Raman image (b) (x:150 μm ; z:50 μm) objective 50x 0.50NA. (c) The single spectra correspond to the image, the colors of the spectra correspond to the colors in the image; spectra were achieved with a integration time of 0.3 s





New look inside human breast ducts with Raman imaging



Analytica Chimica Acta

Volume 909, 25 February 2016, Pages 91–100



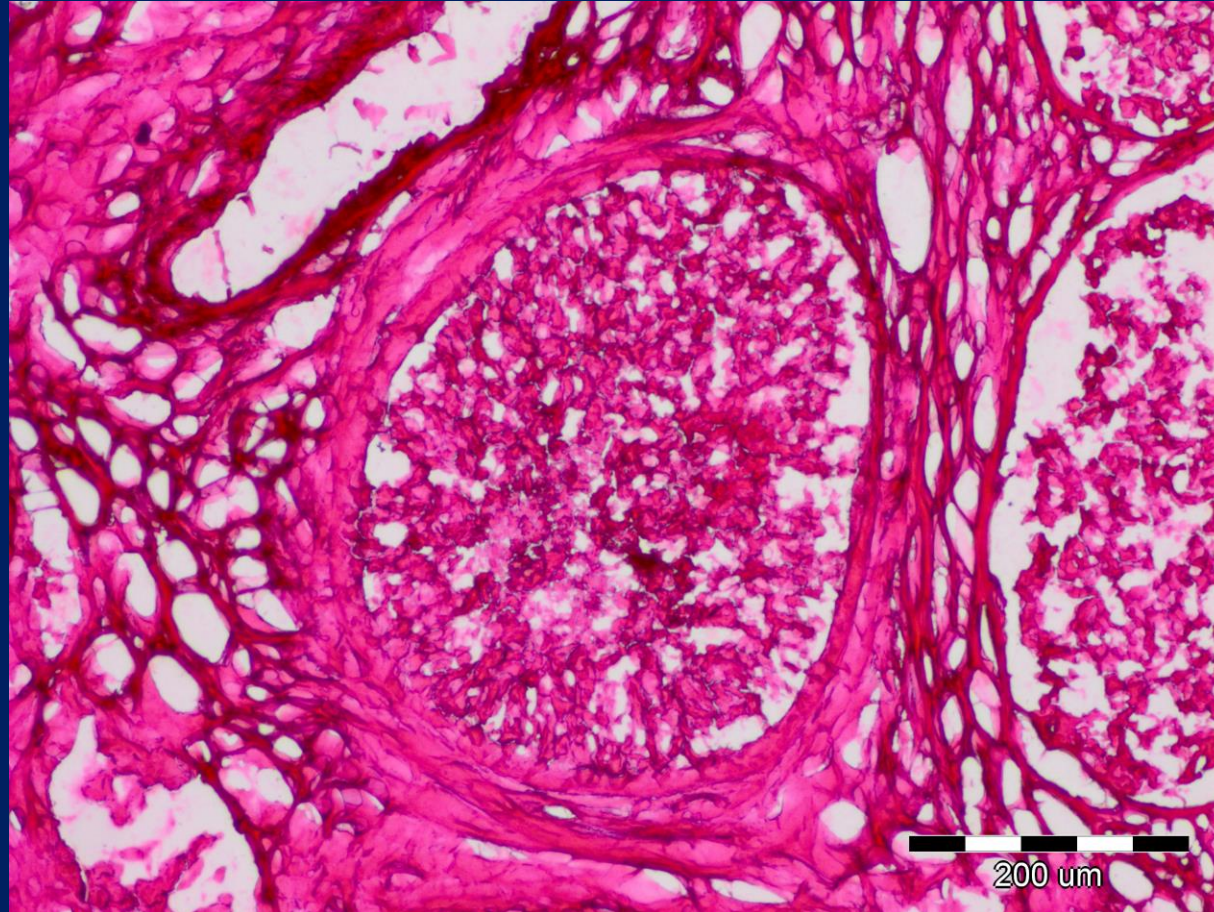
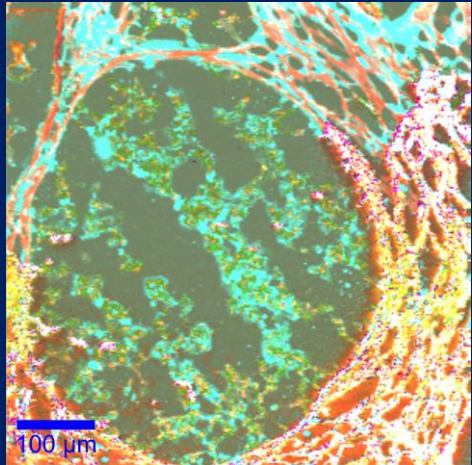
New look inside human breast ducts with Raman imaging.
Raman candidates as diagnostic markers for breast cancer prognosis: Mammaglobin, palmitic acid and sphingomyelin

Halina Abramczyk  · , Beata Brozek-Pluska

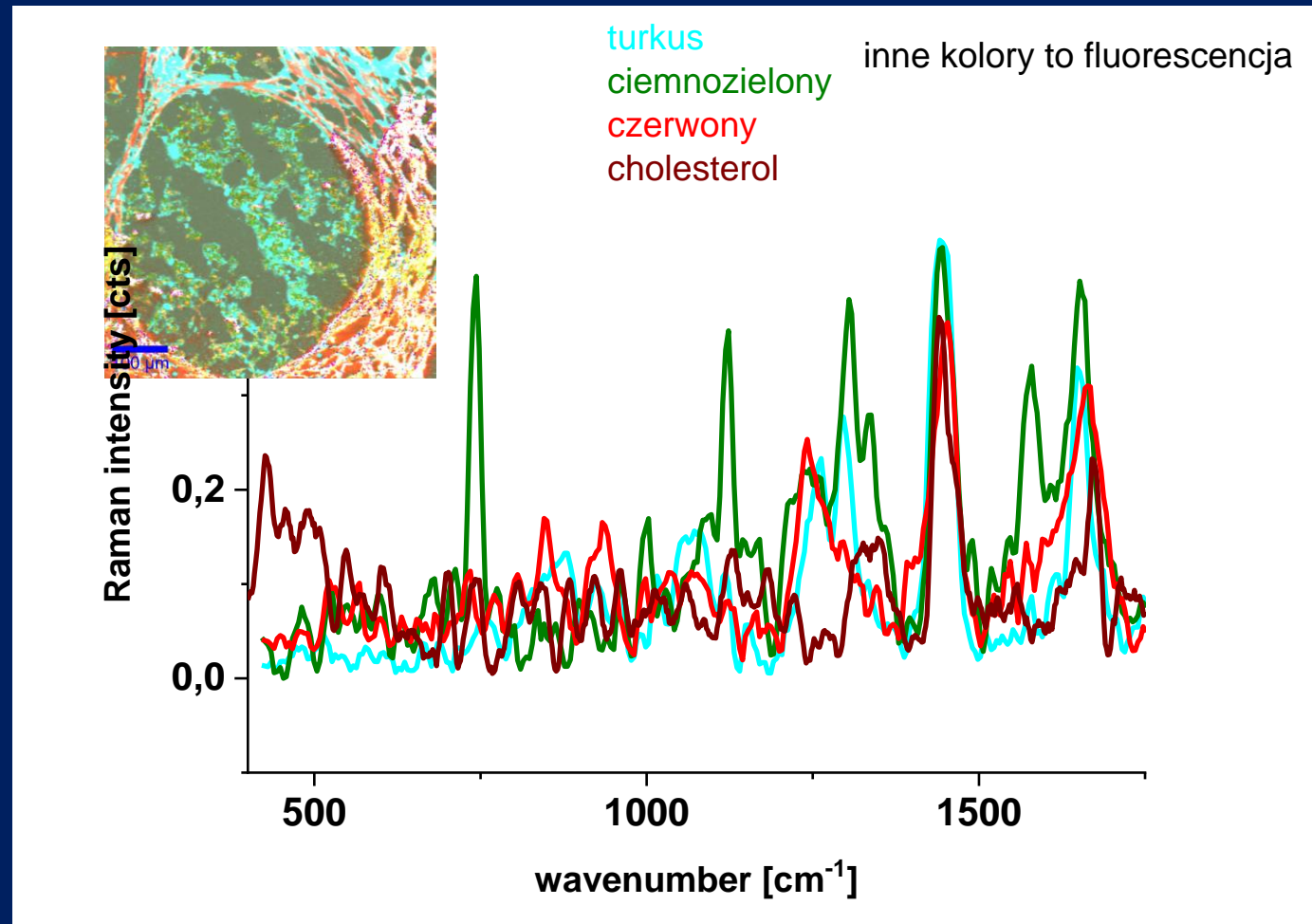
[+ Show more](#)

We can look inside human breast ducts answering fundamental questions about location and distribution of various biochemical components inside the lumen, epithelial cells of the duct and the stroma around the duct during cancer development.

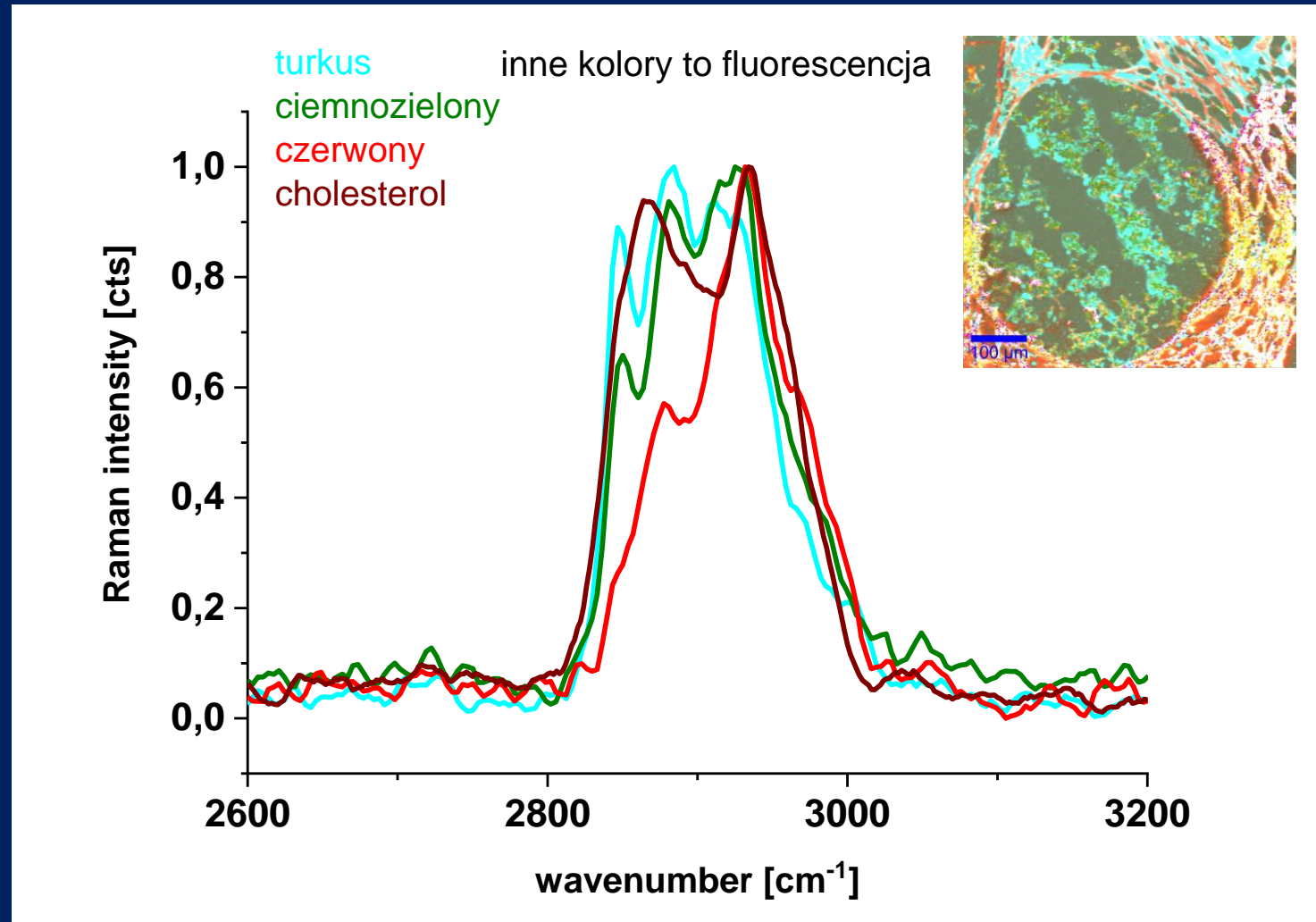
DUCTAL CANCER



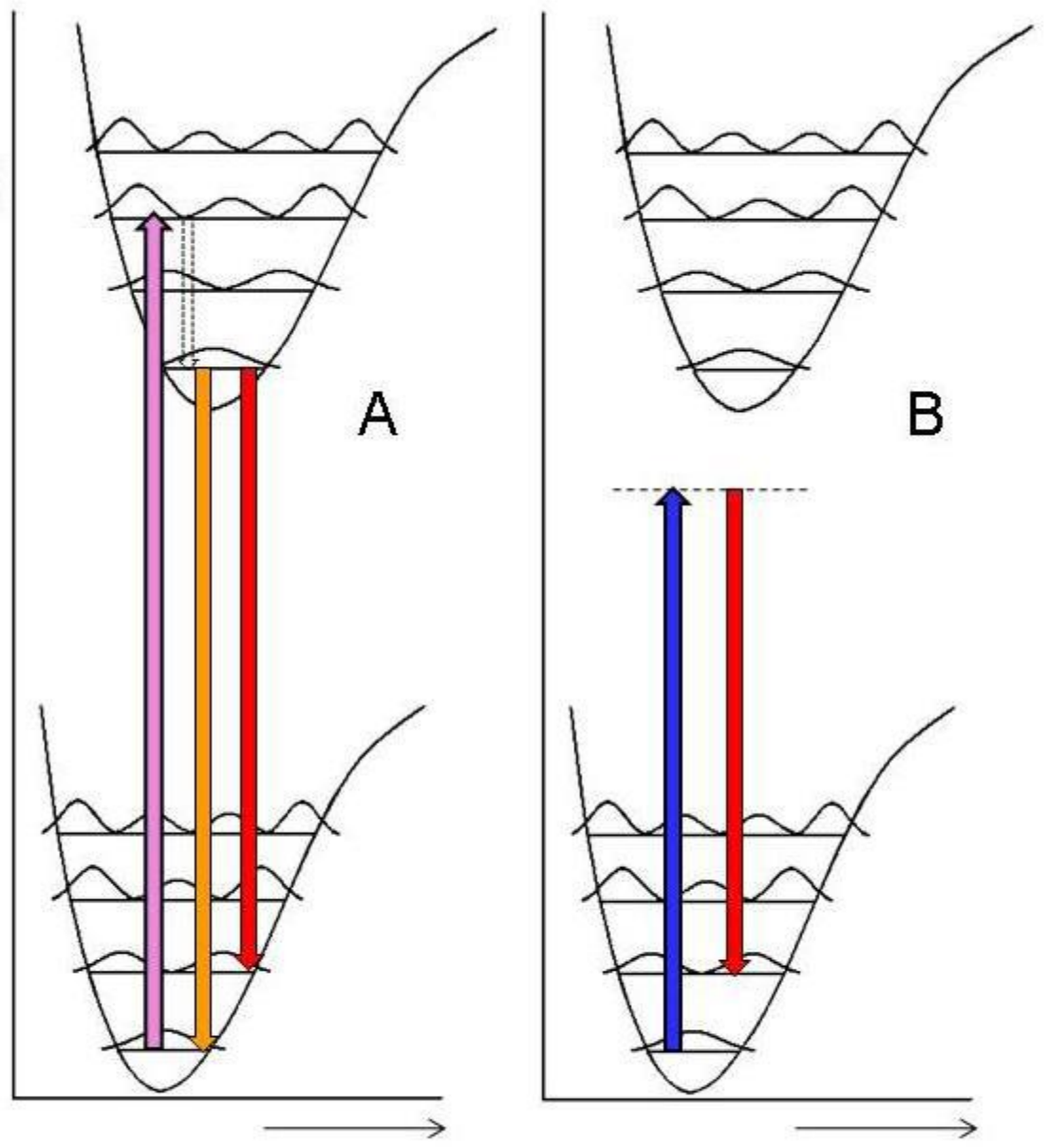
P115 guz vs cholesterol Cytochrome C in cancer duct



P115 guz vs cholesterol



Energy

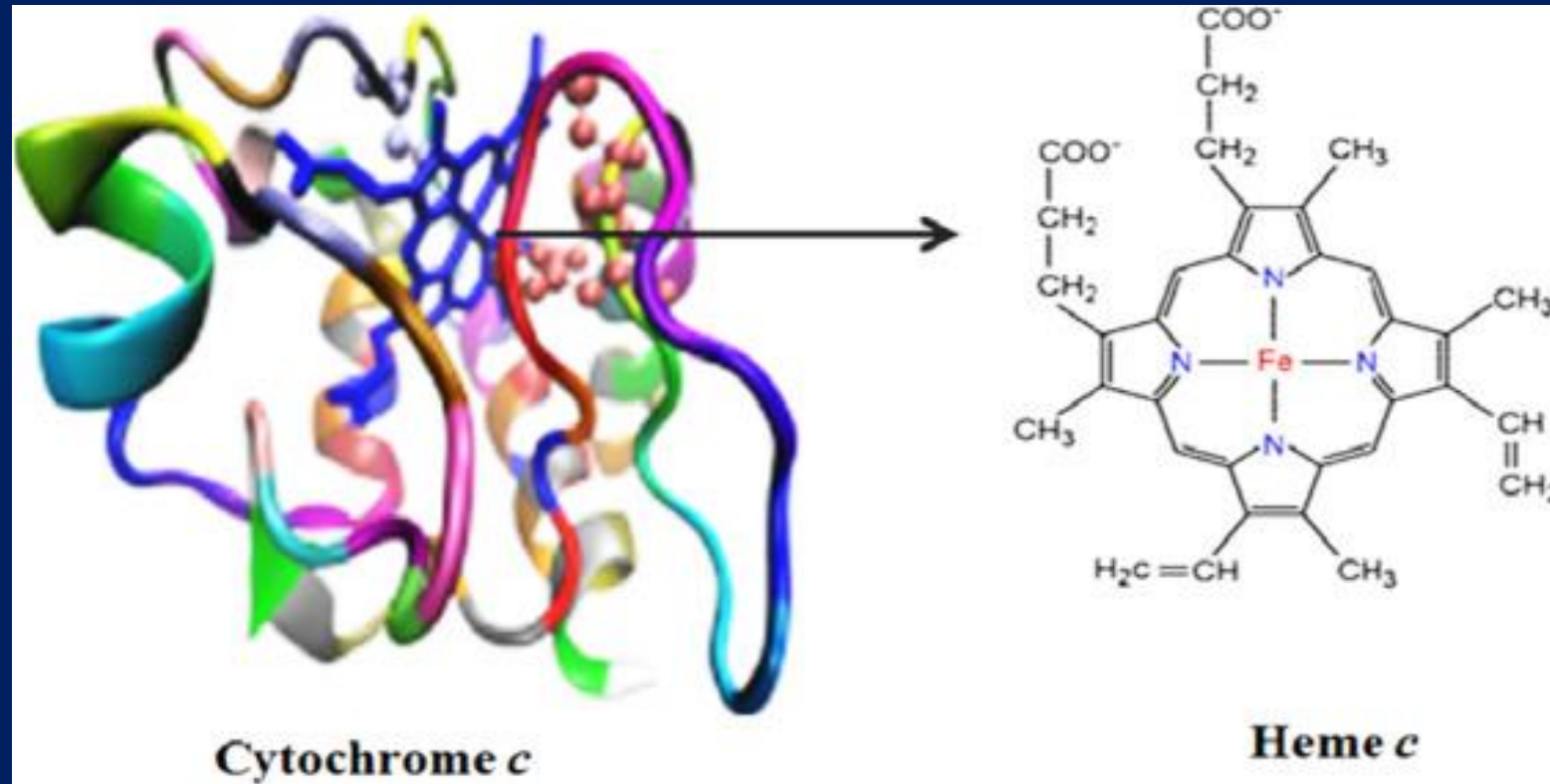


A

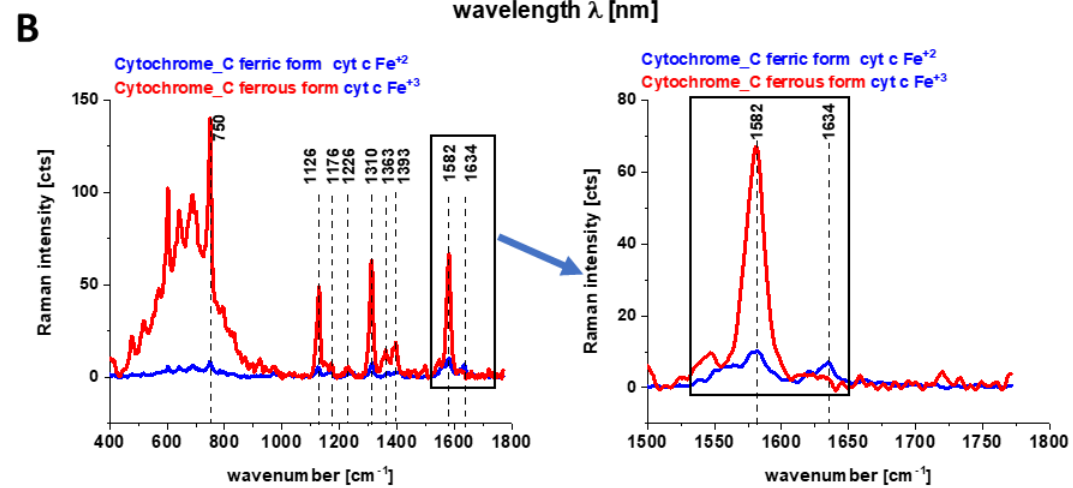
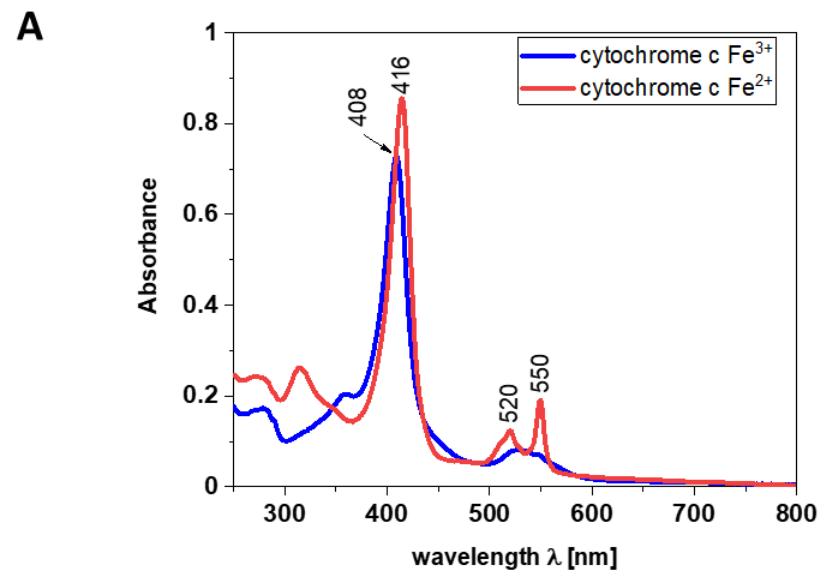
B

Internuclear distance

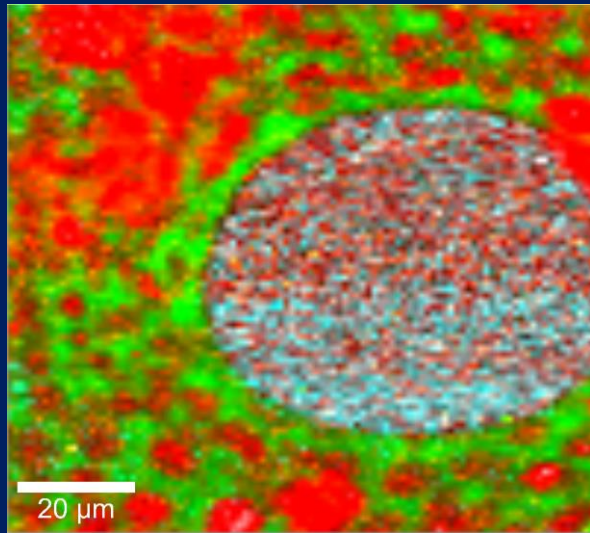
CYTOCHROME C



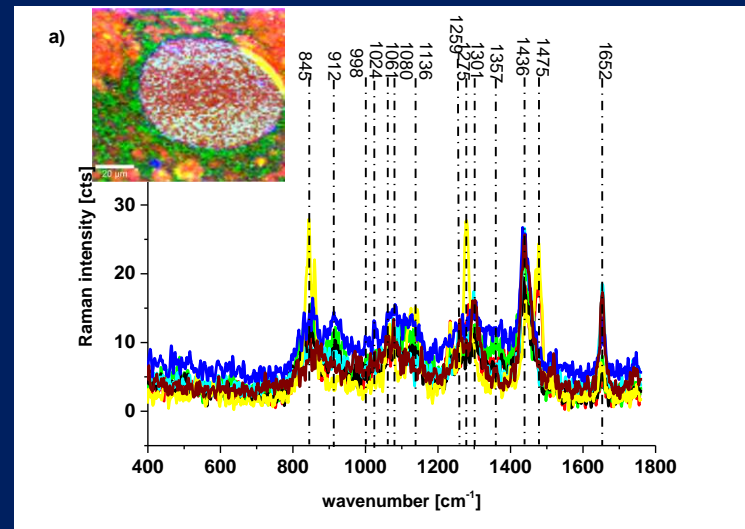
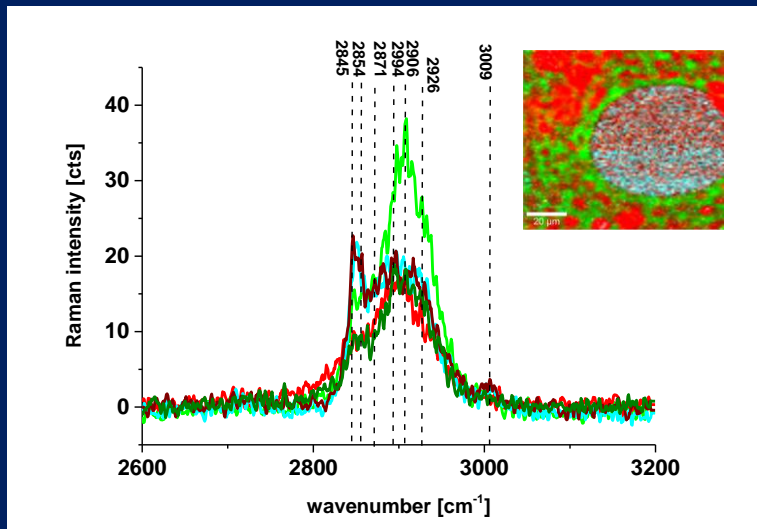
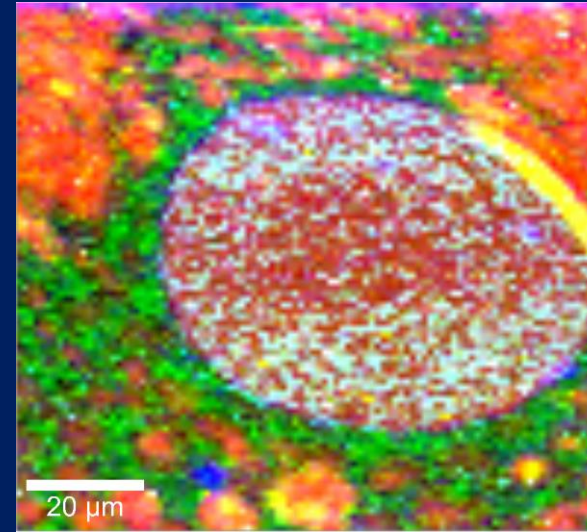
The release of cyt *c* from mitochondria is a key initiative step in the activation of cell death pathways.

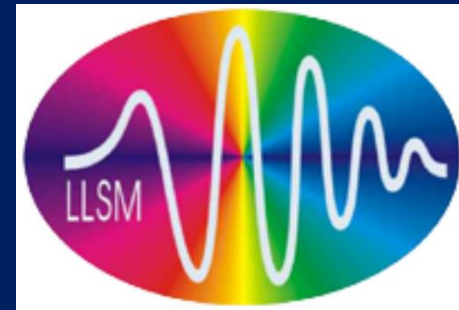


WYSOKI ZAKRES



NISKI ZAKRES





The biochemical, nanomechanical and chemometric signatures of brain cancer

2018

Spectrochimica Acta Part A: Molecular and Biomolecular Spectroscopy 188 (2018) 8–19



ELSEVIER

Contents lists available at ScienceDirect

Spectrochimica Acta Part A: Molecular and Biomolecular Spectroscopy

journal homepage: www.elsevier.com/locate/saa



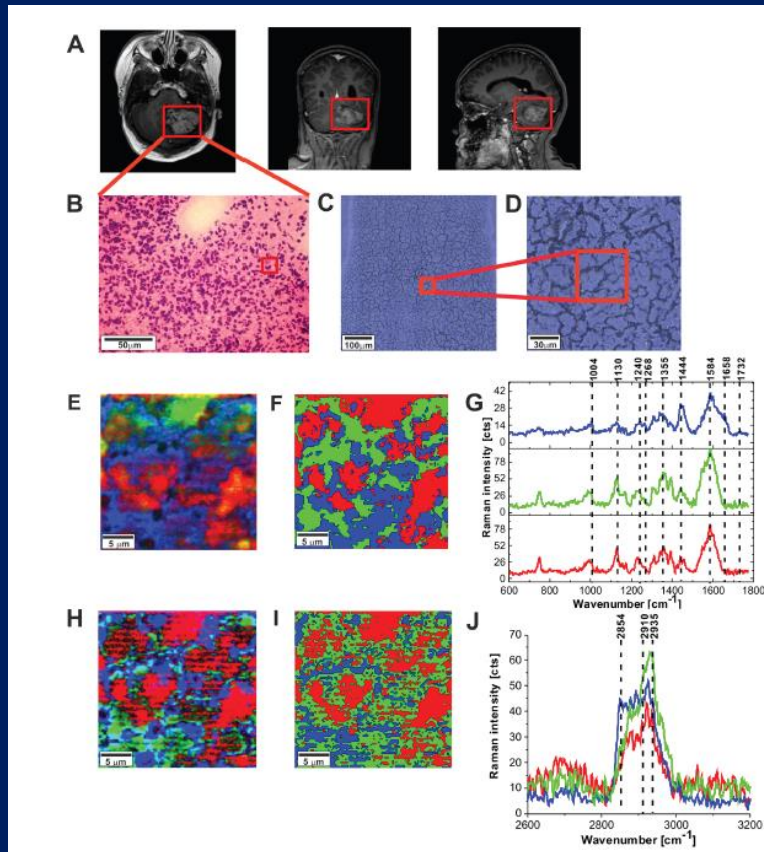
The biochemical, nanomechanical and chemometric signatures of brain cancer

Halina Abramczyk*, Anna Imiela

Lodz University of Technology, Faculty of Chemistry, Institute of Applied Radiation Chemistry, Laboratory of Laser Molecular Spectroscopy, Wroblewskiego 15, 93-590 Lodz, Poland

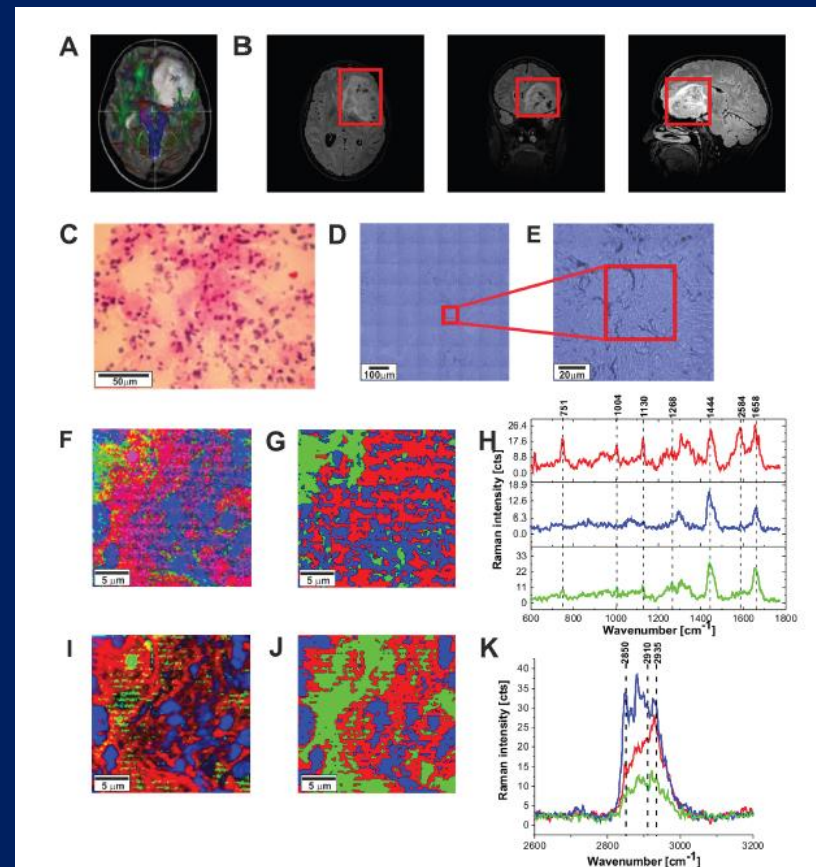


Novel strategies of Raman imaging for brain tumor research



Medulloblastoma , grade IV

Figure 5: The MRI image (A) H&E-stained histological image (B) stitching microscopy image (520 μm x 520 μm) (C) microscopy image (155 μm x 155 μm) (D) Raman images (50 μm x 50 μm) obtained by basis analysis (E) and cluster analysis (F) and the characteristic vibrational Raman spectra in the fingerprint frequency region (G) Raman images (50 μm x 50 μm) obtained by basis analysis (H) and cluster analysis (I) and the characteristic vibrational Raman spectra in the high frequency region (J) of the tumor CNS (medulloblastoma, grade WHO IV, infratentorial. Left cerebellar hemisphere) (P9). The line colors of the spectra correspond to the colors of the Raman maps. Raman integration time for images 0.5 s, resolution step: 1 μm , laser excitation power: 10m W.



Astrocytoma , grade II

Figure 9: The tractography image (A) MRI image (B) H&E-stained histological image (C) stitching microscopy image (550 μm x 550 μm) (D) microscopy image (120 μm x 120 μm) (E) Raman image (50 μm x 50 μm) by basis analysis (F) and cluster analysis (G) and the characteristic vibrational Raman spectra in the fingerprint frequency region (H) Raman image (50 μm x 50 μm) by basis analysis (I) and cluster analysis (J) and the characteristic vibrational Raman spectra in the high frequency region (K) of the tumor (Astrocytoma fibrillare, grade WHO II) (P9). The line colors of the spectra correspond to the colors of the Raman maps. Raman integration time for images 1s for low frequencies and 0.5 s for high frequencies, resolution step: 1 μm , laser excitation power: 10m W.

Novel strategies of Raman imaging for brain tumor research

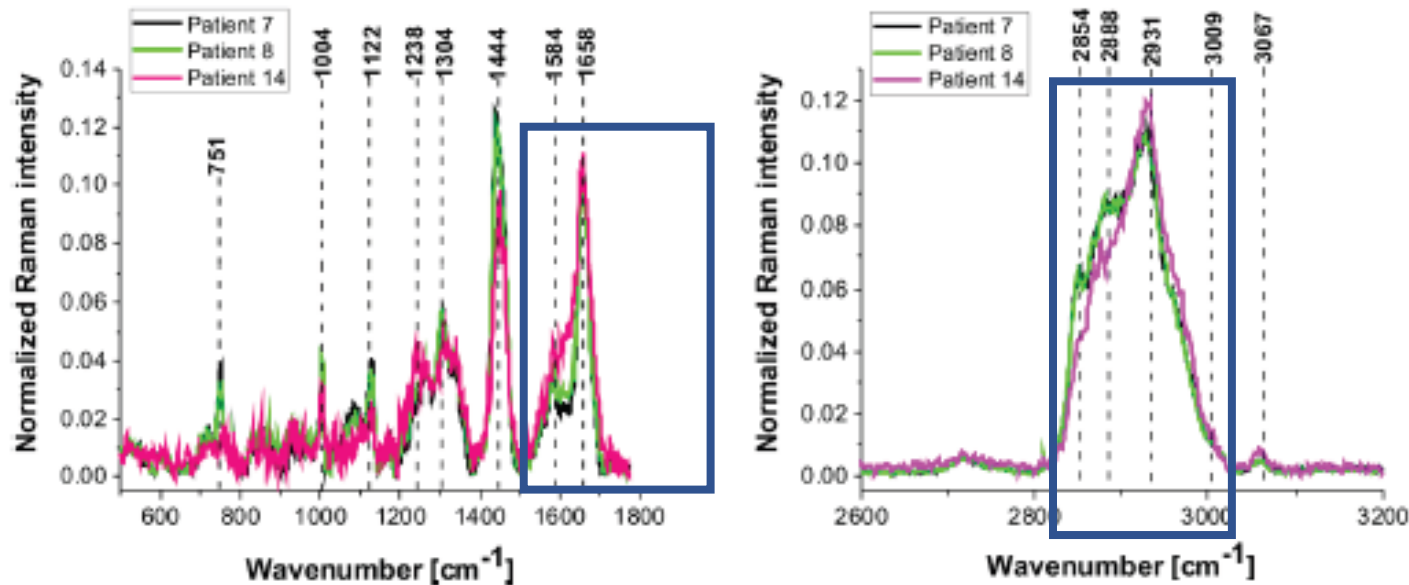


Figure 10: The average vibrational Raman spectra in the low and high frequency region for different areas of the low-grade brain tumor (astrocytoma, grade WHO I and II) (P7, P8, P14), Raman integration time for images 0.5 s for high frequency and 1s for low frequency region, resolution step: 1 μm , laser excitation power: 10m W.

Astrocytoma , grade II

Novel strategies of Raman imaging for brain tumor research

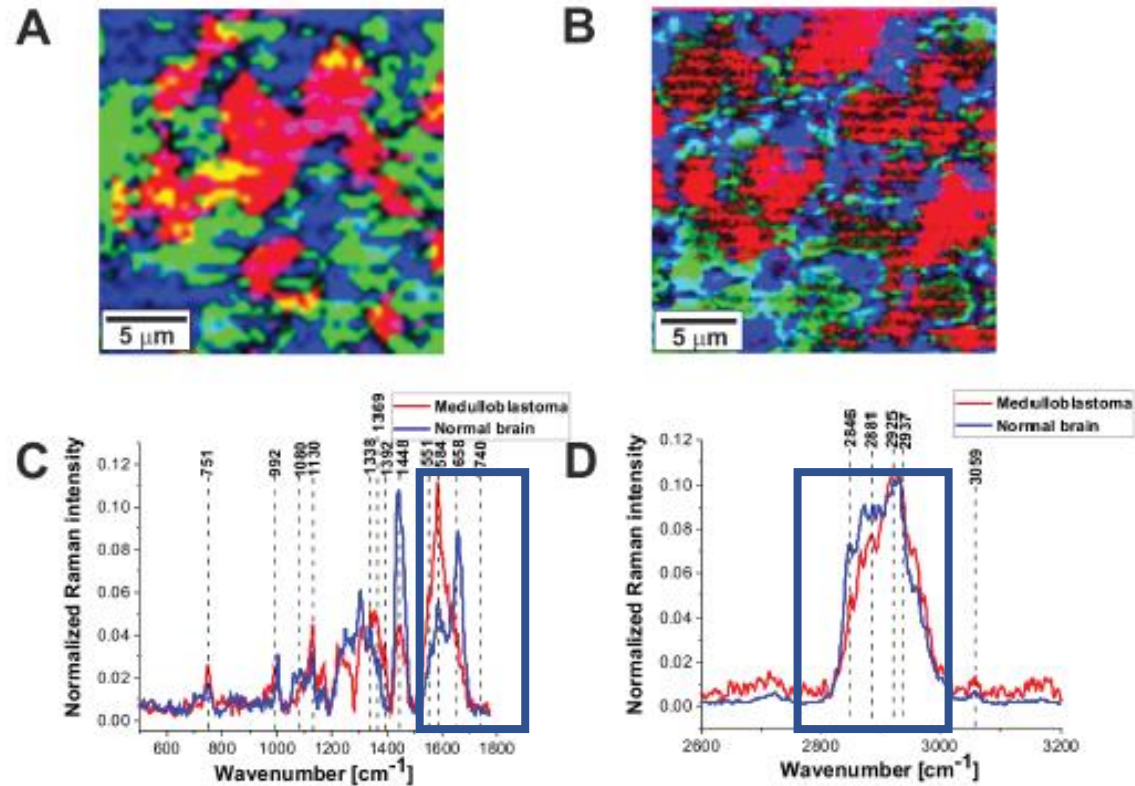


Figure 6: The comparison of the Raman images of the normal (A) and tumor (medulloblastoma, grade WHO IV) (B) tissues. The average vector normalized Raman spectra in the fingerprint region (C) and the high frequency region (D) for the high-grade medulloblastoma (medulloblastoma, grade WHO IV, infratentorial. Left cerebellar hemisphere) (P9), compared with the spectra for normal brain.

Medulloblastoma , grade IV

Novel strategies of Raman imaging for brain tumor research

- We have found that metabolism of proteins, nucleic acids, and lipids is markedly deregulated in malignant medulloblastomas. Our results indicates marked metabolic differences between high grade medulloblastoma and normal brain tissue. The Raman spectra for high-grade brain tumors show many significant differences compared to the normal brain spectra. Detailed inspection shows notable differences in vibrations of proteins, lipids, and nucleic acids:

Novel strategies of Raman imaging for brain tumor research

- 1) the high-grade tumors of central nervous system (medulloblastoma) exhibit enhanced level of β -sheet conformation and down-regulated level of α -helix conformation when comparing against normal tissue.
- 2) almost all tumors studied in the paper have increased Raman signals of nucleic acids. This increase can be interpreted as increased DNA/RNA turnover in brain tumors.
- 3) The ratio of Raman intensities I_{2930}/I_{2845} at 2930 and 2845 cm^{-1} is a good source of information on the ratio of lipid and protein contents. We have found that the ratio reflects the different lipid and protein contents of tumorous brain tissue compared to the non-tumor tissue. Almost all brain tumors have the Raman intensity ratios significantly higher than that found in non-tumor brain tissue, and indicates that the relative amount of lipids compared to proteins is significantly higher in the normal brain tissue.
- 4) We found that levels of the saturated fatty acids were significantly reduced in the high grade medulloblastoma samples compared with non-tumor brain samples and low grade astrocytoma. Differences were also observed in the n-6/n-3 PUFA (polyunsaturated FA) content for medulloblastoma and non-tumor brain samples. The content of the oleic acid (OA) was significantly smaller in almost all brain high grade brain tumors than that observed in the control samples. It indicates that the fatty acid composition of human brain tumors is different from that found in tumor-free brain tissue.

HOW DOES RAMAN SPECTROSCOPY AND IMAGING BENEFIT CANCER RESEARCH?

•POLARITY OF CELLS

The cause-and-effect relationship between metabolic/epigenetic changes and polarity disruption of tissue structure is not clear



Journal of Molecular Liquids

Available online 1 June 2017
In Press, Accepted Manuscript



Apical-basal polarity of epithelial cells imaged by Raman microscopy and Raman imaging: Capabilities and challenges for cancer research

H. Abramczyk  , B. Brozek-Pluska

H. Abramczyk, B. Brozek-Pluska, Apical-basal polarity of epithelial cells imaged by Raman microscopy and Raman imaging: Capabilities and challenges for cancer research, J Mol Liq, 2017, S0167-7322(17)30910-8

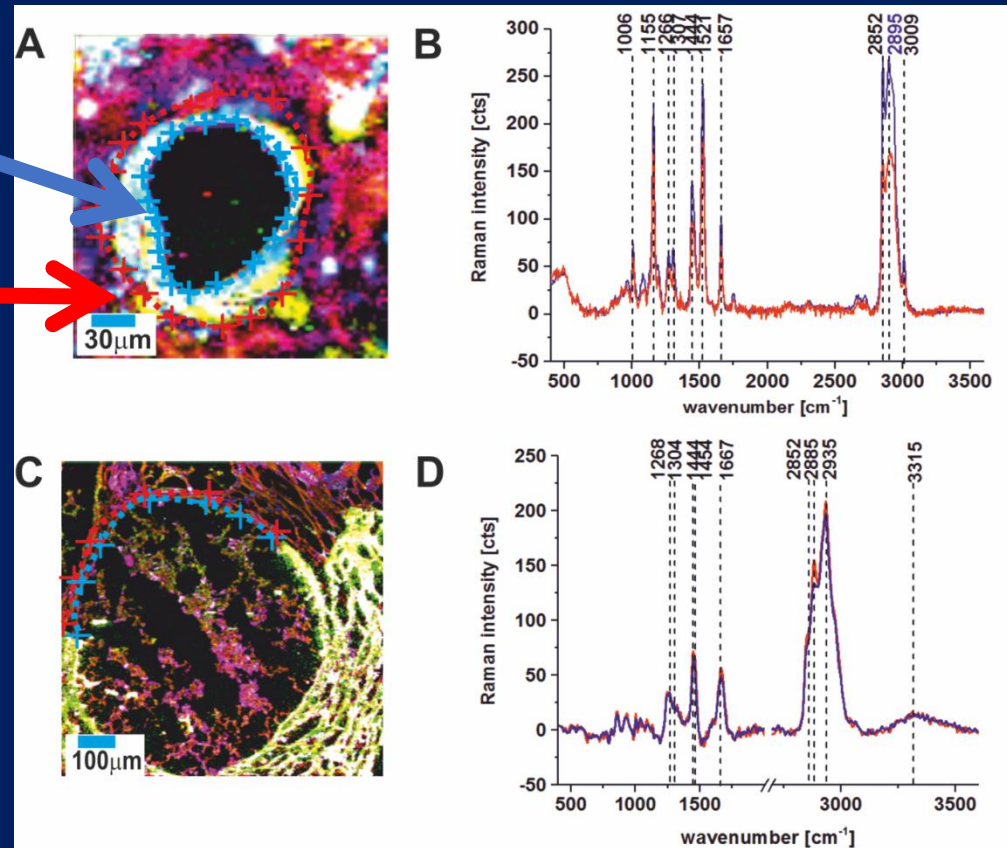
No technology has proven effective for detecting polarity changes in cancer

- **The biochemistry of cancer due to metabolic or epigenetic alterations is related to second important feature of cells – polarity of cells**
- There is also a significant need to develop ways to define and quantify polarity changes in cancer. The conventional method of monitoring the localization of membrane proteins such as E-cadherin, ZO-1 and mucins to monitor apical-basal polarity is misleading and inconclusive [Annu Rev Cell Dev Biol. 2012 ; 28: 599–625].

APICAL-BASAL POLARITY OF EPITHELIAL CELLS BY RAMAN IMAGING

APICAL

BASAL

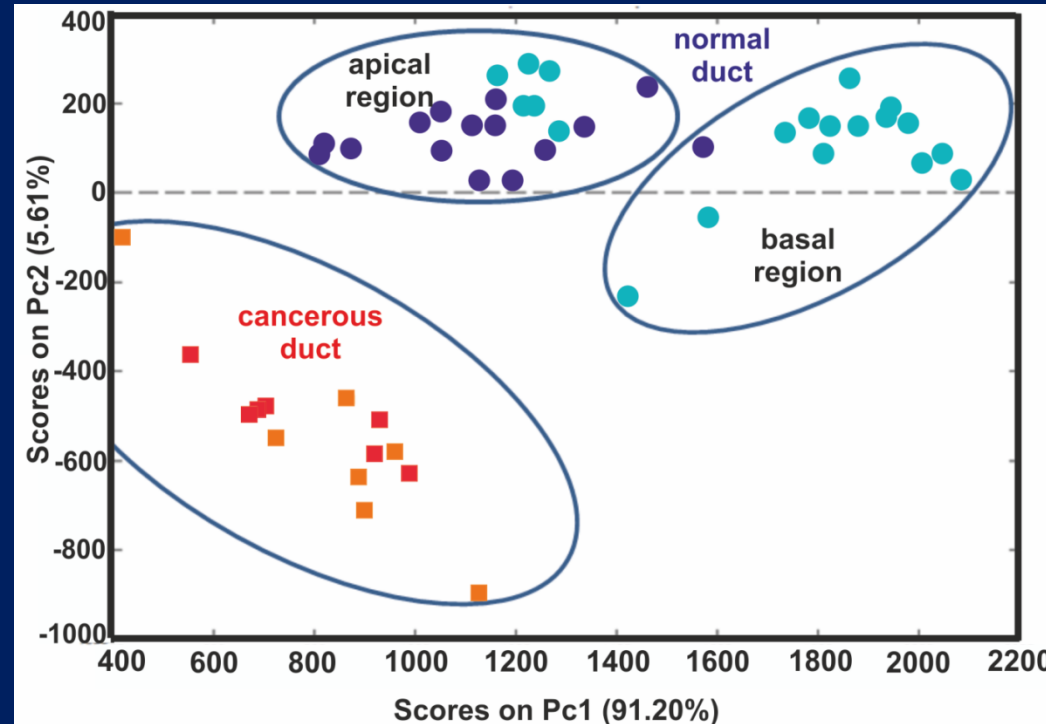


Apical - basal polarity of epithelial cells is critical in the correct functioning of an organism and constitutes an important parameter to assess epithelial integrity and homeostasis. Loss of cell polarity results in epithelial tissue disorganization and is a hallmark of cancer development.

Abramczyk H. J. Mol. Liquids, 2017

The common feature of cancer development is the increased loss of cell polarity that results in epithelial tissue disorganization. Despite intense interest in determining the origin of tumor tissue disorganization, the function of cell polarity remains unclear. In the proposal we will monitor the epithelial cell asymmetry and concentration gradient of main constituents of the cells along the apical-basal axis and monitor ordering at the apical membranes compared to basal membranes in normal and cancerous human cells.

APICAL-BASAL POLARITY OF EPITHELIAL CELLS BY RAMAN IMAGING



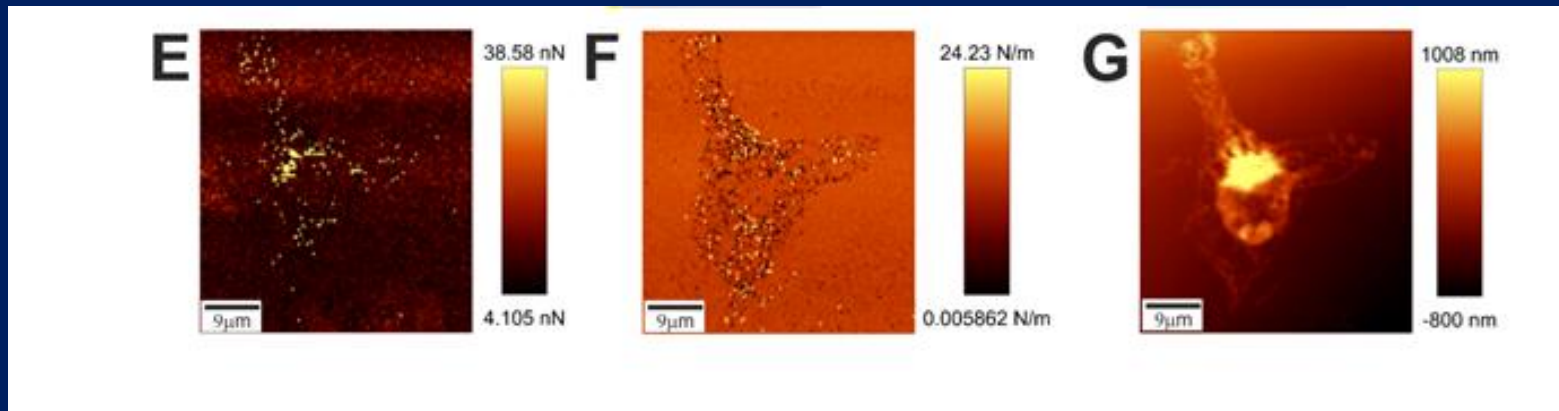
Abramczyk H. J. Mol. Liquids, 2017

The common feature of cancer development is the increased loss of cell polarity that results in epithelial tissue disorganization. Despite intense interest in determining the origin of tumor tissue disorganization, the function of cell polarity remains unclear. We traced the epithelial cell asymmetry and concentration gradient of main constituents of the cells along the apical-basal axis and monitored ordering at the apical membranes compared to basal membranes in normal and cancerous human breast duct.

Nanomechanical signatures of cancer

The ability of epithelial cells due to polarity to interact with each other and with the surrounding environment to maintain tissue organization that is lost in cancer is related to next important feature of cells – stiffness and adhesion.

U-87 MG cell (glioblastoma - brain)



adhesion image (E), stiffness image (F) and topography image (G) of air-dried cell

AFM stiffness and adhesion of cancer cells and tissue by DPFM

To calculate the stiffness of the sample the information on the slope of the rising part of the DPFM curve is needed. Fig. II. presents the force-distance curve recorded by DPFM mode, the fitting range (in light blue) and the fitting curve (in dark blue).

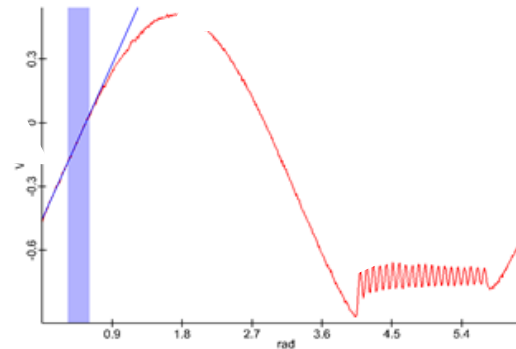


Fig. II. The force-distance curve recorded by DPFM, the selected range of interest with the fitting curve.

We will measure cancer cells and tissues by DPFM to learn how rigid, how sticky, how adherent cancer cells are.

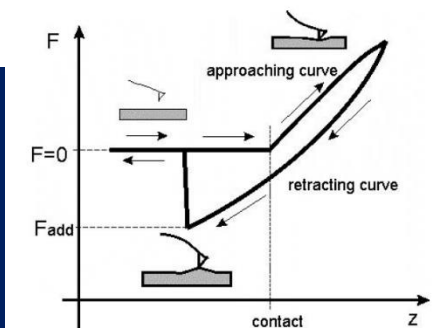
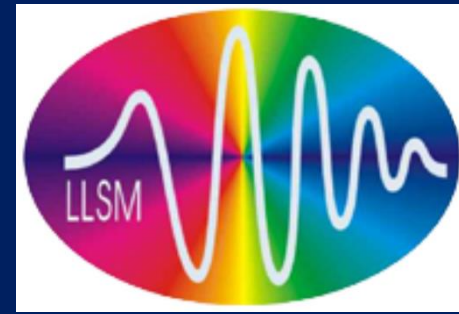


Figure 2. A typical force-distance curve recorded by AFM in force mode. Both the approaching and retracting curves are shown.



Novel strategies for brain tumor research

2017

www.impactjournals.com/oncotarget/

Oncotarget, Advance Publications 2017

Novel strategies of Raman imaging for brain tumor research

Imiela Anna¹, Polis Bartosz², Polis Lech² and Abramczyk Halina¹

¹Lodz University of Technology, Institute of Applied Radiation Chemistry, Laboratory of Laser Molecular Spectroscopy, 93-590 Lodz, Poland

²Polish Mother's Memorial Hospital Research Institute, Department of Neurosurgery and Neurotraumatology, 3-338 Lodz, Poland

Correspondence to: Abramczyk Halina, **email:** abramczy@mitr.p.lodz.pl

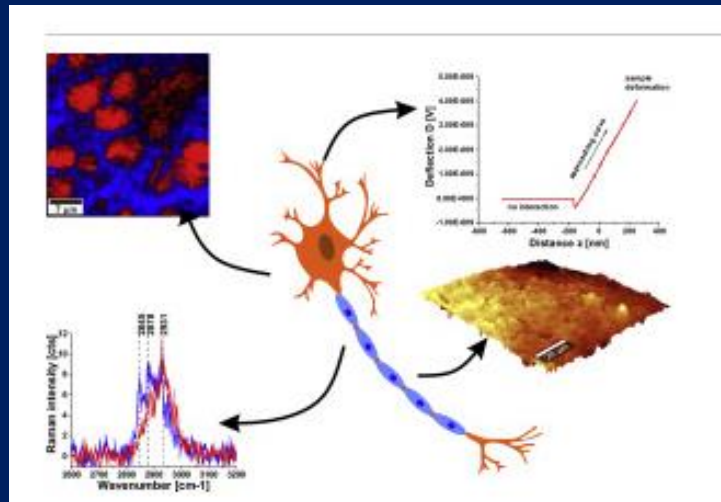
Keywords: Raman spectroscopy, Raman imaging, brain tumor, CNS, iodine number

Received: January 21, 2017

Accepted: April 29, 2017

Published: July 28, 2017

The biochemical and nanomechanical signatures of brain cancer



A. [Imiela, B. Polis, L. Polis, H. Abramczyk, Novel strategies of Raman imaging for brain tumor research, Oncotarget, 2017, 8:85290-85310](#)

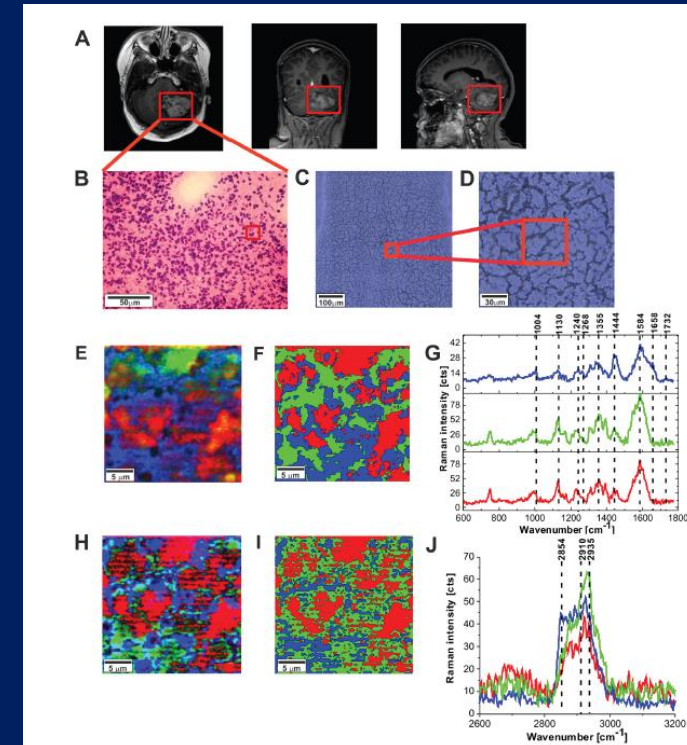
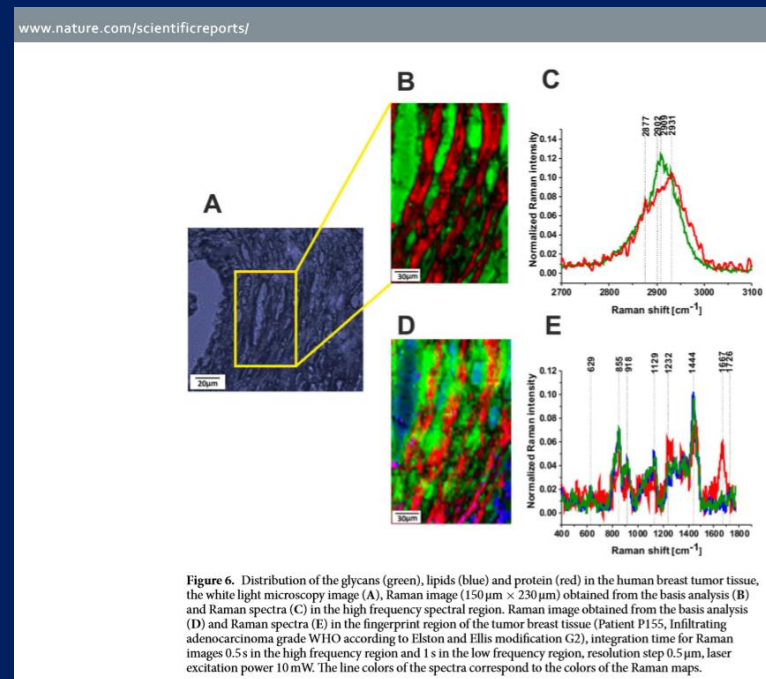


Figure 5: The MRI image (A) H&E-stained histological image (B) stitching microscopy image (520 μm x 520 μm) (C) microscopy image (155 μm x 155 μm) (D) Raman images (50 μm x 50 μm) obtained by basis analysis (E) and cluster analysis (F) and the characteristic vibrational Raman spectra in the fingerprint frequency region (G) Raman images (50 μm x 50 μm) obtained by basis analysis (H) and cluster analysis (I) and the characteristic vibrational Raman spectra in the high frequency region (J) of the tumor CNS (medulloblastoma, grade WHO IV, infratentorial. Left cerebellar hemisphere) (P9). The line colors of the spectra correspond to the colors of the Raman maps. Raman integration time for images 0.5 s, resolution step: 1 μm, laser excitation power: 10m W.

Visualization techniques of glycocalyx- Raman imaging wins once again

- Because of the functional importance of the epithelial glycocalyx, development of direct visualization techniques is crucial to establish its exact role.
- The glycocalyx can be labeled by administration of specific markers that attach to one or more of its components, making them fluorescent or detectable, but Raman imaging wins once again.



M. Kopeć, A. Imiela, H. Abramczyk, Monitoring glycosylation metabolism in brain and breast cancer by Raman imaging, Scientific Reports, Nature, 2019

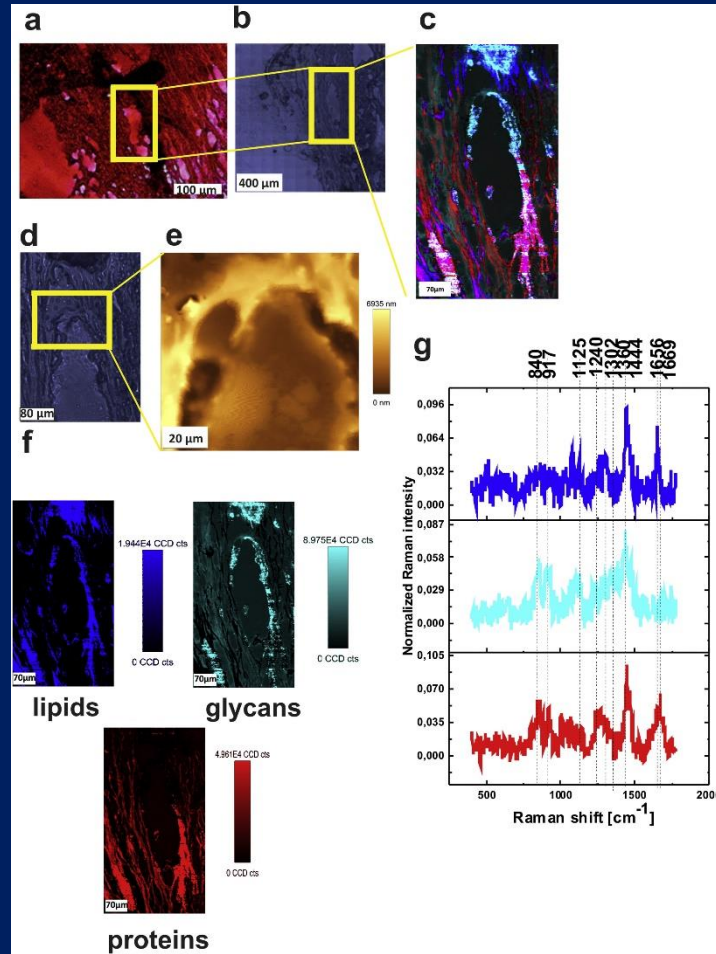


Fig. 1. Histological image, Raman images, AFM image and Raman spectra of tumor mass in human breast tissue in the fingerprint spectral region.

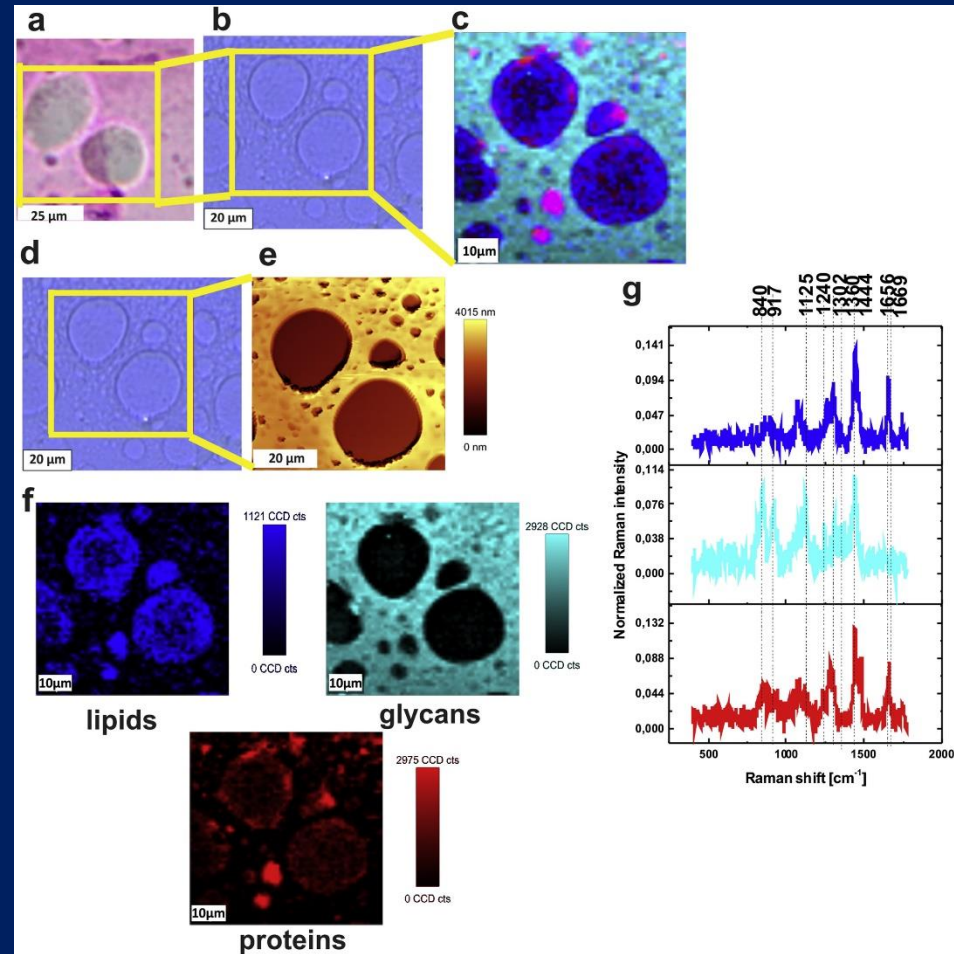
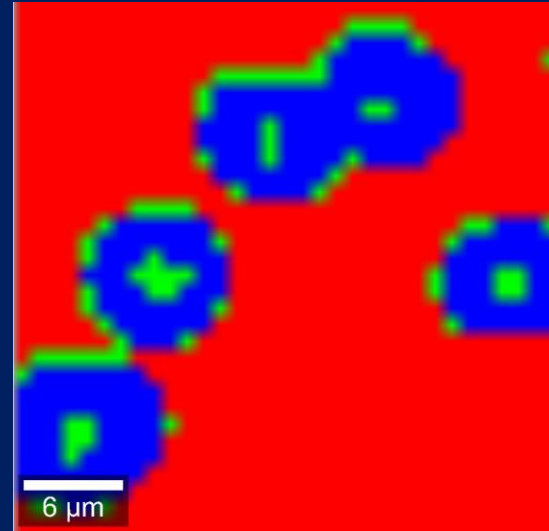
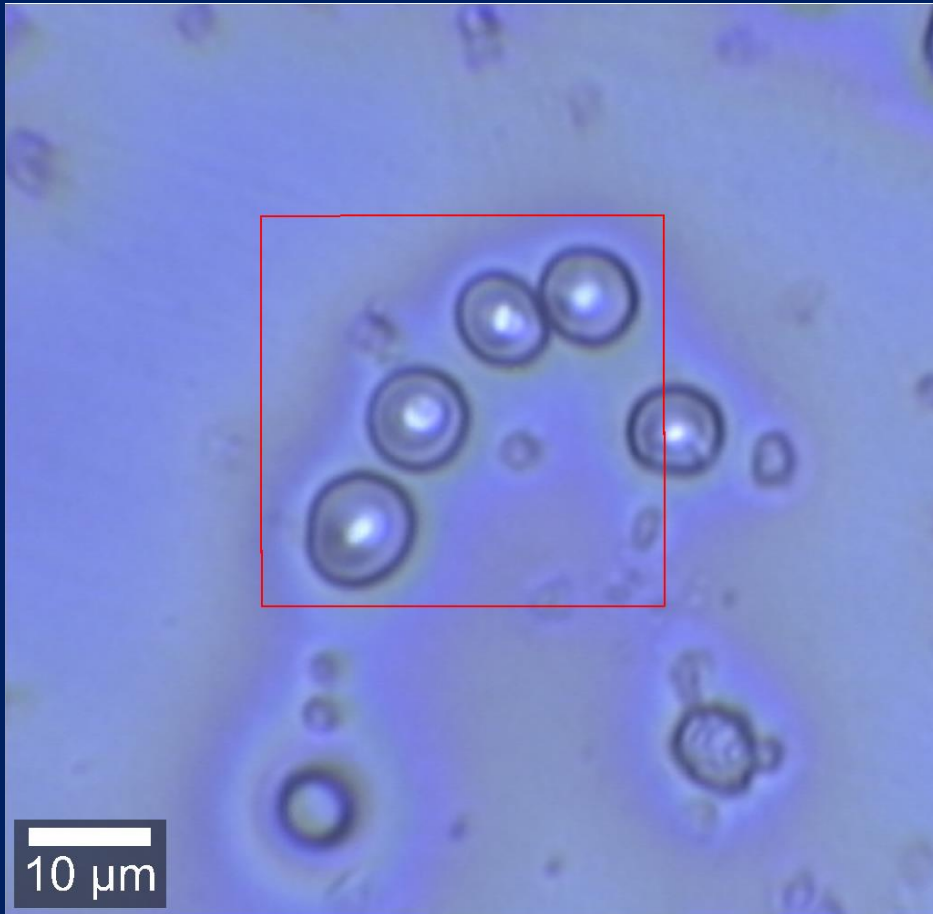


Fig. 2. Histological image, Raman images, AFM image and Raman spectra of a normal breast tissue from a negative margin of a tumor mass from the same patient (G3, ductal cancer P149).

ELUSIVE OUTCOMES IN THE WAR ON CANCER

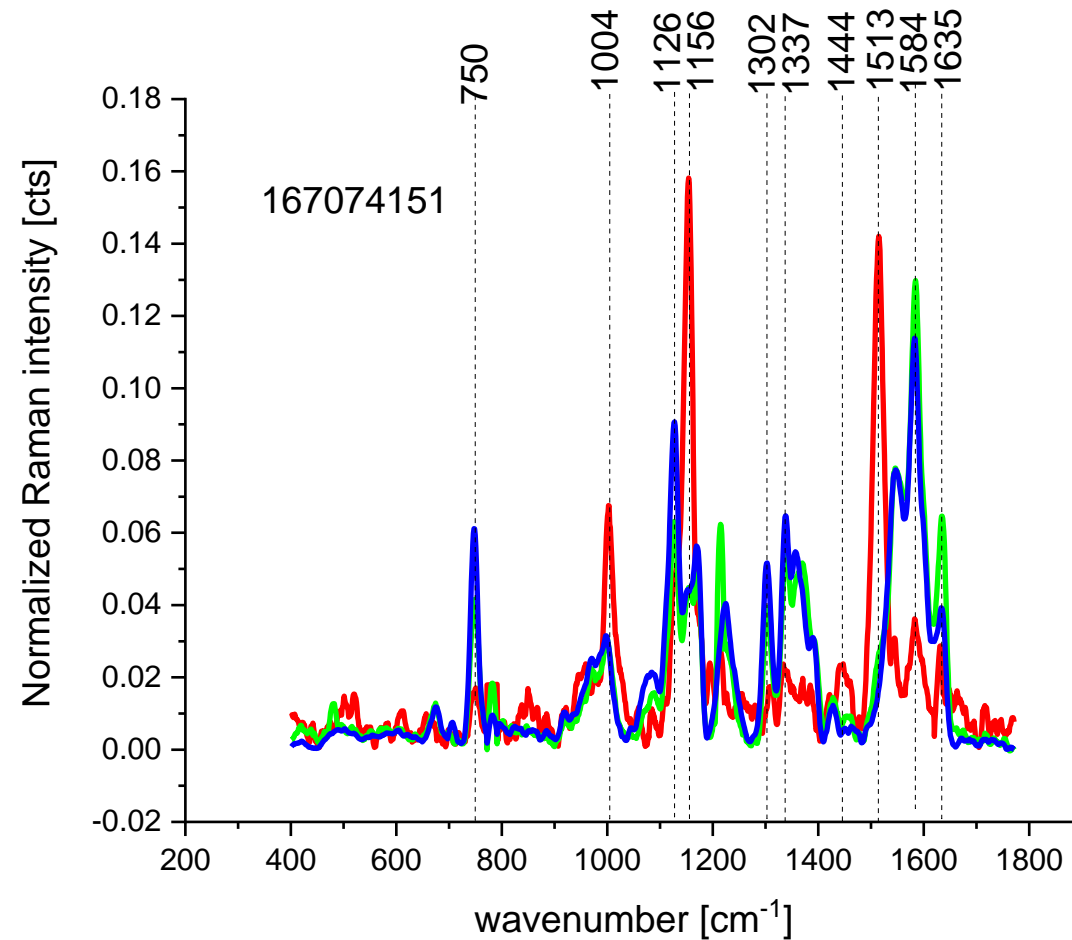
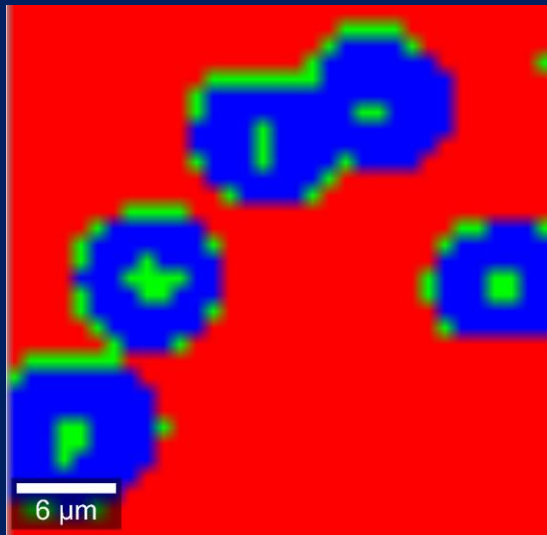
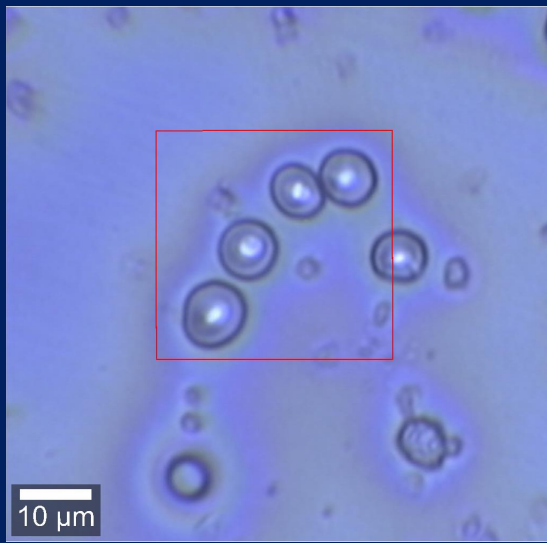
In a recent study, TCGA reported that over 30,000 mutations were identified in breast cancer tissue (Cancer Genome Atlas Network, 2012). The evidence seems to suggest that science based only on cancer genomics, cannot be continued.

KREW



W skład krwi wchodzi składniki komórkowe (ok. 44%) i osocze (ok. 55%). Dalsze składniki krwi to hormony, rozpuszczone gazy oraz substancje odżywcze (cukier, tłuszcze i witaminy), transportowane do komórek, a także produkty przemiany materii (np. mocznik i kwas moczowy), niesione z komórek do miejsc, gdzie mają być wydalone.

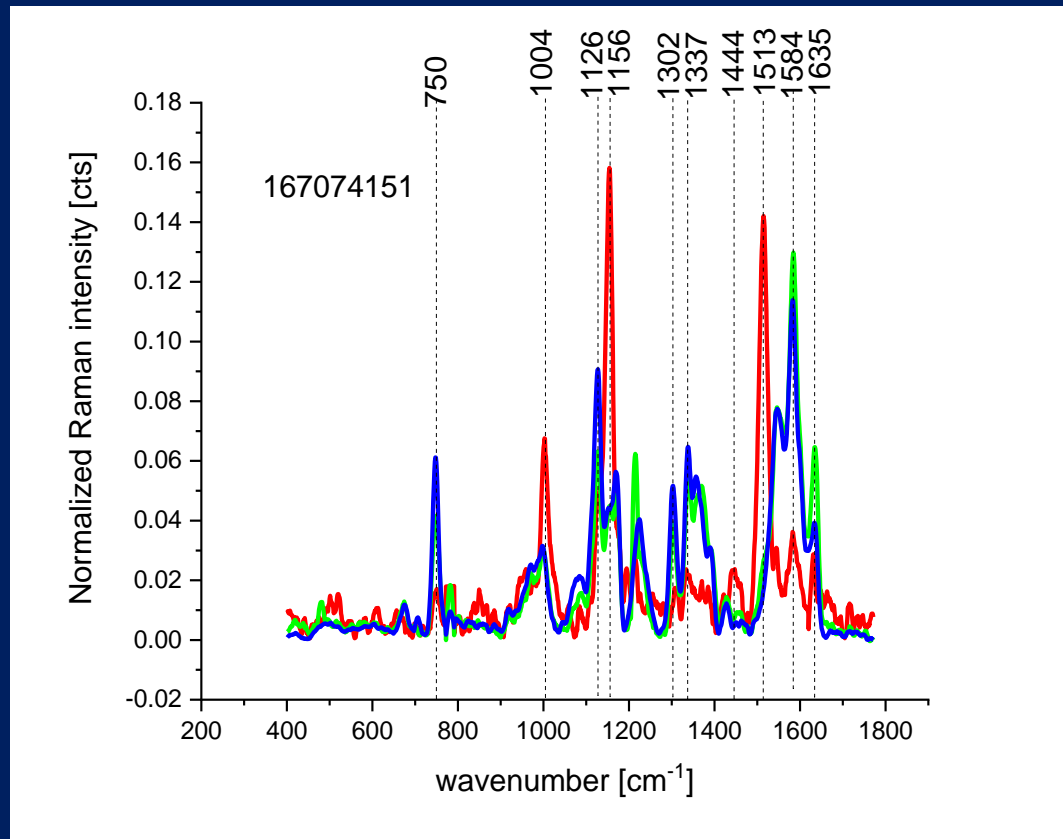
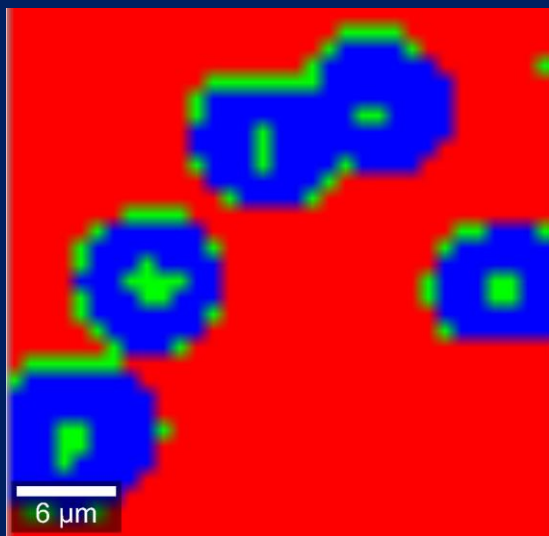
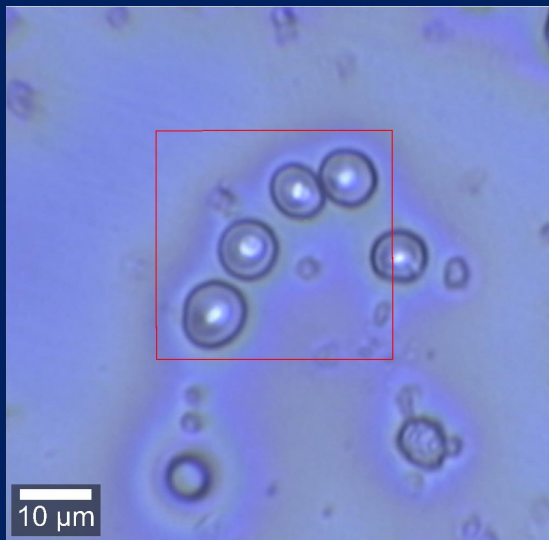
151_kro



Osocze czyli wodny roztwór (90% wody) białek, soli i związków chemicznych o niewielkiej masie cząsteczkowej, jak np. monosacharydy. Zawiera głównie jony sodu, potasu, magnezu, wapnia oraz fosforany i chlorki.

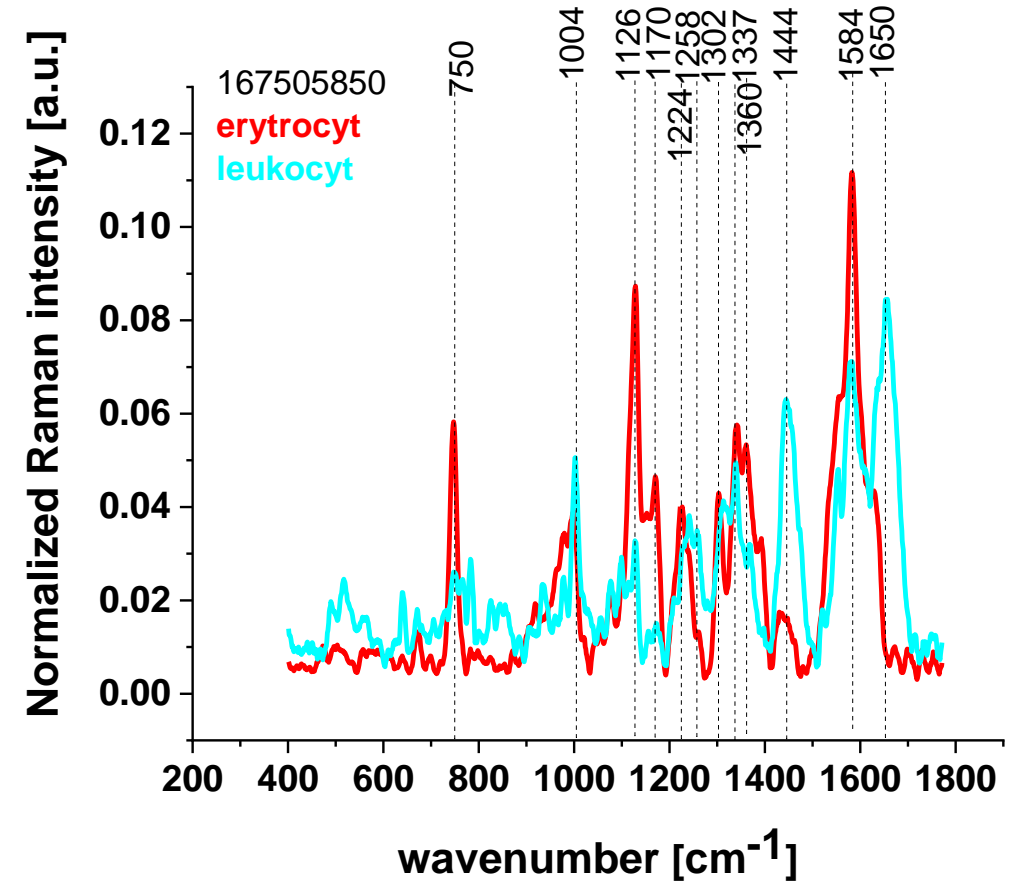
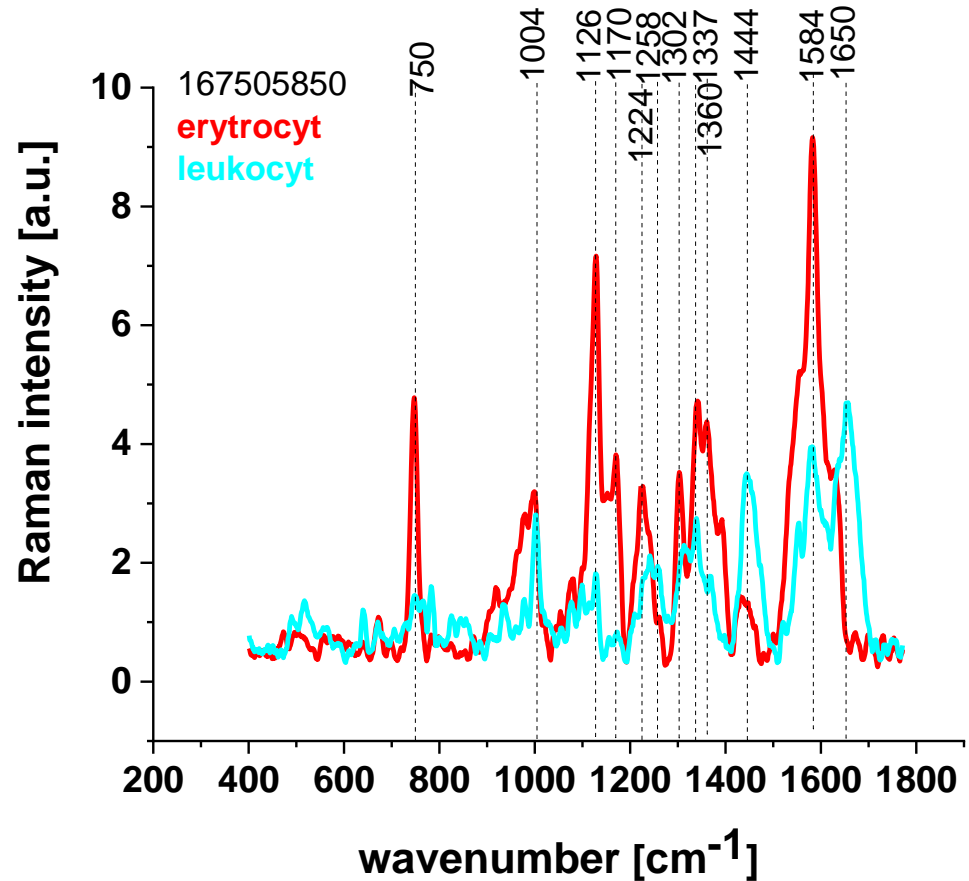
167074151 BRCA1/ (BRCA2)

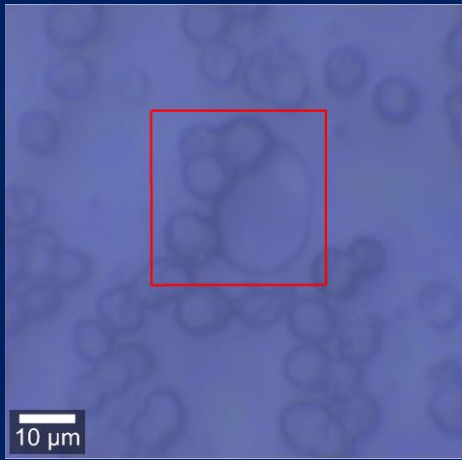
151_krew



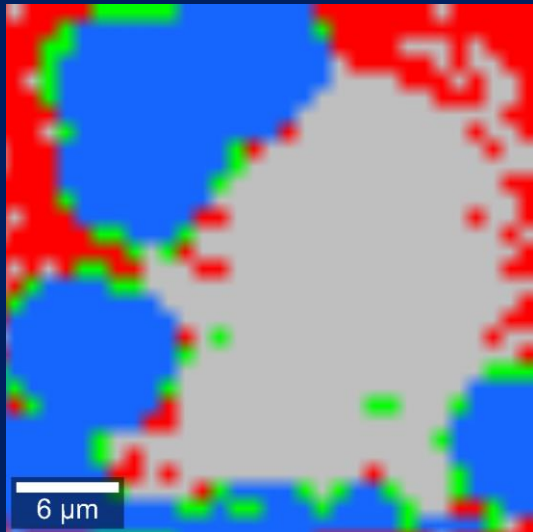
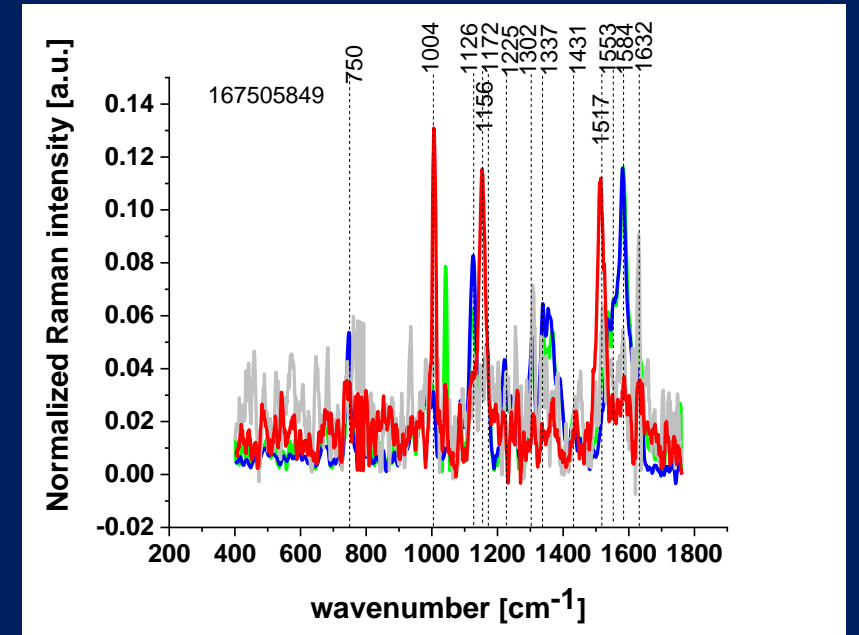
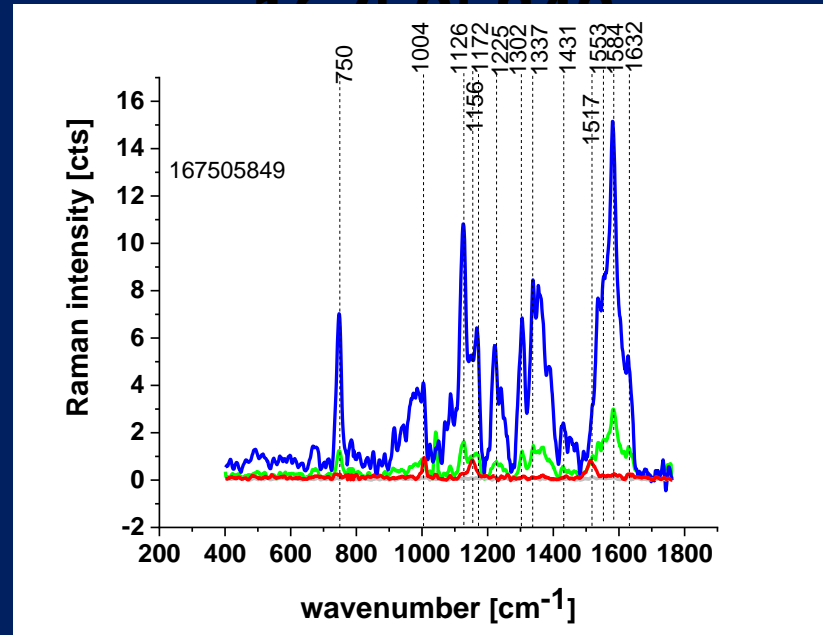
Erytrocyty (czerwone krwinki) – u człowieka nie posiadają jądra komórkowego oraz licznych organelli komórkowych – aktywność metaboliczna jest ograniczona, żeby zmniejszyć zużycie tlenu, który mają te komórki transportować. Erytrocyty mają kształt dwuwklęsłego dysku, a ich średnica wynosi 7–8 mikrometrów. Erytrocyty stanowią ok. 90–94% ogółu elementów morfotycznych. U człowieka występują w liczbie 4,5–5,5 mln/mm³. U innych kręgowców erytrocyty mogą posiadać jądro. Służą do transportu tlenu i dwutlenku węgla. Zawierają hemoglobinę, białko odpowiedzialne za przyłączanie i transport tlenu w krwi; złożone z właściwego białka – *globiny* oraz *grupy hemowej*, która razem z żelazem tworzy kompleks

167505850_porównanie widma erytrocytów i leukocytów





erytrocyt i leukocyt



167505849 brca1

Leukocyty lub białe krwinki u człowieka prawidłowo występują w liczbie 4–9 tys/mm³. Są to komórki jądrowe, o średnicy 6–40 mikrometra, odpowiadają za odpowiedź immunologiczną. Występują w kilku postaciach jako:

- *agranulocyty* – cytoplazma nie zawiera ziarnistości
 - monocyty
 - limfocyty
- *granulocyty* – cytoplazma zawiera ziarnistości
 - neutrofile – granulocyty obojętnochłonne
 - bazofile – granulocyty zasadochłonne
 - eozynofile – granulocyty kwasochłonne.

Granulocyty odpowiadają za niespecyficzną odpowiedź immunologiczną, natomiast limfocyty i monocyty biorą udział w obronie specyficznej.

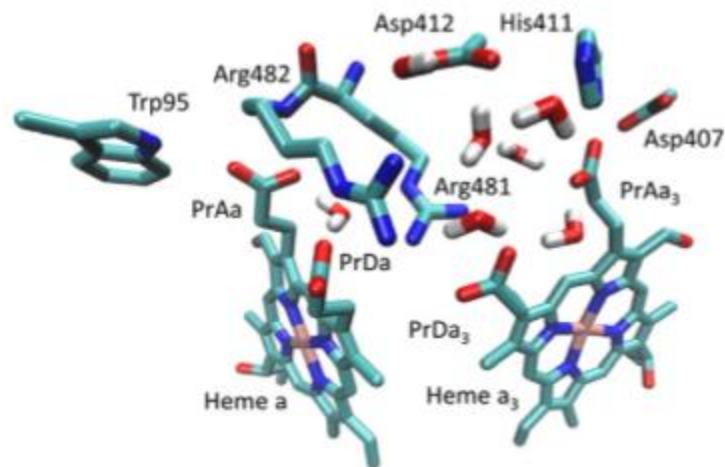


Fig. 1. Structure of the heme *a* and *a*₃ environment of CcO from *Rhodobacter sphaeroides* (PDB 1M56).

PrDa and therefore these propionates are accessible for external protons. These findings are in agreement with the measurements of Behr et al. [13], who observed a protonated PrDa in the fully reduced enzyme using CcO variants with ¹³C modified propionic acids. However, in their work, PRDa was considered to be the only protonated propionic acid, whereas we observe partial protonation of at least three propionates when both hemes are reduced. From electrostatic considerations, heme *a* reduction would favor protonation of one of its own propionates [36,37]. However, as this process would terminate further electron and proton movement, direct proton transfer from Glu286 to PrDa must be highly inefficient. Only in a situation, where heme *a*₃ is reduced, protonation of PrDa would not hinder further progression of the oxygen reaction and the proton pumping process. This is in line with our results: we do not see a protonated PrDa if heme *a*₃ is oxidized ruling

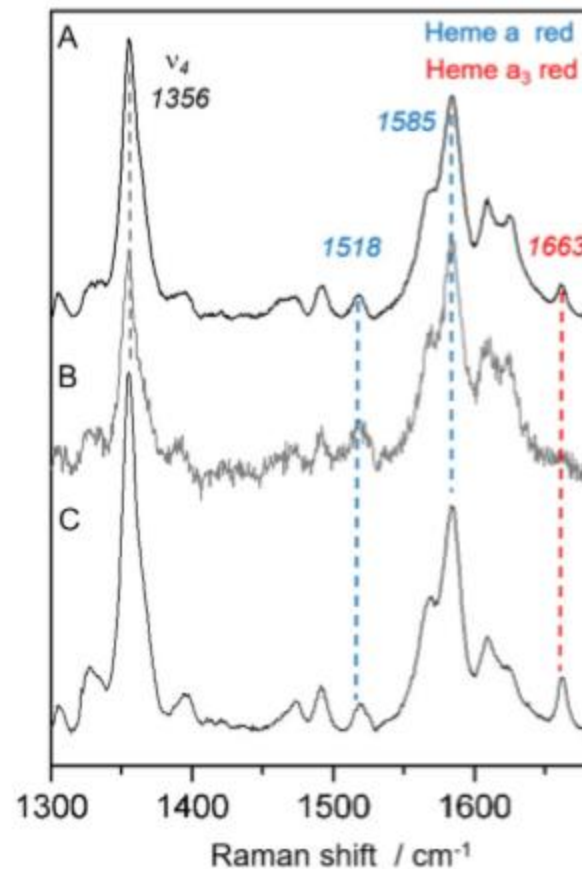
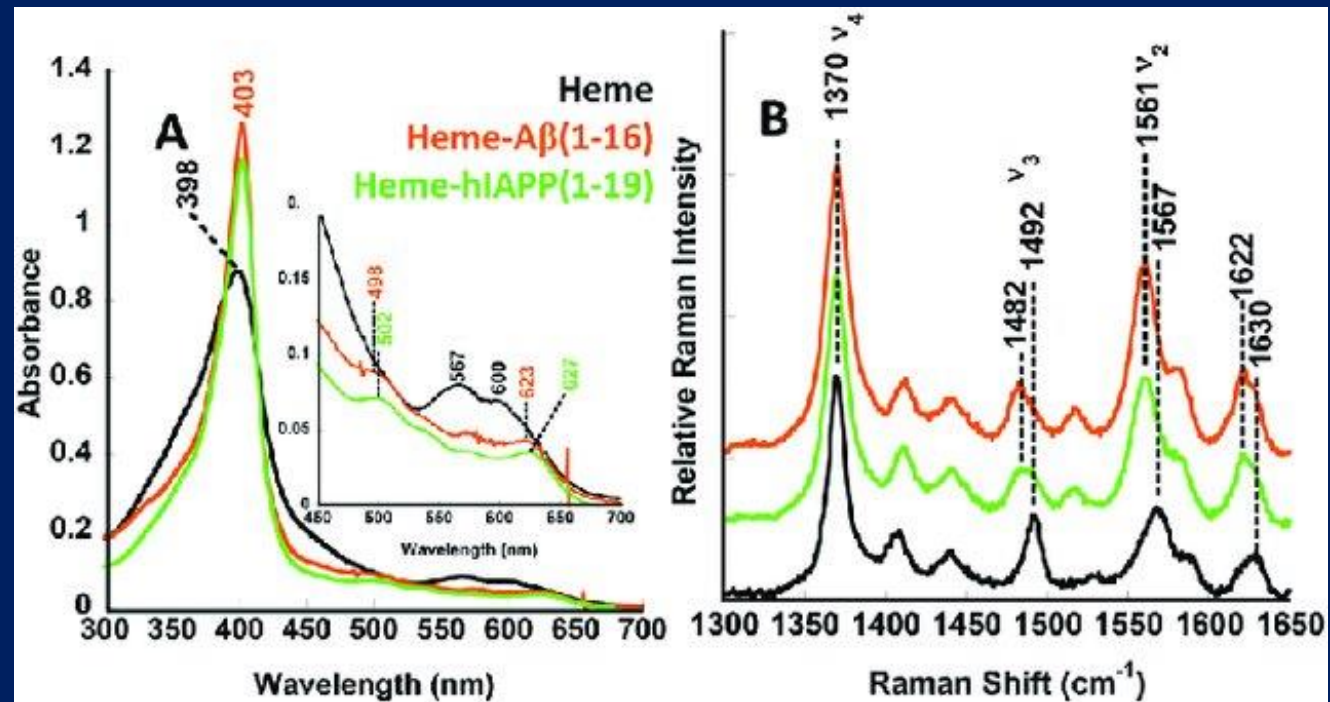


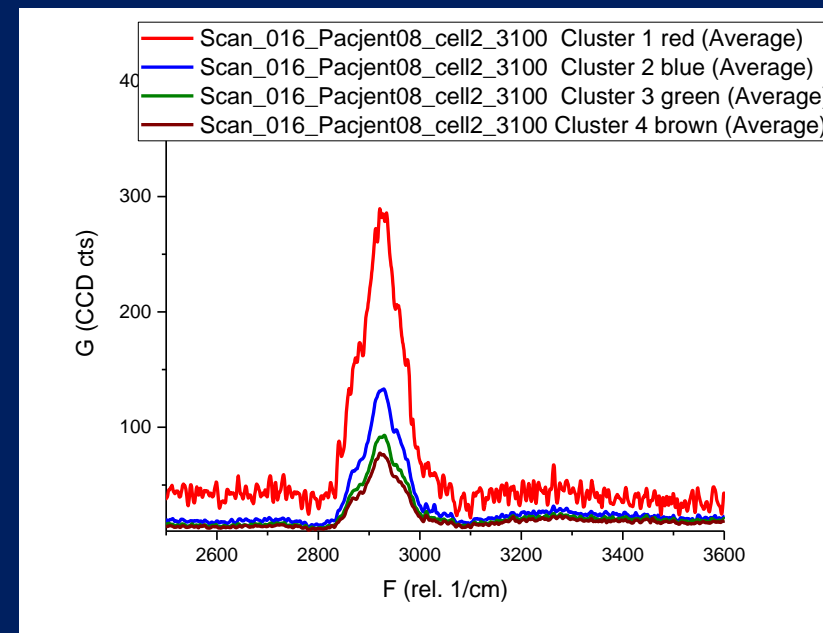
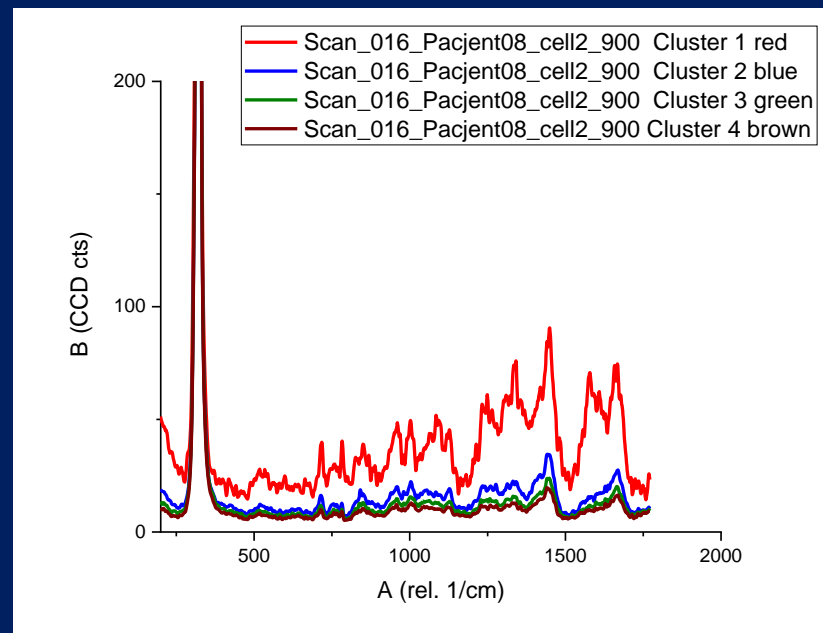
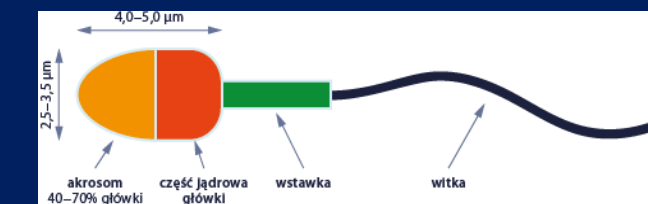
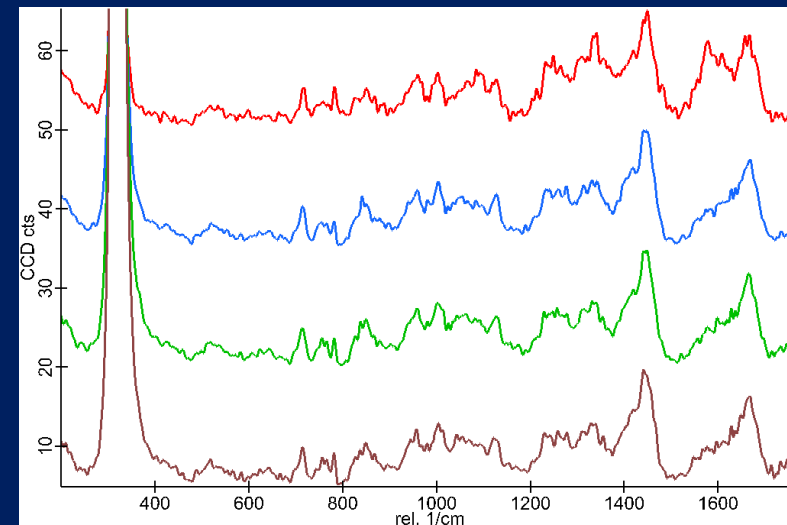
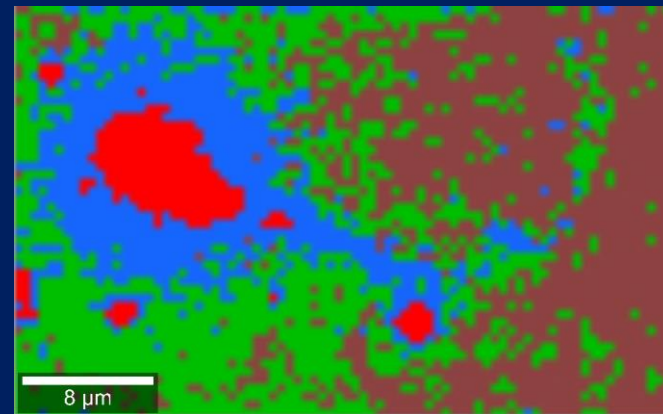
Fig. 2. SERR spectra of CcO in the high frequency region recorded under different conditions. (A) Open circuit potential, traces of oxygen and presence of dithionite, (B) electrode potential of -250 mV and traces of oxygen, (C) electrode potential of -400 mV in the absence of oxygen. The peaks assigned with blue numbers are associated with reduced heme *a*, whereas the peak assigned with a red number is associated with reduced heme *a*₃. All potentials are presented vs. Ag/AgCl. Laser excitation is 442 nm.

reduced heme-Ab

Fe-oxy adducts of heme-A β and heme-hIAPP complexes:
Intermediates in ROS generation



spermatozoid fertility



cellular signal transduction

- **Vitamin A plays an important role in cellular signal transduction in many vital processes. Proton gradient triggers the synthesis ATP. There are two types of generation of proton gradient.**
-
- **the light-activated mechanism in vision processes (rhodopsin family)**
-
- **the electron transport chain forms a proton gradient across the inner mitochondrial membrane, which drives the synthesis of ATP via chemiosmosis.**
-

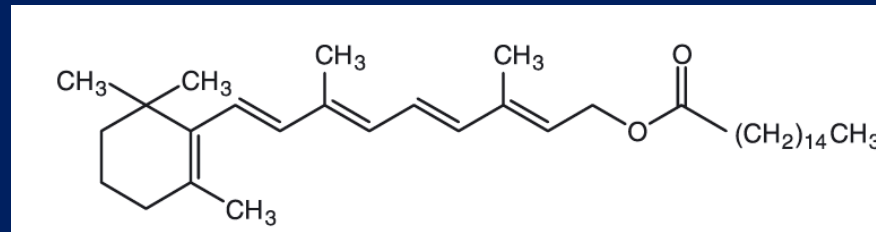
rola retinoidów w przewodzeniu sygnałów komórkowych

- Aby zrozumieć rolę retinoidów w przekazywaniu sygnałów komórkowych w wielu ważnych procesach w organizmach żywych, musimy znaleźć odpowiednie narzędzia do wykrywania retinoidów *in vivo* w celu monitorowania dystrybucji retinoidów w komórkach i tkankach oraz dynamiki czasowej.

Moja prezentacja nie jest w pełni wyczerpująca, ale raczej przedstawia przegląd ostatnich postępów z perspektywy badań w LLSM.

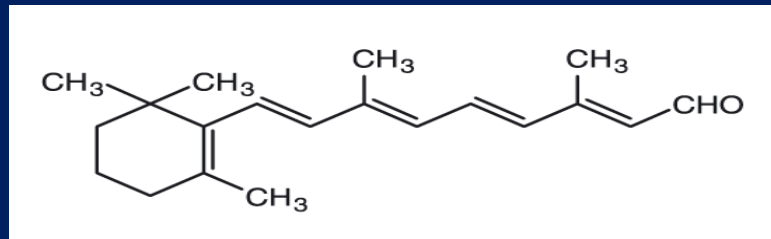
RETINOIDY

ester



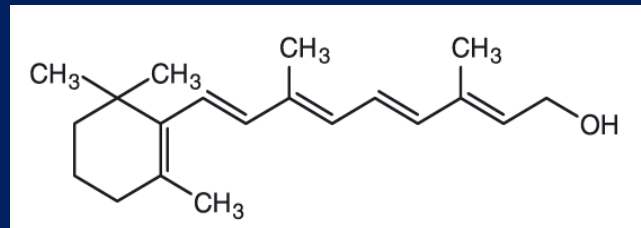
Retinyl palmitate

aldehyd



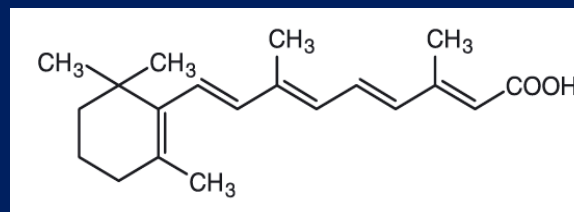
All-trans retinal

alkohol



Retinol

Podstawowa struktura hydrofobowej cząsteczki retinoidu składa się z cyklicznej grupy końcowej, polienowego łańcucha bocznego i polarnej grupy końcowej



Retinoic acid

Metabolizm retinoidów u kręgowców

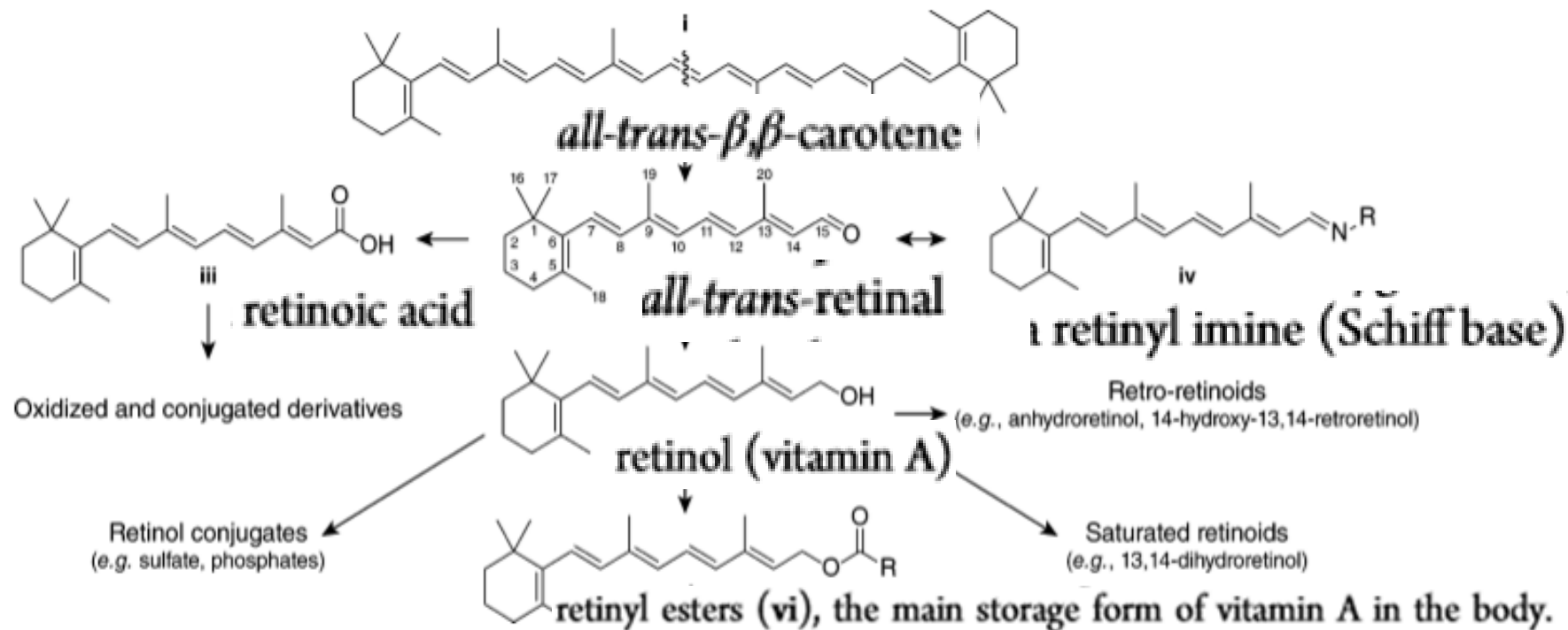
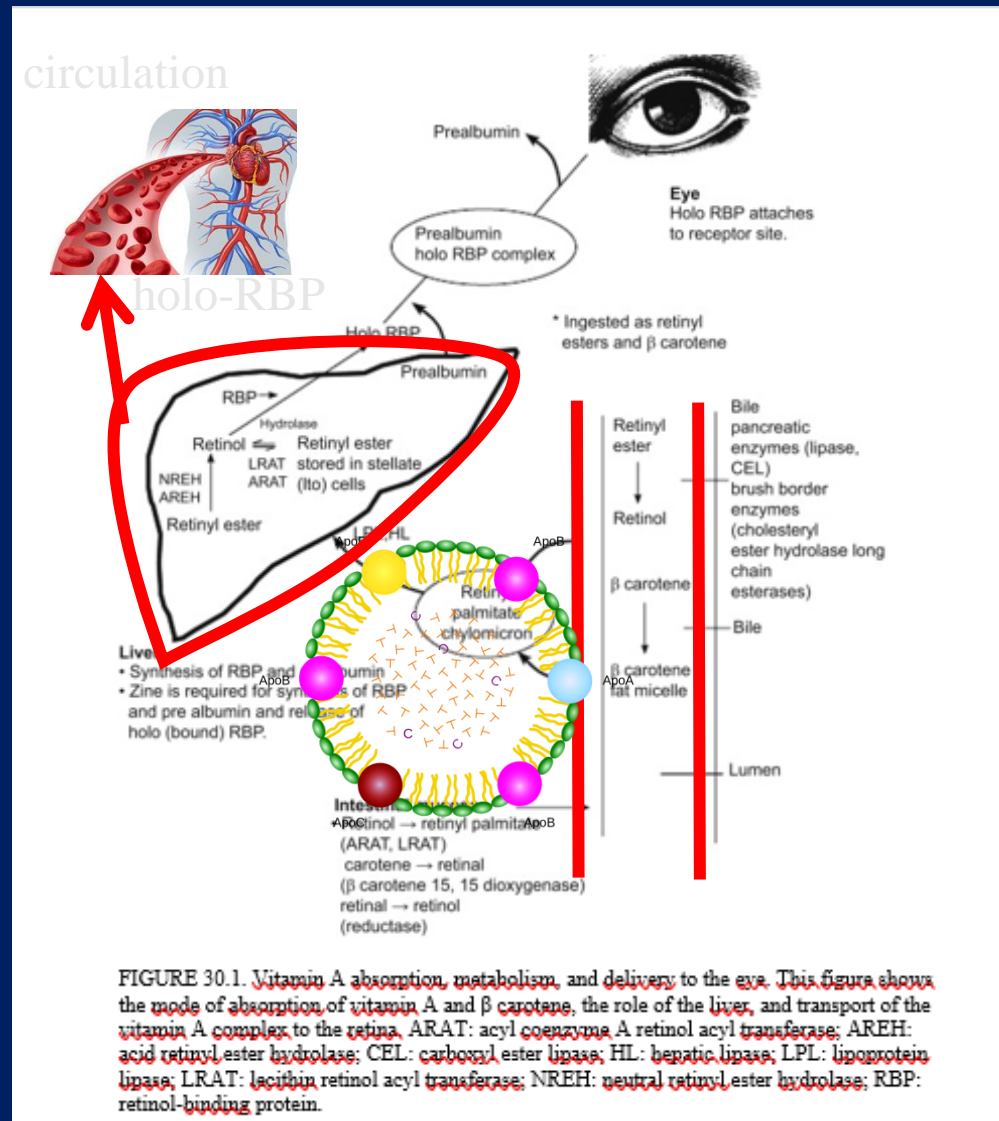


Figure 5. Retinoid metabolism in vertebrates. Dietary *all-trans- β,β -carotene* (i), obtained primarily from plants, is oxidatively cleaved in a symmetric manner by β -carotene monooxygenase I (BCMO I), yielding two molecules of *all-trans-retinal* (ii). Retinal can reversibly combine with an amino group to form a retinyl imine (Schiff base) (iv). Retinal is also subject to oxidation and reduction to form retinoic acid (iii) and retinol (vitamin A) v, respectively, the latter in a physiologically reversible manner. Retinoic acid can be converted into several conjugated and/or oxidized derivatives, some of which exert biological effects. Retinol also can be converted into several derivatives including retro-retinoids, saturated retinols, and phosphate conjugates. Retinol is also reversibly esterified to produce retinyl esters (vi), the main storage form of vitamin A in the body.

Wchłanianie witaminy A, metabolizm i dostarczanie do oka



Wątroba gromadzi witaminę A w postaci estru retinolu, gdy spożycie witaminy A przekracza zapotrzebowanie organizmu. W warunkach optymalnych dla witaminy A większość uwolnionego retinolu jest przenoszona z hepatocytów do komórek gwiaździstej wątroby, gdzie retinol jest wiązany z CRBP2 i reestryfikowany przez LRAT, a następnie przechowywany jako estry retinolu w cytoplazmatycznych kropelkach lipidów.³³ Przechowywanie służy również jako mechanizm detoksykacji, usuwając nadmiar „wolnego” retinolu. Gdy tkanki obwodowe wymagają retinolu, te zmagazynowane estry ulegają hydrolizie, a retinol jest ponownie mobilizowany do hepatocytów. Hepatocyty są również głównym miejscem syntezy RBP. Nowo uwolniony retinol łączy się z apo-RBP, tworząc kompleks holo-RBP, który jest uwalniany z wątroby do krwiobiegu.

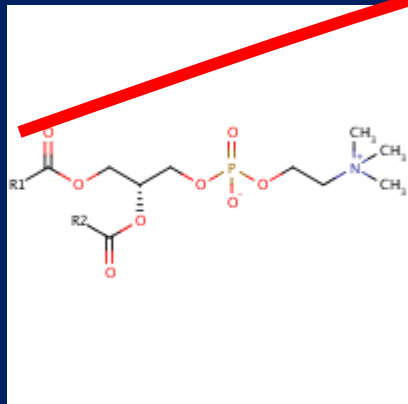
Komórkowe białka wiążące retinoidy (CRBP) (ang. Cellular retinoid-binding proteins (CRBP))

Chylomikrony transportują zawarte w pożywieniu lipidy i estry z jelit do innych miejsc w organizmie.

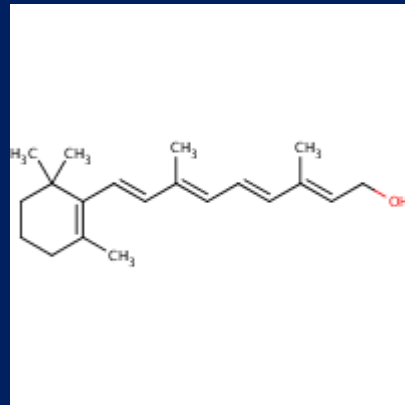
Komórki gwiaździste wątroby
 Komórki gwiaździste wątroby znajdują się pomiędzy hepatocytami a małymi naczyniami krwionośnymi w wątrobie. Charakteryzują się obecnością kropelek lipidowych i cienkimi wypustkami rozciągającymi się wokół naczyń krwionośnych. Ich aktywacja w uszkodzonej wątrobie prowadzi do wydzielania kolagenu i tworzenia się tkanki bliznowatej, prowadząc do przewlekłego zwłóknienia lub marskości.

LRAT

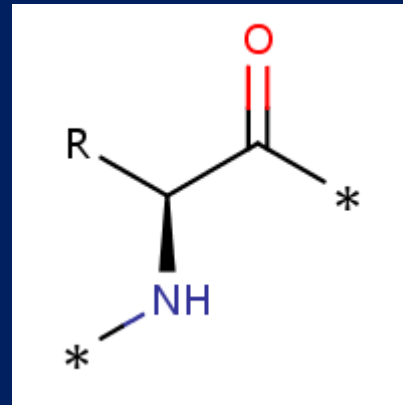
Acylotransferaza retinolowa lecytyny



a 1,2-diacyl-*sn*-glycero-3-phosphocholine

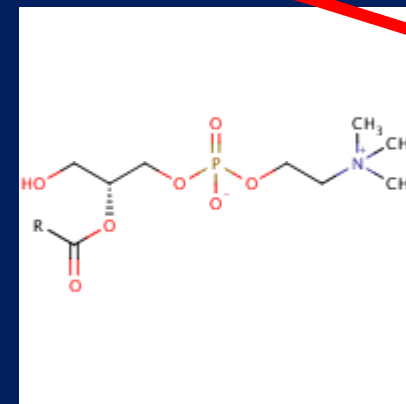


all-trans-retinol

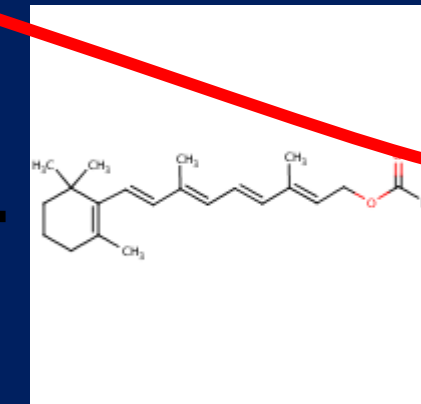


an L- α amino acid residue

all-trans-retinol--[retinol-binding protein RBP]



a 2-acyl-*sn*-glycero-3-phosphocholine



an *all-trans*-retinyl ester

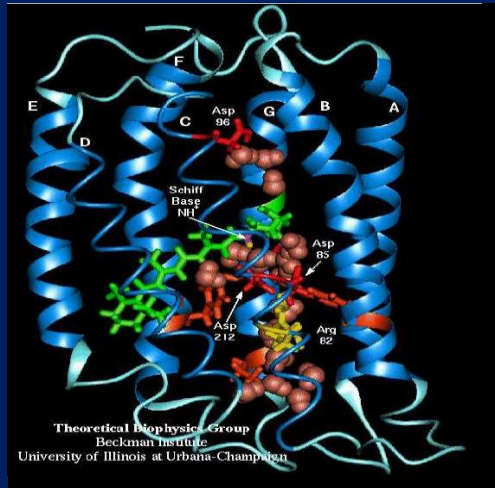
LRAT przenosi grupę acylową z pozycji *sn*-1 fosfatydylocholiny na *all-trans* retinol, wytwarzając estry *all-trans*-retinyłowe. Estry retinyłu są magazynami witaminy A.

Modyfikacje epigenetyczne w patogenezie guza mózgu

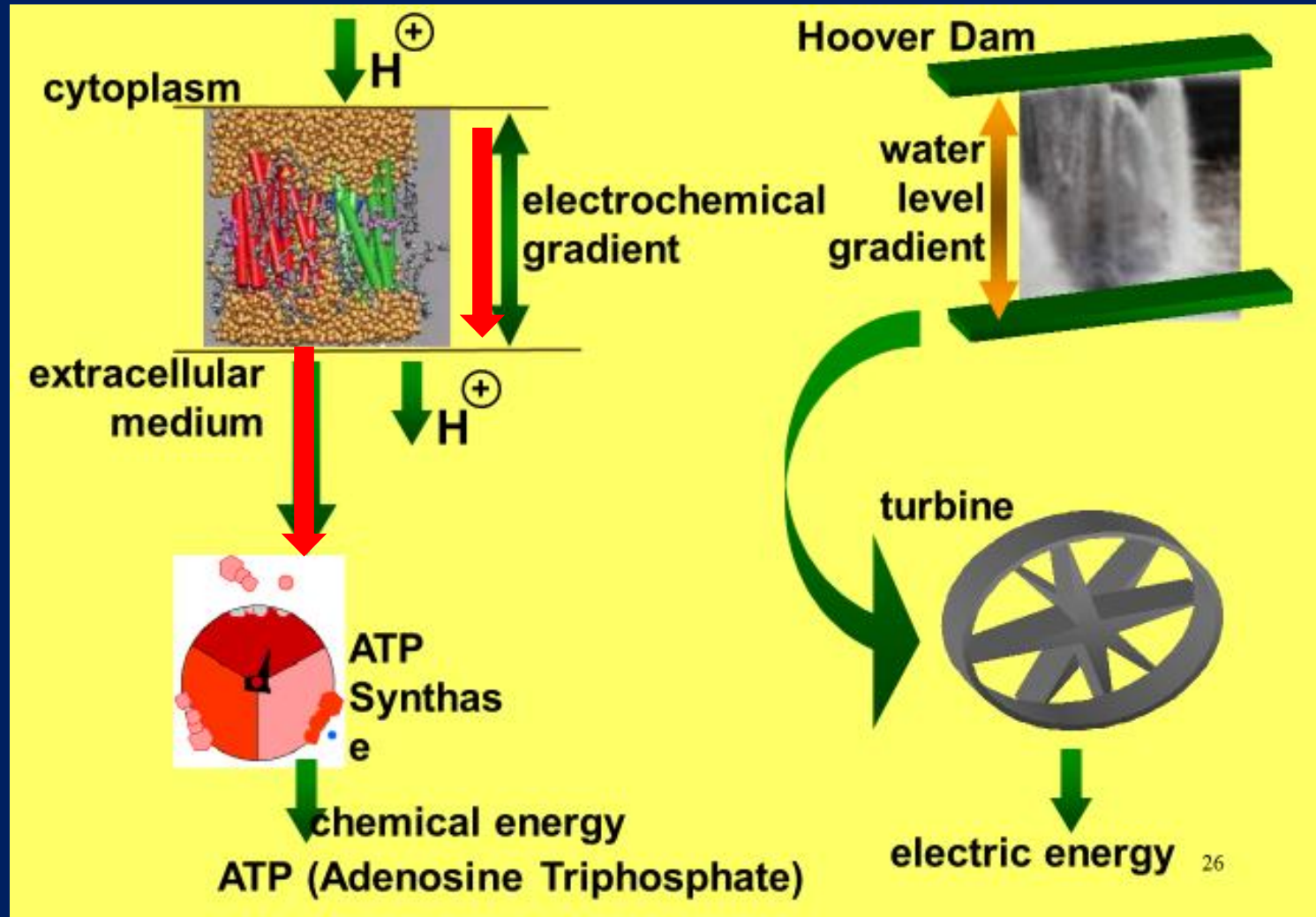
- Istnieje coraz więcej dowodów na to, że kwas retinowy i receptory kwasu retinowego (RAR) odgrywają ważną rolę w wywoływaniu zmian epigenetycznych i regulowaniu zmian epigenetycznych w karcynogenezie. [Subcell Biochem. 2014; 70: 129–149.](#)

Czy glejak wielopostaciowy jest złośliwą zmianą o podłożu epigenetycznym?

The light-activated mechanism of proton gradient



Light activation *triggers* trans to cis isomerization of a bound retinal



It acts as a proton pump; that is, it captures light energy and uses it to move protons across the membrane out of the cell. The resulting proton gradient across the membrane triggers ATP synthesis used for metabolism and phosphorylation by ATP synthase

the electron transport chain forms a proton gradient across the inner mitochondrial membrane, which drives the synthesis of ATP via chemiosmosis.

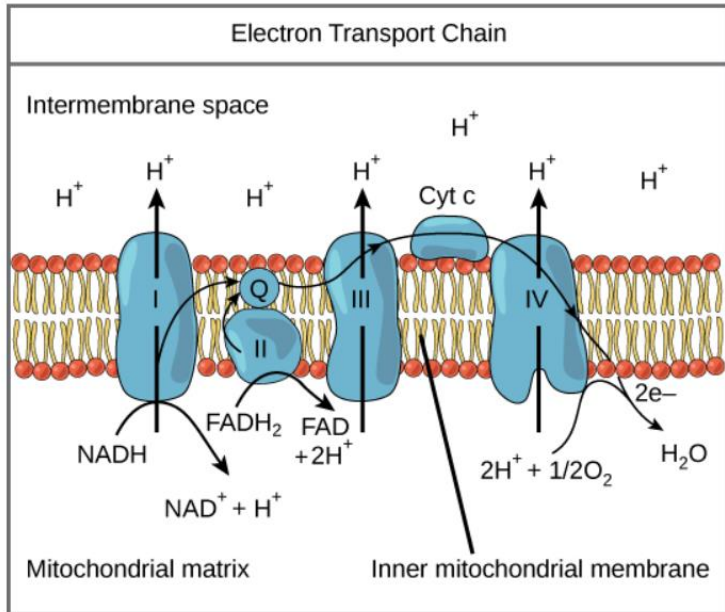
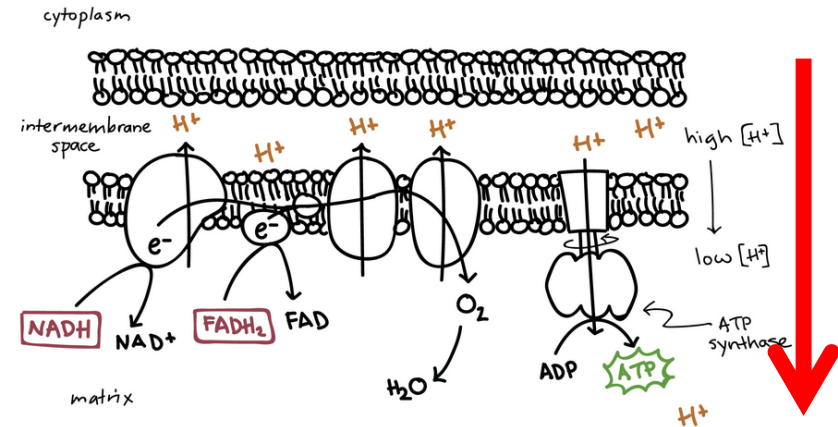


Image modified from "Oxidative phosphorylation: Figure 1", by OpenStax College, Biology (CC BY 3.0).

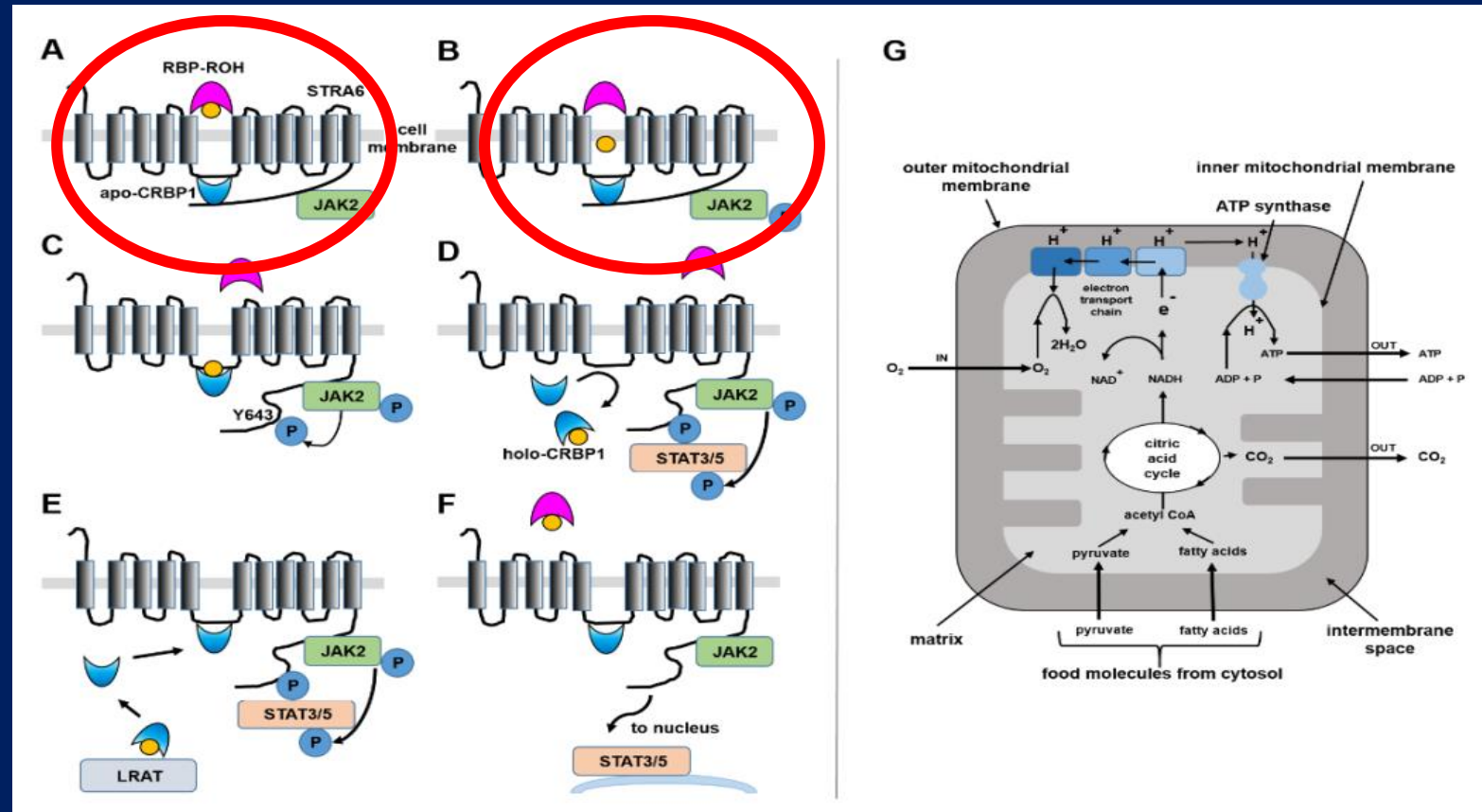
Overview: oxidative phosphorylation



The **electron transport chain** is a series of proteins and organic molecules found in the inner membrane of the mitochondria. Electrons are passed from one member of the transport chain to another in a series of redox reactions. Energy released in these reactions is captured as a proton gradient, which is then used to make ATP in a process called **chemiosmosis**. Together, the electron transport chain and chemiosmosis make up **oxidative phosphorylation**. The key steps of this process, shown in simplified form in the

RETINOIDS BOUND TO PROTEINS

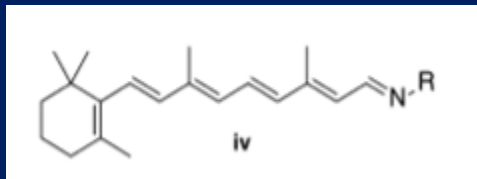
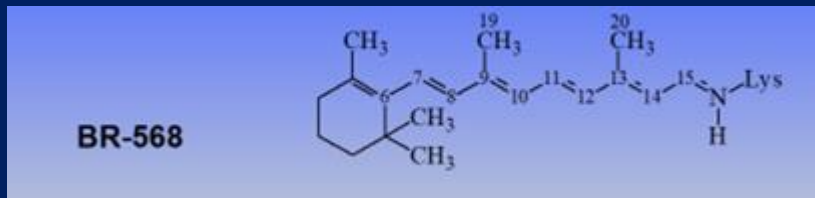
„FREE” RETINOIDS



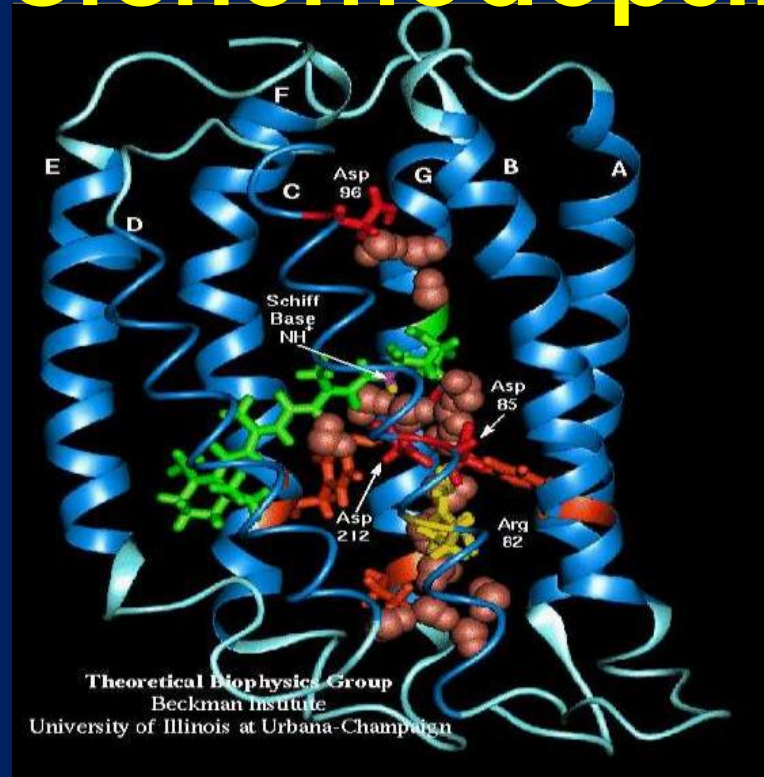
RETINOIDS BOUND TO PROTEINS

1. H. Abramczyk, *Femtosecond primary events in bacteriorhodopsin. Revision of commonly accepted interpretation of electronic spectra of transient intermediates*, J. Chem.Phys. 120 11120 (2004)
1. A. Terentis, L.Uji, H. Abramczyk, G. H. Atkinson, *Primary events in Bacteriorhodopsin photocycle: torsional vibrational dephasing in the first excited electronic state*, Chem. Phys. 313(2005) 51-62

bacteriorhodopsine

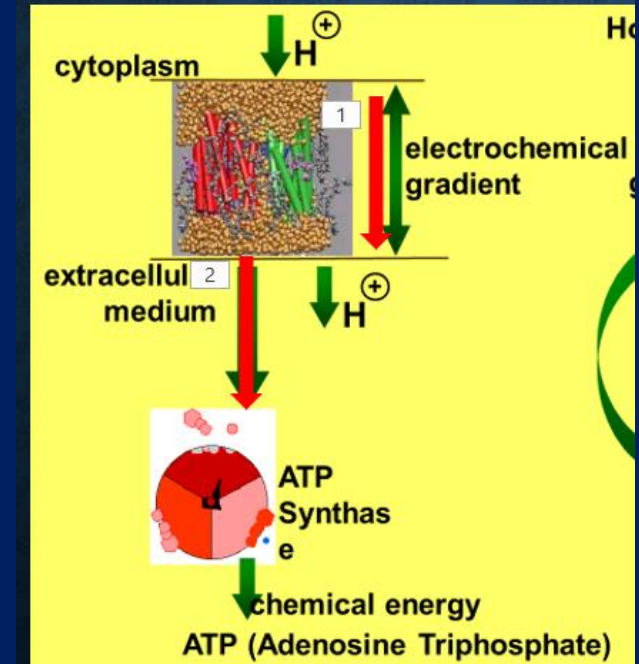
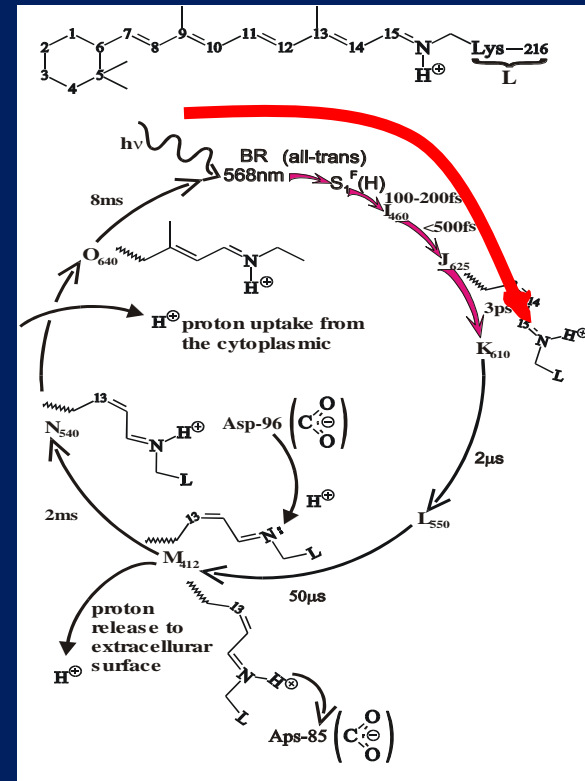
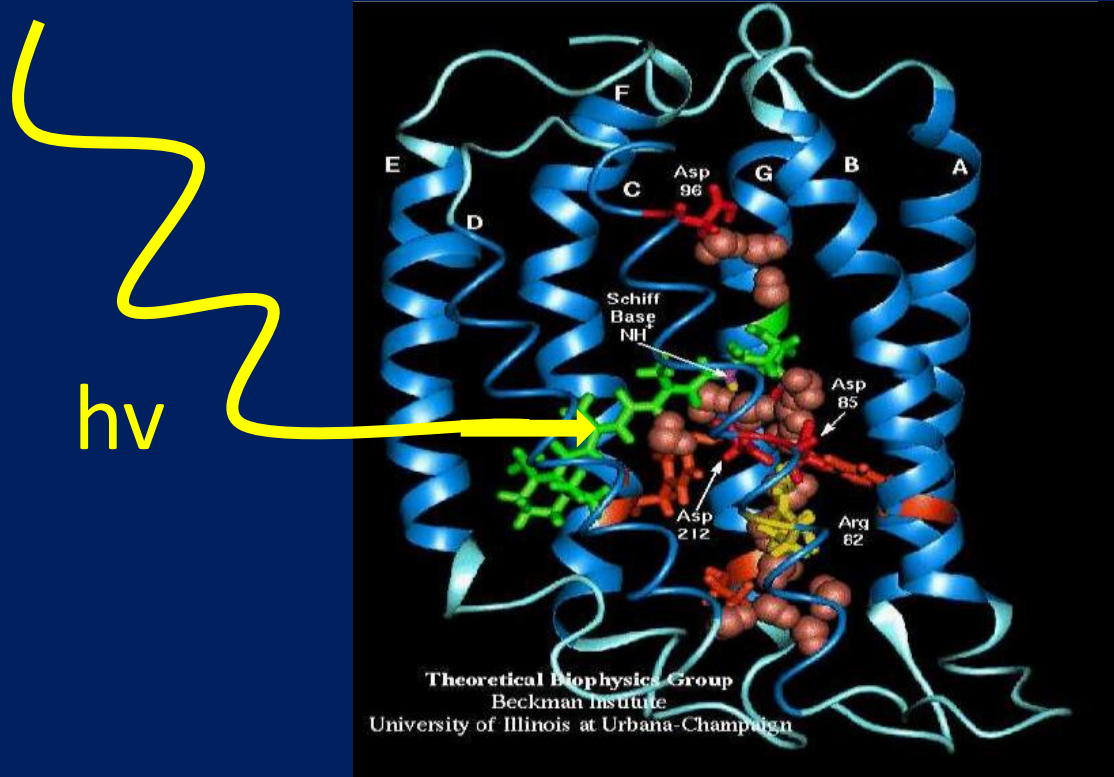


Retinyl imine (Schiff base)



BR contains a polyene chromophore, retinal, which is covalently bound to the Lys²¹⁶ residue of the protein by a protonated Schiff base linkage

RETINOIDS bound TO PROTEINS



The absorption of a photon from the visible range (568 nm) initiates in bacteriorhodopsin a cyclic sequence of reactions that is completed on the millisecond time scale (Scheme 1) leading to the proton moving from the cytoplasmic side to the extracellular surface and generation of an electrochemical potential that is used by a bacterium to maintain its metabolism. As one can see from the Scheme 1 the observed time constants of BR photocycle span about 11 decades. The photocycle can be divided into two distinct parts. The first one comprises very fast molecular processes occurring on femto- and picosecond time scale upon BR-568 (all-trans) excitation up to the formation of the K intermediate that has the 13-cis configuration. The second part of the photocycle is much slower.

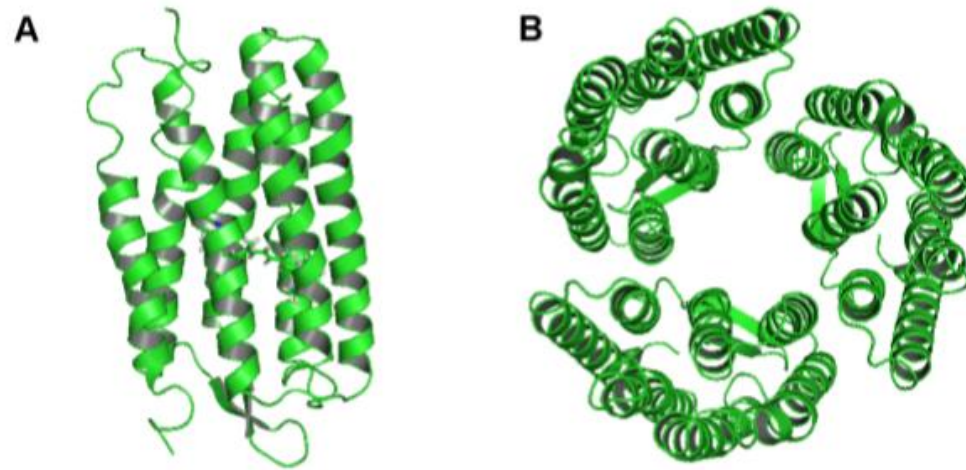


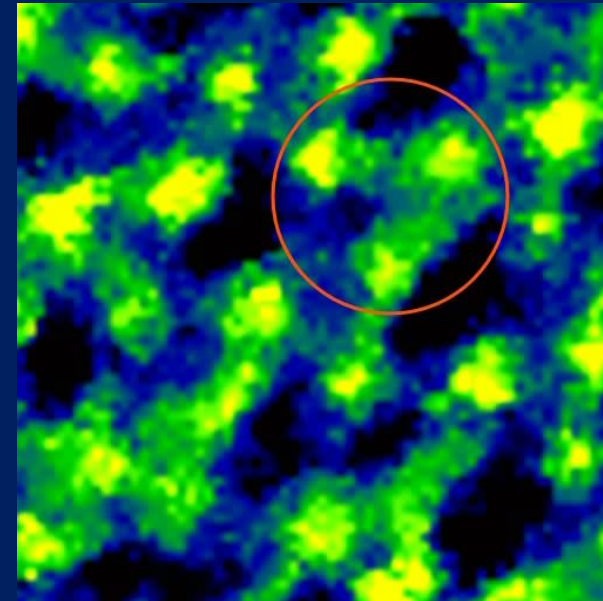
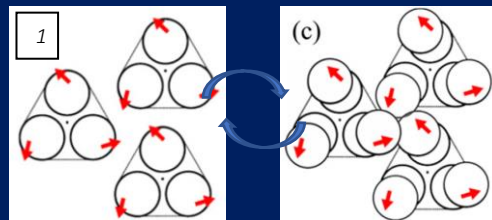
Figure 2.5: Ribbon diagram of bacteriorhodopsin. A: Protein monomer (side view). The retinal is drawn in a stick representation. B: Top view of a bacteriorhodopsin trimer from the cytoplasmic side.

Photoactivation of bacteriorhodopsine



- Fast imaging AFM na BR Mutant D96N
- w 10 mM TRIS, 150 mM KCl, pH 7.6
- AM AFM z A=1.0 nm
- 1 kl / s (64 px2)
- Eksperyment trwał 200 fps
- To samo miejsce (te same molekuly)

To optimize AFM for the investigation of dynamical biological systems, each component of AFM can be modified to improve the speed of AFM scanning. As a result, high-speed AFM (HS-AFM) achieved scanning speeds several orders of magnitude faster than that of conventional AFM, thus enabling monitoring of conformational dynamics of single proteins on substrates with a subsecond temporal resolution.



x,y-range=18x18nm², z=325pm

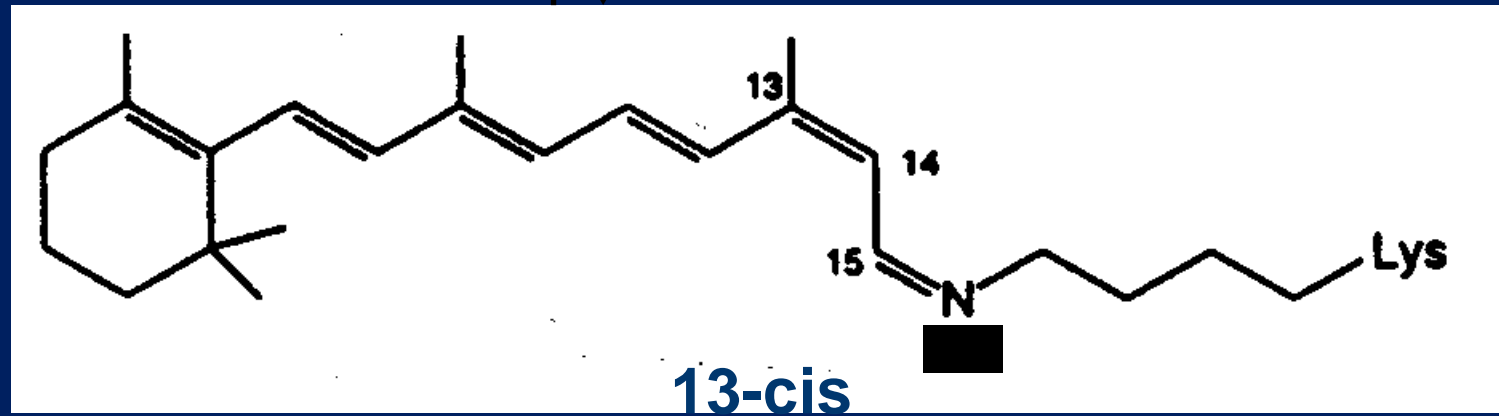
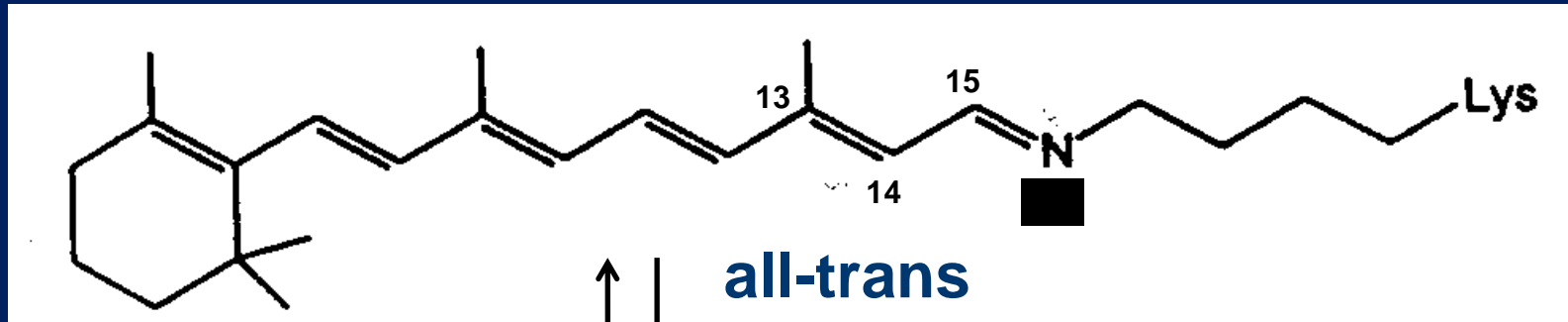
¹ Ando T et al., Nanotechnology 23 (2012) 062001

Time resolved CARS

frequency domain

University of Arizona
Department of Chemistry
85 721 Tuscon, AZ, USA

- **H. Abramczyk, Femtosecond primary events in bacteriorhodopsin. Revision of commonly accepted interpretation of electronic spectra of transient intermediates, J. Chem. Phys. 120 11120 (2004)**
-
- **A. Terentis, L. Uji, H. Abramczyk, G. H. Atkinson, Primary events in Bacteriorhodopsin photocycle: torsional vibrational dephasing in the first excited electronic state, Chem. Phys. 313(2005) 51-62**



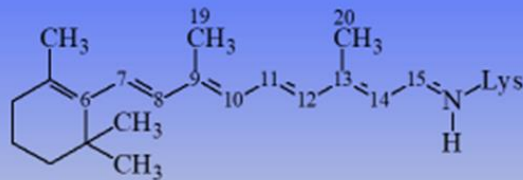
Light activation *triggers* trans to cis isomerization of a bound retinal

Native BR-568 and unlocked analogs BR 6.11 and 6.9

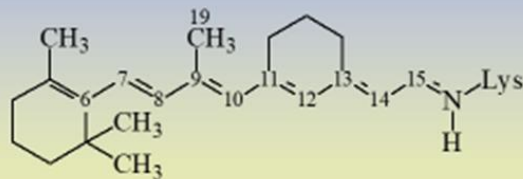
The artificial BR pigments examined here contain a retinal with six-membered carbon ring incorporated into the retinal backbone that remains the 13C=C14 bond free to isomerize

Native BR-568 and unlocked analogs BR 6.11 and 6.9

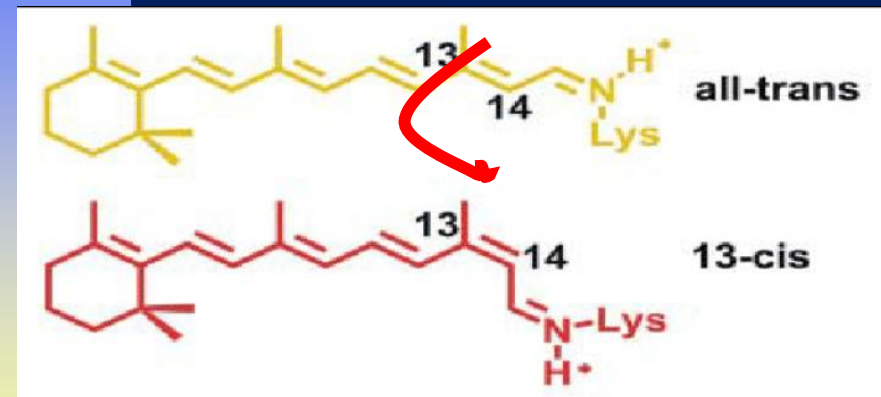
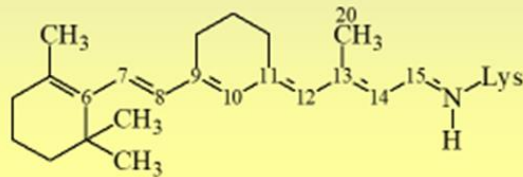
BR-568



BR 6.11



BR 6.9

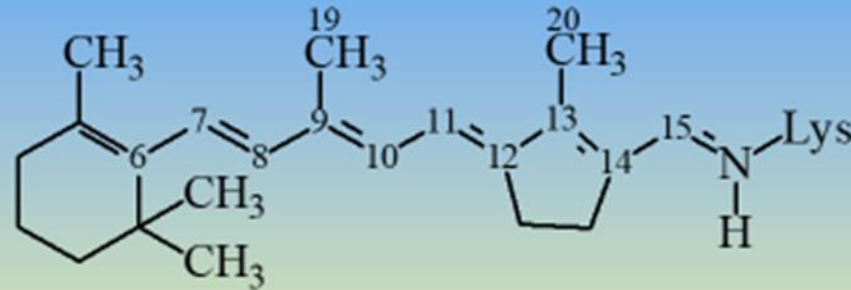


22

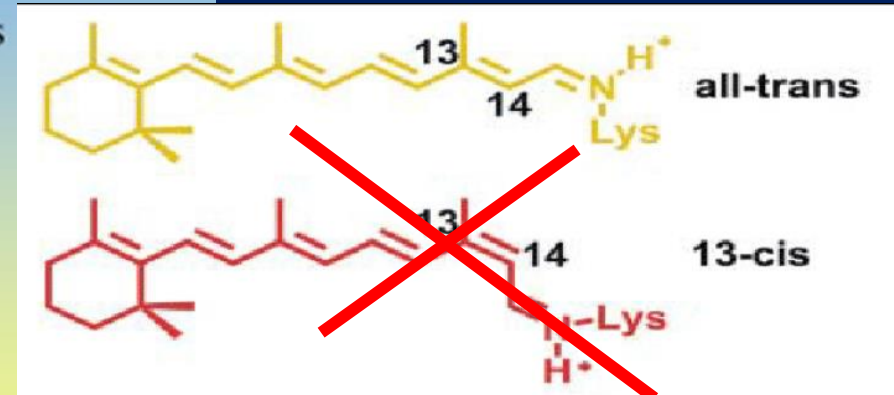
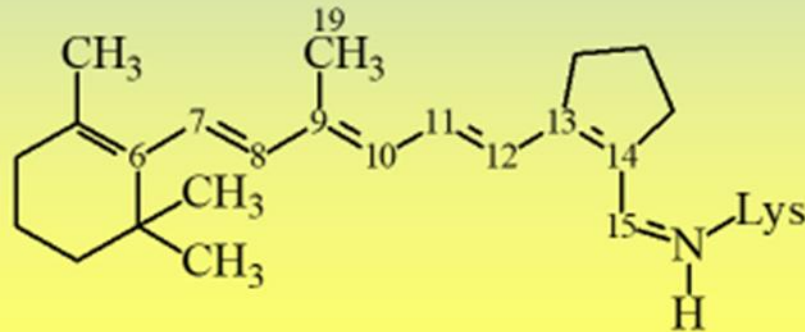
Primary events in the bacteriorhodopsin photocycle: Torsional vibrational dephasing in the first excited electronic state Andrew C. Terentis, Laszlo Ujj, Halina Abramczyk, George H. Atkinson* Chemical Physics 313 (2005) 51-6

Locked analogs BR 5.12 and BR 5.13

BR 5.12



BR 5.13



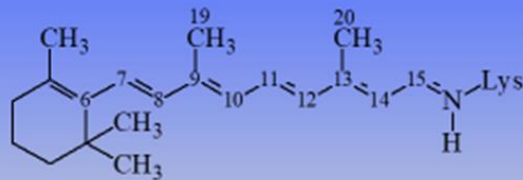
For BR5.12, the C13=C14 retinal bond is locked in the trans configuration by a rigid, five-membered carbon ring

Native BR-568 and unlocked analogs BR 6.11 and 6.9

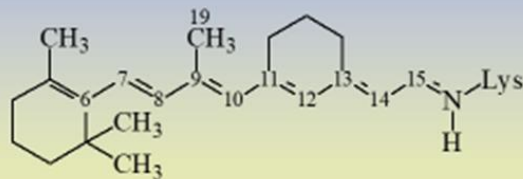
The artificial BR pigments examined here contain a retinal with six-membered carbon ring incorporated into the retinal backbone that remains the 13C=C14 bond free to isomerize

Native BR-568 and unlocked analogs BR 6.11 and 6.9

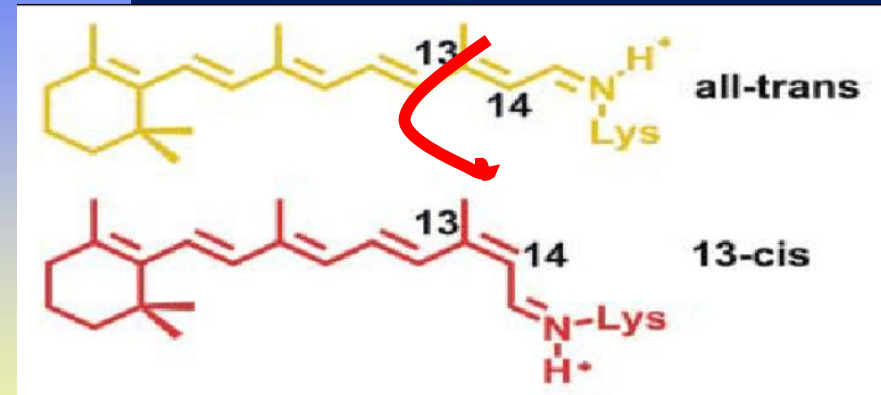
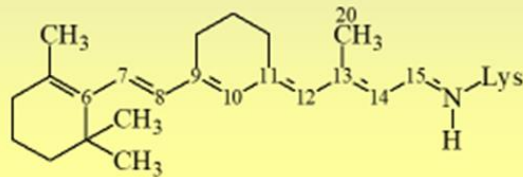
BR-568



BR 6.11



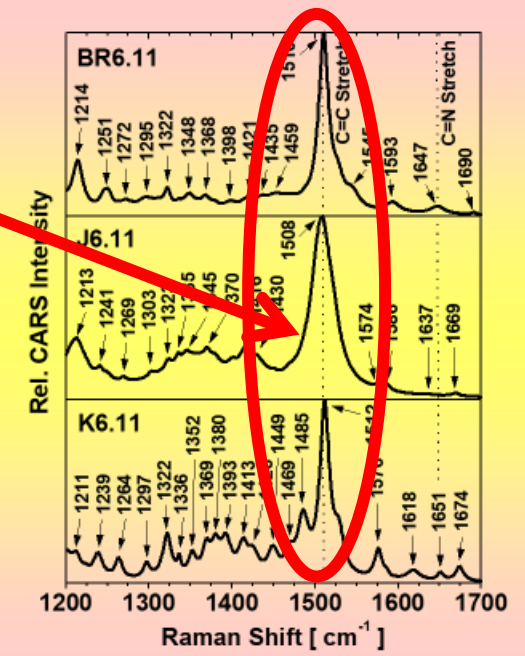
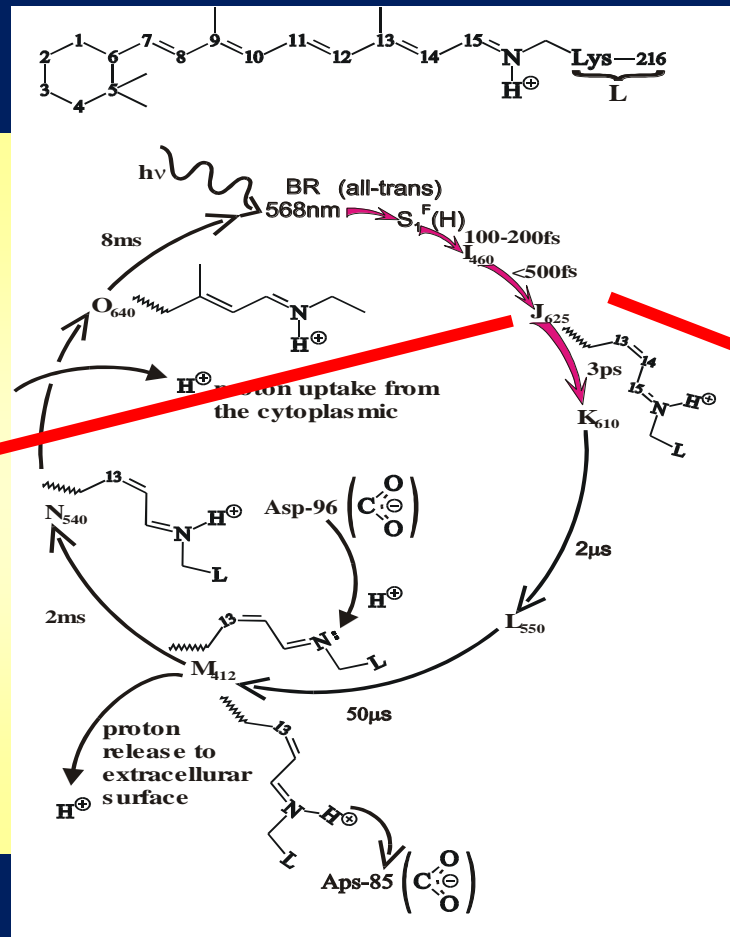
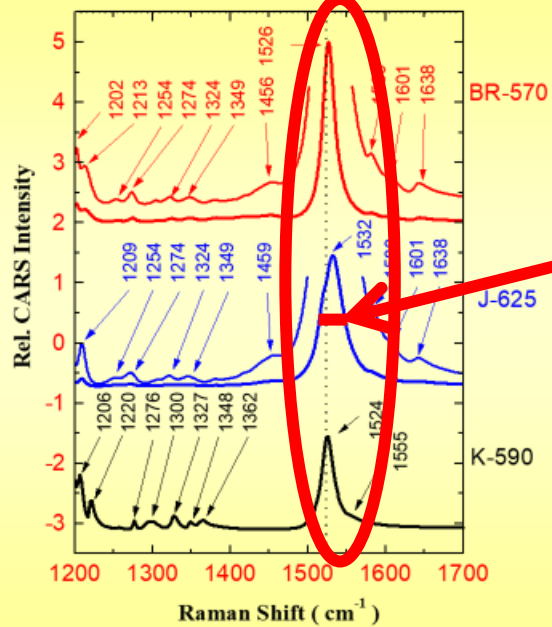
BR 6.9



22

Primary events in the bacteriorhodopsin photocycle: Torsional vibrational dephasing in the first excited electronic state Andrew C. Terentis, Laszlo Ujj, Halina Abramczyk, George H. Atkinson* Chemical Physics 313 (2005) 51-6

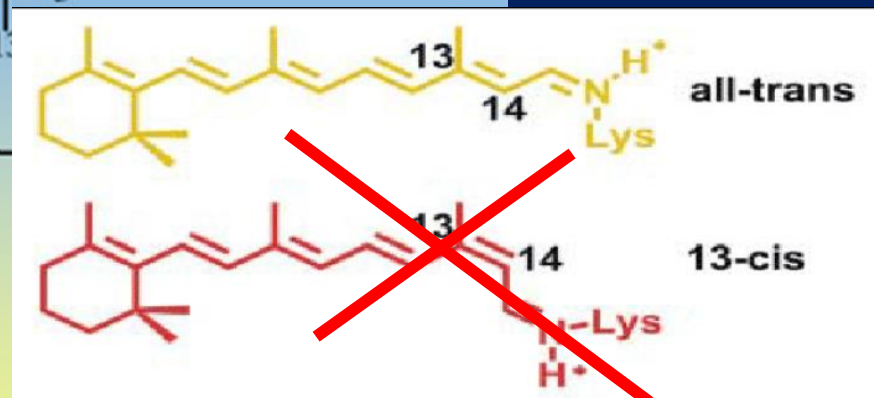
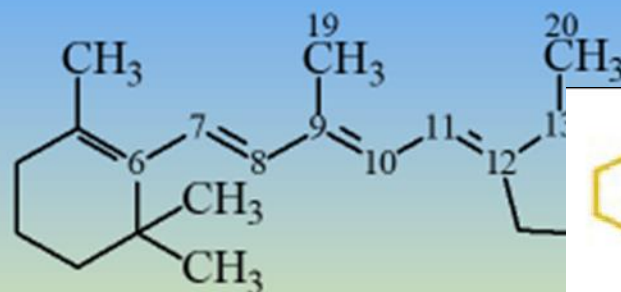
Native BR-568 and unlocked analogs BR 6.11 and 6.9



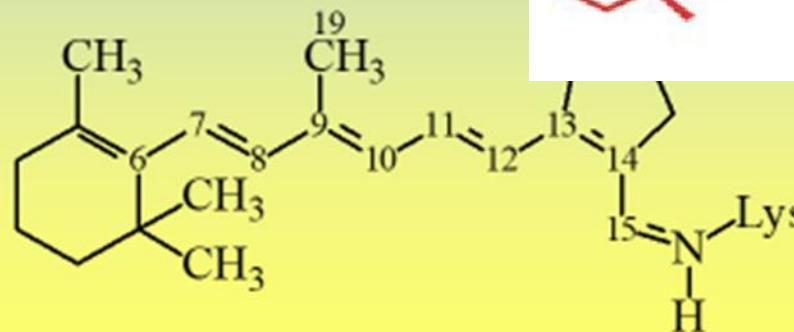
vibrational spectra of BR-570 (top), J-625 (center, derived from the 0-ps PTR/CARS data), and K-590 (bottom, derived from the 200-ps PTR/CARS data) in the 1200–1700 cm⁻¹ region

Locked analogs BR 5.12 and BR 5.13

BR 5.12



BR 5.13



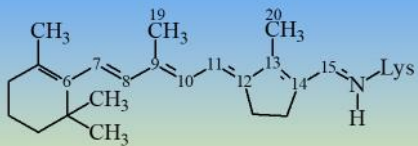
Andrew C.
Terentis, Laszlo
Ujj, Halina
Abramczyk,
George H.
Atkinson*
Chemical Physics
313 (2005) 51–6

28

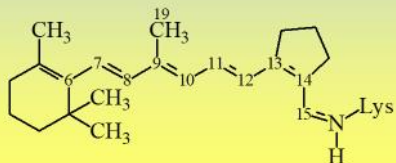
For BR5.12, the C13=C14 retinal bond is locked in the trans configuration by a rigid, five-membered carbon ring

Locked analogs BR 5.12 and BR 5.13

BR 5.12

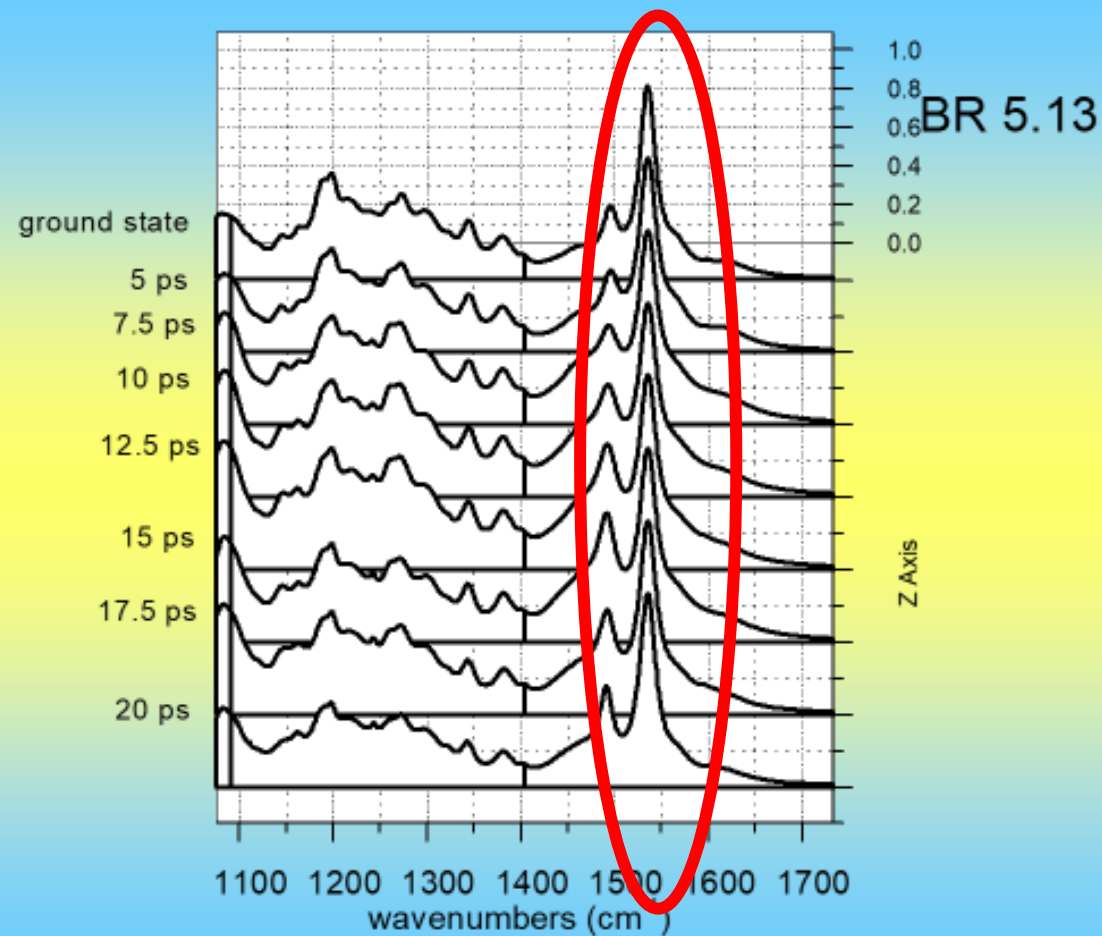


BR 5.13



28

Andrew C. Terentis, Laszlo Ujj, Halina Abramczyk, George H. Atkinson* *Chemical Physics* 313 (2005) 51–6

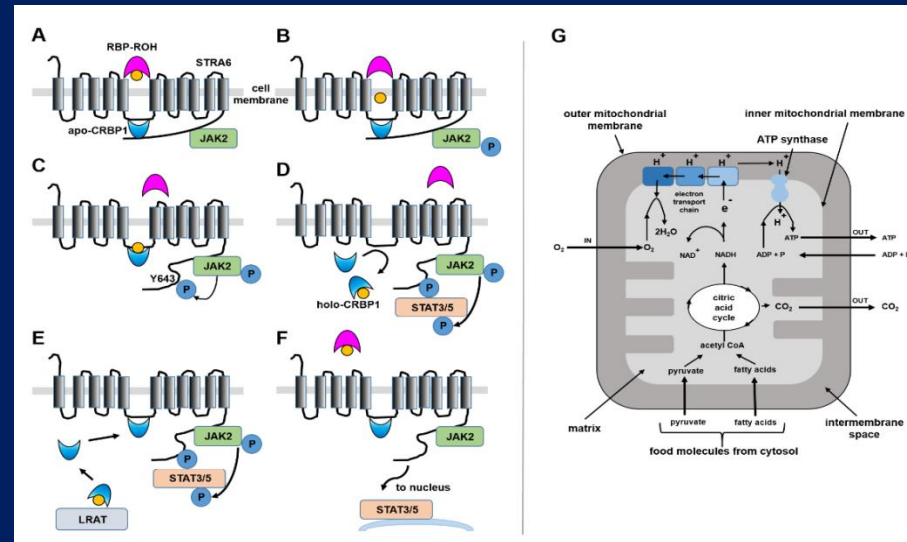


30

Free retinoids and RETINOIDS bound TO PROTEINS

Is femtosecond dynamics of retinoids „free” in solution different from that in retinoids bound to proteins?

Answering this question is very important , because femtosecond dynamics could monitor free retinol and retinol bound to proteins in cells providing information on the mechanism of retinol uptake and signalling by STRA6



CYTOCHROME C

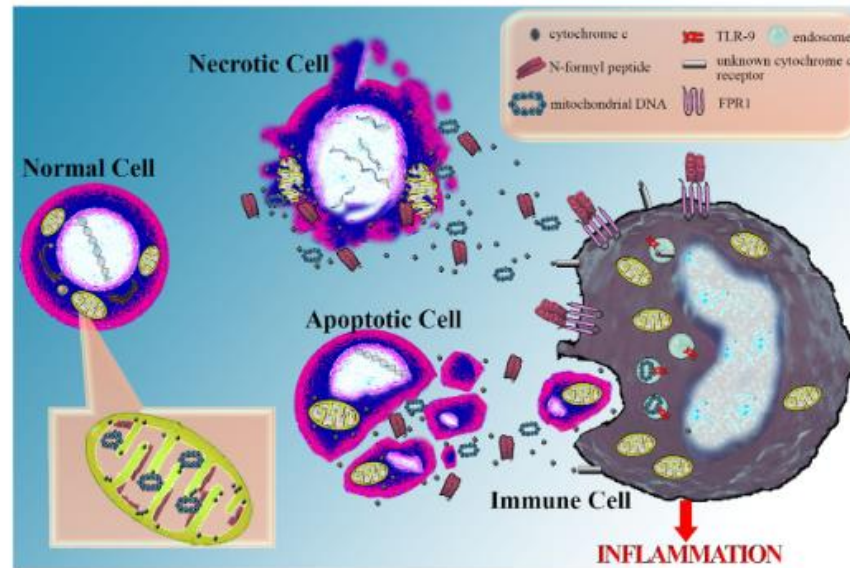
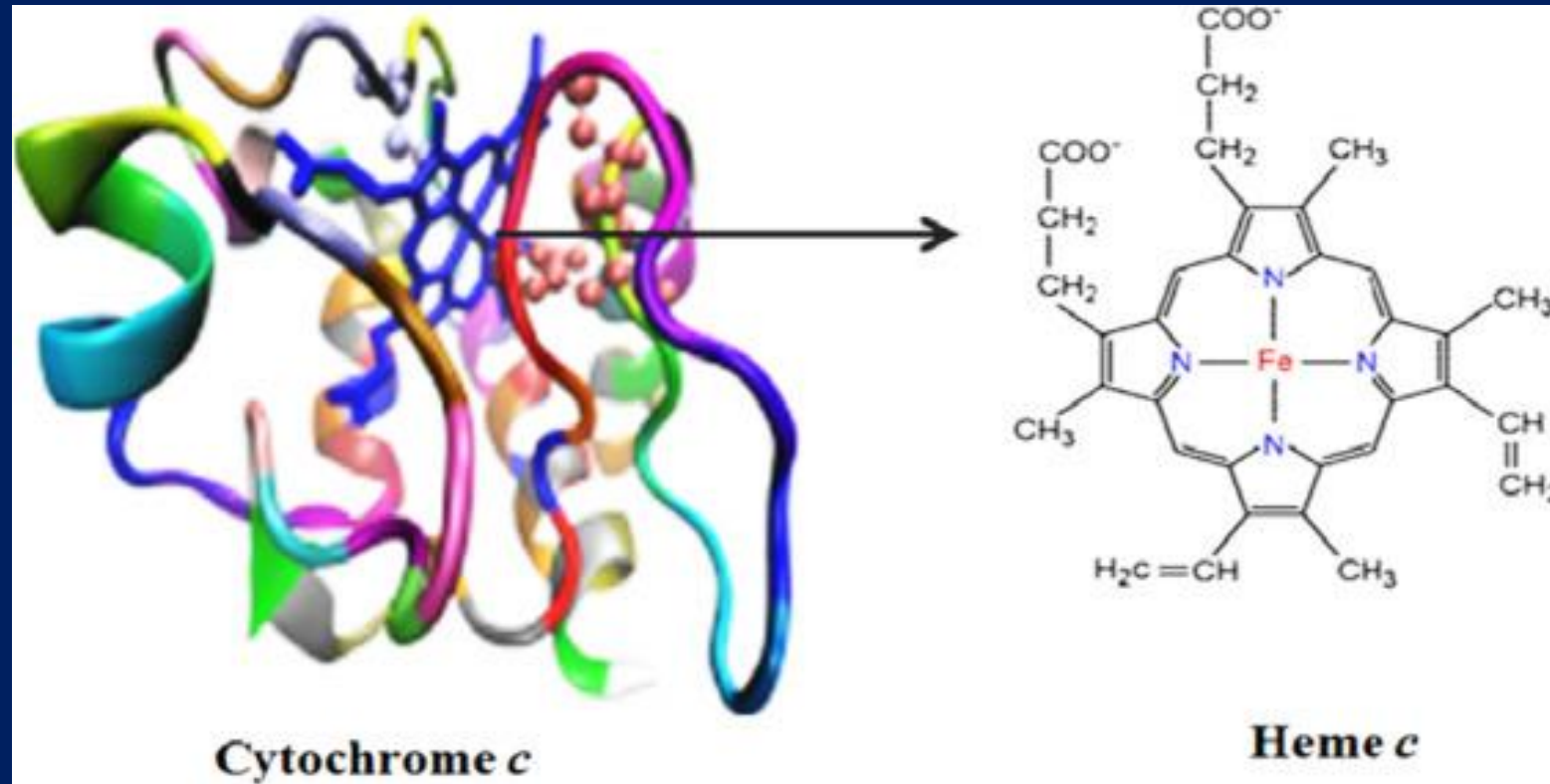


FIGURE 1 | Cytochrome c as a marker of cellular damage and its potential role as a danger-associated molecular pattern. Serious cellular damage results in cell apoptosis or necrosis. In both cases, cytochrome c is released into the extracellular space and can be easily measured in the serum serving as a marker of severe cellular damage and death. Possibly, along with cytochrome c, other mitochondrial molecules are also released into the extracellular space. Among them are annotated some well-defined danger-associated molecular patterns (DAMPs), such as mitochondrial DNA, recognized by the toll-like receptor 9 (TLR9) into the endosomes of immune cells and *N*-formyl peptides, sensitized by the formyl peptide receptor 1 (FPR1) on the cell membrane of immune cells. Besides the above DAMPs, which resemble bacterial structures, there is evidence that cytochrome c, a universal self-molecule, when is inappropriately located into the extracellular space may behave as a DAMP and elicit an inflammatory response. However, further studies are required for supporting this role for cytochrome c and the responsible pattern recognition receptor(s) remain to be discovered.

CYTOCHROME C

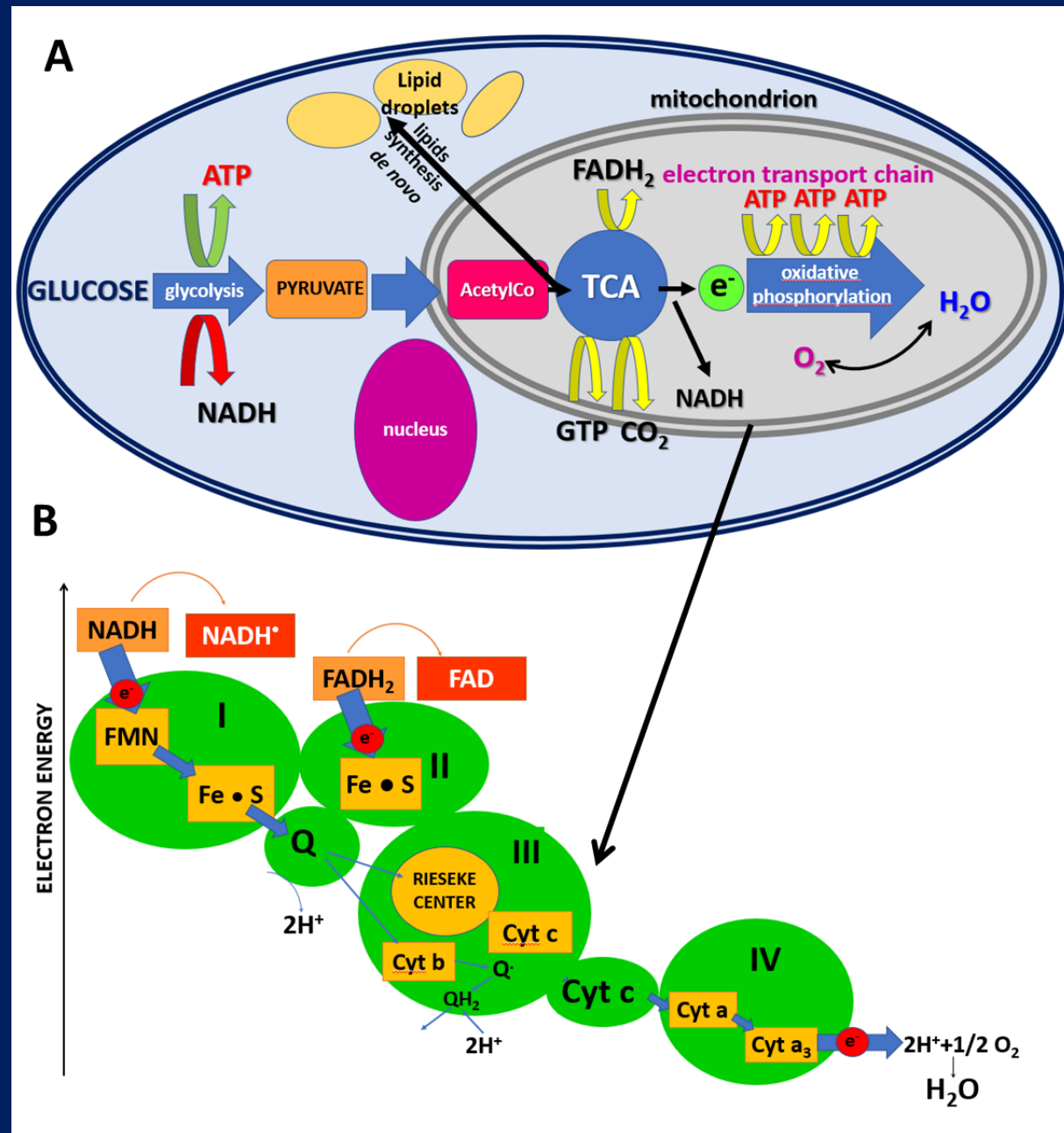


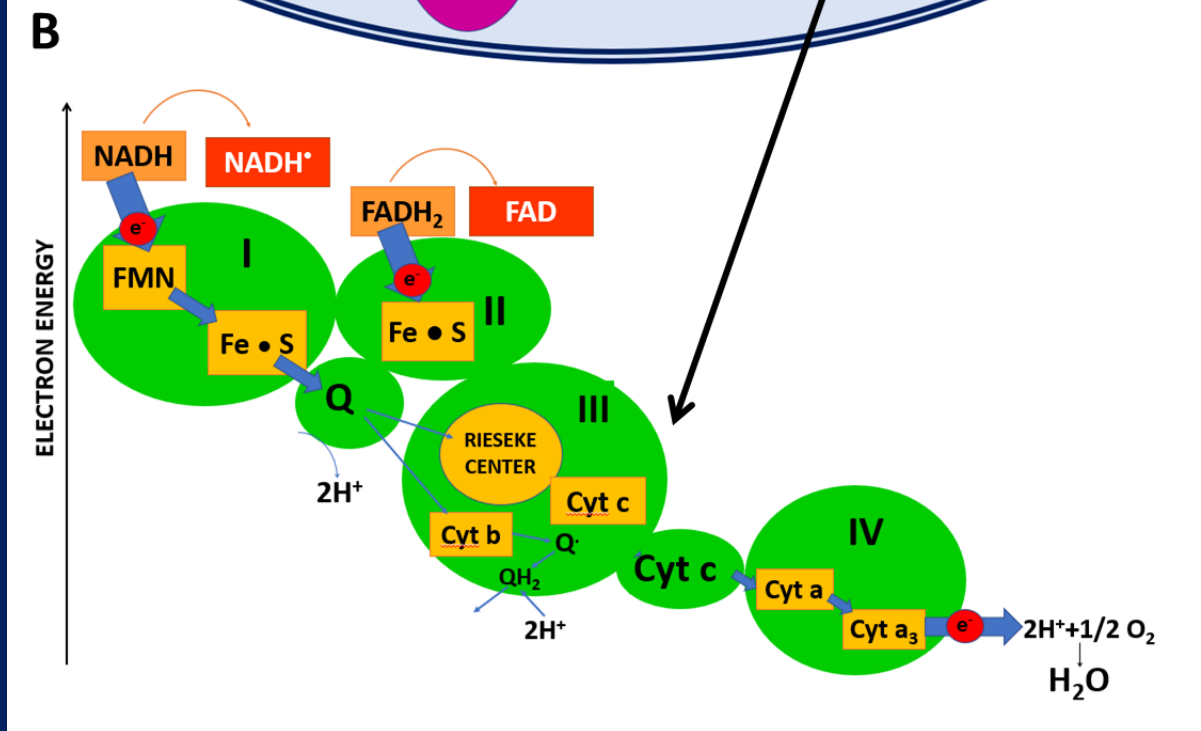
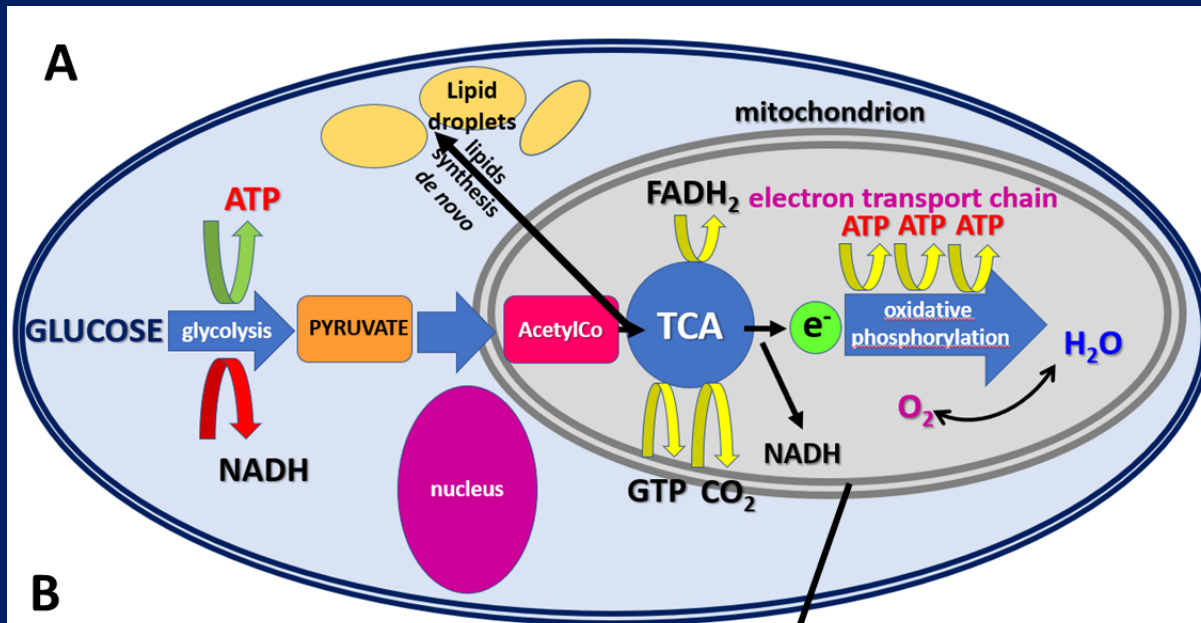
The release of cyt *c* from mitochondria is a key initiative step in the activation of cell death pathways.

Cyt c, a heme containing [metalloprotein](#) is located in the [intermembrane space](#) of [mitochondria](#) and released into bloodstream during pathological conditions. The release of cyt c from mitochondria is a key initiative step in the activation of cell death pathways. Circulating cyt c levels represents a novel in-vivo marker of mitochondrial injury after [resuscitation](#) from heart failure and chemotherapy. Thus, cyt c detection is not only serving as an apoptosis [biomarker](#), but also is of great importance to understand certain diseases at cellular level. Various existing techniques such as [enzyme-linked immunosorbent assays](#) (ELISA), [Western blot](#), [high performance liquid chromatography](#) (HPLC), [spectrophotometry](#) and [flow cytometry](#) have been used to estimate cyt c. However, the implementation of these techniques at POC (point of care) application is limited due to longer analysis time, expensive instruments and expertise needed for operation.

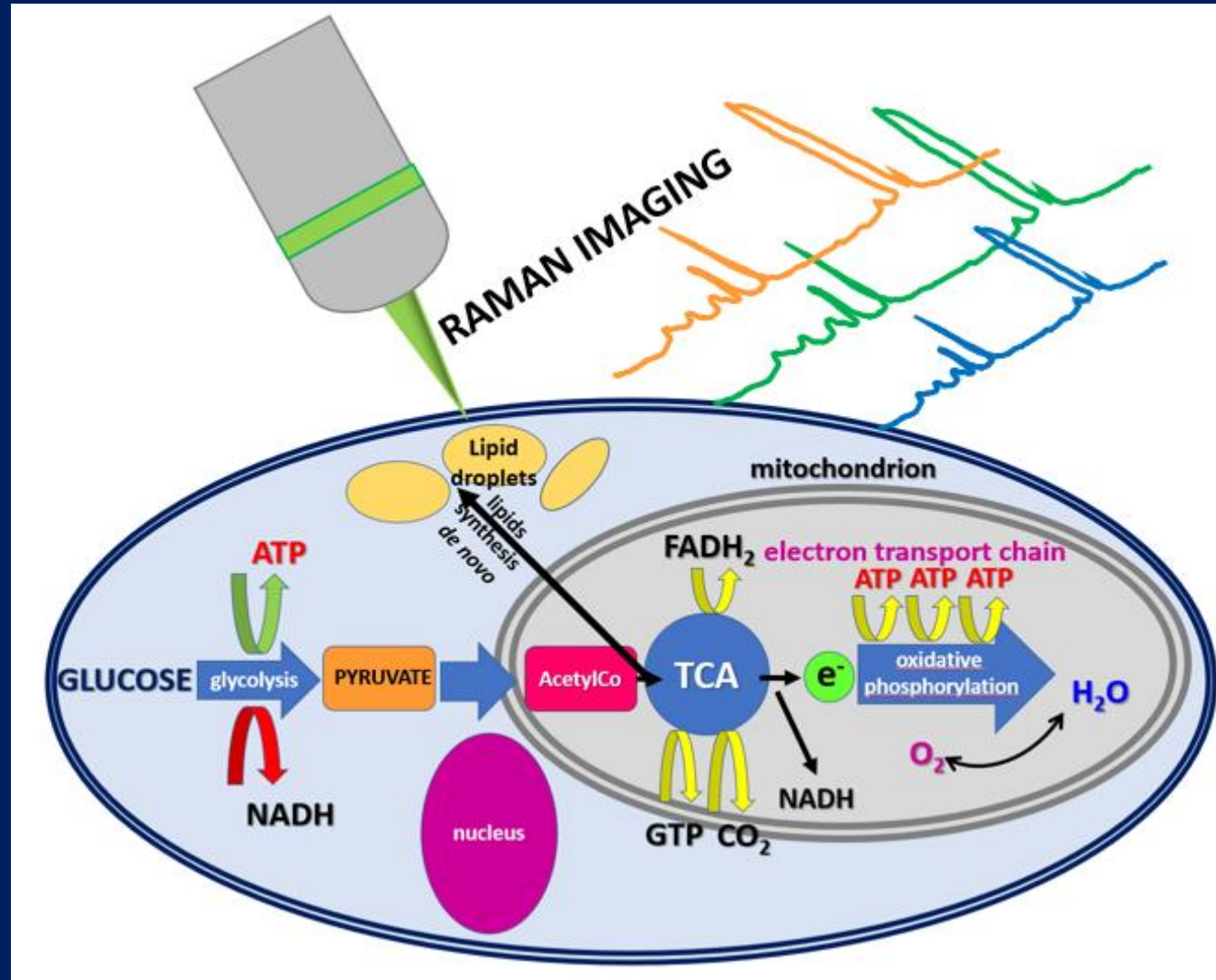
[Biosensors and Bioelectronics](#)

[Volume 87](#), 15 January 2017, Pages 654-668





<https://sciencemusicvideos.com/ap-biology/module-10-cellular-respiration/the-electron-transport-chain-atp-synthase-and-chemiosmosis/>



Cytochromes in cancer living brain (in vivo animal model)

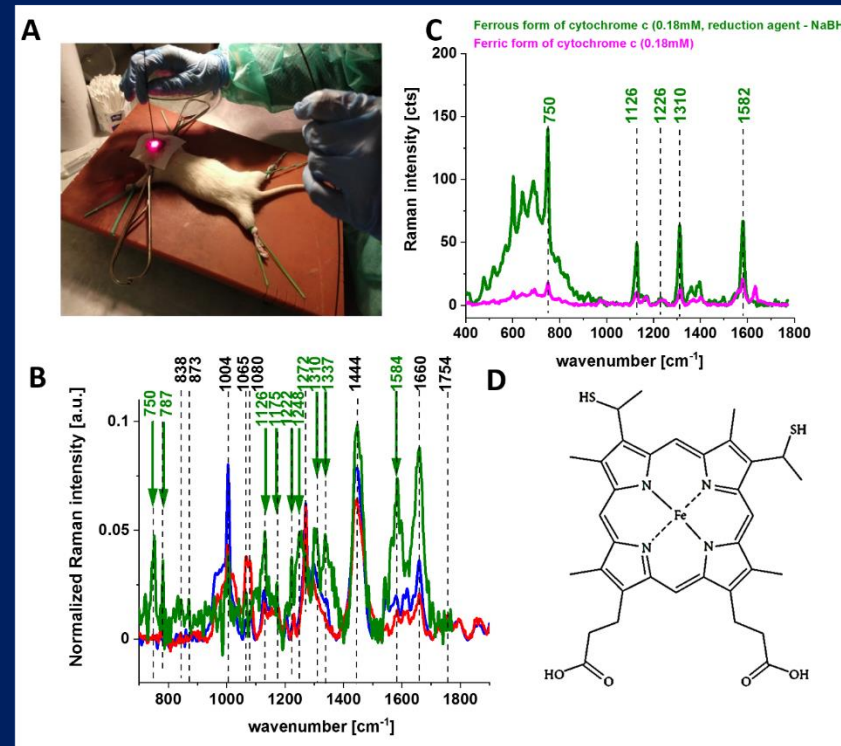


Figure 1. Raman- guided *in vivo* animal (rat) brain analysis (A), the average (number of animals, n=6) Raman spectrum of the *in vivo* brain of animal model (rat) at the excitation 785 nm — and of the *ex vivo* brain of animal model (rat) at the excitation 532 nm — and 785 nm — (B), Raman spectrum of ferrous and ferric forms of cytochrome c —, — (green, magenta) (0.18 mM solution in PBS (PBS - phosphate-buffered saline), excitation line 532 nm, laser power 0.5 mW, accumulation time 2.0 sec., number of accumulation 20) (C), structural formula of heme c in cytochrome c (D).

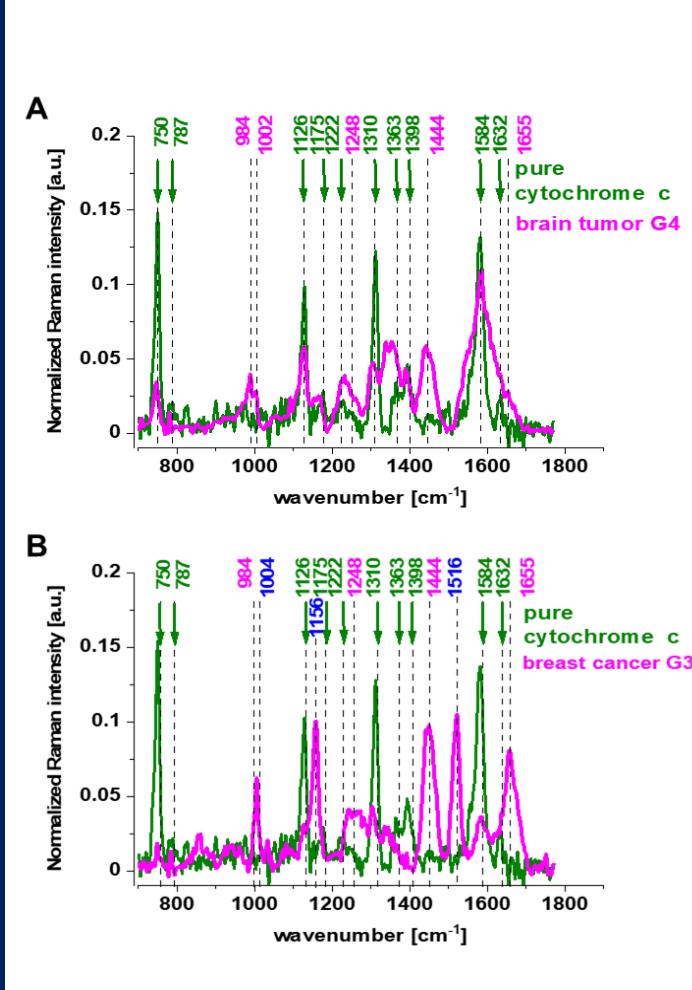


Figure 1. The average (number of patients n (G4)=13, number of single Raman spectra 85 000) Raman spectra of the *ex vivo* human tissue of brain tumor, medulloblastoma (G4) —,cytochrome c — at the excitation at 532 nm (A), the average (number of patients n (G3)=5, number of single Raman spectra $n= 40\ 000$) Raman spectrum of the *ex vivo* human tissue of breast cancer, infiltrating ductal carcinoma (IDC)) (G3) —, cytochrome c — at the excitation at 532 nm (B).

Cytochromes in cancer human tissues

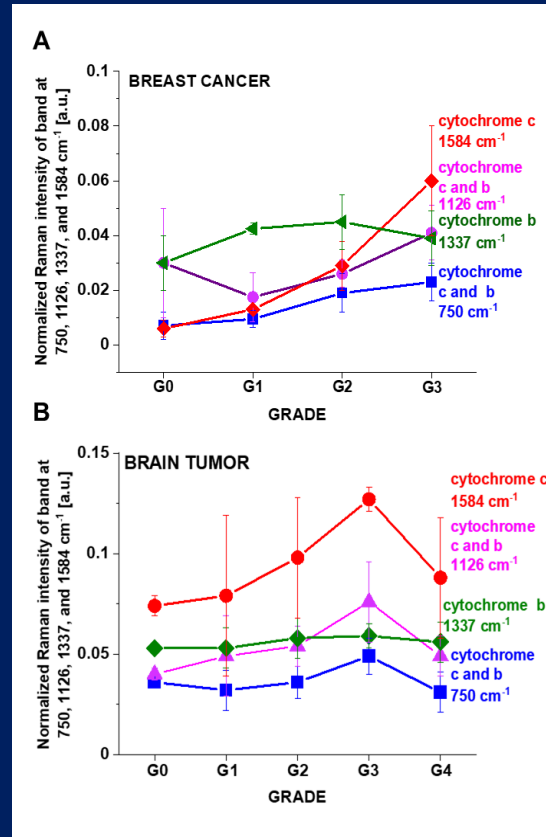
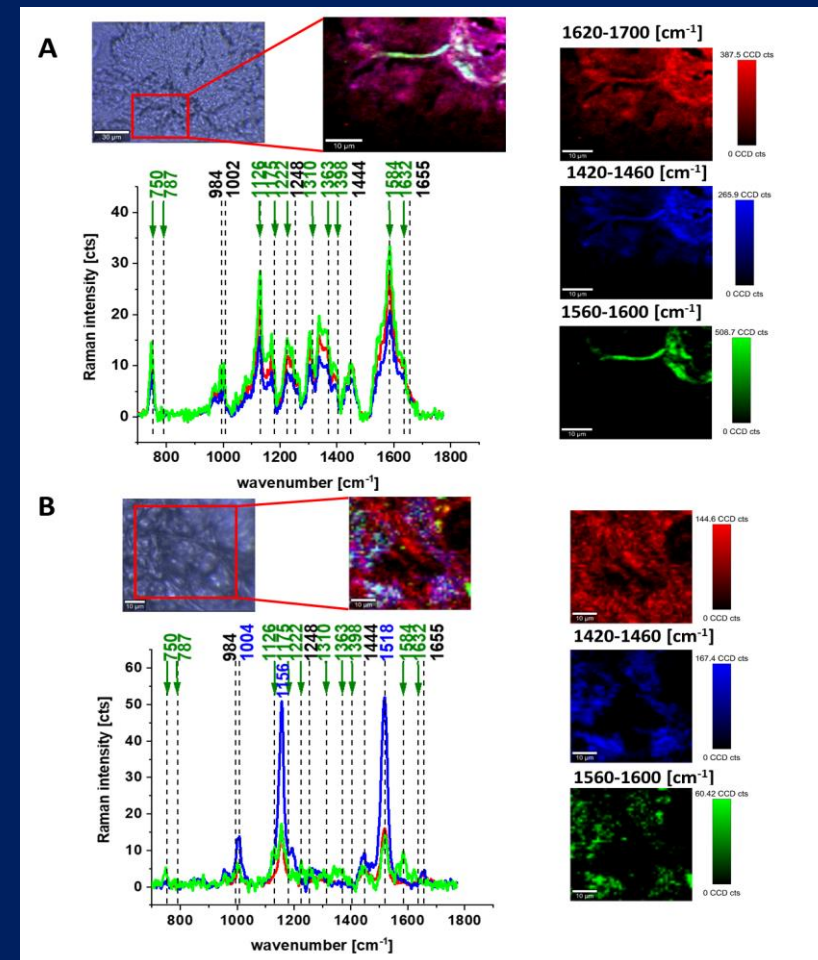


Figure 3. Raman intensity of the 750, 1126, 1337 and 1584 cm⁻¹ as a function of grade for breast normal (G0) and cancer (invasive ductal cancer) human tissue (G1, G2, G3) (average \pm SD from number of patients n=39, number of single Raman spectra =305 000) (A), Raman intensity of the 750, 1126, 1337 and 1584 cm⁻¹ as a function of grade for brain normal (G0) and tumor tissues (G1, G2, G3, G4) (average \pm SD from number of patients n=44, number of single Raman spectra = 280 000) (B).

Cytochromes in cancer human tissues

Figure 2. Microscopy image, Raman images of distribution of proteins (red color), lipids and carotenoids (blue color) and cytochrome c (green) for brain tumor, grade IV medulloblastoma (40x40 μm , resolution 0.5 μm , integration time 1.0 sec, the average Raman spectra of lipids – blue, proteins – red, cytochrome – green at 532 nm (A), Microscopy image, Raman images of distribution of proteins (red color), lipids (blue color) and cytochrome c (green) for breast cancer, grade I ductal cancer (40x40 μm , resolution 0.5 μm , integration time 1.0 sec, the average Raman spectra of lipids and carotenoids – blue, proteins – red, cytochrome – green at 532 nm (B).



Cytochromes in cancer human single cells

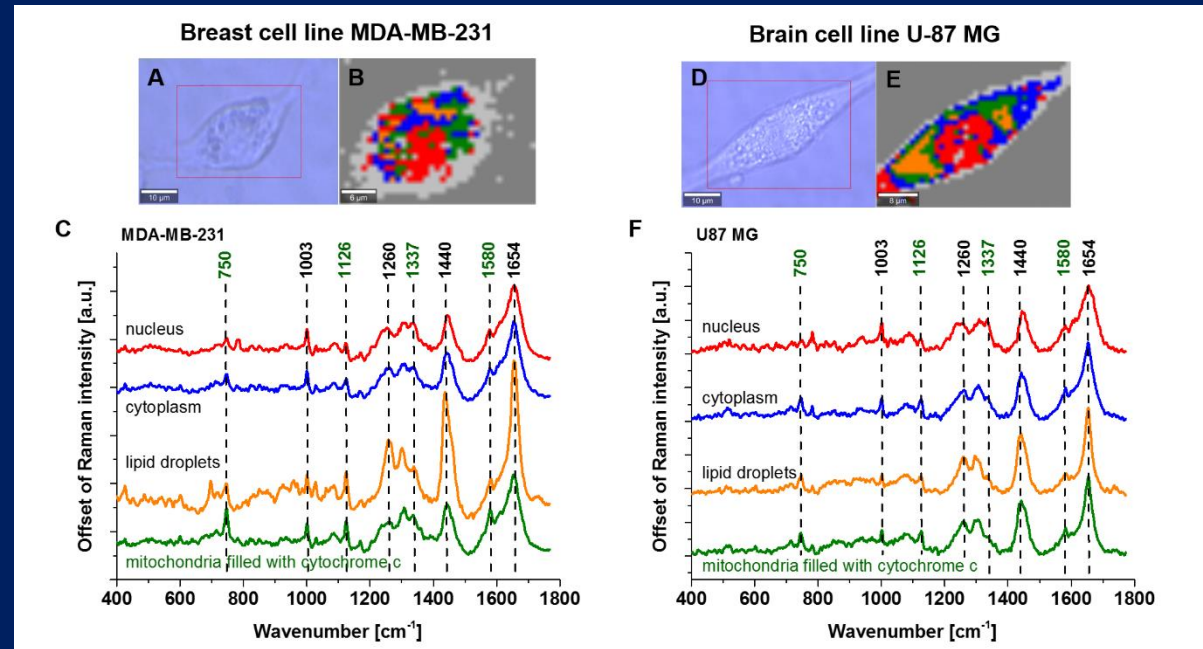


Figure 4. Microscopy image (A), Raman image (35x26 μm , resolution 0.5 μm , integration time 1.0 sec) (B), the average Raman spectra (number of cells $n=3$, number of single Raman spectra $n=10920$) of nuclei (red), cytoplasm (blue), lipid droplets (orange), mitochondria green) (C) at 532 nm of single cell MDA-MB-231 and Microscopy image (D), Raman image (40x30 μm , resolution 0.5 μm , integration time 1.0 sec) (E), the average Raman spectra (number of cells $n=3$, number of single Raman spectra $n=14400$) of nuclei (red), cytoplasm (blue), lipid droplets (orange), mitochondria green) (F) at 532 nm of single cell U-87 MG.

Cytochromes in cancer human single cells

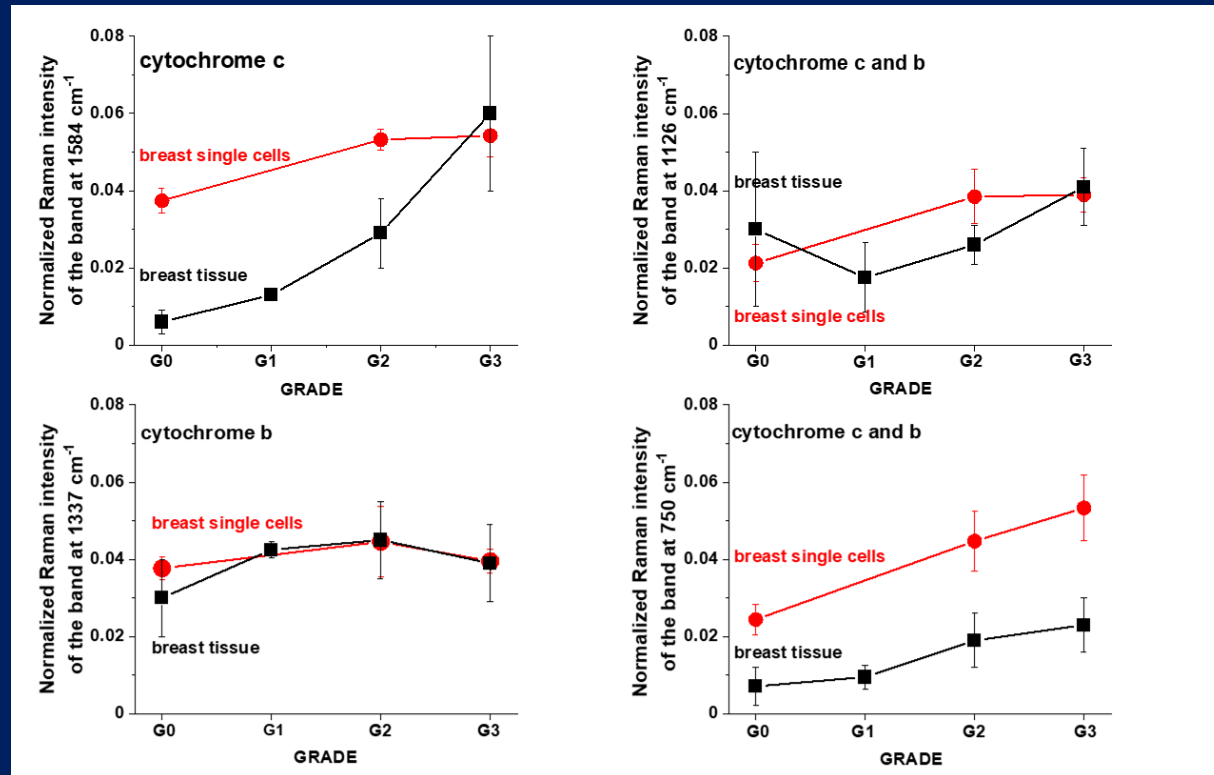
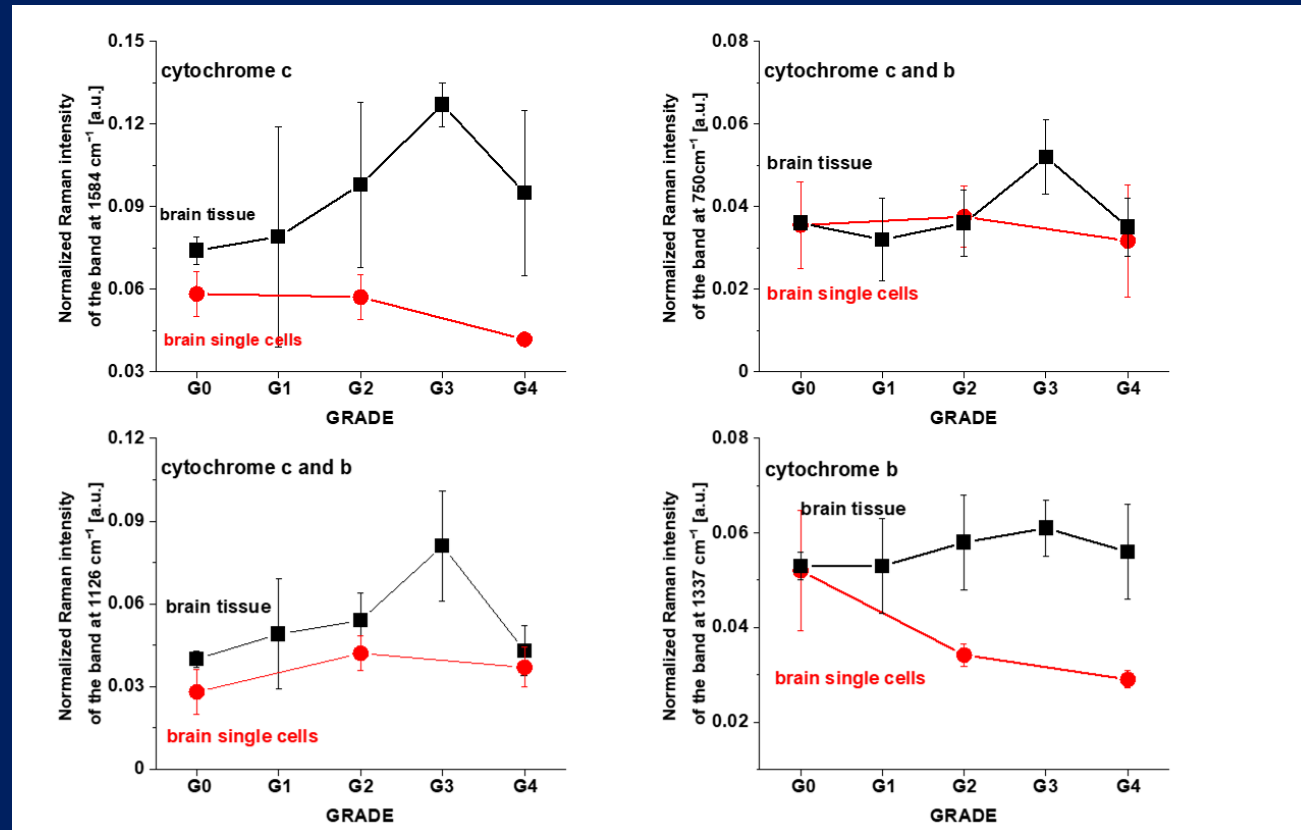
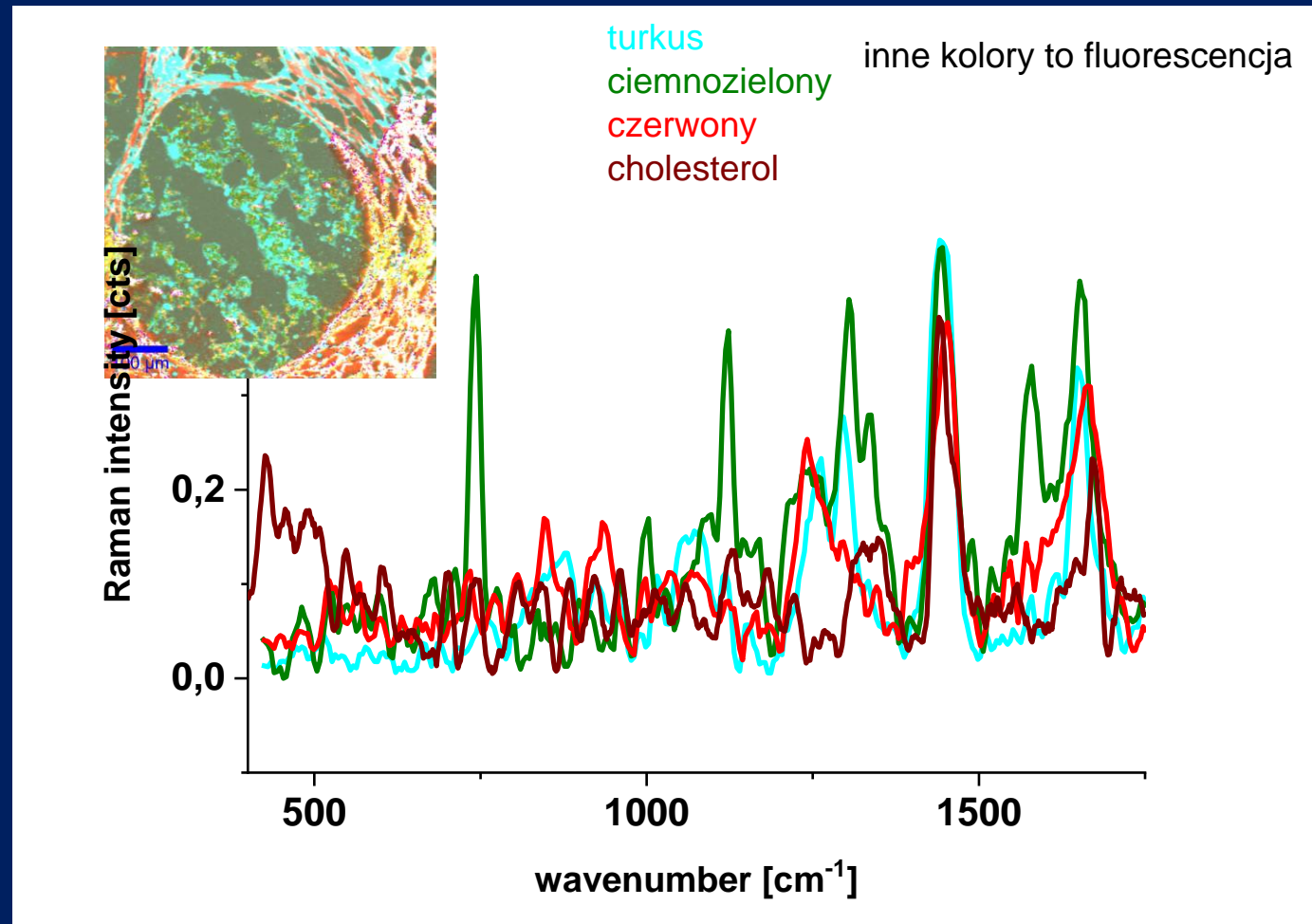


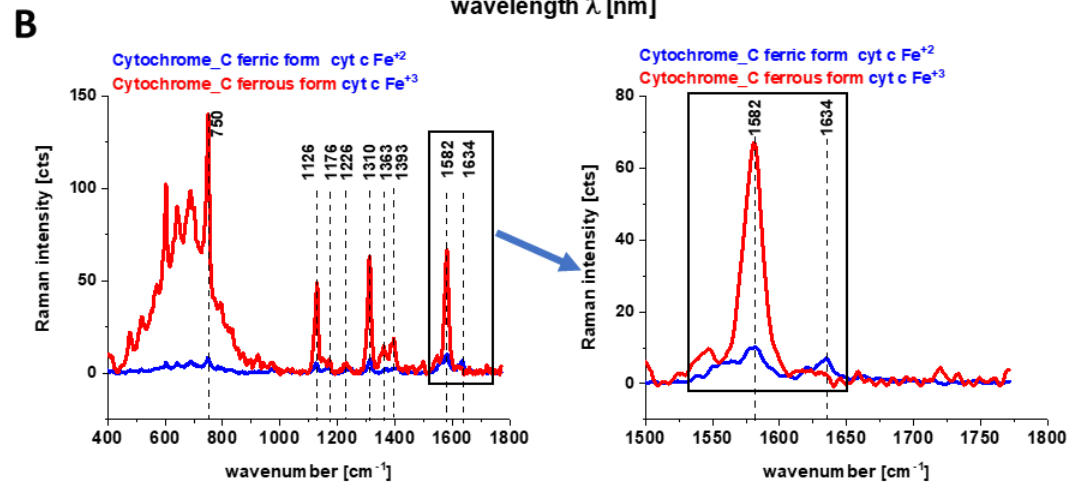
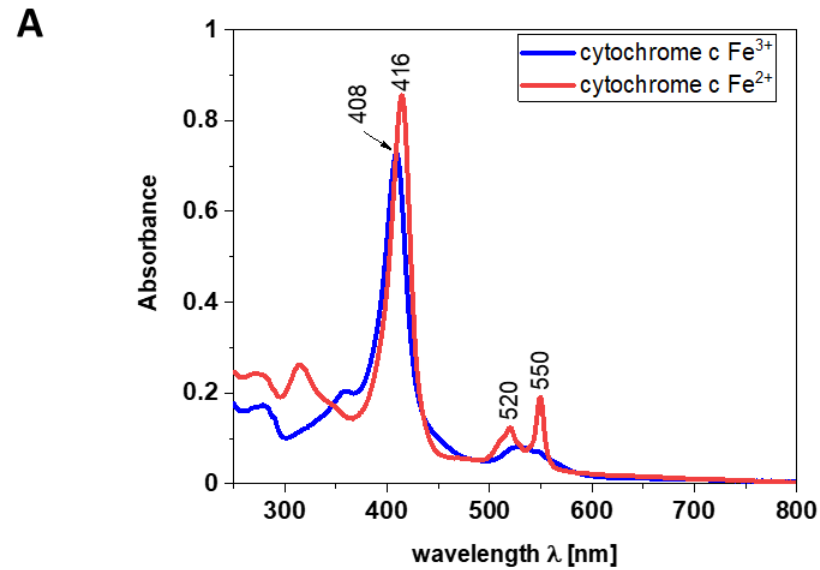
Figure 5. The Raman intensities of cytochrome c and cytochrome b in mitochondria of single cells in vitro culturing and in breast tissues: I_{1584} , I_{1126} , I_{1337} , I_{750} as a function of breast cancer grade malignancy G0-G3 at excitation 532 nm.

Discrepancies between tissues and in vitro cells vs cancer aggressiveness

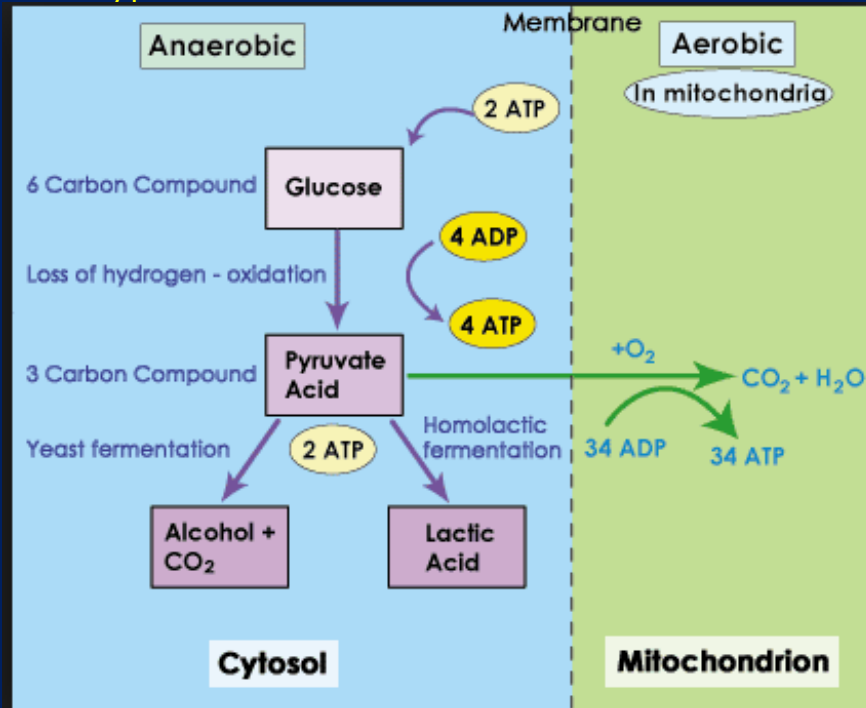


P115 guz vs cholesterol Cytochrome C in cancer duct





The primary **difference** between the **aerobic** and **anaerobic** systems is in the byproduct produced. The **aerobic** byproduct, carbon dioxide, can be easily expelled by regular breathing, while the **anaerobic** byproduct is lactic acid.



During this stage, the glucose molecule is broken down into two molecules of **pyruvate**, an organic acid that can supply cells with energy.

First, it is converted into acetyl-coenzyme A, an event that triggers a series of biochemical reactions that begins with the **oxidation** of glucose components into carbon dioxide during cellular respiration and results in the production of adenosine triphosphate (ATP) which is used to fuel cells.

The outcome of aerobic glycolysis is that the glucose molecule is broken down into two pyruvate, or pyruvic acid, molecules, which are broken down further in the Krebs cycle, and two water molecules.

In oncology, the Warburg effect is the observation that most cancer cells predominantly produce energy by a high rate of glycolysis followed by lactic acid fermentation in the cytosol,^[4] rather than by a comparatively low rate of glycolysis followed by oxidation of pyruvate in mitochondria as in most normal cells.^{[5][6][7]} The latter process is aerobic (uses oxygen). Malignant, rapidly growing tumor cells typically have glycolytic rates up to 200 times higher than those of their normal tissues of origin; this occurs even if oxygen is plentiful.

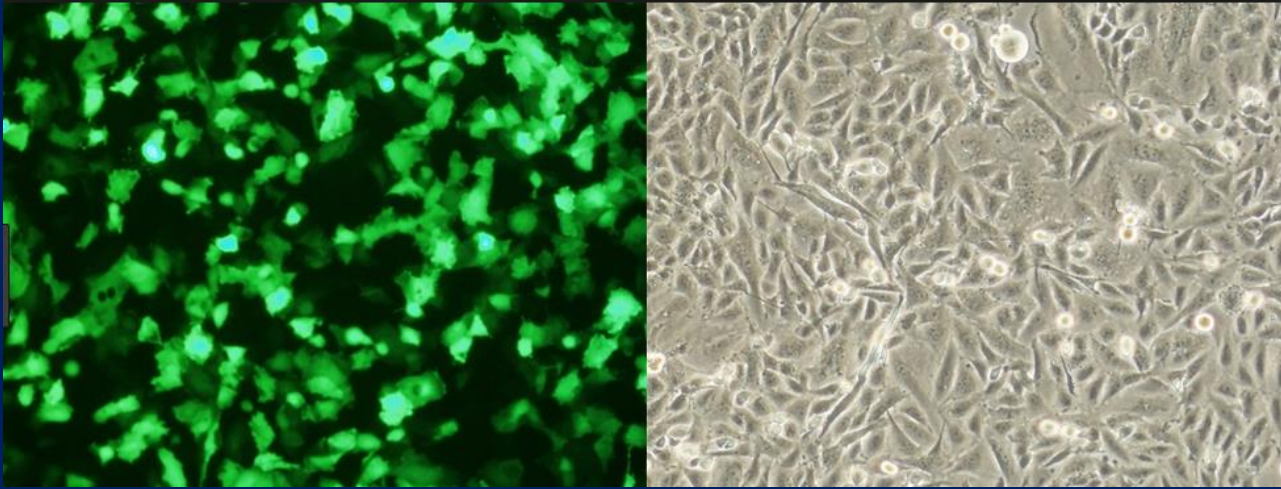
Brain cell lines



Normal Human Astrocytes (NHA) can be used to study the function of the central nervous system and how neural cells interact. Astrocytes are glial cells found in the brain and spinal cord that play a critical role in maintenance, support, and repair of nervous tissue

- **Applications:**
 - Astrocyte-mediated neurotoxicity
 - Neurogenesis research
 - Injury
 - Drug development
 - Parkinson's disease
 - Alzheimer's disease

glioblastoma (U87MG)



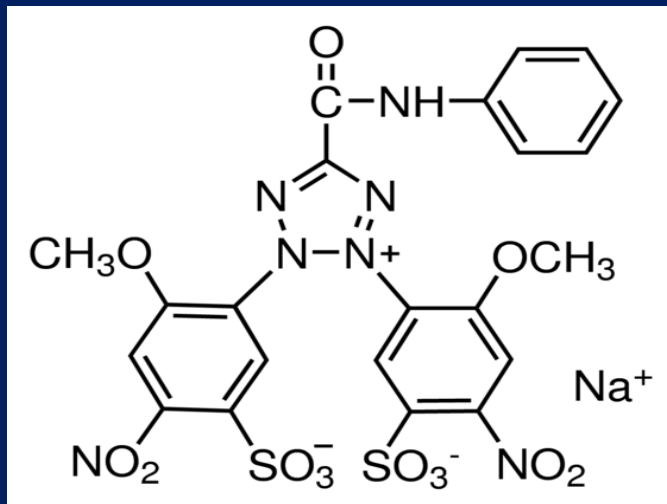
In cell biology, *U87* is a human primary *glioblastoma* cell line formally known as *U-87 MG*. It has epithelial morphology.

Culture Medium

EMEM (EBSS) + 2mM Glutamine + 1% Non Essential Amino Acids (NEAA) + 1mM Sodium Pyruvate (NaP) + 10% Foetal Bovine Serum (FBS).

Cell viability

Cell viability was estimated by Cell Proliferation Kit (XTT based, no. 20-300-1000) following manufacture's instruction (Biological Industries Israel Beit Haemek Ltd.). Briefly seeded cells were mixed with prepared XTT working solution for 3 and 5 hours at 37°C under 5% CO₂ and absorbance value obtained at 450 nm with a reference correction at 690 nm using Synergy HT Multi-Mode Microplate Reader (BioTek).



XTT (sodium 3'-[1-[(phenylamino)-carbony]-3,4-tetrazolium]-bis(4-methoxy-6-nitro)benzene-sulfonic acid hydrate)

Principle

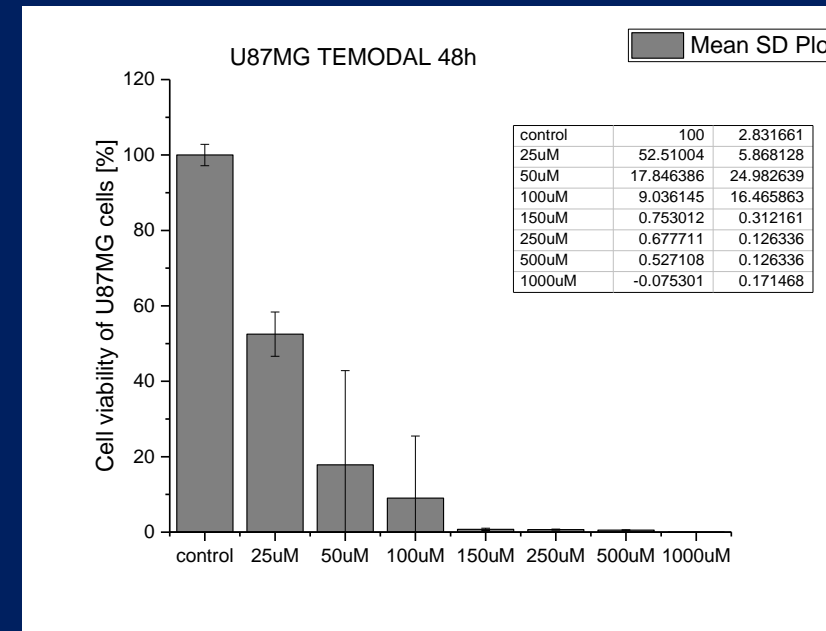
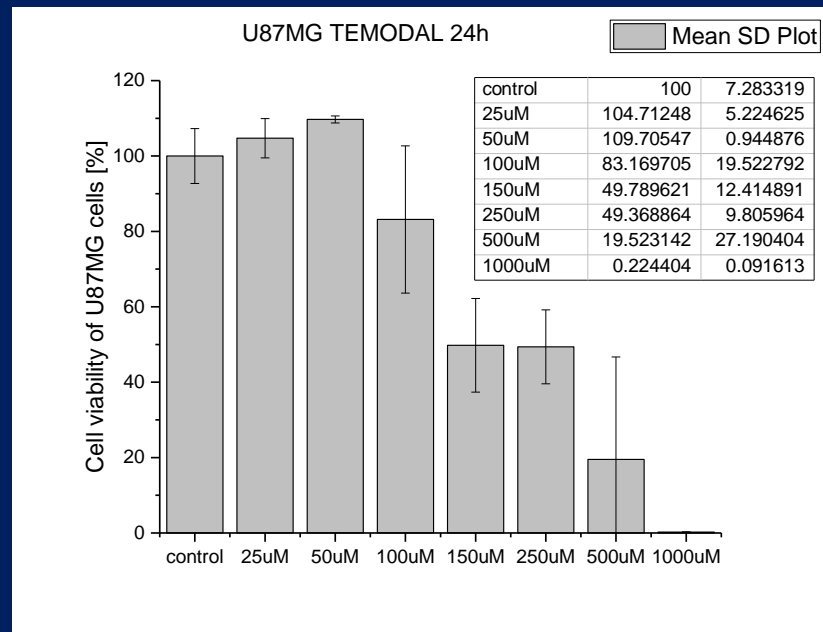
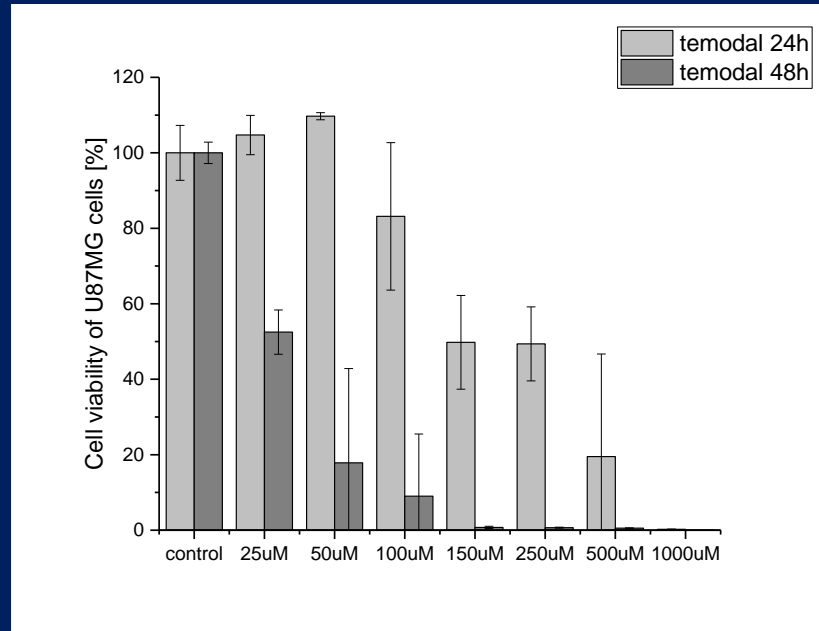
In living cells, XTT is metabolically reduced to produce a colorimetric, water-soluble formazan product.

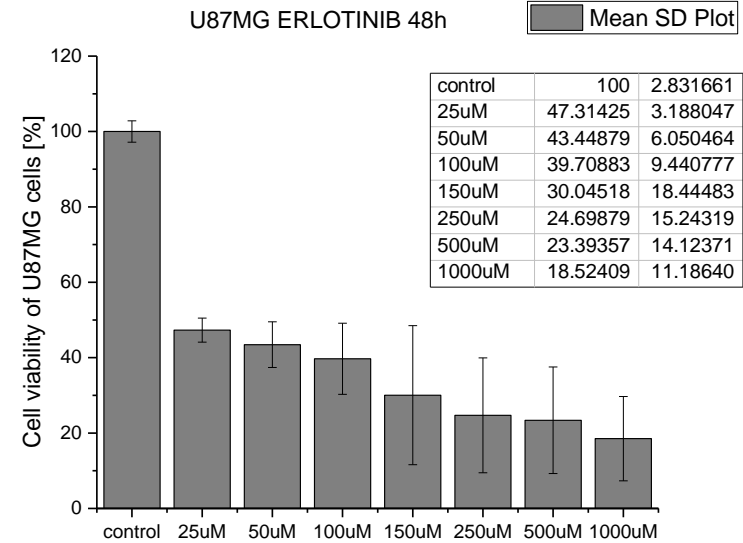
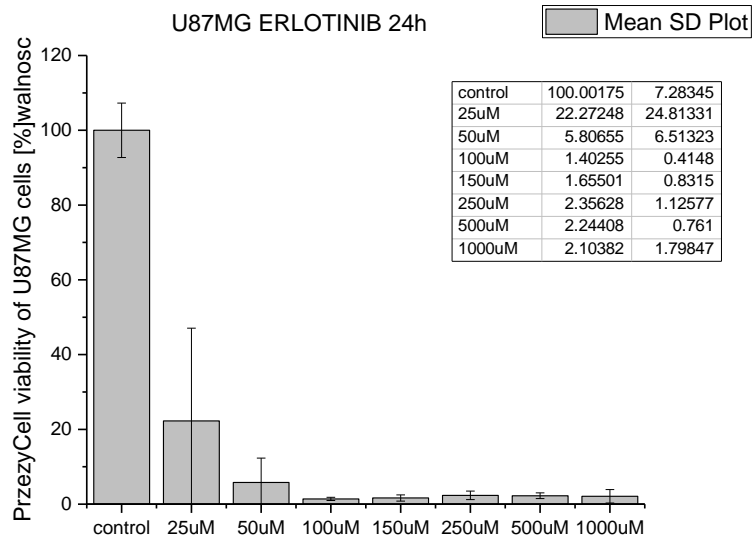
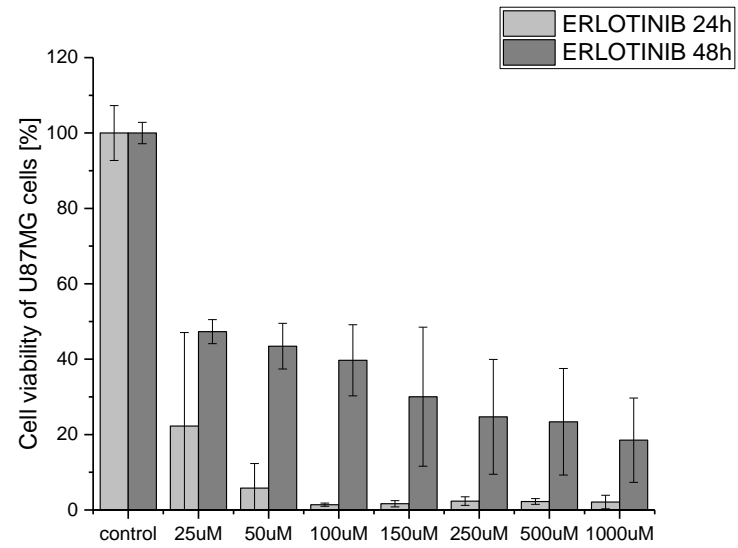
Biochem/physiol Actions

XTT (sodium 3'-[1-[(phenylamino)-carbony]-3,4-tetrazolium]-bis(4-methoxy-6-nitro)benzene-sulfonic acid hydrate) is acted upon by dehydrogenases present in metabolically active cells. This produces water soluble formazan, which is a highly colored product. Thus, it offers an advantage in colorimetric proliferation assays, as opposed to MTT, as the product is already soluble and no formazan crystals are formed.^[1]

General description

XTT (sodium 3'-[1-[(phenylamino)-carbony]-3,4-tetrazolium]-bis(4-methoxy-6-nitro)benzene-sulfonic acid hydrate) is a tetrazolium salt, which forms water-soluble formazan on bio-reduction

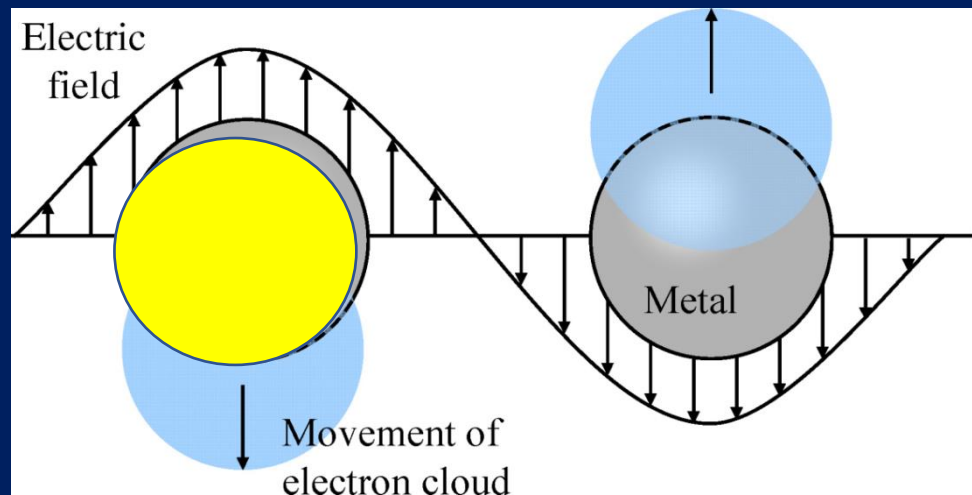




SERS methods

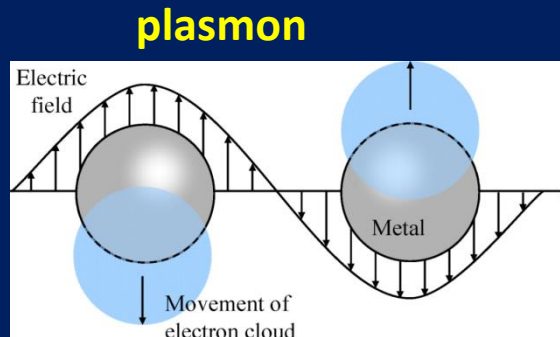
- Despite the high specificity (vibrational fingerprint) , traditional Raman spectroscopy was considered limited because of the very poor efficiency of the inelastic scattering processes and thus the relatively weak signal.
- The SERS technique is based on the fact that if a molecule is brought into close proximity with a metal (Au, Ag) nanostructure or nanoparticle that results in significant increase in the intensity of the Raman spectra.

plasmon



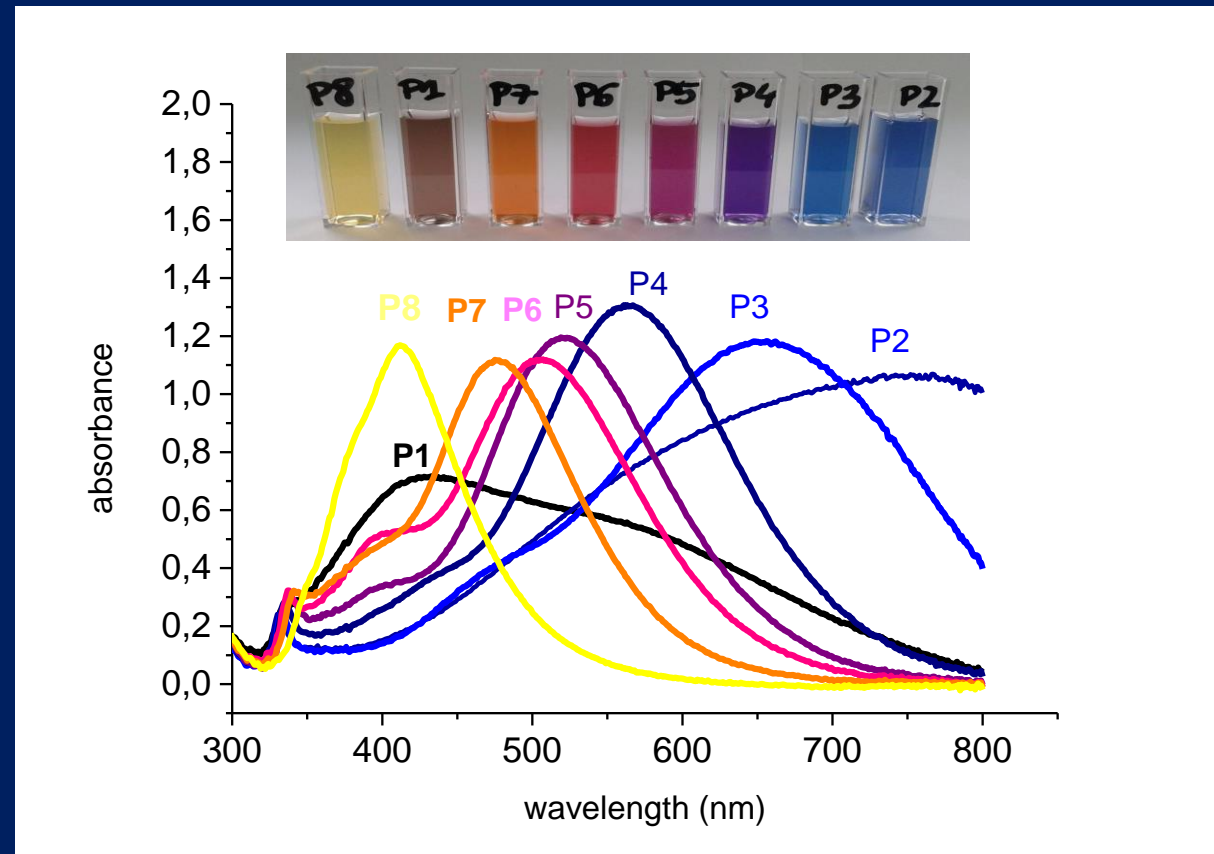
the enhancement mechanism for SERS comes from intense localized fields arising from surface plasmon resonance in metallic (e.g. Au, Ag, Cu) nanostructures with sizes of the order of tens of nanometers, a diameter much smaller than the wavelength of the excitation light.

Silver nanoparticles to SERS



the enhancement mechanism for SERS comes from intense localized fields arising from surface plasmon resonance in metallic (e.g. Ag) nanostructures with sizes of the order of tens of nanometers, a diameter much smaller than the wavelength of the excitation light

Sebastian Schlücker (Ed.): Surface enhanced Raman spectroscopy: analytical, biophysical and life science applications



Nanoparticles produced by chemical reduction.

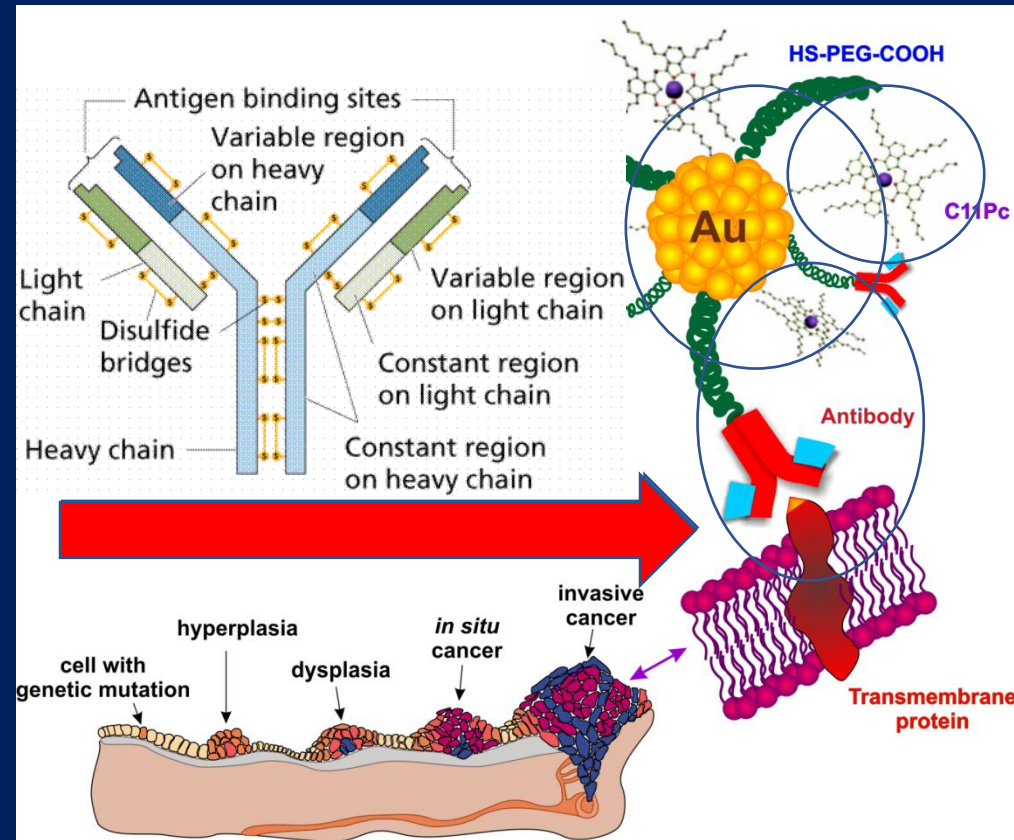
Next step is to enhance the SERS signal with help of nanotechnology.

By immobilising a coloured molecule (Raman reporter) onto a suitably roughened metal surface of the nanoparticle, extremely strong SERRS signals can be obtained with an overall enhancement factor of up to 10^{14} enabling monitoring the genetic and immunological responses in biological systems.

Biocojugates

There are a number of formats used to provide Raman signal. Currently, a promising way to catch cancer lesions early is to use Raman reporters coupled with nanoparticles and antibodies that recognise and bind to cancer cells.

When conjugated with biomolecular targeting ligands such as monoclonal antibodies, peptides or small molecules, these nanoparticles can be used to target malignant tumors with high specificity and affinity.



Raman nanospectroscopy of single DNA molecules

Among biological molecules a deoxyribonucleic acid (DNA) is the most important one because it is found in all living organisms. DNA is often referred to as a double helix because of its appearance. DNA is made of two long strands called nucleotides that run in opposite directions from one another. Nucleotides are made of sugars and phosphate groups that are joined together by ester bonds. Attached to each of the sugars is a molecule called a base. Four different types of bases encode the information that is used for cell replication. Among current DNA detection techniques the Raman scattering is the most powerful tool for gaining information on the chemical structure of the molecule. Raman study of DNA molecules or their basic constituents has a long history since 80th (for example, [1]) and has provided a valuable information on this molecule, however the ultimate goal of Raman measurements has been to work with a minimal concentration of the molecules in a sample, ideally to obtain Raman signals from a single molecule. A single-molecule approach makes it possible to explore individual molecular details that cannot be obtained by ensemble-averaged results. The main obstacle to achieve this aim is the inherent low efficiency of the Raman scattering.

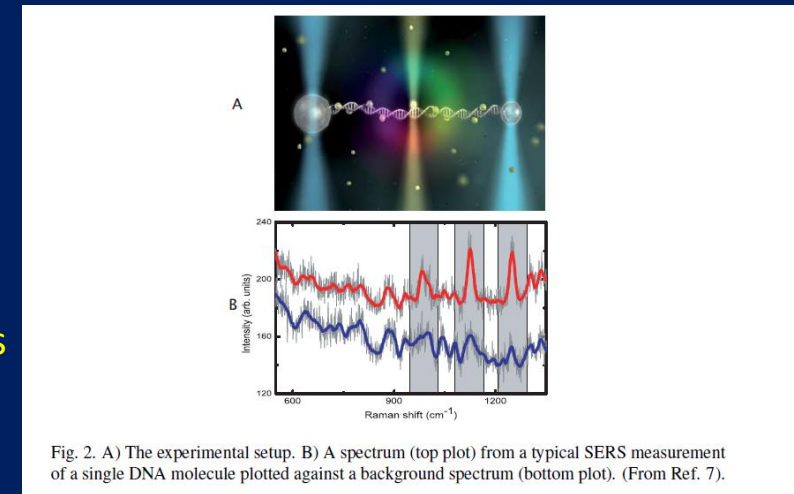


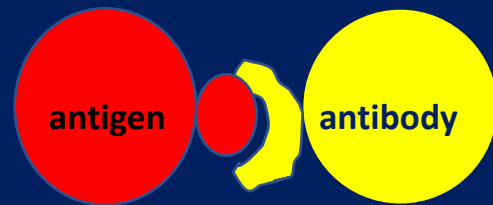
Fig. 2. A) The experimental setup. B) A spectrum (top plot) from a typical SERS measurement of a single DNA molecule plotted against a background spectrum (bottom plot). (From Ref. 7).

Experiments showed that now SERS and TERS may permit one to obtain Raman signals of single DNA molecules. *Journal of Nanophotonics*, Vol. 4, 040306 (2010)

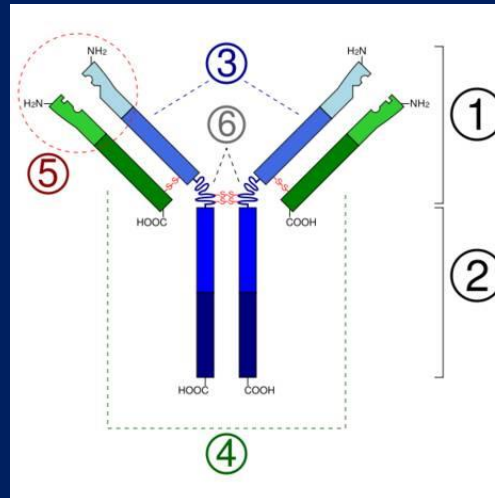
How to reach selective interaction?

binding specificity

Answer: antibody-antigen interactions

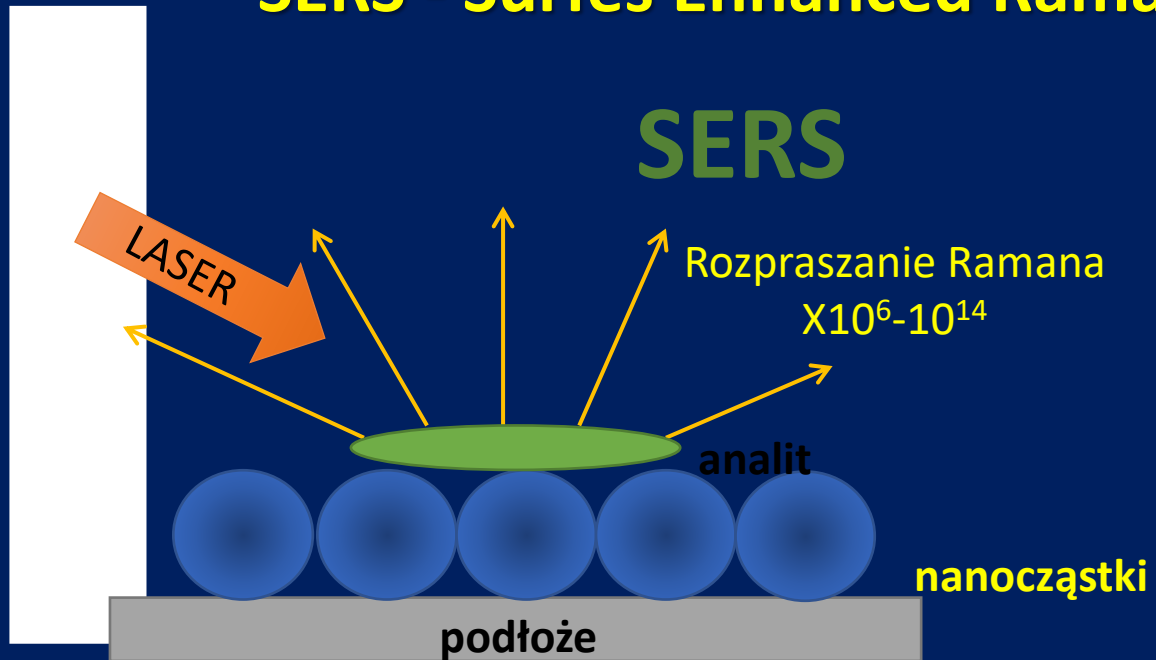


An antigen is a protein molecule that triggers antibody generation

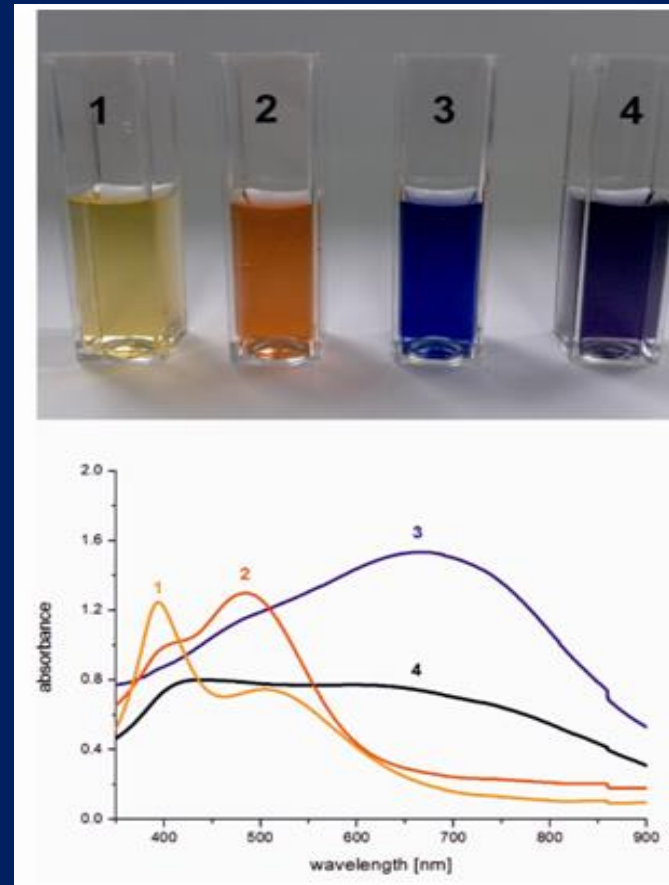


Fortunately, nature provides a solution. The antibody has a unique ability to bind with high specificity to the antigen. Each antibody binds to a specific antigen; an interaction is similar to a lock and key.

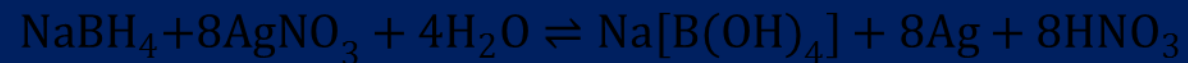
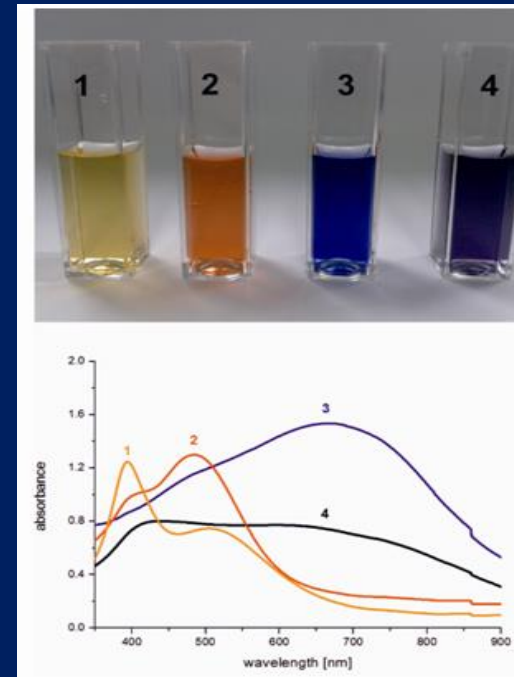
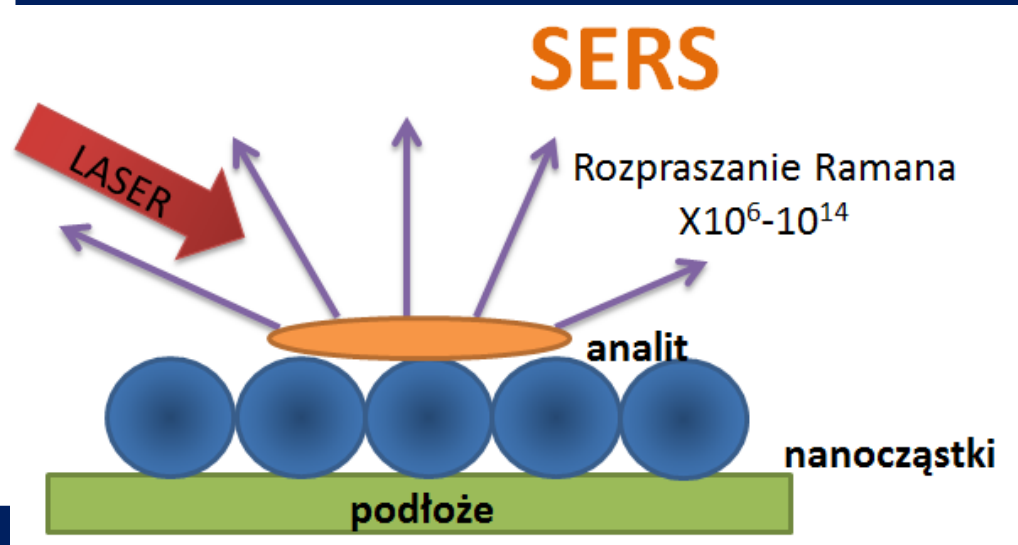
SERS - Surfes Enhanced Raman Spectroscopy



METODY REDUKCJI CHEMICZNEJ
METODY MIKROEMULSYJNE
METODY SONOCHEMICZNE
ABLACJA LASEROWA
METODY RADIACYJNE
TERMICZNA DEKOMPOZYCJA



SERS - Surfes Enhanced Raman Spectroscopy



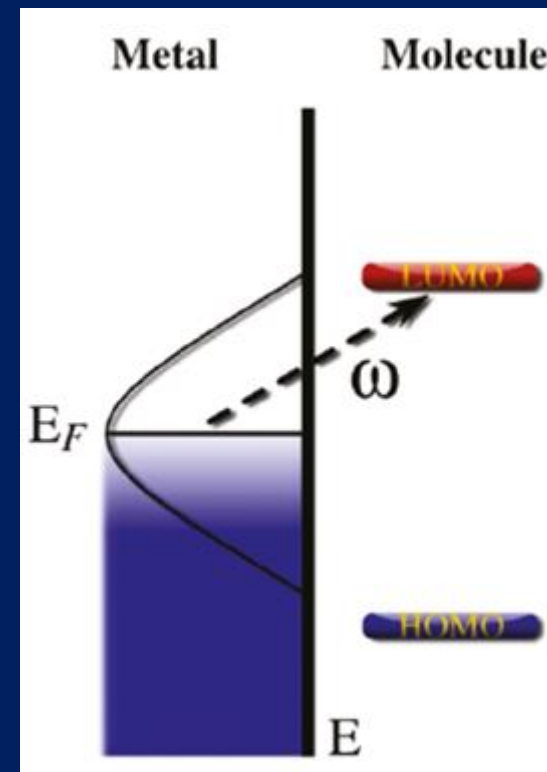
cytrynian sodu
bromek potasu
nadtlenek wodoru

Obecnie przyjmuje się, że obserwowane wzmocnienie sygnału jest wypadkową dwóch mechanizmów: **wzmocnienia chemicznego** oraz **wzmocnienia pola elektromagnetycznego**.

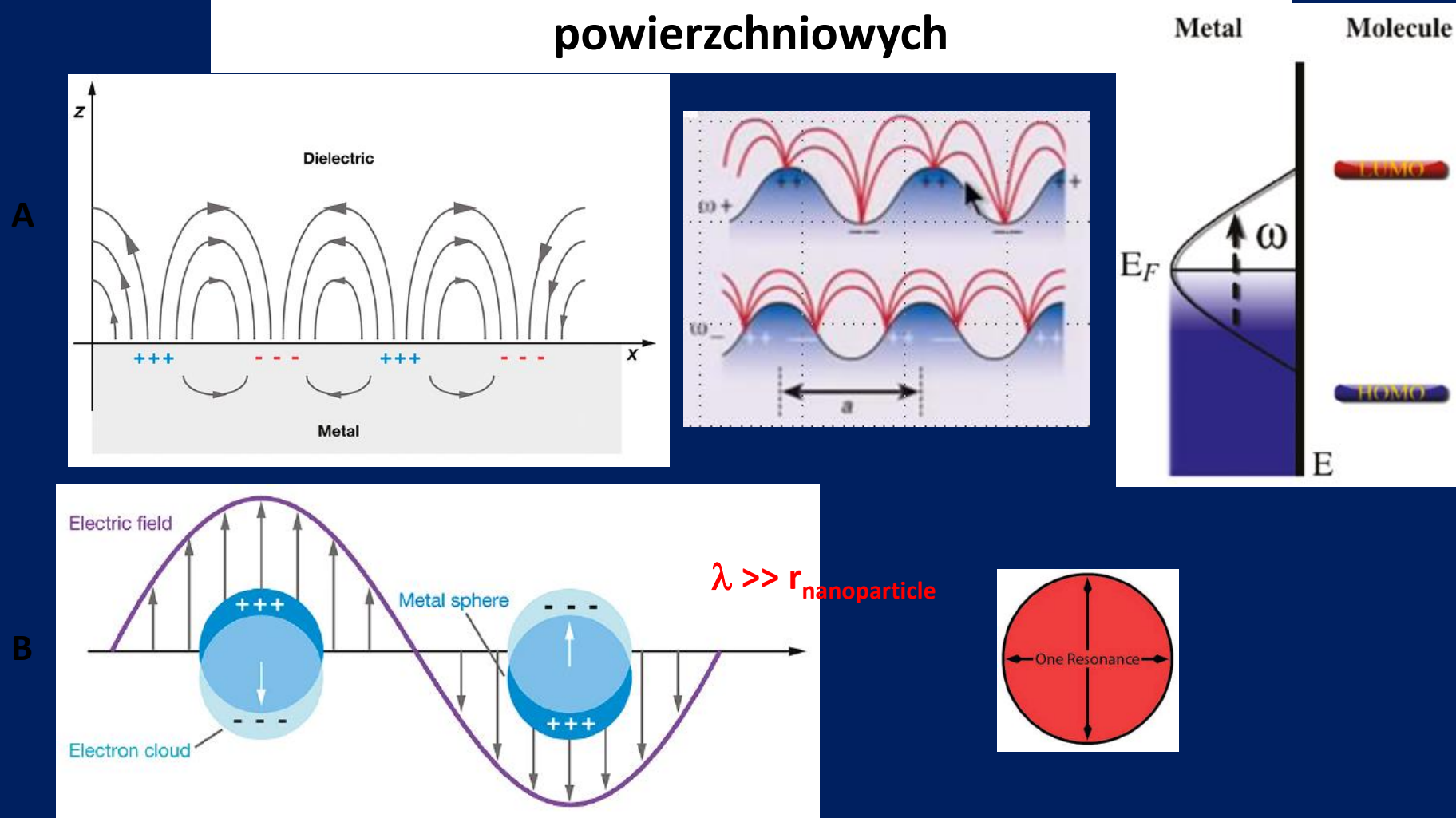
Wzmocnienie chemiczne

W wyniku nałożenia się na siebie orbitali walencyjnych cząsteczki zaadsorbowanej oraz pasma przewodnictwa metalu możliwe staje się przeniesienie ładunku (ang. *charge transfer*) z adsorbatu do metalu (lub na odwrót).

- Wzmocnienie natężenia światła rozproszonego ramanowsko w stosunku do zwykłych warunków rejestracji widma jest rzędu 10^2 .
- Wzmocnienie występuje jedynie dla cząsteczek bezpośrednio oddziałujących z metalem - zasięg ograniczony do monowarstwy adsorbatu (duża specyficzność powierzchniowa).
- Wielkość wzmocnienia chemicznego zależy od położenia poziomu Fermiego metalu i zmienia się w zależności od przyłożonego do elektrody potencjału.

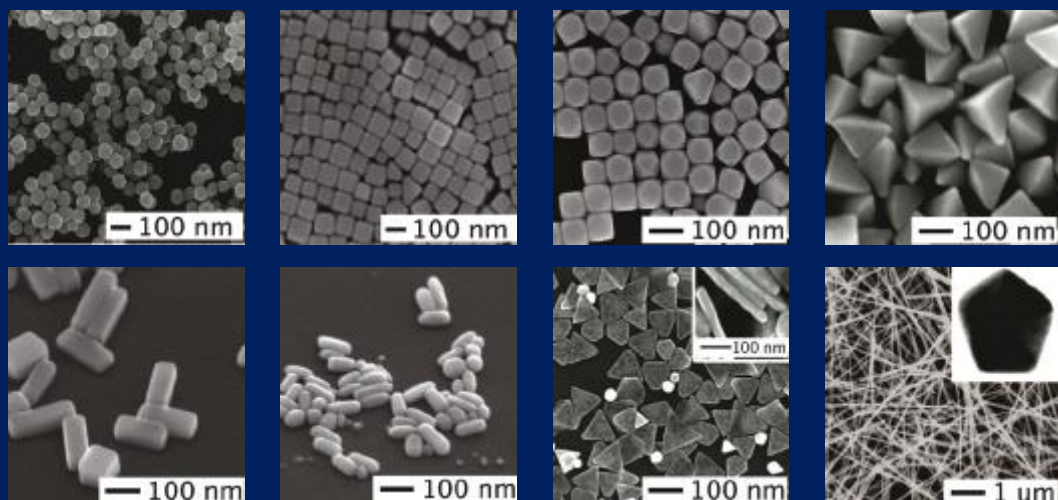
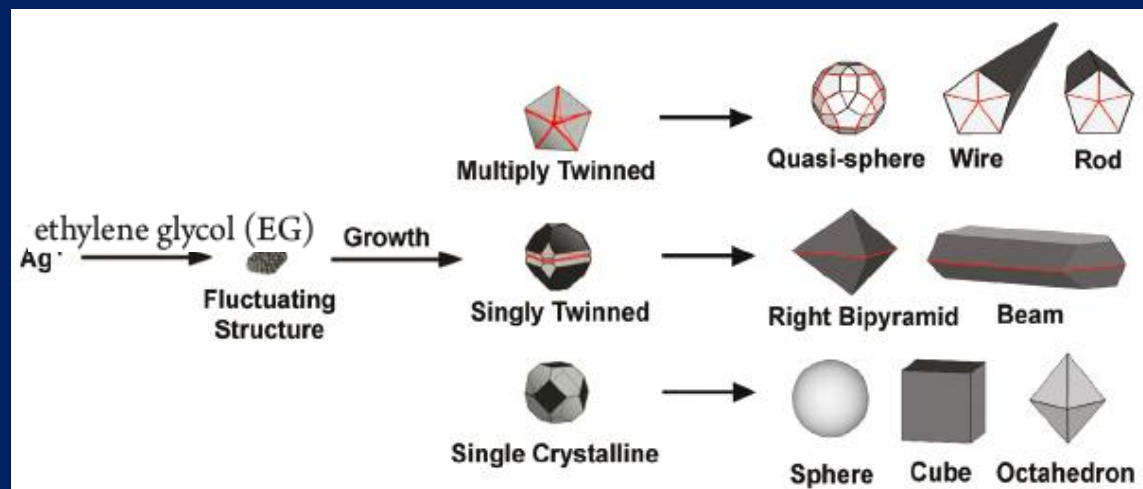


Wzmocnienie pola elektromagnetycznego - rezonansowa oscylacja plazmonów powierzchniowych



Schematic diagrams illustrating (A) a surface plasmon polariton and (B) localized surface plasmon resonance

Polyol method for synthesizing Ag nanostructures



Shape	Illustration	LSPR
Sphere and quasi-sphere		320 - 450
Cube and truncated cube		400 - 480
Tetrahedron and truncated tetrahedron		350 - 450
Octahedron and truncated octahedron		400 - 500
Bar		350 - 900
Spheroid		350 - 900
Right bipyramid		500 - 700
Beam		-
Decahedron		350 - 450
Wire and rod		380 - 460
Polygonal plates and disc		350 - 1000
Branched structures		400 - 1100
Hollow structures		380 - 800

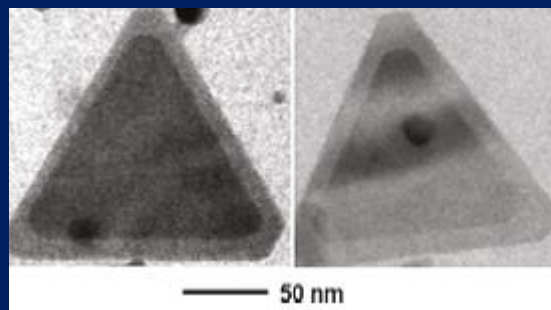
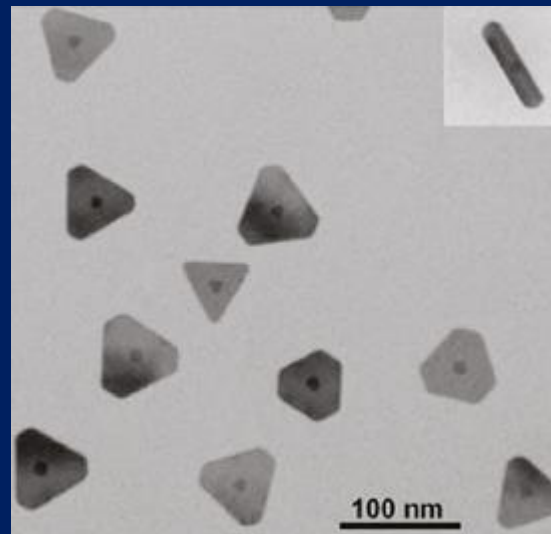
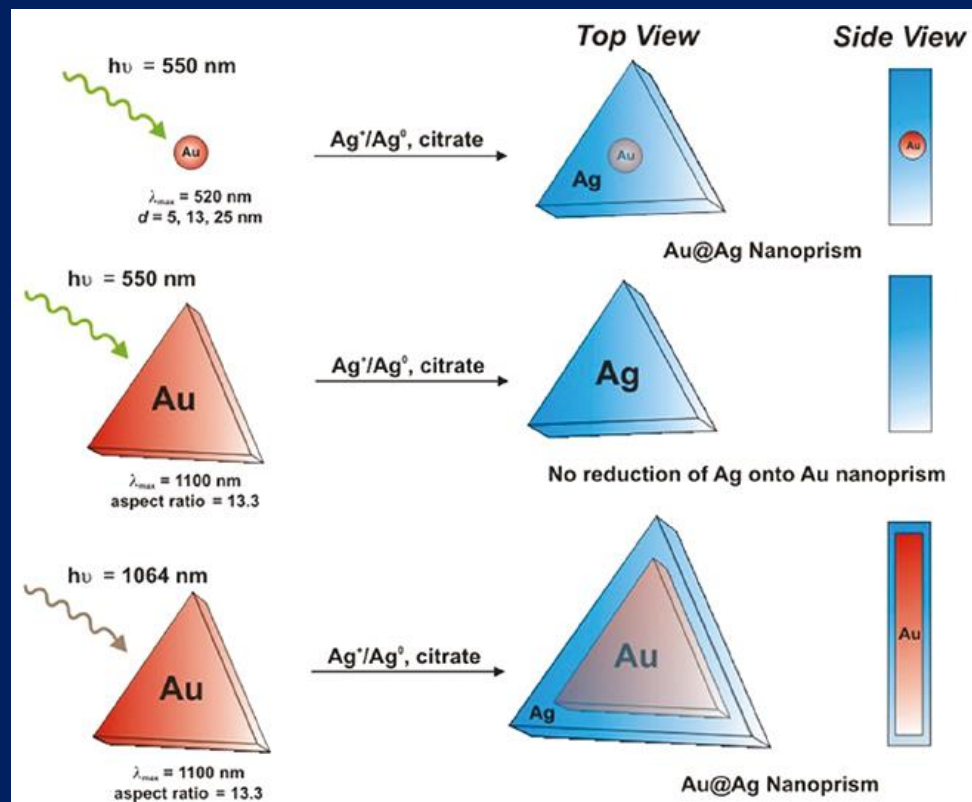
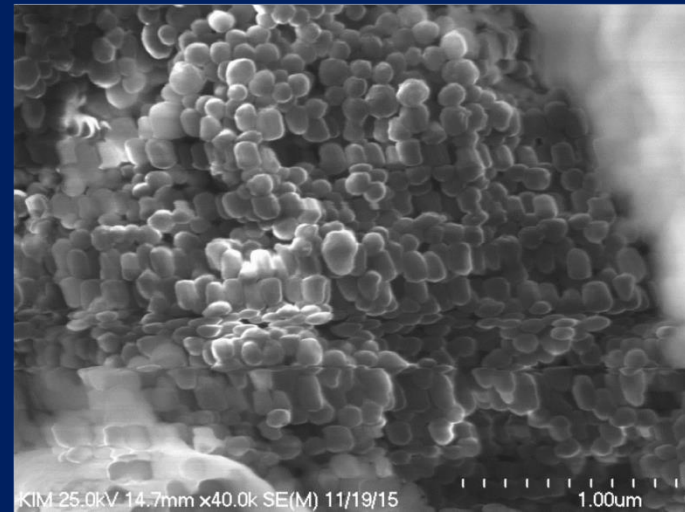
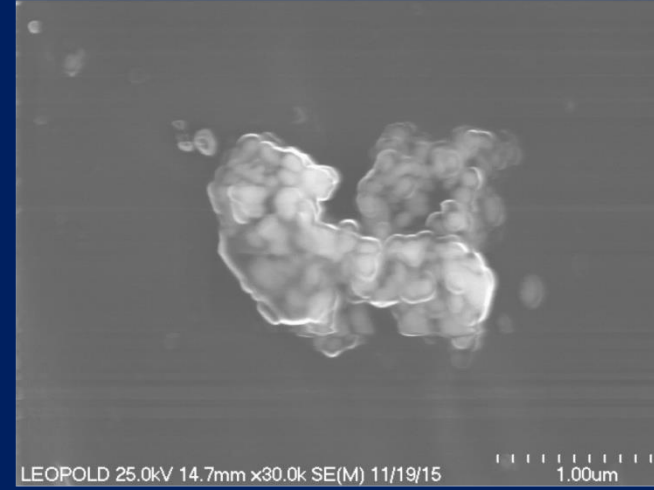
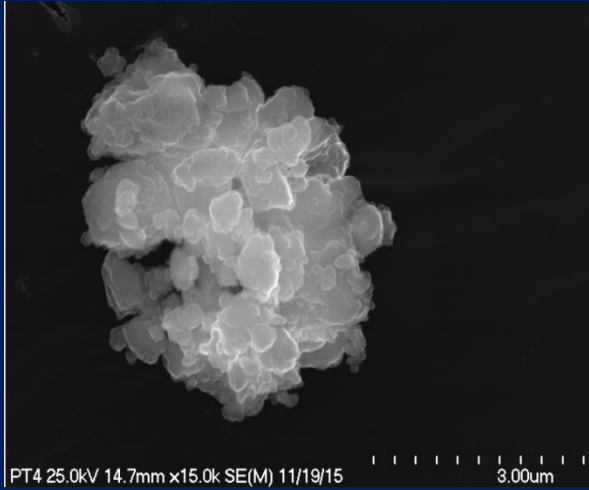


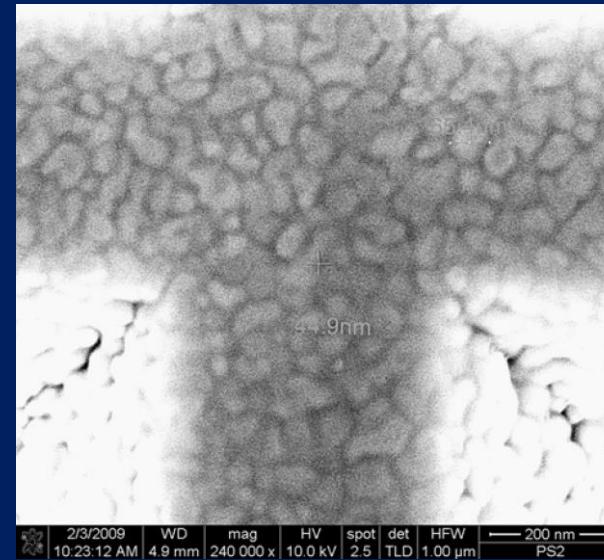
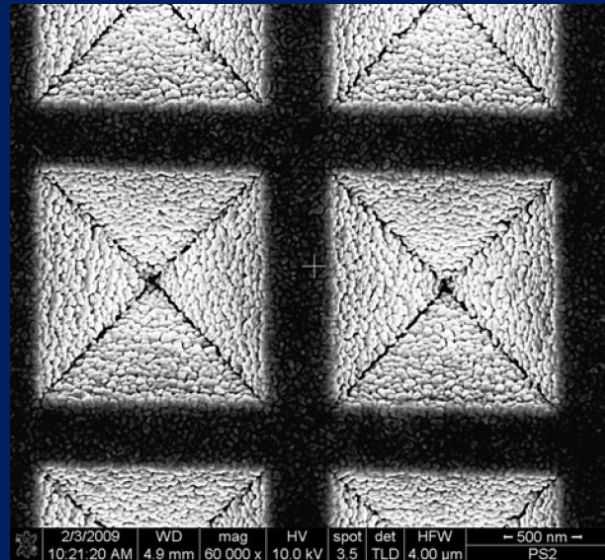
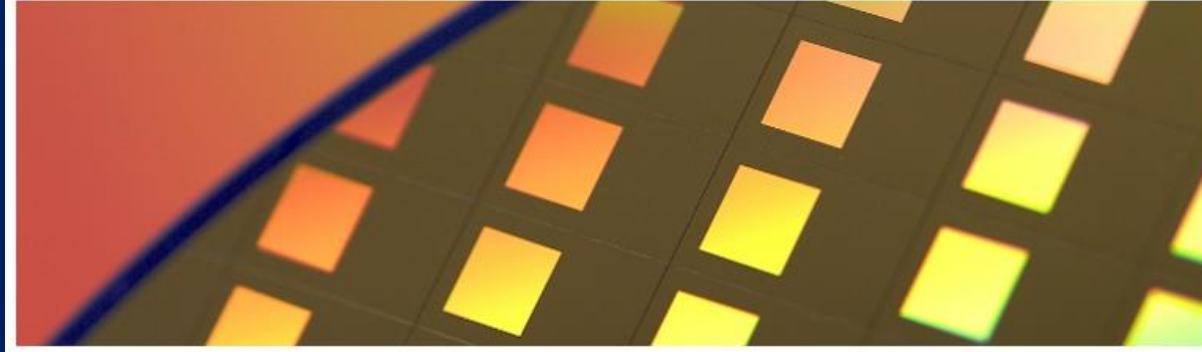
Illustration of the growth pathways for the Au core Ag shell nanostructures

Xue, C.; Millstone, J. E.; Li, S. Y.; Mirkin, C. A. *Angew. Chem., Int. Ed.* 2007, 46, 8436

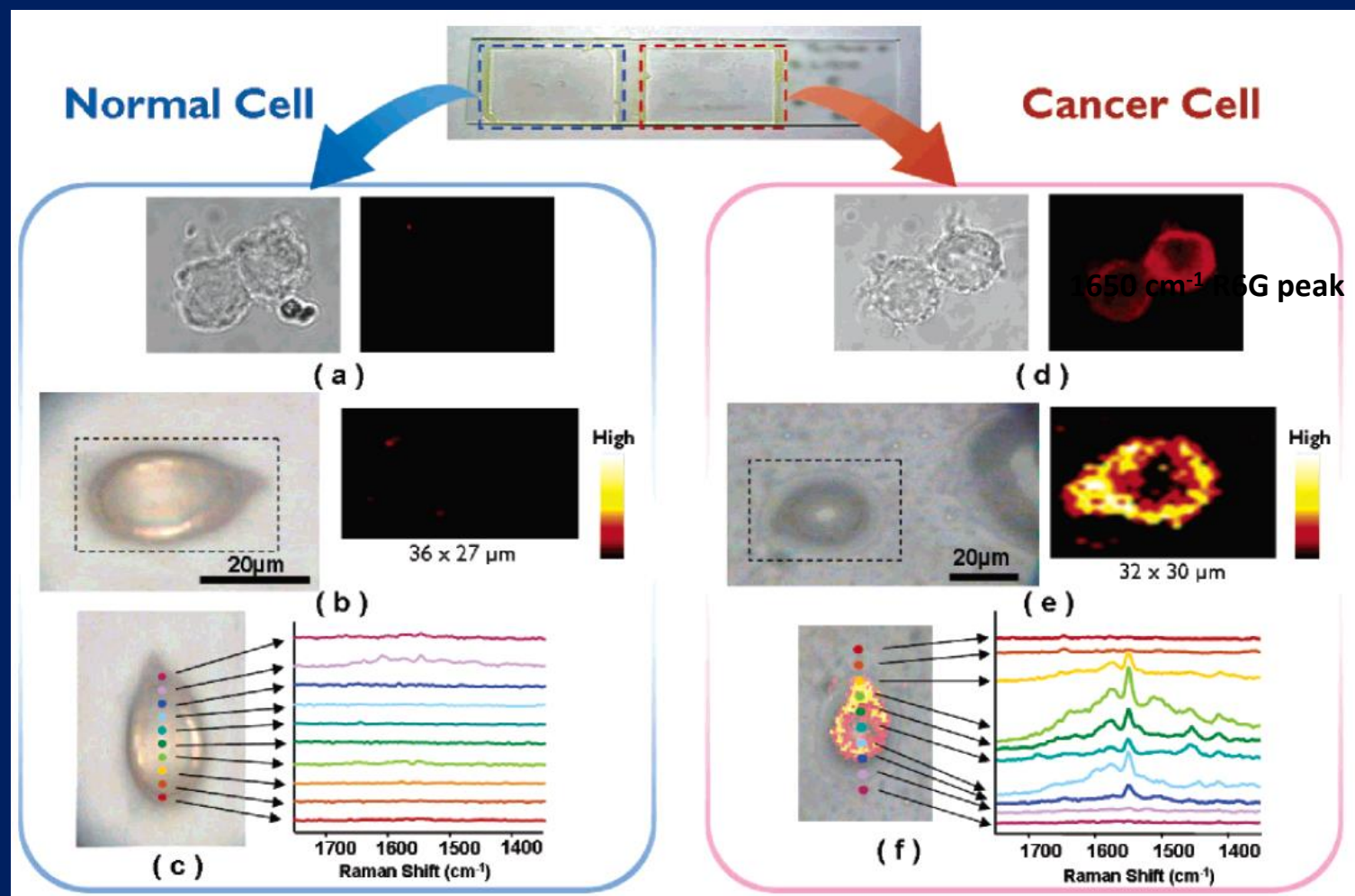
SERS - Surfaces Enhanced Raman Spectroscopy



Klarite® SERS substrates

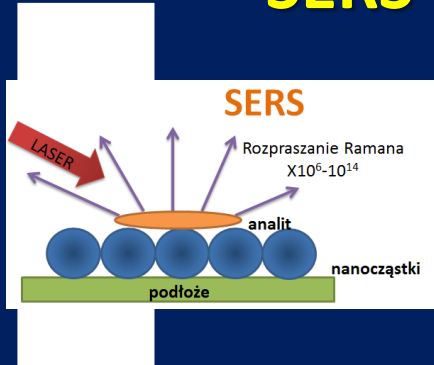


SEM images of a commercial Mesophotonics Klarite substrate



**Fluorescence and SERS images of normal HEK293 cells
and PLC-gamma1-expressing HEK293 cells**

SERS - Surfes Enhanced Raman Spectroscopy



Sample Details

Sample Name: seria_5_SiO2-MPTS_PO-MYCIU 3
 SOP Name: mansettings.nano
 General Notes: seria_5_SiO2-MPTS_PO-MYCIU_23.09.2013

File Name: seria_5_SiO2-MPTS_P... Dispersant Name: etanol
 Record Number: 5 Dispersant RI: 1,359
 Material RI: 1,33 Viscosity (cP): 1,0780
 Material Absorbtion: 0,17 Measurement Date and Time: 23 września 2013 13:59:15

System

Temperature (°C): 25,0 Duration Used (s): 60
 Count Rate (kcps): 441,4 Measurement Position (mm): 0,45
 Cell Description: Disposable sizing cuvette Attenuator: 4

Results

	Diam. (nm)	% Intensity	Width (nm)
Z-Average (d.nm): 384,4	Peak 1: 292,3	94,6	40,60
Pdl: 0,394	Peak 2: 2936	5,4	393,8
Intercept: 0,916	Peak 3: 0,000	0,0	0,000

Result quality **Good**

